Development of novel nanoemulsions as delivery systems

Anges Hwee Ming Teo

2016

Development of novel nanoemulsions as delivery systems

A thesis presented in partial fulfilment of the requirements
for the degree of
Doctor of Philosophy in Food Technology
at Massey University, New Zealand

Anges Hwee Ming Teo

2016

ABSTRACT

In the past decades, emulsions have been widely used as delivery systems for incorporating bioactive compounds into foods. With the advancing of nanotechnology, smaller particles in the nanometric range (i.e. nanoemulsions) can be created with better properties that are more advantageous than conventional emulsions in terms of their stability to gravitational separation, optical clarity and better absorption of nutrients in drug delivery (with increased bioavailability). In particular, emulsification and solvent evaporation method has been used to produce nanoemulsions with optimum results. However, like conventional emulsions, protein-stabilised nanoemulsions become unstable when exposed to certain environmental stresses such as high temperatures, salt addition and extreme pH changes. Additionally, liquid emulsions are difficult to transport and use in some food systems while being susceptible to microbial spoilage. To remedy, a dry, stable emulsion system has to be obtained for their prospective future in food applications.

The objective of this research was to develop nanoemulsions with useful attributes. The thesis consists of three main parts in which the first part studied the formation and properties of nanoemulsions using emulsification and solvent evaporation method; the second part delved into the making of dried nanoemulsion powders and the third part focused on the structural modifications of nanoemulsions and encapsulation of a bioactive compound lutein.

To begin, an experimental study to optimise the conditions for producing nanoemulsions using emulsification and solvent evaporation methodology was performed under different processing conditions (microfluidisation pressures and number of passes), organic phase ratios and materials (oil types and emulsifiers). It was found that smaller oil droplets (around 80 nm in diameter) were achieved when increasing the microfluidisation pressure up to 12000 psi (80 MPa) for 4 passes at an organic phase ratio of 10:90. There was a progressive decrease in particle size with increasing emulsifier concentration up to a 1% (w/w) level for whey protein isolate (WPI) and lactoferrin but it did not decrease further at higher concentration. On the other hand, much larger oil droplets were formed in Tween 20 emulsions (120 – 450 nm). The environmental study showed that lactoferrin and Tween 20 emulsions have

a better stability to pH changes (pH 2 – 12) and salt addition (0 – 500 mM NaCl or 0 – 90 mM $CaCl_2$) than WPI stabilised nanoemulsions.

After successful preparation of nanoemulsions, liquid nanoemulsions were converted to dried powders by spray drying or freeze drying. The nanoemulsions were mixed with different wall materials consisting of maltodextrin alone, trehalose alone or a 1:1 ratio of maltodextrin and trehalose at 10, 20 or 30% (w/w) solid concentration. Results showed that the powders containing 20% trehalose have better powder properties with lower moisture content and water activity, higher bulk density and good reconstitution in water. The freeze-dried powders showed excellent wettability and dispersibility in water but lower encapsulation efficiency than spray dried powders.

In another part of study, nanoemulsions with modified interfacial structure were used to improve their stability to environmental stresses. The interactions between WPI and lactoferrin in aqueous solutions were first studied to explore the feasibility of using these two proteins to form complex interfacial structures at the droplet surface in the emulsions. Based on ζ-potential and turbidity measurements, both proteins were shown to interact with each other via electrostatic interactions at pH values between 6 and 8. The adsorption of protein layers on a gold surface that mimics the hydrophobic oil surface was also confirmed by a quartz crystal microbalance with dissipation (QCM-D) study.

Next, a series of bi-layer nanoemulsions at different pH values and lactoferrin concentrations were prepared so as to determine the best conditions on the overall emulsion stability. It was shown that the stability of emulsions was dependent on both pH and lactoferrin concentration. At pH values close to pI of WPI (around pH 5), the nanoemulsions remained unstable regardless of the lactoferrin concentration used (0.25 – 5% w/w). The nanoemulsions at pH 6 were also unstable at low concentrations (0.5 – 1% w/w) presumably due to “bridging flocculation” and exhibited phase separation. Consequently, a lactoferrin concentration of 3% (w/w) was used to produce bi-layer nanoemulsions at pH 6. At pH 7 – 10, the bi-layer nanoemulsions were stable at all lactoferrin concentrations and formed a bi-layer structure at the interface of droplet.

The formulated nanoemulsions (single layer and bi-layer emulsions) were subjected to a variety of environmental stresses and *in vitro* digestion under simulated gastrointestinal conditions. The emulsion stability to pH changes and salt addition was improved in the bi-layer emulsions containing WPI and lactoferrin when compared to the single layer nanoemulsions stabilised by WPI alone. However, the bi-layer emulsions were more susceptible to destabilisation on heating at temperatures above 60^{o}C. The *in vitro* digestion of bi-layer nanoemulsions was similar to single layer nanoemulsions in which the protein hydrolysis of the interfacial layers results in extensive droplet flocculation.

In subsequent formulations, lutein was incorporated in the emulsions as a model of bioactive compound for the application of nanoemulsions as a novel delivery system. The nanoemulsions well encapsulated lutein in their matrices with an encapsulation efficiency of 80% and contained small oil droplets (70 – 80 nm). All the emulsions were physically stable under the tested conditions up to 28 days at different storage temperatures (5, 20 and 40^{o}C). However, there was a significant decrease in lutein content during storage especially at higher temperatures due to oxidative degradation. Nevertheless, the bi-layer nanoemulsions showed a better stability to lutein degradation. Based on *in vitro* cell toxicity studies on Caco-2 cells using MTT assay, both nanoemulsions did not show toxicity as the cell viability was more than 80% at 10 times or more dilution after 24 hours of incubation. The cellular uptake of lutein was higher in bi-layer nanoemulsions when compared to single layer emulsions.

The present work demonstrated that nanoemulsions can be formed using emulsification and a solvent evaporation method. Dried microcapsules of nanoemulsions were formed with similar properties as their original nanoemulsions after reconstitution in water. The nanoemulsions with bi-layer interfacial structure have better stability to environmental changes than single layer emulsions. Nanoemulsions did not show more toxicity than their corresponding conventional emulsions with large oil droplets produced without the use of organic solvent. These have important implications in the use of nanoemulsions for encapsulation lutein or other bioactive compounds for applications in foods and beverages.

ACKNOWLEDGEMENTS

It was indeed my pleasure to study at Massey University (School of Food & Nutrition). First of all, I would like to thank all my supervisors, Dr. Sung Je Lee, Associate Professor Kelvin Goh and Professor Matt Golding for their supervision, guidance and support throughout my study. I am honoured to have Dr. Lee as my chief supervisor. It has been a great learning experience to work under his supervision. His thorough thinking, scientific knowledge, suggestions, valuable inputs and advices have helped me to complete this research. This thesis would not have been possible without the great input from him. I am also thankful to my co-supervisor, Associate Professor Goh for his guidance and continuous support in the experimental work by providing his constructive feedbacks and suggestions as well as in writing of the thesis.

I am very grateful to the Ministry of Business, Innovation and Employment (MBIE) for funding this research project through the Royal Society of New Zealand as well as providing the travel grants to attend conferences both locally and overseas.

I would also like to thank Professor Conan Fee, Dr. Simone Dimartino and Ms. Rayleen Fredericks (Chemical and Process Engineering Department, University of Canterbury) for giving me the opportunity to work in their laboratory. It was indeed a pleasure to work with Dr. Simone on the QCM-D to study the interactions between protein molecules. His advice and feedbacks were useful to the research work.

I am also thankful to Dr. Fran Wolber for her teaching and guidance on the cell culture studies. It has been a wonderful experience to work with her and the little laboratory tricks that she shared with me.

I would like to thank all the laboratory managers, Ms. Michelle Tamehana, Mr. Steve Glasgow and Ms. Gabrielle Plimmer from School of Food & Nutrition and Ms. Janiene Gilliland and Mr. Chris Hall from Riddet Institute. They have been very helpful to provide the trainings on the use of laboratory equipment and ordering of chemicals. I am also grateful to Ms. Michelle McGrath for her assistance on the HPLC. I would also like to acknowledge the help from Ms. Jordon Taylor and Ms.

Niki Murray (Manawatu Microscopy and Imaging Centre) for preparing the samples for TEM and SEM imaging. I am thankful to Ms. Yvonne Parkes and Ms. Christine Ramsay for their help on the administrative works.

I would also like to thank the students from Singapore, Ms. Lam Yi Shi and Mr. Chiang Jie Hong for helping me with some of the experimental works and the data they provided.

This journey would not have been more than enjoyable without the fun and support of my friends, Yap Sia Yen, Karen Khaw, Noor Soffalina, Daisy Wen, Anynda Yuris, Li Mo, Deng Le and fellow Singaporean friends. It is a pleasure to know them here especially Soffalina who had helped me got my driver license. There was so much wonderful and memorable time we spent in the laboratory doing our research.

Finally, I would like to thank my grandma, my mom and my brother for their unconditional love and continuous support.

TABLE OF CONTENTS

LIST OF FIGURES

LIST OF TABLES

LIST OF SYMBOLS

C	Mass sensitivity constant
D	Translational diffusion coefficient
$D_{3,2}$	Surface weighted mean
$D_{4,3}$	Volume weighted mean
f(κa)	Henry's function
g	Gravitational acceleration
h	Thickness
K	Boltzmann's constant
k	Rate constant
n	Overtone number
r	Radius
T	Temperature
U_E	Electrophoretic mobility
v	Creaming velocity
$t_{½}$	Half-life
ΔD	Dissipation shift
Δf	Frequency shift
Δm	Adsorbed mass
ΔP	Laplace pressure
γ	Interfacial tension
δ	Interfacial layer thickness
η	Viscosity
λ	Wavelength
ε	Dielectric constant
μ	Shear elastic modulus
ρ	Density
ρ_{eff}	Effective surface density
ϕ	Volume fraction
ω	Angular frequency of oscillation

LIST OF ABBREVIATIONS

AMD	Age-related macular degeneration
AMY	Amylase
ANOVA	Analysis of Variance
APS	Ammonium persulphate
BHT	butylated hydroxyl toluene
$CaCl_2$	Calcium chloride
CC	Coconut oil
CCP	Colloidal calcium phosphate
CIE	Commission Internationale de L'Eclairage
CR	Corn oil
DE	Dextrose Equivalence
DLS	Dynamic Light Scattering
DMEM	Dulbecco's modified eagle medium
DMSO	Dimethyl sulfoxide
EE	Encapsulation efficiency
GI	Gastrointestinal
HCl	Hydrochloric acid
HPLC	High Performance Liquid Chromatography
pI	Isoelectric point
kBar	Kilobar
kDa	Kilodalton
L	Lipase
LBL	Layer-by-layer
LCT	Long chain triglycerides
LF	Lactoferrin
LO	Lemon oil
LSCM	Laser Scanning Confocal Microscopy
MCT	Medium chain triglycerides
MD	Maltodextrin
MPa	Mega pascal
MTT	3-(4,5-dimethylthiazol-2-yl)-2,5-diphenyltetrazolium bromide

Na_3N	Sodium azide
NaCas	Sodium caseinate
NaCl	Sodium chloride
nm	nanometre
O.D.	Optical Density
O/W	Oil-in-water
PDI	Polydispersity Index
PIT	Phase inversion temperature
pmol	picomol
psi	Pound force per square inch
QCM-D	Quartz Crystal Microbalance with Dissipation
RNase	Ribonuclease
ROS	Reactive oxygen species
SAM	Self-assembled monolayer
SCT	Short chain triglycerides
S.D.	Standard Deviation
SDS	Sodium dodecyl sulphate
SDS PAGE	Sodium dodecyl sulphate polyacrylamide gel electrophoresis
SEM	Scanning Electron Microscopy
SGF	Simulated Gastric Fluid
SIF	Simulated Intestinal Fluid
SLS	Static Light Scattering
SNEDDS	Self-Nanoemulsifying Drug Delivery System
SOR	Surfactant to oil ratio
SPR	Surface plasmon resonance
TEM	Transmission Electron Microscopy
TEMED	N,N,N',N'-tetramethylethylene diamine
TR	Trypsin
TRE	Trehalose
WI	Whiteness Index
WPC	Whey protein concentrate
WPH	Whey protein hydrolysate
WPI	Whey protein isolate

W/O	Water-in-oil
α-lac	Alpha-lactalbumin
β-lg	Beta-lactoglobulin
ζ-potential	Zeta-potential

LIST OF PUBLICATIONS & CONFERENCE PROCEEDINGS

1. Teo, A., S. Dimartino, S. J. Lee, K. K. T. Goh, J. Wen, Indrawati, O., S. Ko & H. S. Kwak (2016). Interfacial structures of whey protein isolate (WPI) and lactoferrin on hydrophobic surfaces in a model system monitored by quartz crystal microbalance with dissipation (QCM-D) and their formation on nanoemulsions. *Food Hydrocolloids*, 56, 150-160.

2. Teo, A., Goh, K. K. T., Wen, J., Oey, I., Ko, S., Kwak, H. S. & Lee, S. J. (2016). Physicochemical properties of whey protein, lactoferrin and Tween 20 stabilised nanoemulsions: effect of temperature, pH and salt. *Food Chemistry*, 197(Part A), 297-306.

3. Anges Teo, Sung Je Lee & Kelvin K. T. Goh (2015). Stability of lutein in protein-stabilized nanoemulsions prepared by emulsification and solvent evaporation method, 19th International Conference of Functional Food Center, 17-18 November, Kobe, Japan.

4. Teo, A., S. Dimartino, K. K. T. Goh, J. Wen, Indrawati, O., S. Ko, H. S. Kwak, M. Golding & S. J. Lee. (2015). Characterisation of interfacial bi-layer or complex structures of nanoemulsions coated with WPI and lactoferrin studied by QCM-D, NZIFST Annual Conference, 29 June-2 July, Palmerston North, New Zealand.

5. Teo, A., Goh, K. K. T. & Lee, S. J. (2014). Nanoparticles and nanoemulsions. In: Noomhorm, A., Ahmad, I. & Anal, A. K., Functional Foods and Dietary Supplements: Processing Effects and Health Benefits (pp. 405-435). United Kingdom: Wiley Blackwell.

6. Teo, A., Lee, S. J. & Goh, K. K. T. (2014). Modulation of interfacial composition on the physico-chemical stability and lipid digestibility of nanoemulsions stabilised by whey protein isolates (WPI) and lactoferrin, Food Structure and Functionality Forum Symposium from Molecules to Functionality, 30 March-2 April, Amsterdam, The Netherlands.

7. Teo, A., Lee, S. J. & Goh, K. K. T. (2012). Nanotechnology in emulsions: preparation and characterisation of protein-stabilised nanoemulsions and their stability against heat, ionic strength and pH changes, NZIFST Annual Conference, 26-28 June, Hamilton, New Zealand.

Chapter One:

Introduction

1.1 Background Information

Nanotechnology is emerging in the food industry with many potential applications in the arena of functional foods. The U.S. National Science and Technology Council (2006) defines nanotechnology as matters with dimensions of 1 – 100 nm in length. The nanoscale size of materials generally exhibits different physicochemical properties from larger particles and can be potentially used to improve or modify the nutritional, sensorial and structural properties of foods. Particularly, nanoemulsions are being increasingly used in the food industry for encapsulation of bioactive compounds or nutraceuticals. There are a number of potential benefits of using nanoemulsions when compared to conventional emulsions owing to their relatively small droplet size. These include higher stability to gravitational separation, optical clarity, enhanced absorption and higher bioavailability of nutrients (McClements & Rao, 2011). Despite these remarkable benefits, some challenges are faced when developing nanoemulsions containing droplets, especially those smaller than 100 nm in diameter, for use in foods.

At present, nanoemulsions can be produced by high energy or low energy emulsification methods. High energy methods use mechanical devices e.g. high pressure homogenisers or ultrasonic devices to generate large disruptive forces to break up large oil droplets into smaller ones (Anton, Benoit & Saulnier, 2008; McClements & Rao, 2011). However, they are less energy efficient to produce very small droplet size due to the capacity of equipment and materials used (e.g. oil type) (McClements & Rao, 2011). On the contrary, low energy methods such as spontaneous emulsification and phase inversions are more effective in producing nanoemulsions but also have some limitations due to the types of materials (e.g. synthetic surfactants) and processing conditions used. Low energy methods depend on the spontaneous formation of small oil droplets by altering the solution conditions such as surfactant-oil-water ratio, ionic strength, temperature and etc. (McClements

& Rao, 2011; Yang, Marshall-Breton, Leser, Sher & McClements, 2012). However, there are also some limitations as described above and they are not readily suitable for food applications due to the use of high amounts of synthetic surfactants (McClements & Rao, 2011).

Recently, a relatively novel technique to produce nanoemulsions by combining high pressure homogenisation and solvent evaporation appears to be a more desirable approach to overcome the limitations of making nanoemulsions (< 100 nm). In this method, the droplet size of nanoemulsions can be controlled by optimising the emulsification conditions. Thus, it is necessary to understand the processing conditions and the materials used to make nanoemulsions using this approach. If the liquid nanoemulsions can be converted to dry powders, it will also necessarily increase the shelf-life and convenience of using nanoemulsions in encapsulating high-value functional ingredients and bioactive compounds. Therefore, part of this study was to explore the feasibility of drying nanoemulsions using different wall materials and to investigate the physical properties of dried powders.

The performance of nanoemulsions can also be further improved by manipulating the interfacial composition and structure of oil droplets to form multiple layer or mixed layer emulsions. This point is of interest because the interfacial properties of nanoemulsions are considerably different from conventional emulsions as nanoemulsions generally have thicker interfacial layer which is approximately as thick as their droplet diameter (McClements & Rao, 2011). Consequently, a large part of this study was to elucidate the interactions between two oppositely charged biopolymers at the interface which is required for the formation of a stable, multilayer nanoemulsion.

The development of novel biocompatible nanoemulsions with no toxic effects can be of benefit when used to encapsulate bioactive compounds such as lutein which is insoluble in water. However, there was no clear evidence on how these nanoemulsions could improve the stability of the encapsulated compounds and the possible toxicity of nanoemulsions. As such, it was necessary to evaluate the performance of nanoemulsions employed as a delivery system for high value bioactives. In the present study, the development and design of nanoemulsions containing lutein and no lutein (blank emulsions) were investigated. The process

parameters and formulation variables for making nanoemulsions using emulsification and solvent evaporation were systematically studied. The physicochemical properties and stability of nanoemulsions as well as *in vitro* studies on cytotoxicity were also evaluated for their potential applications in food products and for human consumption.

The objectives of this research project were:

1. To investigate the effect of various processing parameters (i.e. homogenisation parameters, organic phase ratios, oil types, emulsifier types and concentrations) on the formation and stability of nanoemulsions using emulsification and solvent evaporation method,
2. To explore the feasibility of making dried powders using different wall materials and their powder properties,
3. To determine and characterise the interactions between WPI and lactoferrin in aqueous solution,
4. To elucidate the formation of bi-layer nanoemulsions and their stability under various environmental and physiological conditions,
5. To determine and compare the stability of lutein encapsulated in nanoemulsions with different interfacial structures and,
6. To investigate the *in vitro* cytotoxicity and cellular uptake of lutein in nanoemulsions.

1.2 Overview of Thesis

This thesis entails the development of nanoemulsions with modified interfacial structures for encapsulation of a bioactive compound – lutein. Specifically, the thesis consists of nine chapters briefly described as follows:

Chapter 1 describes the rationale of developing a nanoemulsion-based delivery system and outlines the main framework of the research project.

Chapter 2 is a literature review of the current understanding of nanoemulsions.

Chapter 3 lists the materials and methods used in this research work.

Chapter 4 describes the processing conditions and the use of some materials to optimise the conditions for making nanoemulsions using emulsification and solvent evaporation method.

Chapter 5 discusses the use of different types of wall materials on the properties of dried nanoemulsion powders produced by different drying methods (spray drying and freeze drying).

In Chapter 6, the interaction of two oppositely charged proteins, namely WPI and lactoferrin was studied to facilitate the understanding on the formation of complex interfacial structure in bi-layer nanoemulsions.

Chapter 7 characterises the formation and physicochemical stability of bi-layer nanoemulsions using WPI and lactoferrin. The encapsulation and stability of lutein in nanoemulsions with different interfacial structures were compared and discussed in Chapter 8. Chapter 8 also includes *in vitro* cytotoxicity and cellular uptake studies on lutein nanoemulsions.

The main highlights of all experimental works herein and some directions for future work are presented in Chapter 9.

Chapter Three:

Materials and Methods

In this chapter, the common materials and methodologies used in most of the experimental works are listed here. Other materials or methods relating to a particular set of experiment are described in their respective chapters.

3.1 Materials

3.1.1 Whey protein isolate (WPI)

WPI (Alacen^{TM} 895) containing 93.9% protein (N x 6.38), 0.3% fat, 4.7% moisture and 1.5% ash was supplied by Fonterra Co-operative Group Limited (New Zealand).

3.1.2 Lactoferrin

Lactoferrin was obtained from Tatua Co-operative Dairy Company Limited (New Zealand). According to the manufacturer, the lactoferrin powder contained 97.7% protein, of which 93.5% was lactoferrin, 0.3% moisture and 1.1% ash.

3.1.3 Corn oil

Corn oil was purchased from a local food supplier, Davis Trading Company, Palmerston North, New Zealand. The oil contained α-tocopherol (306) as antioxidant and citric acid (330). It was used directly without further purification.

3.1.4 Chemicals

Milli-Q water purified by treatment with a Milli-Q apparatus (Millipore Corp., Bedford, MA, USA) was used to prepare all the solutions used in the experimental works. Ethyl acetate (HPLC grade) was purchased from Fischer Scientific (New Jersey, USA). Hydrochloric acid (HCl), sodium hydroxide (NaOH), sodium chloride (NaCl), calcium chloride ($CaCl_2$) and sodium azide (Na_3N) were of analytical grade and purchased from Thermo Fisher Scientific (Victoria, Australia) or BDH Chemicals (Poole, England). All other chemicals used in the experiments

were of analytical grade and obtained from BDH Chemicals (Poole, England) unless otherwise stated.

3.2 Preparation Methods of Nanoemulsions

Nanoemulsions were prepared by emulsification and solvent evaporation method following the method reported by Lee et al. (2011) with some modifications. Briefly, the two phases consisting of an aqueous phase (emulsifier solution) and an organic phase (a mixture of oil and ethyl acetate) were mixed together and homogenised at high pressures before solvent evaporation as illustrated in Figure 3.1.

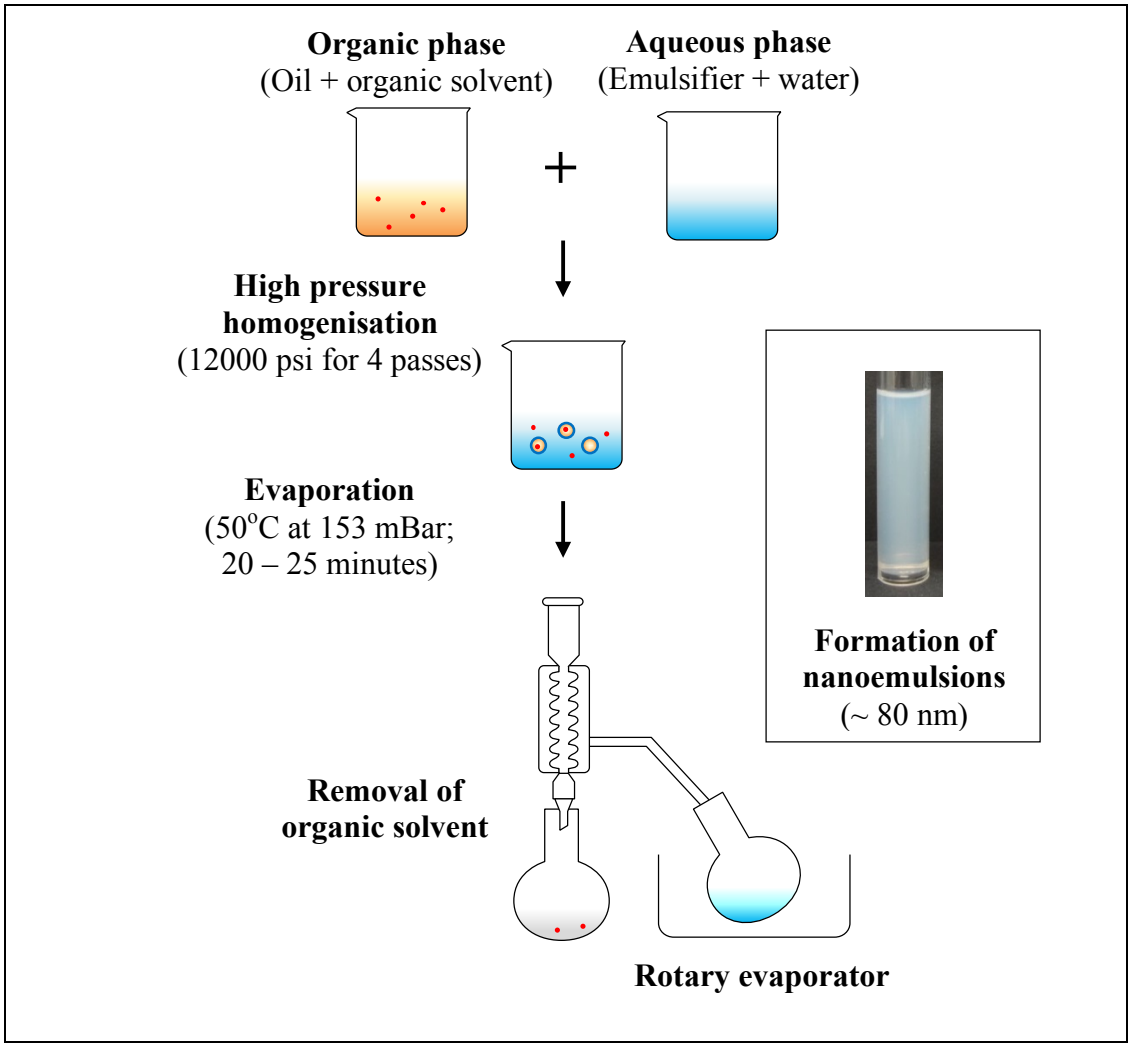

Figure 3.1 Schematic illustration of a combined method of high pressure homogenisation and solvent evaporation used to produce nanoemulsions.

3.2.1 Preparation of solutions

The protein solution used in the aqueous phase was prepared by dispersing appropriate amounts of WPI or lactoferrin powders in Milli Q water (Millipore, 18.2 MΩ cm at 25°C) under gentle stirring for at least 3 hours at room temperature (20^{o}C) and stored at 5^{o}C for overnight to ensure full hydration and dissolution. The pH of the aqueous phase was adjusted to 7 using aliquot solutions of HCl or NaOH.

The organic phase was prepared fresh prior to use by mixing 90% (w/w) ethyl acetate and 10% (w/w) corn oil using a magnetic stirrer at low speed for 2 minutes.

3.2.2 Preparation of nanoemulsions

O/W nanoemulsions were made by mixing organic phase and aqueous phase (10:90 or 20:80 ratios) using a high shear mixer (Ultra Turrax® T25 Basic, IKA, Germany) at 16000 rpm for 3 minutes to form a coarse emulsion. The coarse emulsion was passed through a high pressure homogeniser (M-110P, Microfluidics, USA) (Figure 3.2a) 1 – 4 times at 3000 – 12000 psi (20.7 – 82.7 MPa). After homogenisation, the emulsion was evaporated in a round bottom flask using a rotary evaporator (Buchi Rotavapor R-215, Vacuum Controller V850 and Heating Bath B-491, BUCHI Labortechnik AG, Switzerland) (Figure 3.2b) operating at 50^{o}C with a vacuum pressure of 153 mBar for 20 to 25 minutes. During evaporation, ethyl acetate and some water were removed. The final concentration of oil in the evaporated emulsion was adjusted accordingly to 0.5% (w/w) by replacing the solvent loss with water based on the weight of emulsions before and after evaporation. The pH of the emulsion was adjusted to 7 by adding HCl or NaOH solutions.

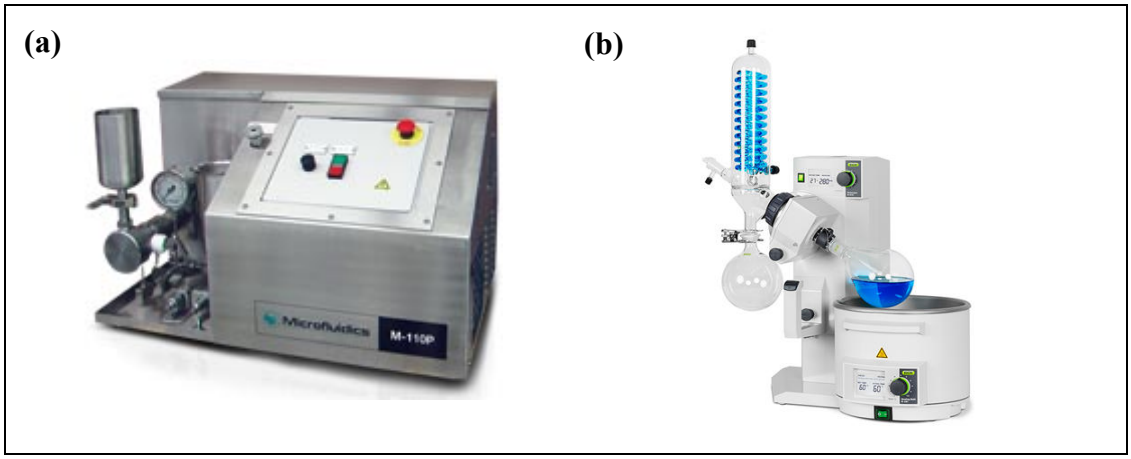

Figure 3.2 Pictures of (a) laboratory scale microfluidiser (M-110P) (Image taken from Microfluidics, USA) and (b) rotary evaporator (Image taken from Buchi, Switzerland).

In chapter 4, several batches of nanoemulsions were prepared under various processing conditions to determine their effects on the formation of nanoemulsions. They were studied by varying the organic phase to aqueous phase ratios (10:90 and 20:80), oil types (corn oil, coconut oil and lemon oil), emulsifier types (WPI, lactoferrin and Tween 20), emulsifier concentrations (0 to 5% w/w) and homogenisation parameters (20 to 80 MPa; 1 to 4 cycles).

The conventional emulsions were also prepared under the same conditions but without the addition of ethyl acetate. In this case, the conventional emulsions contained only corn oil (10% w/w) in the organic phase.

After preparation, all the emulsions were stored overnight at room temperature (20^{o}C) before analysis.

3.3 Characterisation methods

3.3.1 Particle size and size distribution

The particle size and size distribution of emulsions were measured by DLS using a Malvern Zetasizer Nano ZS (Malvern Instruments Ltd, Worcestershire, UK) (Figure 3.3a) equipped with a helium/neon laser at a wavelength of 633 nm and analysed at a backscattering angle of 173^{o}. The DLS technique measures the random movement of particles due to Brownian motion and calculates the particle size by

correlating the intensity of light scattered by the particles using the Stokes-Einstein equation assuming that the particles are spherical (Horne, 2011). A glass cuvette with round aperture (PCS8501) was used for the analysis of samples. The emulsion samples were measured without further dilution during the size measurement, unless otherwise stated. The particle size results were reported as the Z-Average mean diameter and polydispersity index (PDI).

Although the Zetasizer was useful for measuring particle size from 0.3 nm to 10 μm, a Mastersizer instrument (Mastersizer 2000 Hydro MU, Malvern Instruments Ltd, Worcestershire, UK) (Figure 3.3b) was used for measuring larger particles. This applies to those aggregated samples used in the environmental study. Their particle size was reported as the volume mean diameter, $d_{4,3} = \frac{\Sigma_i n_i d_i^4}{\Sigma_i n_i d_i^3}$, where n_i is the amount of droplets with diameter d_i.

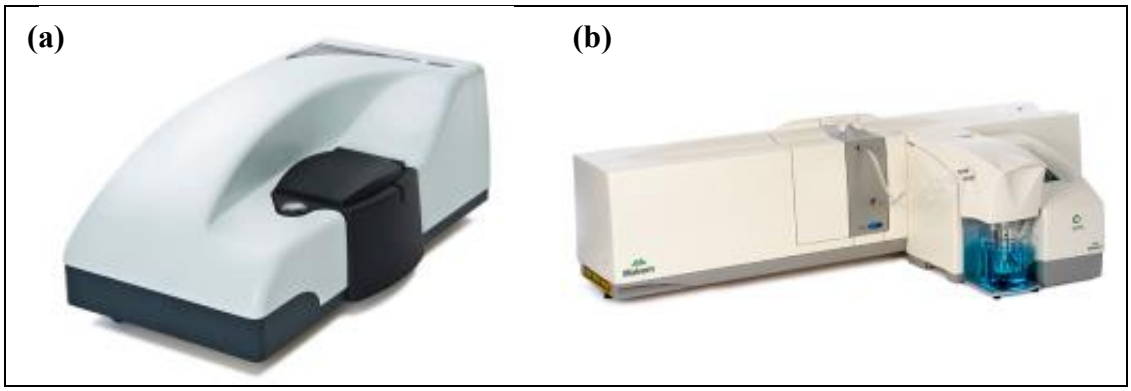

Figure 3.3 Pictures of (a) Zetasizer Nano ZS and (b) Mastersizer 2000 equipped with the Hydro 2000MU (Images taken from Malvern Instruments, Worcestershire, UK).

3.3.2 Zeta potential (ζ-potential) measurements

The ζ-potentials of emulsions were determined using a Malvern Zetasizer Nano ZS (Malvern Instruments Ltd, Worcestershire, UK) (Figure 3.3a) and disposable zeta potential cells ("Size & Zeta" folded capillary cell, Model DTS1070, Malvern Instruments Ltd, Worcestershire, UK). The samples were used without further dilution during the measurement. The measurement was carried out after 30 seconds of equilibration at 25^{o}C and the ζ-potential was calculated by the instrument software using the Smoluchowski model (Zetasizer Software, Version 7.10, Malvern Instruments Ltd, Worcestershire, UK).

3.3.3 Transmission electron microscopy (TEM)

The microstructure of emulsions was determined by TEM and the emulsion samples were embedded in resin according to the method described by Gallier, Tate & Singh (2013). The samples were injected into freshly made 3% agarose tubes (Hydragene Co. Ltd., Xiamen, China) and sealed at the end of each tube with remaining agarose. The embedded samples in agarose tubes were fixed with 3% glutaraldehyde in 0.1 M cacodylate buffer (Merck, Darmstadt, Germany) at pH 7.2 and subjected to a second fixture with 1% osmium tetraoxide (ProSciTech, Thuringowa, Australia) in the same buffer. The samples were dehydrated in a series of acetone washes consisting of 25% acetone (15 minutes), 50, 75 and 90% acetone (30 minutes each) and 100% acetone (30 minutes for 3 times) (Merck, Darmstadt, Germany). This was then embedded in fresh 100% resin (ProSciTech, Thuringowa, Australia) and polymerised at 63^{o}C for 48 hours.

The embedded samples in resin blocks were cut using a glass knife on the ultramicrotome (Leica EM UC7, Heidelberg, Germany) and trimmed down to ultrathin sections using a diamond knife (Diatome, Hatfield, PA, USA). The thin sections of the embedded samples were placed on a copper grid using a Coat Quick "G" adhesive pen (Saiko, Japan) and stained with saturated uranyl acetate (BDH Chemicals, Poole, England) in 50% ethanol (Merck, Darmstadt, Germany) followed by 0.25% lead citrate (BDH Chemicals, Poole, England). This was mounted in a specimen holder and inserted into the microscope cooled by liquid nitrogen. The samples were viewed using a transmission electron microscope (FEI Tecnai^{TM} G2 Spirit BioTWIN, Czech Republic) operated at 60 kV and equipped with a LaB_6 filament. TEM images were captured with a 2K x 2K Veleta camera (14 bit) (Olympus Soft Imaging Solutions GmbH, Münster, Germany).

Figure 3.4 Picture of a transmission electron microscope (Image taken from FEI, Czech Republic).

3.4 Data Analysis

All experimental works were carried out in duplicates and the results were reported as averages and standard deviations of the measurements. Averages and standard deviations were calculated using Microsoft Excel 2010. The data were analysed statistically (Minitab® 17.2.1 statistical software, Minitab, Inc, USA) by analysis of variance (ANOVA) at significant different level set at 0.05. A P value less than 0.05 was considered to be statistically significant.

Chapter Four:

Development of Nanoemulsions Using Emulsification and Solvent Evaporation

4.1 Abstract

The formation of nanoemulsions using a combined method of high pressure homogenisation and solvent evaporation was investigated. The processing conditions (homogenisation pressures, number of cycles, organic phase ratios) and materials (oil types and emulsifiers) used to prepare nanoemulsions were studied. It was shown that WPI-stabilised nanoemulsions containing small droplets with Z-average diameters (80 nm) were produced using this method. The droplet size of the nanoemulsions decreased from 120 to 80 nm with increasing homogenisation pressures (20 – 80 MPa) and cycles (1 – 4). After establishing the optimum processing conditions, the influence of different types of oil (corn oil, coconut oil and lemon oil) and emulsifiers (WPI, lactoferrin and Tween 20) on the properties and stability of nanoemulsions were investigated. Nanoemulsions produced by corn oil or coconut oil formed small droplets (around 80 nm) and were more stable compared to lemon oil emulsions (890 nm). Protein-stabilised nanoemulsions showed a decrease in particle size with increasing protein concentrations from 0.25 to 1% (w/w) level with Z-average diameter between 70 and 90 nm. However, larger droplets were produced by Tween 20 (120 – 450 nm) especially at concentration above 0.75% (w/w). The stability of nanoemulsions to temperature (30 – 90^{o}C), pH (2 – 10) and ionic strength (0 – 500 mM NaCl or 0 – 90 mM $CaCl_2$) was also tested. Tween 20 nanoemulsions were unstable to heat treatment at 90^{o}C for 15 minutes. WPI-stabilised nanoemulsions exhibited droplet aggregation near the pI at pH 4.5 and 5 and they were also unstable at salt concentration above 30 mM $CaCl_2$. These results indicated that stable nanoemulsions can be prepared by careful selection of emulsifiers.

4.2 Introduction

Over the last two decades, considerable studies have been carried out to design novel emulsion systems with improved stability and delivery in the human GI tract. One of the possible delivery systems used for this purpose is in the form of nanoemulsions. Nanoemulsions contain smaller droplets with particle diameter of 10 to 100 nm whereas conventional emulsions have larger droplet size ranging from 0.1 to 100 μm in diameter (McClements, 2010; Lee et al., 2011). The relatively small droplet size of nanoemulsions compared to conventional emulsions means that nanoemulsions have different physicochemical properties with potential applications in food systems (Weiss et al., 2009; McClements, 2010). For instance, nanoemulsions tend to appear transparent or translucent due to the small particle size (smaller than the wavelengths of light) which results in lower reflectance of light (McClements, 1999). Therefore, nanoemulsions can be used to subtly incorporate bioactive compounds into transparent or translucent food systems without affecting their visual appearance. Nanoemulsions also have better physical stability against gravitational separation and droplet aggregation than conventional emulsions (Weiss et al., 2009; McClements & Rao, 2011).

As discussed in the literature review (Section 2.1.3), nanoemulsions can be produced using various emulsification methods. Particularly, emulsification and solvent evaporation is a suitable method to prepare nanoemulsions since it is effective at producing small oil droplets and can be used with a variety of food-grade materials. The droplet size of nanoemulsions produced by this method can be controlled by varying the emulsification conditions and the choice of materials used such as the homogenisation pressure, organic phase ratios, types of oil and emulsifier. However, these emulsification conditions need to be optimised in order to obtain translucent nanoemulsions with good stability. Additionally, the emulsifiers play an important role in the formation of nanoemulsions but there is no systematic study on the role of emulsifiers on the physical functionality of nanoemulsions prepared using this method. Moreover, the physicochemical characteristics and stability of nanoemulsions when exposed to environmental conditions encountered during food processing such as heating, salt addition and extreme pH changes have not yet been extensively reported.

The objectives of this work were to investigate the effect of processing conditions (homogenisation pressure, number of cycle, organic phase ratios, oil types and emulsifier types and concentrations) on the properties of nanoemulsions and the physicochemical stability of nanoemulsions under different environmental conditions (heating temperature, ionic strength and pH changes). The research attempts to provide insight into the development of nanoemulsions with great potential for delivery of lipophilic bioactive compounds in foods.

4.3 Materials and Methods

4.3.1 Materials

The main materials used for making nanoemulsions are as listed in Chapter 3 (Section 3.1). Coconut oil (93% medium chain fatty acids) was purchased from Nature's Way Products, LLC (Lehi, UT, USA). Lemon oil and Tween 20 was purchased from Sigma Chemical Co. (St. Louis, MO, USA). All the chemicals used were of analytical grade.

4.3.2 Formulation of nanoemulsions

Nanoemulsions were prepared using emulsification and solvent evaporation method as described in Chapter 3 (Section 3.2.2). Conventional emulsions (10% w/w corn oil) were prepared under the same conditions as nanoemulsions but without the use of ethyl acetate. An example of the composition of conventional emulsion and nanoemulsion before and after solvent evaporation and after dilution to 0.5% (w/w) oil level is shown in Table 4.1.

Table 4.1 Composition of conventional emulsion and nanoemulsion prepared at organic phase ratio of 10:90.

	Conventional emulsion			**Nanoemulsion**		
	Before evaporation	**After evaporation**	**Final composition**	**Before evaporation**	**After evaporation**	**Final composition**
Aqueous phase						
WPI	1.80	1.80	0.09	1.80	1.98	0.90
Water	88.2	88.2	99.4	88.2	96.9	98.6
Organic phase						
Ethyl acetate	-	-	-	9.00	0.00	0.00
Corn oil	10.0	10.0	0.50	1.00	1.10	0.50
Total	100	100	100	100	100	100

The effect of experimental parameters on the formation of nanoemulsions was studied under various processing conditions using WPI as the primary emulsifier and corn oil in the organic phase (Table 4.2). Several nanoemulsions were prepared at different concentrations of WPI varying from 0.25 to 5% (w/w) at two different organic and aqueous phase ratios of 10:90 and 20:80. A detailed composition of the nanoemulsions prepared at different protein concentrations and organic phase ratios is shown in the Appendix (Table 1). The effect of homogenisation parameters on the nanoemulsions was also studied at two different organic phase ratios (10:90 and 20:80) using 1% (w/w) WPI under different homogenisation pressures (20 – 80 MPa) and number of cycles (1 – 4). For all the other experimental works, the nanoemulsions were microfluidised for 4 cycles at 80 MPa.

Table 4.2 Variations of the emulsion composition and conditions used in the preparation of nanoemulsions.

Experiment	Organic to aqueous phase ratio	% Emulsifier concentration (w/w)	Microfluidisation pressure (MPa)	No. of cycle
Organic phase ratio and WPI concentration	10:90	0.25	80	4
	10:90	0.50	80	4
	10:90	0.75	80	4
	10:90	1.0	80	4
	10:90	2.0	80	4
	10:90	3.0	80	4
	10:90	5.0	80	4
	20:80	0.25	80	4
	20:80	0.50	80	4
	20:80	0.75	80	4
	20:80	1.0	80	4
	20:80	2.0	80	4
	20:80	3.0	80	4
	20:80	5.0	80	4
Organic phase ratio and homogenisation parameters	10:90	1.0	20	4
	10:90	1.0	40	4
	10:90	1.0	60	4
	10:90	1.0	80	4
	10:90	1.0	80	1
	10:90	1.0	80	2
	10:90	1.0	80	3
	20:80	1.0	20	4
	20:80	1.0	40	4
	20:80	1.0	60	4
	20:80	1.0	80	4
	20:80	1.0	80	1
	20:80	1.0	80	2
	20:80	1.0	80	3

The use of different types of oil on the properties of nanoemulsions was studied using corn oil, fractionated liquid coconut oil or lemon oil. All the oils were used as purchased without any further purification. The nanoemulsions were prepared using 1% (w/w) WPI as the emulsifier at an organic phase ratio of 10:90.

The effect of different types and the concentrations of emulsifier on the properties and stability of nanoemulsions were studied using WPI, lactoferrin or Tween 20 at emulsifier concentrations ranging from 0.25 to 5% (w/w). The nanoemulsions were prepared using corn oil at organic phase ratio of 10:90.

4.3.3 Effects of environmental conditions on nanoemulsions

The effects of heat treatment, pH changes and ionic strength on the environmental stability of nanoemulsions stabilised by different emulsifiers (WPI, lactoferrin and Tween 20) at 1% (w/w) level were studied.

- The effect of heat treatment on the stability of emulsions was examined by heating the emulsions in water bath at different temperatures (30, 40, 50, 60, 70, 80 and 90^{o}C) for 15 minutes. After heating, the emulsions were immediately cooled to room temperature by placing them in an ice water bath.
- The pH stability of emulsions was determined by adjusting the pH of emulsions to different pH levels (2, 3, 4, 5, 6, 7, 8, 9 and 10) using different concentrations of HCl and NaOH solutions.
- The addition of salt on the stability of emulsions was determined by using NaCl and $CaCl_2$. The emulsions were mixed with an equal amount of different concentrations of salt solutions to achieve oil concentration of 0.5% (w/w) and the final concentration of salt in the emulsions was 0, 50, 100, 200 and 500 mM NaCl or 0, 10, 30, 60 and 90 mM $CaCl_2$.

4.3.4 Characterisation of nanoemulsions

The particle size and size distribution of nanoemulsions were measured using a Malvern Zetasizer Nano ZS (Malvern Instruments Ltd, Worcestershire, UK). The emulsion samples were measured without further dilution during the size measurement. For those aggregated samples (with large particles ≥ 5000 nm) in the environmental study, they were measured using a Malvern Mastersizer 2000 Hydro MU (Malvern Instruments Ltd, Worcestershire, UK). This applies to the WPI-

stabilised nanoemulsions with pH adjusted to 4.5 and 5 and those with salt concentrations above 30 mM $CaCl_2$. The ζ-potential of nanoemulsions was determined using a Malvern Zetasizer Nano ZS (Malvern Instruments Ltd, Worcestershire, UK) and disposable ζ-potential cells ("Size & Zeta" folded capillary cell; DTS1070). The samples were used without further dilution during the measurement. The mesurements were carried out in triplicates on two independent samples. Details of the particles size analysis and ζ-potential measurements are described in Chapter 3 (Section 3.3.1 and 3.3.2). The microstructure of selected nanoemulsions (1% w/w WPI, lactoferrin and Tween 20 nanoemulsions) was determined by TEM using resin embedding method as described in Section 3.3.3 of Chapter 3.

4.4 Results and Discussion

4.4.1 Preparation of nanoemulsions using emulsification and solvent evaporation technique

Nanoemulsions containing 1% (w/w) WPI and 0.5% (w/w) corn oil were prepared at 10:90 ratio of organic and aqueous phases by an emulsification method combined with solvent evaporation. Changes in the mean particle size of nanoemulsions during emulsion preparation in each step were measured as shown in Figure 4.1. Mixing of aqueous phase and organic phase using a high-shear mixer produced a coarse emulsion containing large oil droplets with a wide particle size distribution (Figure 4.1). The large particle size of the coarse emulsion decreased from around 900 to 90 nm after microfluidisation for 4 cycles at 80 MPa (Table 4.3), which involves a combination of high shear, impact and cavitation forces to break up the large oil droplets into smaller ones (Anton et al., 2008; Jo & Kwon, 2014). A further decrease in the particle size to 80 nm was also observed after solvent evaporation of ethyl acetate. The particle size distribution of emulsions was observed to change after microfluidisation from multimodal to monomodal (Figure 4.1) and the PDI decreased from 0.43 to 0.21 (Table 4.3).

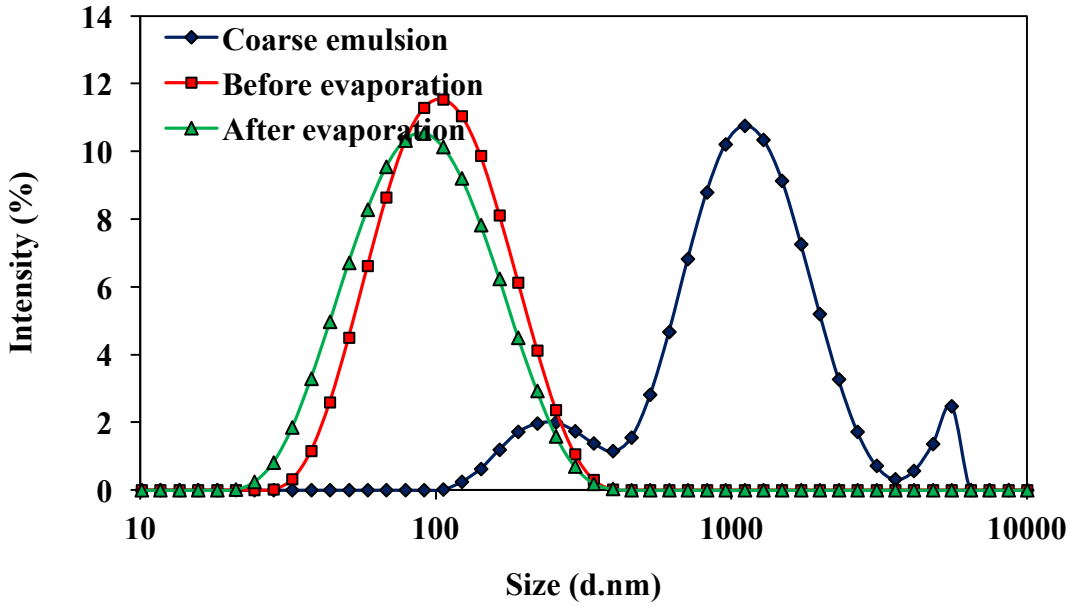

Figure 4.1 Particle size distributions of WPI-stabilised nanoemulsion during preparation. A coarse emulsion was formed by mixing the aqueous phase and organic phase using high shear mixer. The coarse emulsion was homogenised using a microfluidiser at 80 MPa for 4 cycles and evaporated using a rotary evaporator (50^{o}C; 153 mBar) to remove ethyl acetate.

Table 4.3 Mean particle diameter (Z-Average) and PDI of coarse emulsion and nanoemulsion before and after evaporation. Data are presented as the mean and standard deviation of two independent measurements with triplicates (n=6).

	Coarse emulsion	Nanoemulsion	
		Before evaporation	After evaporation
Z-Average (d.nm)	905.8 ± 46.3	92.5 ± 2.52	78.4 ± 1.81
PDI	0.43 ± 0.05	0.20 ± 0.01	0.21 ± 0.01

In this method, the use of solvent is crucial for reducing the droplet size of nanoemulsions by decreasing the interfacial tension and viscosity of the oil and water phases. The interfacial tension at the interface of ethyl acetate and water (≈ 6.8 mN m^{-1}) was much lower than corn oil and water (≈ 31.5 mN m^{-1}) (Lee et al., 2011). As such, the addition of solvent can lower the interfacial tension to form small droplets during homogenisation. This was demonstrated in a previous study done on the impact of alcohol to form small droplets in nanoemulsions produced by high pressure homogenisation (Zeeb, Herz, McClements & Weiss, 2014). The authors showed that the addition of alcohol (10% w/w 1-butanol) into the water phase can help to reduce the droplet size of sodium caseinate stabilised emulsions from 169 to

92 nm in diameter due to a lower interfacial tension. Also, there was a decrease in the viscosity of the dispersed phase containing a mixture of ethyl acetate and corn oil which helps to increase the mixing efficiency during homogenisation which results in more droplet disruption. The viscosity of corn oil measured at 25^{o}C was 51.9 ± 2.6 mPa.s while those of a mixture of ethyl acetate and corn oil were below the limit of the instrument (TA Instruments AR-G2 Rheometer, USA).

Previous studies have suggested that the use of very high pressures in microfluidic devices were able to produce emulsion droplets in the nanometric range (Solans et al., 2005; Qian & McClements, 2011). For instance, the droplet size of 5% (w/w) corn oil emulsion stabilised by 2% (w/w) β-lactoglobulin was around 150 nm after homogenisation by microfluidiser for 6 passes at 14 kBar (400 MPa) (Qian & McClements, 2011). However, the mean particle size of nanoemulsions produced by high pressure homogenisation at 80 MPa (4 cycles) combined with solvent evaporation was even smaller without the use of very high pressures. Therefore, this technique is more efficient and effective to produce nanoemulsions with even smaller droplet size.

4.4.2 Comparison of nanoemulsions and conventional emulsions

Conventional emulsions containing 1% (w/w) WPI in the aqueous phase and 10% (w/w) corn oil were also prepared under the same conditions as nanoemulsions but without the addition of solvent (ethyl acetate). After preparation, the conventional emulsions were diluted to the same oil concentration as nanoemulsions (0.5% w/w) but they contained much lower protein concentrations (0.09% w/w) after dilution as shown in Table 4.1. This is because the organic phase of conventional emulsions was made up of corn oil alone without added solvent even though the initial concentration of the protein loaded and the volume fraction ratio of organic phase to aqueous phase applied in the preparation of conventional emulsions were maintained to be the same as the formulation of nanoemulsions.

Based on visual observations, the appearance of these two types of emulsions was very different. The nanoemulsion appeared translucent while the conventional emulsion was opaque as shown in the inserted photograph in Figure 4.2. This is because nanoemulsions contain smaller particles that scatter light weakly McClements, 1999; Lee et al., 2011). The Z-average mean diameter of nanoemulsion

was 78.4 nm and conventional emulsion was 161.5 nm (Table 4.4). The difference in the droplet size between these two emulsion samples was due to some differences in the composition of the two emulsion systems during preparation as described before. The organic phase of nanoemulsions consisted of a mixture of ethyl acetate and corn oil but the conventional emulsions contained only corn oil. Therefore, the viscosity of the dispersed phase in the nanoemulsions was considerably lower than the conventional emulsions resulting in a higher mixing efficiency during homogenisation to form small droplets (Lee et al., 2011). Furthermore, the addition of ethyl acetate helped to form small droplets in nanoemulsions by reducing the interfacial tension as mentioned earlier.

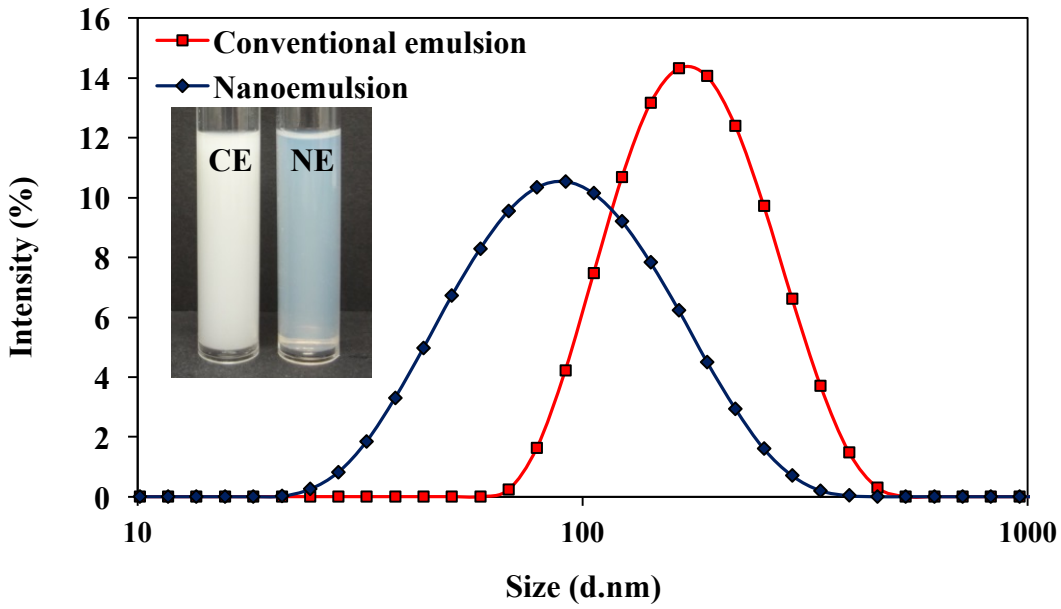

Figure 4.2 Particle size distributions of WPI stabilised conventional emulsion and nanoemulsion (denoted as CE and NE, respectively) adjusted to 0.5% (w/w) oil with photographs inserted.

Table 4.4 Mean particle diameter (Z-Average) and mean ζ-potential of conventional emulsion and nanoemulsion. Data are presented as the mean and standard deviation of two independent measurements with triplicates (n=6).

Emulsion type	Z-Average (nm)	PDI	ζ-potential (mV)
Conventional emulsion	161.5 ± 1.0	0.13 ± 0.01	-69.0 ± 5.4
Nanoemulsion	78.4 ± 1.8	0.21 ± 0.01	-37.1 ± 2.9

The particle characteristics of the two kinds of emulsions stabilised by the same WPI are shown by their TEM images in Figure 4.3. The micrographs clearly show that the nanoemulsion sample contains smaller oil droplets than the conventional emulsion sample. This is in agreement with the results of the particle size measurements.

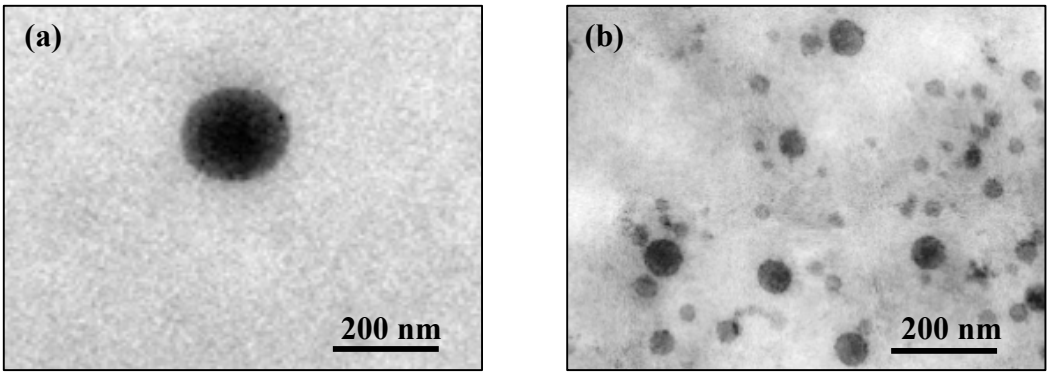

Figure 4.3 TEM images of WPI stabilised (a) conventional emulsions and (b) nanoemulsions adjusted to 0.5% (w/w) oil.

There was an appreciable difference in the electrical characteristics of the two emulsion systems (Table 4.4). The ζ-potential of nanoemulsions and conventional emulsions stabilised by WPI was -37.1 ± 2.9 and -69.0 ± 5.4 mV, respectively. The difference in ζ-potential between the two emulsion systems is not known but a similar observation was also shown in the previous study done on the emulsion properties of protein-stabilised nanoemulsions and conventional emulsions reported by Lee et al. (2011). The authors explained that nanoemulsions contained more proteins than conventional emulsions and consequently, the ionic strength of nanoemulsions was higher, corresponding to a lower ζ-potential value in nanoemulsions.

As demonstrated, nanoemulsions containing small droplets were successfully prepared using emulsification and solvent evaporation method. The oil droplets in nanoemulsions were much smaller than conventional emulsions. However, the particle size of an emulsion can be affected by other variables including homogenisation parameters, organic phase to aqueous phase ratios and materials used, therefore, these variables were further investigated in the following work.

4.4.3 Effect of organic phase ratios and WPI concentrations on nanoemulsions

The effect of organic phase to aqueous phase ratios (10:90 and 20:80) on the properties of nanoemulsions was studied with WPI as the emulsifier at different protein concentrations ranging from 0 to 5% (w/w). The nanoemulsions were prepared under the same processing condition at 80 MPa for 4 cycles. Figure 4.4 shows the photographs of nanoemulsions prepared with different concentrations of WPI at different organic phase ratios of 10:90 and 20:80 (after evaporation) and adjusted to 0.5% (w/w) oil. It is shown that the appearance of the nanoemulsions for both organic phase ratios becomes more translucent with increasing protein concentrations due to a reduction in size.

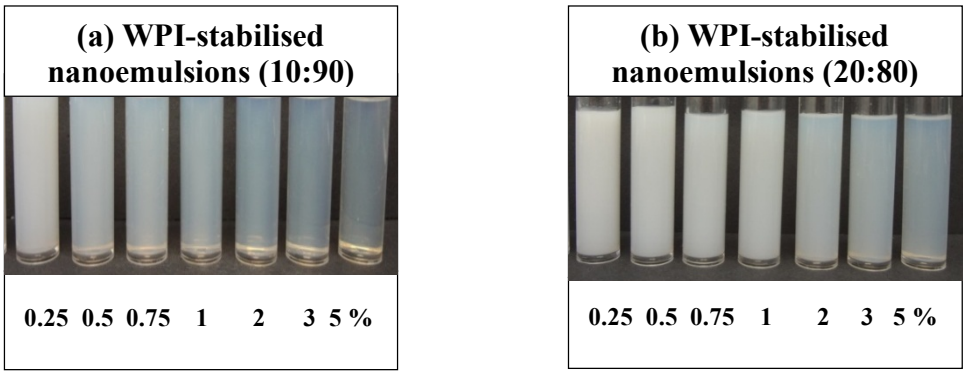

Figure 4.4 Photographs of nanoemulsions prepared with different concentrations of WPI at different organic to aqueous phase ratios of (a) 10:90 and (b) 20:80 (after evaporation) adjusted to 0.5% (w/w) oil.

The particle size of the nanoemulsions before and after solvent evaporation was measured at different WPI concentrations for the two organic phase ratios (10:90 and 20:80) are as shown in Figure 4.5. Overall, there was a decrease in the mean particle size of the nanoemulsions after the solvent evaporation process. At the same 1% (w/w) protein level, the mean particle size of nanoemulsions before and after evaporation decreased from 93.7 ± 2.0 to 82.3 ± 1.2 nm and 131.6 ± 6.5 to 112.1 ± 5.4 nm for the nanoemulsions prepared at 10:90 and 20:80 ratios, respectively. This showed that the removal of ethyl acetate caused the oil droplets to shrink in size but the extent of size reduction was similar for both organic phase ratios. It may be expected that smaller droplets are formed at higher organic phase ratio given a higher concentration of solvent used in the initial system with greater ability for solvent displacement to reduce the droplet size.

As shown in Figure 4.5, the mean particle size of nanoemulsions decreased with increasing protein concentrations for both organic phase ratios. The mean droplet size of nanoemulsions prepared at 10:90 ratio (after evaporation) decreased from 111.3 ± 0.6 to 82.3 ± 1.2 nm in diameter while those prepared at 20:80 ratio (after evaporation) decreased from 159.7 ± 5.7 to 112.1 ± 5.4 nm when the WPI concentration was increased from 0.25 to 1% (w/w) but it did not decrease further at higher concentrations used in this experiment. The mean droplet size which decreases with increasing protein concentrations can be expected as more proteins are available in the aqueous phase to enable them to more readily adsorb to the surface of oil droplets, thus stabilising them against droplet re-coalescence and aggregation (Chu et al., 2007; Jo & Kwon, 2014).

It was observed that larger droplets were formed with nanoemulsions prepared at higher organic phase ratio of 20:80 for all protein concentrations. This is because at the same initial level of protein used, there is a lower ratio of protein to oil for the nanoemulsions with higher organic phase ratio (20:80). For instance, the ratio of protein to organic phase (oil plus solvent) at 1% (w/w) protein levels for both organic to aqueous phase ratios (10:90 and 20:80) were 0.18 and 0.04, respectively. At 3% (w/w) protein level it was 0.54 and 0.12, respectively and it was 0.9 and 0.2, respectively at 5% (w/w) protein level. Details of the formulation of nanoemulsions prepared at different organic phase ratios are shown in the appendix (Table 1). Consequently, there may not have been enough protein emulsifiers at higher organic phase ratio (20:80) to rapidly adsorb at the interface of oil droplets formed during homogenisation and resulted in the formation of larger droplets.

Apart from the lack of sufficient proteins to stabilise the droplets, there could be less mixing efficiency during the homogenisation process at higher organic phase ratios due to an increase in viscosity of the dispersed phase (Tan & Nakajima, 2005b). As discussed earlier, the viscosity of corn oil was higher than ethyl acetate at ambient temperature and so an increase in oil concentration at higher organic phase ratio corresponds to an increase in the viscosity of the system.

For both organic phase ratios, the ζ-potential of nanoemulsions was observed to decrease with increasing WPI concentrations (Figure 4.6). This can be attributed to the fact that at higher protein concentrations, the ionic strength of the system

increases and the proteins may form a thick interfacial coating around the droplets (Lee et al., 2011). The latter may result from some electrostatic screening effects on the droplet surface and thus a reduction in the electrical charge.

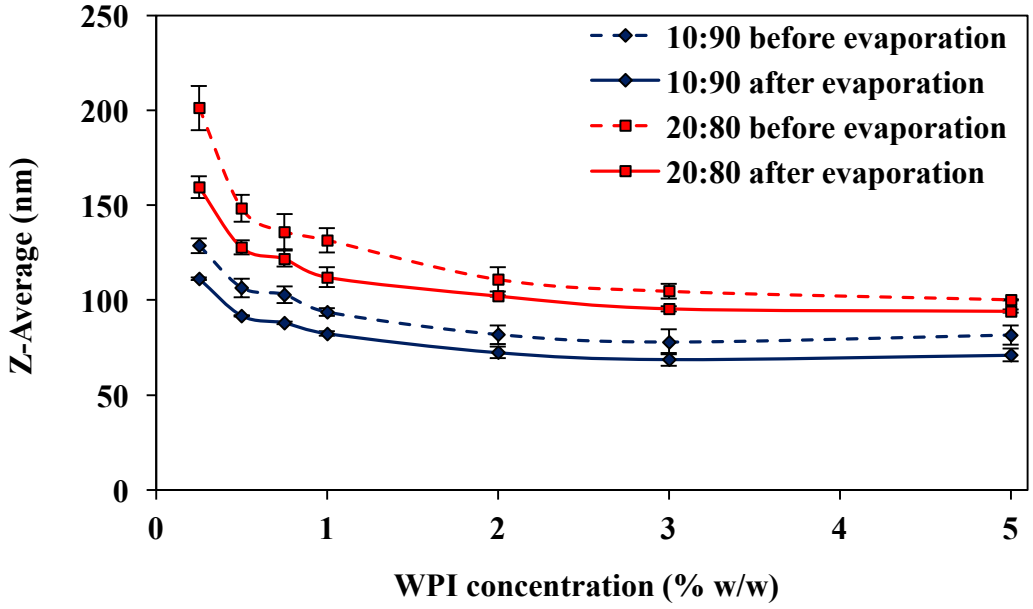

Figure 4.5 Mean particle diameter (Z-Average) of nanoemulsions prepared with different concentrations of WPI at different organic to aqueous phase ratios of 10:90 and 20:80 before and after evaporation and adjusted to 0.5% (w/w) oil. Data are presented as the mean of two independent measurements with triplicates (n=6) and error bars represent the standard deviation.

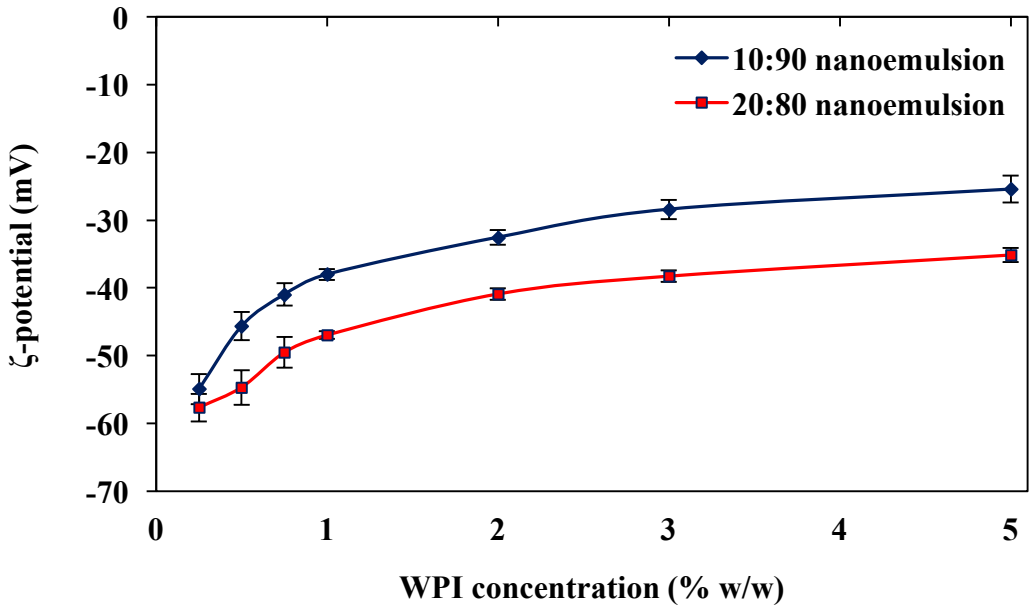

Figure 4.6 Mean ζ-potential of nanoemulsions prepared with different concentrations of WPI at different organic to aqueous phase ratios of 10:90 and 20:80 after solvent evaporation and adjusted to 0.5% (w/w) oil. Data are presented as the mean of two independent measurements with triplicates (n=6) and error bars represent the standard deviation.

4.4.4 Effect of organic phase ratios and homogenisation parameters on nanoemulsions

The effects of homogenisation pressures (20 to 80 MPa) and number of cycles (1 to 4 cycles) on the mean particle size of nanoemulsions prepared at two different organic phase ratios of 10:90 and 20:80 with the same emulsifier level (1% w/w WPI) were compared. As shown in the photographs, the nanoemulsions with organic phase ratio of 10:90 were more translucent with increasing pressures (Figure 4.7) or number of cycles (Figure 4.9) due to a size reduction below 100 nm in diameter while those of 20:80 remained relatively opaque because the size range of particles formed and changed was larger (> 120 nm). In all cases, the particle size distributions were unimodal (Figures 4.8 and 4.10).

The mean particle size of nanoemulsions prepared at organic phase ratio of 10:90 decreased from 117.8 ± 3.0 to 78.4 ± 1.8 nm when the homogenisation pressures was increased from 20 to 80 MPa after 4 cycles (Figure 4.8c). However, the change in mean particle size of nanoemulsions prepared at higher organic phase ratio of 20:80 did not change markedly with increasing pressures (Figure 4.8c). This may be due to the fact that the minimum droplet size of nanoemulsions prepared at 20:80 ratio was reached and any further increase in pressures did not decrease the particle size. As explained, when the organic phase ratio increases, the amount of emulsifiers in the aqueous phase is lower. As a result, there were probably insufficient emulsifiers available to stabilise the oil droplets at the concentration used and therefore an increase in homogenisation pressure did not have any effect on the droplet size of nanoemulsions prepared at higher organic phase ratio.

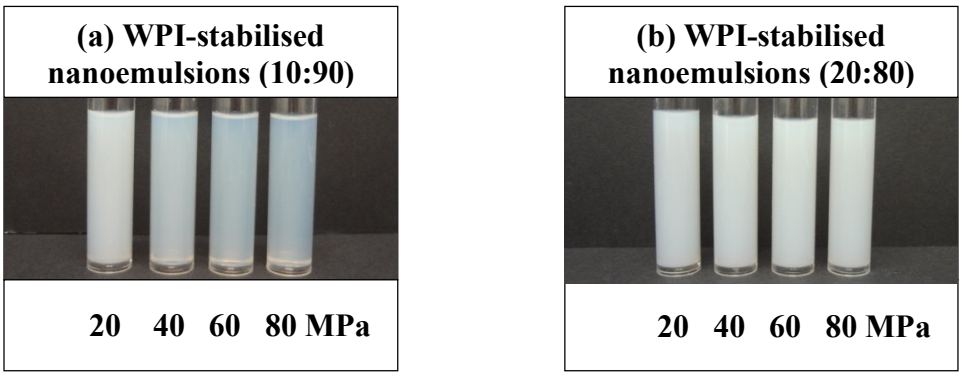

Figure 4.7 Photographs of WPI-stabilised nanoemulsions prepared at different homogenisation pressures for 4 cycles at different organic phase ratios of (a) 10:90 and (b) 20:80 and adjusted to 0.5% (w/w) oil.

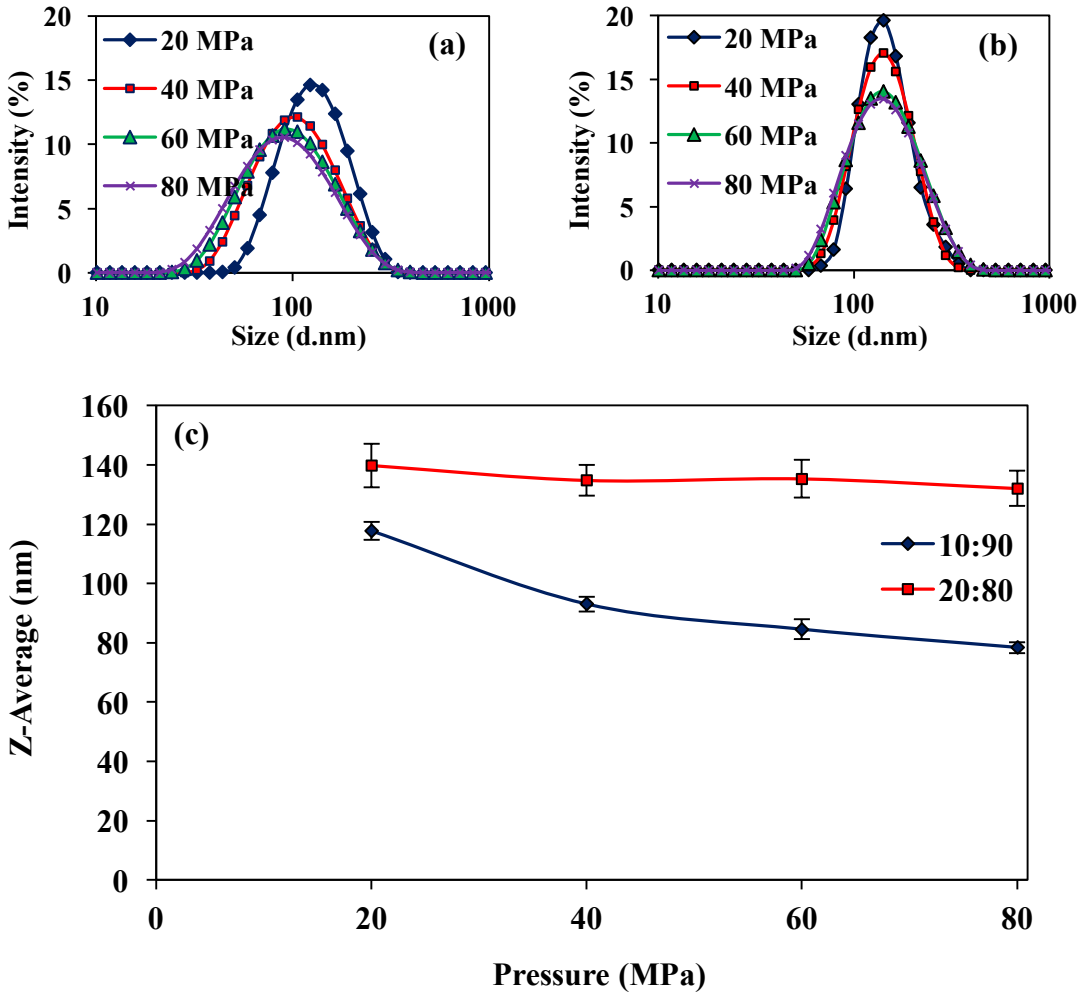

Figure 4.8 Particle size distributions and mean particle diameter (Z-Average) of WPI-stabilised nanoemulsions prepared at different homogenisation pressures for 4 cycles at different organic phase ratios of (a) 10:90 and (b) 20:80 and adjusted to 0.5% (w/w) oil. Data are presented as the mean of two independent measurements with triplicates (n=6) and error bars represent the standard deviation.

On the other hand, it was observed that the mean particle size decreased when both emulsions (10:90 and 20:80 ratios) passed through the homogeniser with increasing number of cycles at the same homogenisation pressure (80 MPa) used (Figure 4.10c). The particle size of emulsions decreased gradually with increasing number of cycles from 1 to 4 cycles. Overall, the results showed that increasing the homogenisation pressures and number of cycles produced nanoemulsions with smaller droplet size as expected.

Subsequently, the homogenisation conditions used to produce nanoemulsions for the investigation on the effects of other variables described below were fixed and the emulsions were passed through the microfluidiser for 4 times at 80 MPa to achieve small droplet size.

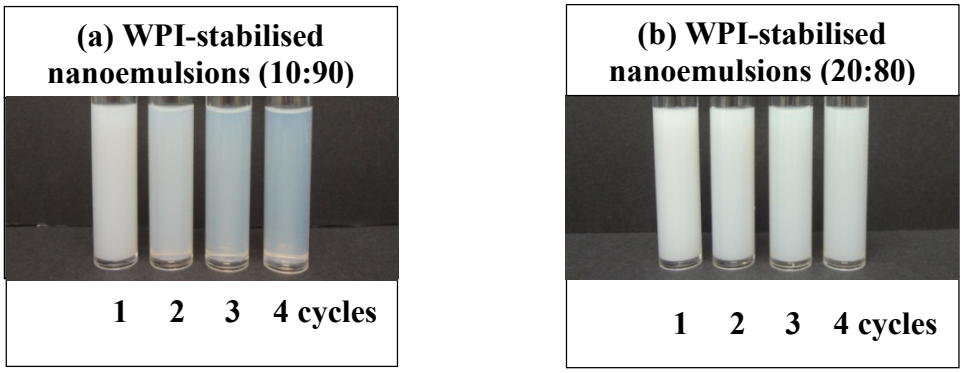

Figure 4.9 Photographs of WPI-stabilised nanoemulsions prepared at 80 MPa with different number of homogenisation cycles for different organic phase ratios of (a) 10:90 and (b) 20:80 and adjusted to 0.5% (w/w) oil.

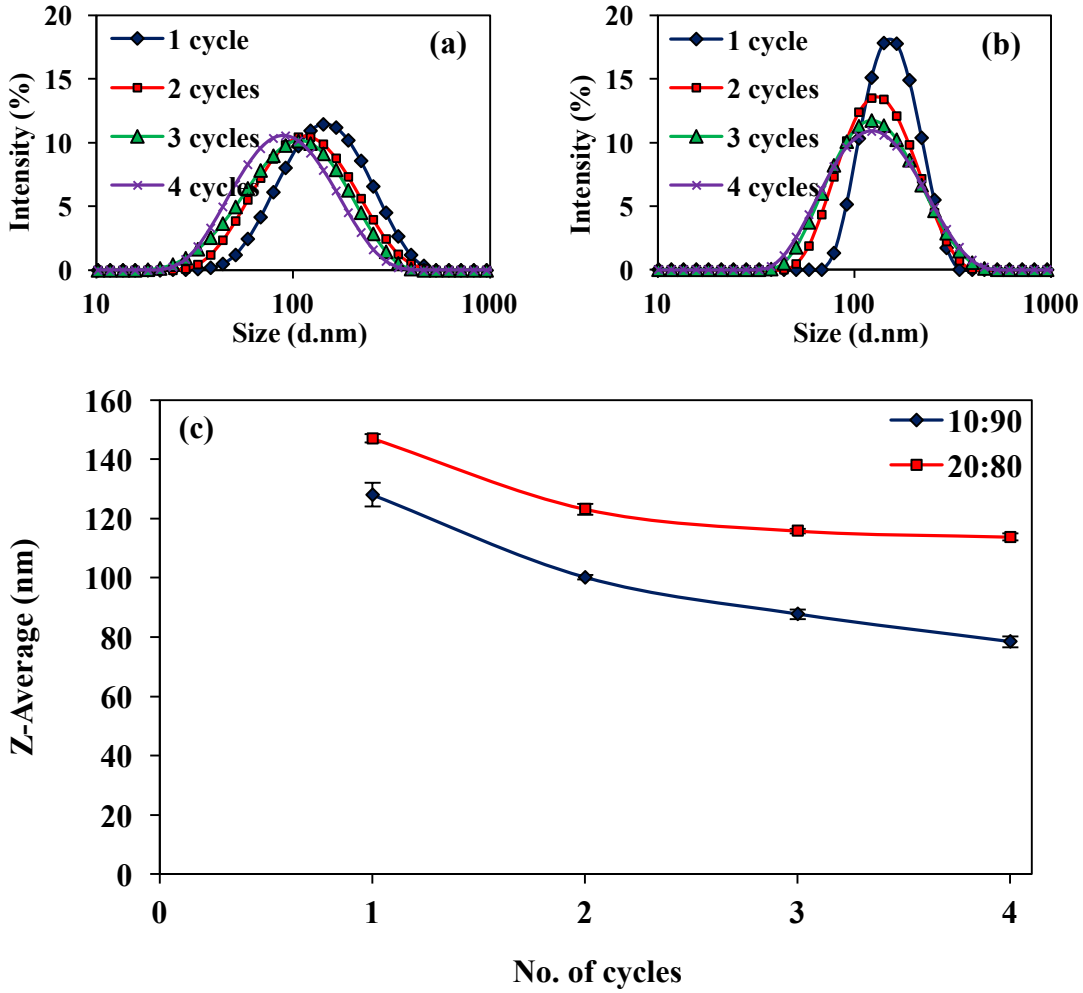

Figure 4.10 Particle size distributions and mean particle diameter (Z-Average) of WPI-stabilised nanoemulsions prepared at 80 MPa with different number of homogenisation cycles for different organic phase ratios of (a) 10:90 and (b) 20:80 and adjusted to 0.5% (w/w) oil. Data are presented as the mean of two independent measurements with triplicates (n=6) and error bars represent the standard deviation.

4.4.5 Influence of oil types on nanoemulsions

Different types of oils can affect the formation, stability and physical properties of emulsions. For instance, the efficiency of droplet disruption during homogenisation can be affected by the physicochemical properties of a bulk oil phase (McClements & Rao, 2011). A lower interfacial tension and viscosity of the oil phase can facilitate the disruption of oil droplets within the homogeniser and lead to the formation of smaller droplets (Lee et al., 2011). For these reasons, three different types of oils were used to prepare nanoemulsions in this study. They were selected based on their molecular and chemical characteristics, namely corn oil as LCT oil, fractionated liquid coconut oil as MCT oil and lemon oil as flavour oil.

Visually, corn oil or coconut oil nanoemulsions appeared translucent but lemon oil emulsions were opaque (Figure 4.11). The physicochemical properties of oils and emulsions formed by the respective oils are shown in Table 4.5. The particle size of the emulsions was significantly different ($P < 0.05$). The particle size of corn oil or coconut oil nanoemulsions was small but larger oil droplets were formed by emulsions made of lemon oil. The difference in the droplet size of emulsions can be attributed to the characteristics of the oils used. It has been reported that curcumin nanoemulsions made using MCT or LCT oils (e.g. Miglyol 812 or corn oil) were physically more stable than emulsions containing flavour oils (e.g. orange oil) (Ahmed et al., 2012). The authors explained that the orange oil emulsions were unstable to coalescence due to Ostwald ripening. This is possible because flavour oil has higher water solubility for the oil droplets to diffuse through the aqueous phase to form large droplets while the smaller ones disappear (McClements & Rao, 2011). On the contrary, Li and co-workers (2012) reported that low viscosity and interfacial tension of orange oil can facilitate the formation of droplet disruption during homogenisation. As a result, the orange oil nanoemulsions formed smaller droplet sizes in comparison to those formed by corn oil or Miglyol 812N. The discrepancies in the results could be due to the different periods of delayed measurements after homogenisation as the extent of Ostwald varies with time. In our case, samples were measured after storage at room temperature for 24 hours.

Clearly, in this experiment, nanoemulsions containing corn oil or coconut oil were more stable than the ones containing lemon oil as they formed small droplets. The ζ-potential of the emulsions was similar for all the oils as they were stabilised by

the same emulsifier using WPI which gave them negative charges at neutral pH (Table 4.5). Based on the above results, nanoemulsions containing corn oil or coconut oil were able to form small droplets and remain physically stable.

Table 4.5 Physicochemical properties of different types of oil used to prepare nanoemulsions and the characteristics of emulsions formed. Data are presented as the mean and standard deviation of two independent measurements with triplicates (n=6). Means with different letters within a column indicate significant difference at $P < 0.05$.

Oil type	Physicochemical properties of oil		Characteristics of emulsion	
	Density ($g\ cm^{-3}$)	Viscosity at 20°C (mPa.s)	Z-Average (nm)	ζ-potential (mV)
Corn oil	0.917 ± 0.000	51.9 ± 2.6	82.3 ± 1.2^{b}	-38.0 ± 0.8^{b}
Coconut oil	0.939 ± 0.001	28.4 ± 0.3	81.2 ± 1.6^{b}	-38.2 ± 0.6^{b}
Lemon oil	0.853 ± 0.001	-	890 ± 56^{a}	-35.5 ± 0.9^{a}

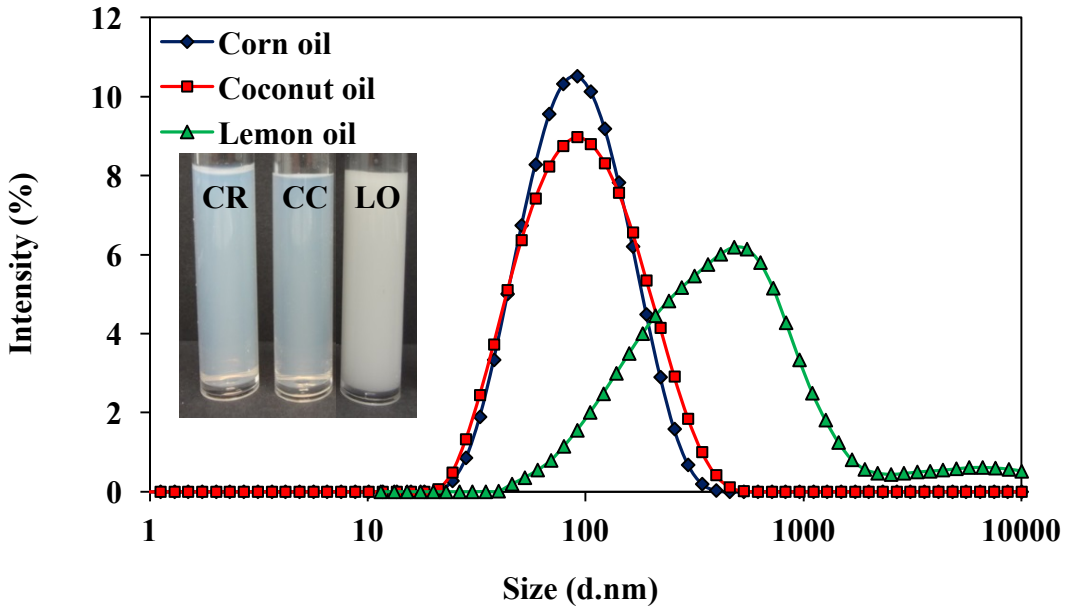

Figure 4.11 Particle size distributions of WPI-stabilised nanoemulsions prepared with different types of oils, corn oil (CR), coconut oil (CC) and lemon oil (LO), at organic phase ratio of 10:90 and adjusted to 0.5% (w/w) oil.

4.4.6 Influence of emulsifier types and concentrations on nanoemulsions

Apart from the oil types, the use of different types and concentrations of emulsifiers had a noticeable influence on the characteristics of nanoemulsions. Protein-stabilised nanoemulsions containing WPI or lactoferrin appeared more translucent than Tween 20 nanoemulsions (Figure 4.12) and the particle size of nanoemulsions was significantly different ($P < 0.05$). WPI or lactoferrin nanoemulsions were smaller than those containing Tween 20 at concentrations above 0.75% (w/w) (Figure 4.13). This result is interesting as many previous studies had shown that smaller droplets were formed by small molecule surfactants rather than proteins (Qian & McClements, 2011; Jo & Kwon, 2014). This is because small molecule surfactants can adsorb more rapidly onto the droplet surface during emulsification as they are more mobile and smaller in size than large globular proteins (McClements, 1999; Jafari et al., 2007; Jo & Kwon, 2014).

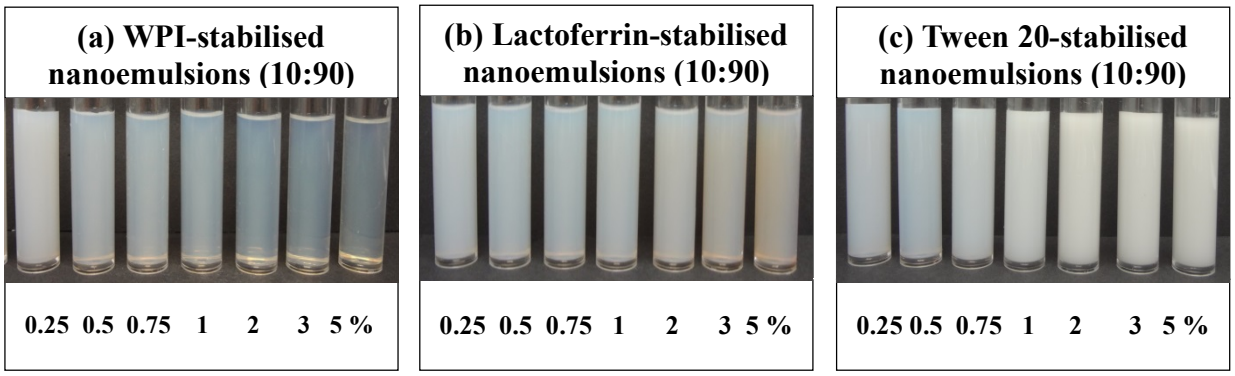

Figure 4.12 Photographs of nanoemulsions prepared with different types and concentrations of emulsifiers at organic phase ratio of 10:90 and adjusted to 0.5% (w/w) oil.

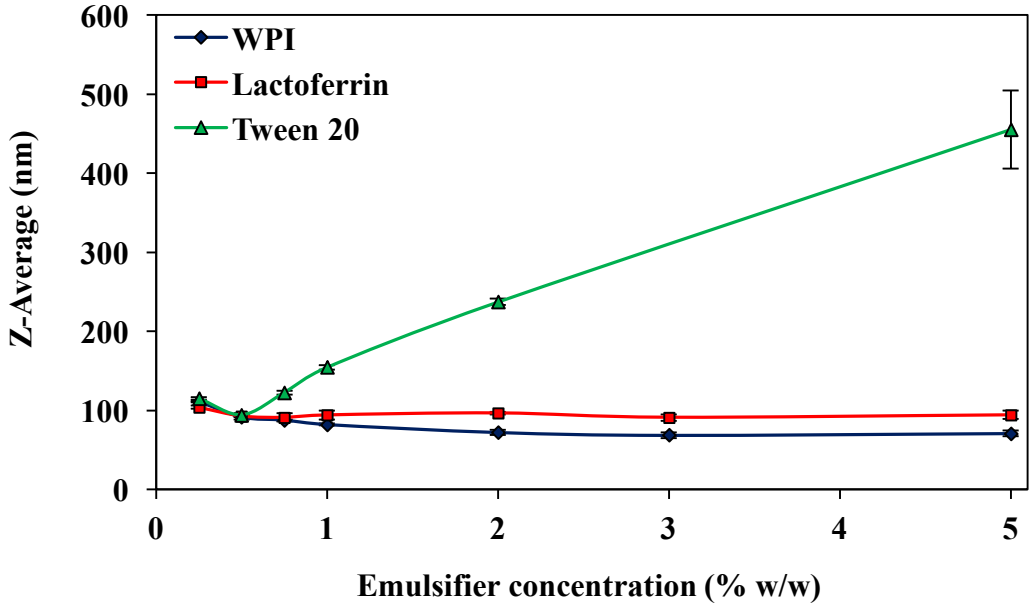

Figure 4.13 Mean particle diameter (Z-Average) of nanoemulsions prepared with different types and concentrations of emulsifiers at organic phase ratio of 10:90 and adjusted to 0.5% (w/w) oil. Data are presented as the mean of two independent measurements with triplicates (n=6) and error bars represent the standard deviation.

The particle size of WPI or lactoferrin nanoemulsions was around 100 nm at 0.25% (w/w) protein which was decreased to 70 and 90 nm, respectively as the protein concentration was increased but remained steady at above 1% (w/w) (Figure 4.13). In the case of Tween 20, the mean particle diameter decreased slightly from 115 to 94.3 nm when Tween 20 concentration was increased from 0.25 to 0.5% (w/w). However, Tween 20 produced nanoemulsions with increasingly larger droplet size (120 to 450 nm) when the concentration was increased from 0.75 to 5% (w/w) (Figure 4.13). Jafari and co-workers (2007) also observed an increase in the droplet size of emulsions stabilised with Tween 20 from 183 to 505 nm ($D_{4,3}$) at high surfactant concentrations above 2.5% (w/w). It was suggested that the unadsorbed Tween 20 when used at high levels formed surfactant micelles which caused the oil droplets to flocculate due to depletion effect. The presence of surfactant micelles in the aqueous phase can result in the exclusion of surfactant molecules between the oil droplets when they are at a distance less than the diameter of the surfactant micelles due to osmotic pressure and eventually cause the droplets to flocculate (McClements, 1999; Jafari et al., 2007).

Interestingly, the ζ-potential of Tween 20 emulsions was negative (around -10 mV) (Figure 4.14) even though Tween 20 is a non-ionic surfactant. It is thought that the negative surface charge was due to adsorption of anionic species from the materials used in making nanoemulsions such as free fatty acids (COO^-) in oils or hydroxyl ions (OH^-) present in NaOH solution when adjusting the pH of emulsion (Jo & Kwon, 2014).

Of the two protein emulsifiers, WPI produced nanoemulsions with slightly smaller particle sizes (70 – 110 nm) at all concentrations (0.25 – 5% w/w) than those stabilised by lactoferrin (90 – 100 nm) (Figure 4.13). The mean particle diameter of nanoemulsions stabilised by WPI decreased from 110 to 70 nm when the protein concentration was increased from 0.25 to 0.75% (w/w) but remained fairly constant thereafter. In a study reported by Cornacchia & Roos (2011), the decrease in droplet size from 1500 to 600 nm ($D_{3,2}$) with increasing WPI concentrations up to 0.8% (w/w) was also reported for emulsions with 10% (w/w) sunflower oil or hydrogenated palm kernel oil. No further decrease in droplet size was observed at higher WPI concentrations. The authors also reported that excessive proteins could result in the formation of multilayer proteins around the droplets as the surface protein coverage was found to increase from 1.5 to 4.8 mg/m^2 with increasing protein concentration. It was suggested that multiple interfacial layers may be formed in WPI-stabilised emulsions as the globular whey proteins become partially denatured during homogenisation. Denatured protein molecules expose amino acids containing reactive groups, such as non-polar and sulfhydryl groups and promote protein-protein interactions via hydrophobic interactions and disulphide bonds.

In this study, at WPI concentration above 0.75% (w/w), the excess WPI molecules could have been adsorbed on the droplet surface and form multilayer coatings. This explains the lower concentrations of non-adsorbed proteins in the continuous phase which is favourable in preventing depletion flocculation. Presumably, the excess proteins form thicker multilayer coatings around the droplets which can provide steric repulsion apart from electrostatic repulsion between the negatively charged droplets. This may also explain why depletion flocculation did not occur in WPI-stabilised nanoemulsions at higher concentrations. As expected, all the WPI-stabilised nanoemulsions were negatively charged at pH 7 (Figure 4.14). The net negative charge was decreased with increasing protein concentration

especially from 0.2% to 1% (w/w) but still high enough to confer electrostatic repulsive force between the droplets.

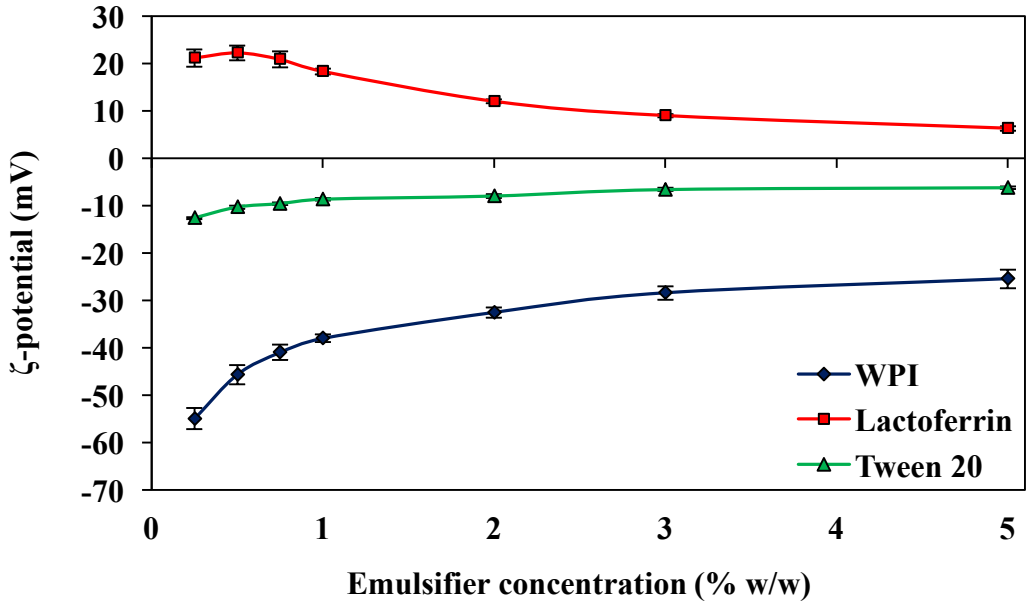

Figure 4.14 Mean ζ-potential of nanoemulsions prepared with different types and concentrations of emulsifiers at organic phase ratio of 10:90 and adjusted to 0.5% (w/w) oil. Data are presented as the mean of two independent measurements with triplicates (n=6) and error bars represent the standard deviation.

There was also a decrease in the particle size of lactoferrin-stabilised nanoemulsions but it did not decrease further at higher concentrations above 0.5% (w/w) (Figure 4.13). In a previous study done on the adsorption behaviour of lactoferrin in oil-in-water emulsions, Ye & Singh (2006) reported that the droplet size of emulsion decreased with increasing lactoferrin concentration from 0.3% up to 1% (w/w) level. They also found the surface protein coverage increased from 1 to 4.7 mg/m^2 when lactoferrin concentration was increased from 0.3 to 3% (w/w), indicating the formation of lactoferrin multilayers at the droplet surface. In our case, the unadsorbed lactoferrin molecules can be thought to form multilayer coatings at higher concentration (0.5% w/w) and stabilise the emulsions through electrostatic and steric hindrance. The higher molecular weight lactoferrin (approximately 84 kDa) with carbohydrate groups attached to the polypeptide backbone also provides a strong steric repulsion in emulsions (Tokle et al., 2012; Steijns & van Hooijdonk, 2000). The ζ-potential measurements of emulsions showed that the lactoferrin nanoemulsions were positively charged (Figure 4.14) as lactoferrin contains a high

proportion of basic amino acids with a high pI of around 9 (Steijns & van Hooijdonk, 2000; Baker & Baker, 2005). The ζ-potential of lactoferrin emulsions was found to decrease with increasing lactoferrin concentration (Figure 4.14) due to some electrostatic screening effects as a result of higher ionic strength at higher lactoferrin concentration has been explained earlier (Section 4.4.3).

The microstructure of selected nanoemulsions stabilised by WPI, lactoferrin and Tween at 1% (w/w) emulsifier level was observed by TEM as shown in Figure 4.15. The TEM images showed that the oil droplets formed by the three different emulsifiers were uniformly spherical and the droplet size corresponded well to the particle size measurements.

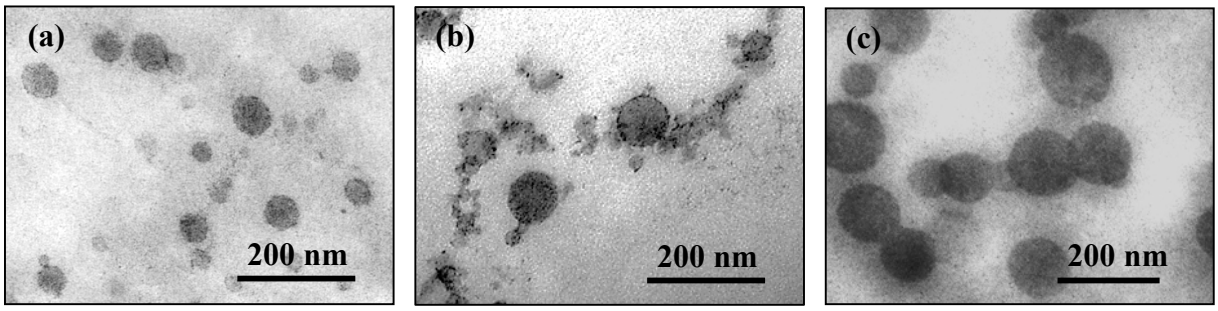

Figure 4.15 TEM images of nanoemulsions prepared with different types of emulsifiers, (a) WPI, (b) lactoferrin and (c) Tween 20 at the same emulsifier concentration (1% w/w). Nanoemulsions were prepared at organic phase ratio of 10:90 and adjusted to 0.5% (w/w) oil.

Overall, the results showed that the three types of emulsifiers can be used to prepare nanoemulsions with an optimal concentration to form small droplets. WPI and lactoferrin produced small droplet sizes (< 100 nm) at all different protein concentrations (0.25 – 5% w/w) used in this study while Tween 20 formed larger droplets at concentration higher than 0.75% (w/w), possibly due to coalescence caused by depletion flocculation. The ζ-potentials of nanoemulsions were different due to the molecular characteristics of different emulsifiers used. The stability of nanoemulsions formed by three different emulsifiers was further evaluated under varying environmental conditions which is discussed in the subsequent sections.

4.4.7 Environmental stability of nanoemulsions

4.4.7.1 Effect of heat treatment

The effect of temperature on the stability of nanoemulsions prepared at 1% (w/w) emulsifier level was examined. Nanoemulsions were heated in water baths at different temperatures ranging from 30 to 90^{o}C for 15 minutes and rapidly cooled to room temperature. The particle size and ζ-potential of the heat-treated nanoemulsions were measured after 1 day of storage at room temperature. The results showed that all the nanoemulsions except Tween 20 heated at 90^{o}C were stable against droplet aggregation as there was no significant change in the appearance and particle size over the temperature range used ($P > 0.05$) (Figure 4.16).

Oil droplet aggregation which could result from heat treatment in protein-stabilised emulsions was not observed in this study. Similar results were shown in a previous study by Lee et al. (2011) that whey proteins stabilised nanoemulsions were stable to heat treatment against droplet aggregation due to strong electrostatic repulsion between them. On the other hand, it has been reported that large particles were formed in β-carotene nanodispersions stabilised by 1% (w/w) WPI after heating them in a water bath at 60^{o}C for 4 hours (Chu et al., 2008). This can be attributed to thermal denaturation and unfolding of adsorbed globular proteins on the droplet surfaces that lead to exposure of non-polar and sulfhydryl groups which increases protein-protein interactions for droplet aggregation to occur (Chu et al., 2008; Tokle & McClements, 2011). The observed difference in results can be attributed to the shorter heating duration of 15 minutes instead of 4 hours used in the current work. This agrees with another previous finding that aggregation of whey proteins in emulsions was dependent on the heating time (Sliwinski, Roubos, Zoet, Boekel & Wouters, 2003). It was shown that the particle size remained constant during heating at 75^{o}C for about 45 minutes but there was an increase in size from 720 to 1350 nm when the heating time was continued from 45 to 130 minutes. In our study, it can be assumed that there was a strong electrostatic repulsion between the droplets in WPI-stabilised nanoemulsions and the relatively shorter time used for heating nanoemulsions did not cause extensive aggregation to occur. The ζ-potential of the nanoemulsions remained the same with only a slight increase at higher temperatures (Figure 4.17).

It has been reported that lactoferrin emulsions were also sensitive to heat treatment due to a lower denaturation temperature of the protein (Tokle & McClements, 2011; Tokle et al., 2012). According to the differential scanning calorimetry studies, bovine lactoferrin has two thermal denaturation temperatures at around 61 and 93^{o}C (Bengoechea et al., 2011). Therefore, it can be expected that lactoferrin emulsions become unstable to droplet aggregation upon heating at temperatures near 60^{o}C since the proteins have low denaturation temperature and relatively low magnitude of droplet charge (Figure 4.17). However, this was not observed in the lactoferrin-stabilised nanoemulsions (Figure 4.16) given the fact that lactoferrin are large glycoprotein with molecular mass of 80 kDa in comparison to β-lactoglobulin (18.2 kDa) in whey proteins (Kinsella & Whitehead, 1989; Shimazaki, 2000) and so the lactoferrin molecules can form thick interfacial coatings around the oil droplets to prevent droplet coalescence via steric hindrance.

In the case of emulsions stabilised by Tween 20, an increase in the particle size of nanoemulsions was notably observed at 90^{o}C (Figure 4.16). This may be related to the droplet coalescence occurring at temperature near the PIT of Tween 20. The phase inversion of an emulsion will occur when the temperature is near the cloud point of non-ionic surfactant (Shinoda & Arai, 1964). The cloud point is defined as the temperature at which the surfactant solution becomes insoluble and undergoes phase separation due to dehydration of the head group of surfactant molecules at higher temperature (Mahajan, Chawla & Bakshi, 2004). According to the manufacturer, the cloud point of Tween 20 is around 76^{o}C and therefore some droplet coalescence could have occurred at higher temperatures as indicated by an appreciable increase in the mean particle size of Tween 20 nanoemulsions, especially after heat treatment at 90^{o}C (Figure 4.16).

These results suggested that the nanoemulsions stabilised by WPI or lactoferrin have better thermal stabilities than those stabilised by Tween 20. This has important implications in the selection of suitable surface active molecules to stabilise nanoemulsions that can withstand thermal processing.

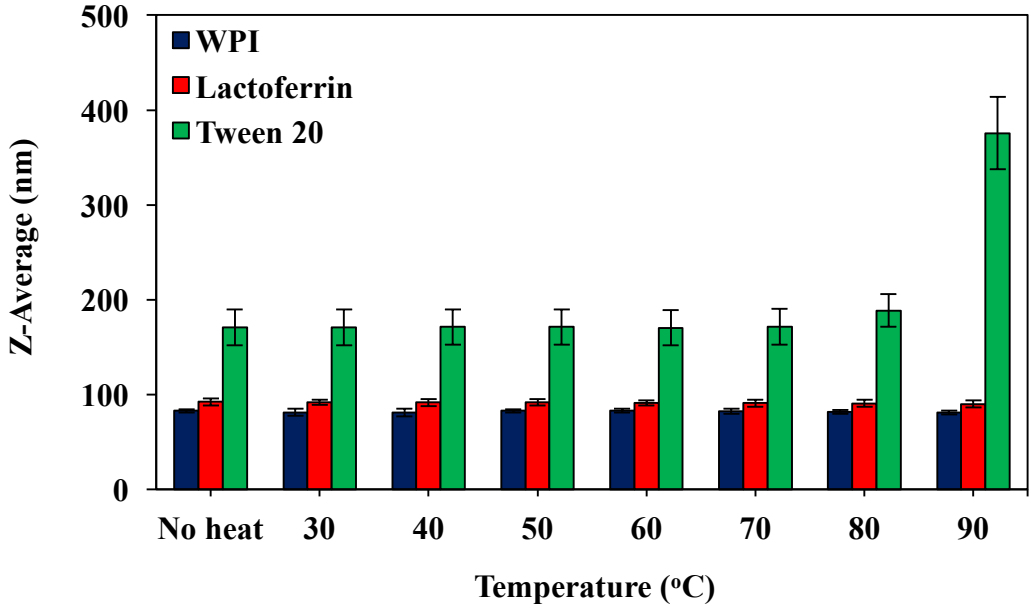

Figure 4.16 Influence of heating temperatures on the mean particle diameter (Z-Average) of nanoemulsions stabilised by different types of emulsifiers. Data are presented as the mean of two independent measurements with triplicates (n=6) and error bars represent the standard deviation.

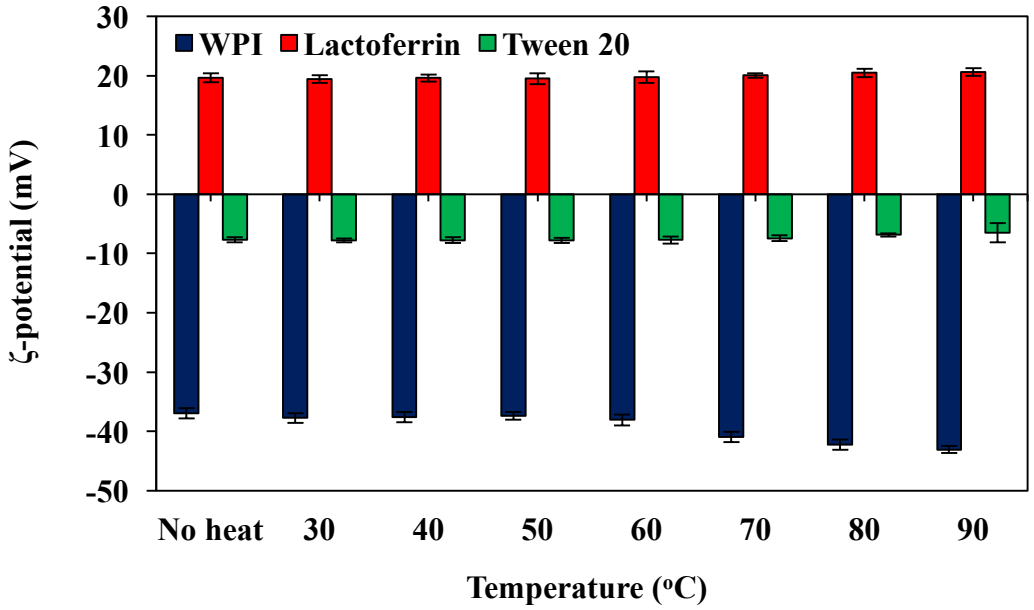

Figure 4.17 Influence of heating temperatures on the mean ζ-potential of nanoemulsions stabilised by different types of emulsifiers. Data are presented as the mean of two independent measurements with triplicates (n=6) and error bars represent the standard deviation.

4.4.7.2 Effect of pH changes

The pH stability of nanoemulsions was investigated for their potential applications in foods. The pH of nanoemulsions stabilised by WPI, lactoferrin or Tween 20 was adjusted to different pH levels ranging from 2 to 10. Visual observations showed that WPI-stabilised nanoemulsions were stable at all pH values except at pH 4.5 and 5 (Figure 4.18a). The particle size measurements showed that the oil droplets remained small at pH below or above the pI but there was a marked increase in the particle size at pH values near to the pI of WPI (Figure 4.19). This is because WPI-stabilised nanoemulsions are stabilised by electrostatic repulsion and they tend to form aggregates via hydrophobic attractions and van der Waals interactions when the electrostatic repulsion is not strong enough to overcome these attractive forces at pH near to the pI of the proteins (McClements, 1999; Harnsilawat, Pongsawatmanit, McClements, 2006). This was confirmed by the ζ-potential measurements of the emulsions as the electric net charges of droplets were small at the pI but became highly positive or negative at pH below or above the pI, respectively (Figure 4.20).

It is interesting to note that the phase separation of nanoemulsions did not form a cream layer on top of the emulsion but instead they formed white precipitation at the bottom of the tube at pH values of 4.5 and 5 (Figure 4.18a). This phenomenon was similar to a previous study done on the pH stability of WPI-stabilised nanoemulsions and conventional emulsions (Lee et al., 2011). It was shown that a cream layer was formed on top of the conventional emulsions but a suspension of white particulates was found at the bottom of the tube for nanoemulsions. The observed difference in the phase separation behaviour of the two emulsion systems was explained by the overall particle density difference between the oil and water phases. The oil droplets in the conventional emulsions were relatively large in size and surrounded by a thin layer of protein and the particle density was thus less than the surrounding liquid for the droplets to exhibit creaming. However, the droplets in the nanoemulsions were smaller and coated by a thicker layer of protein which causes the particle density to be higher than the surrounding liquid for sedimentation to occur. This could explain why the particle characteristics between nanoemulsions and conventional emulsions are different.

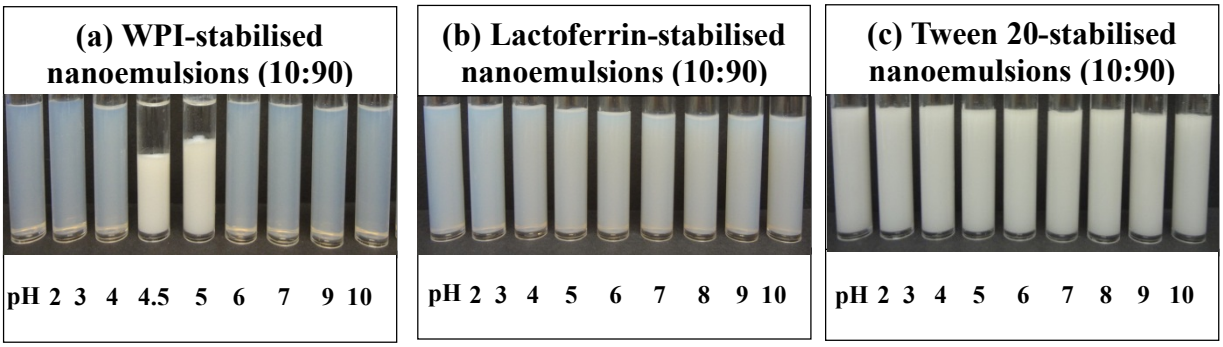

Figure 4.18 Photographs of nanoemulsions prepared with different types of emulsifiers at different pH levels.

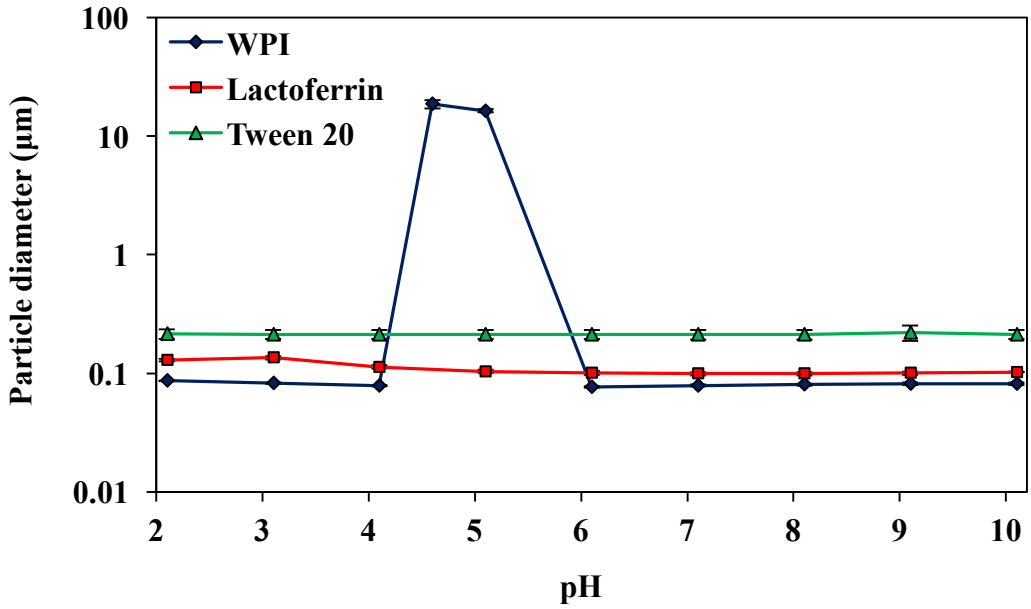

Figure 4.19 Influence of pH changes on the mean particle diameter (Z-Average) of nanoemulsions stabilised by different types of emulsifiers measured using a Zetasizer Nano ZS. Particle size of WPI emulsions at pH 4.5 and 5 is reported as the $D_{4,3}$ measured using a Mastersizer 2000. Data are presented as the mean of two independent measurements with triplicates (n=6) and error bars represent the standard deviation.

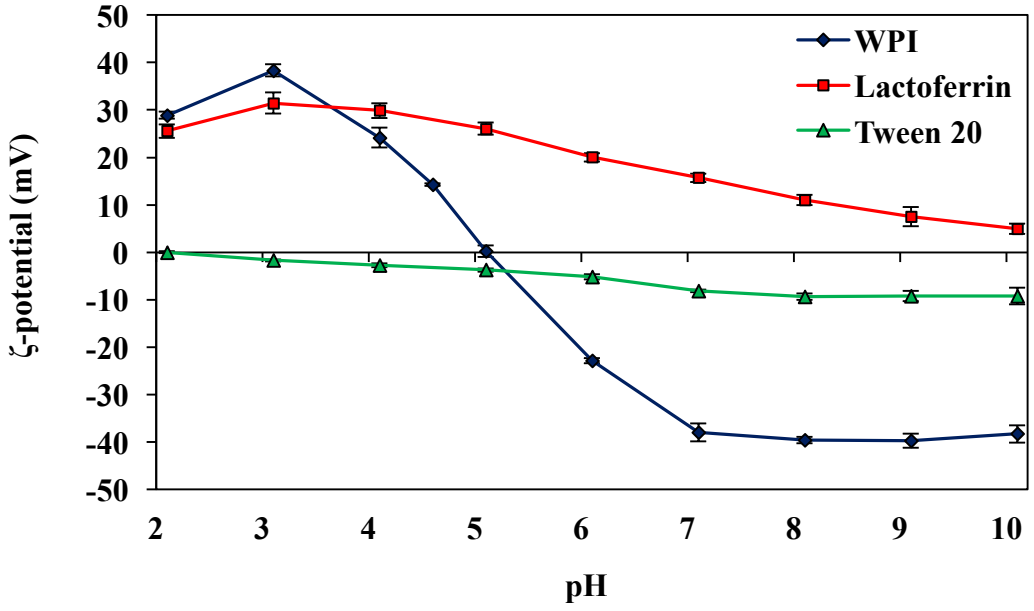

Figure 4.20 Influence of pH changes on the mean ζ-potential of nanoemulsions stabilised by different types of emulsifiers. Data are presented as the mean of two independent measurements with triplicates (n=6) and error bars represent the standard deviation.

The pH stability of lactoferrin-stabilised emulsions (5% w/w corn oil and 0.5% w/w lactoferrin) has been reported to be stable in the pH range from 2 to 6 with Z-average diameter less than 250 nm. However, droplet aggregation was observed at higher pH values from 7 to 9 which are close to the pI of lactoferrin (Tokle & McClements, 2011). Interestingly, the latter was not observed in this study as lactoferrin-stabilised nanoemulsions did not form large aggregates at higher pH values (Figure 4.19) and remained positively charged (Figure 4.20). It is thought that the stability of nanoemulsions coated with lactoferrin can be maintained by both electrostatic and steric repulsive forces as mentioned above. This is because lactoferrin is a glycoprotein with carbohydrate moieties that stabilises emulsions against aggregation by a combination of electrostatic and steric repulsion (Tokle et al., 2012; Mao, Dubot, Xiao & McClements, 2013). However, the decrease in positive charges of lactoferrin nanoemulsions with increasing pH (Figure 4.20) suggests that the higher pH stability of nanoemulsions observed in this study could be largely attributed to steric repulsion.

The nanoemulsions stabilised by Tween 20 were also stable to pH changes as the particle size did not increase across the pH range studied (Figure 4.19) and the ζ-

potential of the emulsions remained the same (Figure 4.20). This is so because Tween 20 is a non-ionic surfactant and thus the stability of emulsions was not affected by pH changes.

Based on the results, all the nanoemulsions were stable across the pH range found within most food products except those stabilised by WPI at pH 4.5 and 5. The WPI-stabilised nanoemulsions were unstable to droplet aggregation at pH near the pI. This could pose a problem for WPI-stabilised nanoemulsions in food systems with pH values around 4.5 and 5.

4.4.7.3 Effect of type and concentration of salt

The stability of nanoemulsions in the presence of NaCl (0 to 500 mM) or $CaCl_2$ (0 to 90 mM) at different salt concentrations was examined. All the nanoemulsions exhibited good stability to NaCl with little changes in their particle size at all NaCl concentrations up to 500 mM (Figure 4.21). However, WPI-stabilised nanoemulsions became opaque and exhibited phase separation at salt concentrations above 10 mM $CaCl_2$ while those stabilised by lactoferrin or Tween 20 remained physically stable at all salt concentrations studied (Figure 4.22). As shown in Figure 4.23, the mean particle size of WPI-stabilised nanoemulsions increased slightly when the $CaCl_2$ concentration was increased from 0 to 10 mM but they formed larger aggregates and phase separated at higher concentrations. The phase separation behaviour of nanoemulsions which resulted in sedimentation instead of creaming can be similarly explained by the pH-induced aggregation of nanoemulsions.

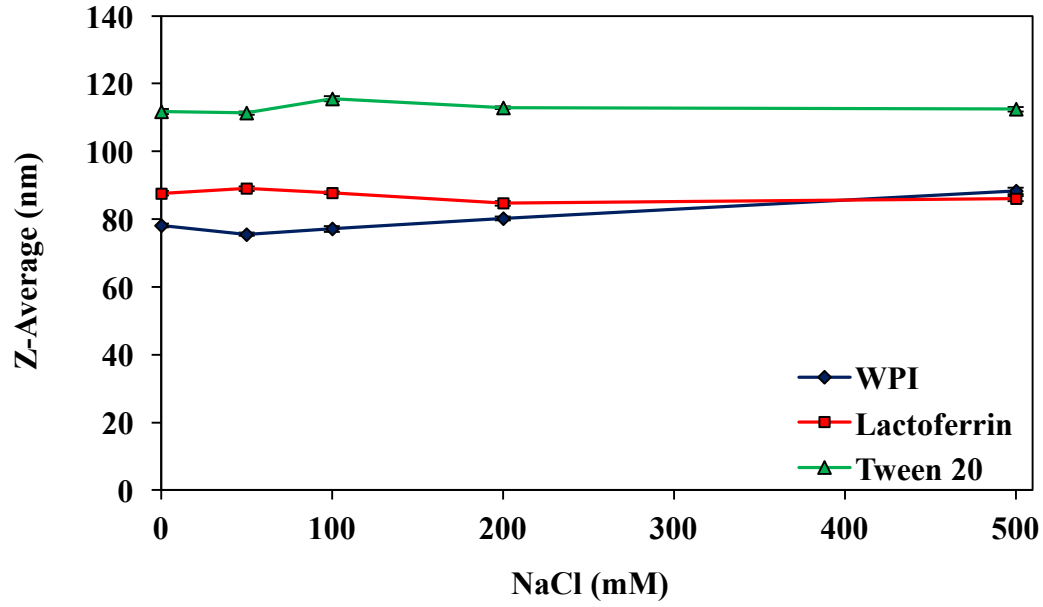

Figure 4.21 Influence of NaCl concentrations on the mean particle diameter (Z-Average) of nanoemulsions stabilised by different types of emulsifiers. Data are presented as the mean of two independent measurements with triplicates (n=6) and error bars represent the standard deviation.

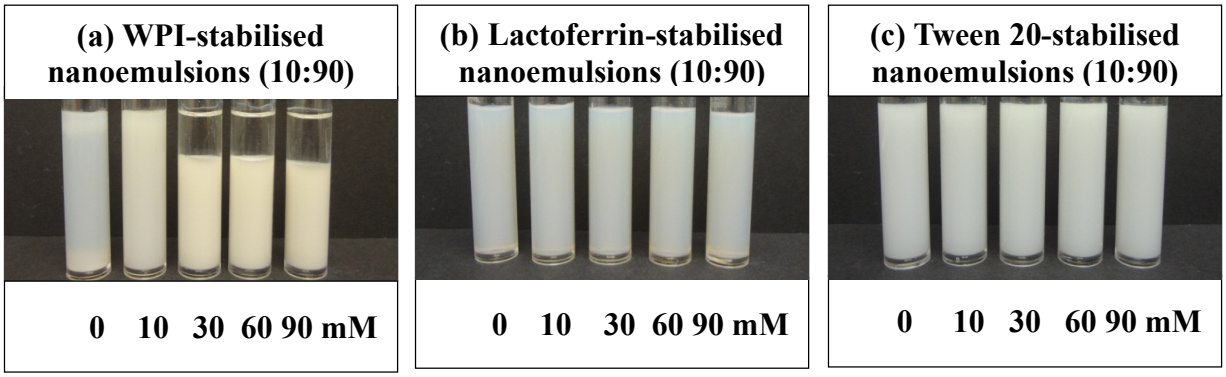

Figure 4.22 Photographs of nanoemulsions prepared with different types of emulsifiers adjusted to different $CaCl_2$ concentrations.

Initially, WPI-coated emulsion droplets were stabilised by electrostatic repulsive forces due to their negative charges. However, the presence of the dissociated Ca^{2+} cations screened the electrical charges and reduced the electrostatic repulsion between the droplets for aggregation to occur (Ye, Lo & Singh, 2012; Degner, Chung, Schlegel, Hutkins & McClements, 2014). This was confirmed by the measurement of electrical charges on the emulsions. The ζ-potential of WPI-stabilised nanoemulsions decreased with the addition of $CaCl_2$ and eventually reached almost neutrality at higher concentrations (Figure 4.24). In addition to the

screening of negative charges, the divalent Ca^{2+} ions could also form calcium bridges between the adsorbed proteins on the droplets to promote extensive aggregation. This is similar to a previous study done on the destabilisation of protein-stabilised emulsions caused by adding $CaCl_2$ in conventional emulsions (Ye et al., 2012).

In the case of nanoemulsions stabilised by lactoferrin or Tween 20, they were stable against droplet aggregation in the presence of NaCl or $CaCl_2$. Their particle size remained the same without any sign of phase separation at different salt concentrations (Figures 4.21 & 4.23). However, the ζ-potential of the nanoemulsions decreased as compared to their original value in nanoemulsions without the addition of salt (Figures 4.24). The emulsions stabilised by lactoferrin became less positively charged (from +25.5 to +2.19 mV) while those of Tween 20 became less negatively charged (from -16.0 to -2.84 mV) with increasing $CaCl_2$. The change in ζ-potential measurements suggested that there was some charge screening by the Cl^- ions in the case of lactoferrin and Ca^{2+} ions in the case of Tween 20. In this case, one might expect a stronger affinity for the divalent Ca^{2+} ions in lactoferrin and Tween 20 emulsions than the monovalent Cl^- ions in WPI emulsions. Nevertheless, the nanoemulsions stabilised by lactoferrin or Tween 20 remained stable as the ion binding effect was not sufficient to induce droplet aggregations to overcome their steric repulsion. Similarly, Tokle & McClements (2011) did not find any droplet aggregations in 0.5% (w/w) lactoferrin-stabilised conventional emulsions (containing 5% corn oil) up to 100 mM $CaCl_2$ but some aggregation was found at higher concentrations above 150 mM $CaCl_2$. In another study, Tween-stabilised conventional emulsions (10% MCT oil) were also reported to be stable up to 500 mM NaCl (Yang, Leser, Sher & McClements, 2013). The good salt stability of lactoferrin or Tween 20-stabilised nanoemulsions suggested that their stability was largely dominated by steric repulsion rather than electrostatic repulsion.

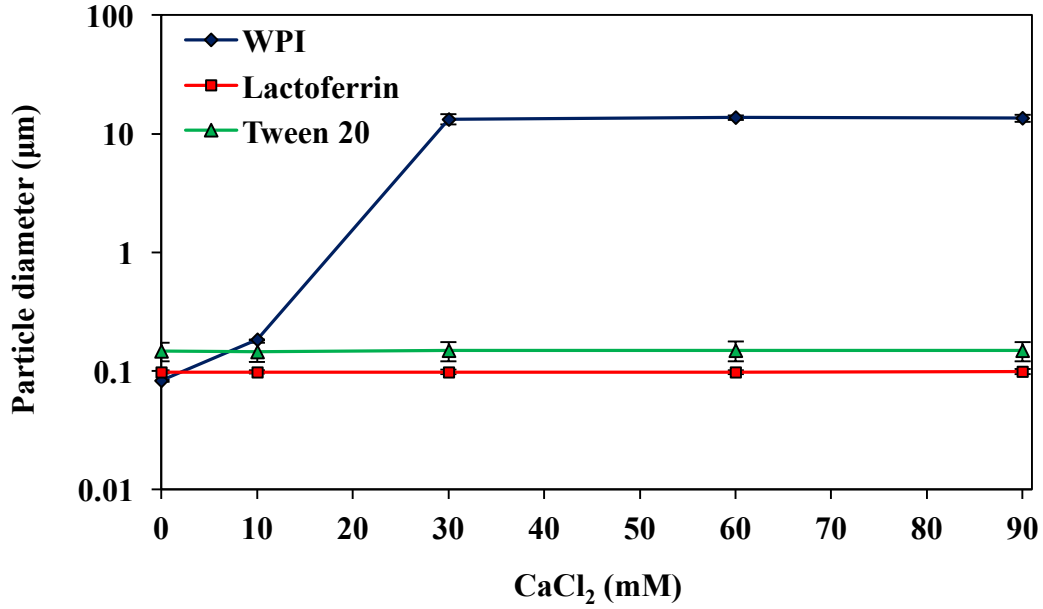

Figure 4.23 Influence of $CaCl_2$ concentrations on the mean particle diameter (Z-Average) of nanoemulsions stabilised by different types of emulsifiers measured using a Zetasizer Nano ZS. Particle size of WPI emulsions at salt concentrations above 30 mM $CaCl_2$ is reported as the $D_{4,3}$ measured using a Mastersizer 2000. Data are presented as the mean of two independent measurements with triplicates (n=6) and error bars represent the standard deviation.

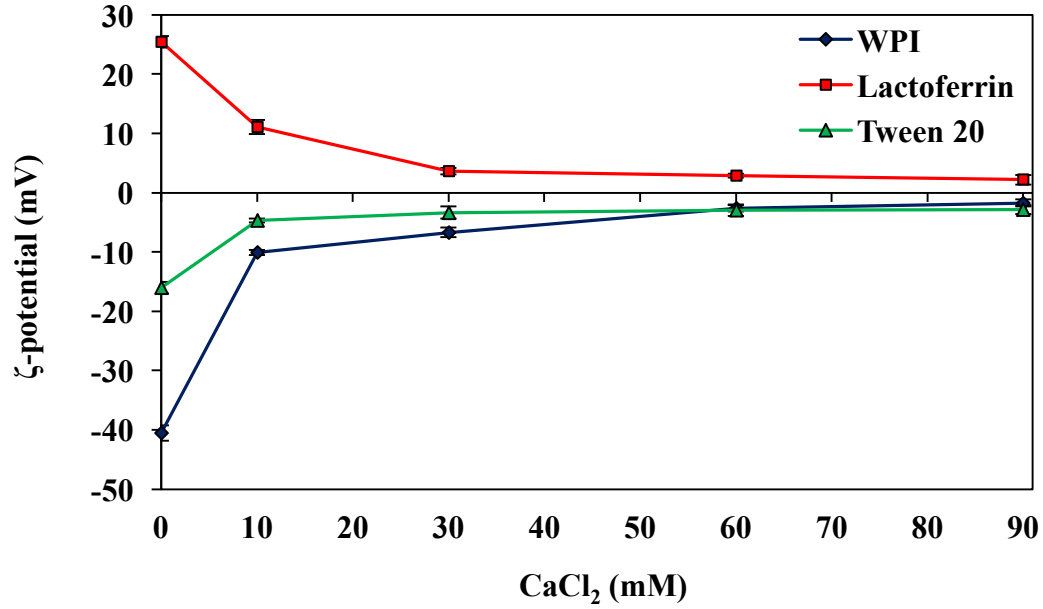

Figure 4.24 Influence of $CaCl_2$ concentrations on the mean ζ-potential of nanoemulsions stabilised by different types of emulsifiers. Data are presented as the mean of two independent measurements with triplicates (n=6) and error bars represent the standard deviation.

4.5 Conclusions

This experiment work demonstrated that nanoemulsions containing small droplets can be prepared using emulsification and solvent evaporation method. The droplet size of nanoemulsions can be controlled by optimising the processing conditions and the materials used. The droplet size of nanoemulsions decreased with increasing homogenisation pressures and cycles in which their optimum size were achieved (80 nm) at 80 MPa for 4 cycles and organic phase ratio of 10:90. Nanoemulsions produced by this method can also be formed using different emulsifiers in which protein emulsifiers produced smaller droplets than Tween 20. Protein-stabilised nanoemulsions were stabilised by a combination of electrostatic and steric repulsion whereas Tween 20 nanoemulsions was stabilised by steric repulsion. This could explain why Tween 20 nanoemulsions were more susceptible to depletion flocculation and thus formed large droplets at high surfactant concentrations. The environmental study also found that WPI-stabilised nanoemulsions were unstable to pH near to the pI of whey proteins as compared to those of lactoferrin or Tween 20. The WPI-stabilised nanoemulsions phase separated and exhibited sedimentation instead of creaming which is normally observed in the conventional emulsions. Similar phenomenon was observed in WPI nanoemulsions in the presence of $CaCl_2$ addition when the concentration went above 30 mM. Salt destabilised WPI nanoemulsions via screening of the negative charge and formed calcium bridges which then led to droplet aggregation. However, the presence of $CaCl_2$ up to 90 mM did not affect the stability of lactoferrin or Tween 20 stabilised nanoemulsions. The results indicated that the selection of emulsifier type used is important to producing stable nanoemulsions under different environmental conditions.

Chapter Five:

Influence of Wall Materials and Drying Methods on Physicochemical Properties of Dehydrated Nanoemulsions

5.1 Abstract

Nanoemulsions were spray dried in different wall materials containing maltodextrin, trehalose or a combination of maltodextrin and trehalose (1:1 ratio) at different wall concentrations with a total dry matter of 10, 20 or 30% (w/w) in the feed solutions. The powders were characterised for their moisture content, water activity, bulk density, particle size, microstructure, encapsulation efficiency, and wettability and dispersibility in water. Results showed that all the powders produced by spray drying at an inlet temperature of 150 ± 1°C and an outlet temperature of 65 ± 5°C contained small oil particles ranging from 6.8 to 17.4 μm ($D_{4,3}$) with high encapsulation efficiencies of oil droplets (97.1 – 98.9%). In terms of their physical properties, powders containing trehalose were superior as they had lower moisture content (3.9 – 4.4% w/w) and water activity (0.19 – 0.22), higher bulk density (0.28 – 0.46 g/mL) and better wettability (3.9 – 5.1 minutes) and dispersibility in water (62 – 82% w/w) as compared to other powders, particularly produced from only maltodextrin as a wall material. Nevertheless, all the spray dried powders displayed good reconstitution ability as the emulsion properties of the reconstituted powders were similar to the initial nanoemulsions before spray drying. Reconstituted nanoemulsions were monodispersed with Z-Average of around 80 nm in diameter and highly negatively charged at pH 7 similar to the original particle size before spray drying. The properties of selected nanoemulsions (20% w/w trehalose) were further investigated using freeze drying. Results showed that freeze dried powders had lower moisture content (1.5% w/w) and water activity (0.04) with good dispersibility (96.2%) and shorter wetting time of less than 3 seconds in water. However, freeze dried powders had higher surface oil (0.16g/100g powder) with lower encapsulation efficiency (93.7%) than spray dried powders. This study showed that nanoemulsions with suitable wall material consisting of trehalose can be used to produce dried powders by spray drying or freeze drying process with good particle characteristics and reconstitution properties.

5.2 Introduction

As discussed in the literature review (Section 2.1.6), nanoemulsions have many potential applications in foods due to their minute droplet size. However, there are some concerns over the shelf stability of liquid nanoemulsions during storage as liquid products are more susceptible to microbiological spoilage. Furthermore, it is not feasible to use liquid nanoemulsions in dry food systems and they are also difficult to handle during transportation. Therefore, conversion to powders from liquid nanoemulsions using drying technologies can overcome these limitations. Among various drying methods, spray drying is one of the most widely used to produce emulsion powders. It is a relatively simple method of drying to produce large amounts of powders. During spray drying, water is being removed and the oil droplets are embedded in the solid matrix of the powder particles. Therefore the wall materials used must be carefully selected to ensure desired properties of powders are achived after drying and during storage.

Generally, the wall materials used must be soluble in water with low viscosity at high concentration so that the solution can be pumped and sprayed during the process and they must have good film forming and drying properties (Bae & Lee, 2008; Turchiuli Munguia, Sanchez, Ferre & Dumoulin, 2014). As discussed in Section 2.2.2 of the literature review, several wall components have been used for spray drying and freeze drying including maltodextrin, modified starches, sugars, and proteins (Gharsallaoui et al., 2007; Jafari et al., 2008). Of which, maltodextrin is the most common wall materials used for microencapsulation by spray drying due to their low viscosity, good solubility and good oxidative stability (Gharsallaoui et al., 2007). However, maltodextrin has poor emulsifying properties and emulsion stability. Hence it is often used in conjunction with other wall materials such as whey proteins and gum arabic in spray dried powders (Gharsallaoui et al., 2007; Carneiro et al., 2013; Turchiuli et al., 2014). Trehalose is another material suitable for use in spray drying. It is a non-reducing disaccharide consisting of two α-glucose units joined by α-(1-1) linkage and possesses a high glass transition temperature ranging from 79 to 113^{o}C which can provide good physical stability to the powders (Willart, de Gusseme, Hemon, Descamps, Leveiller & Rameau, 2002; Richards & Dexter, 2011). The properties of these two wall materials appear to be very promising for encapsulation although each presents its own desirable characteristics. In this aspect,

the use of a mixture of maltodextrin and trehalose may be advantageous to improve the characteristics of the microparticles synergistically.

Although spray drying is an efficient method to produce dried powders, the use of relatively high temperature makes it unsuitable for drying heat sensitive materials and often resulted in a loss of product quality and their sensory attributes (Chen et al., 2013). On the other hand, freeze drying is a preferred method to dry heat sensitive food products but energy consumption is significantly higher with low throughput. The freeze drying process is carried out at temperatures lower than ambient temperature under vacuum which can prevent oxidative deterioration or any undesirable chemical changes (Fang & Bhandari, 2012). Therefore, freeze drying method helps to minimise product damage due to the use of high temperature in spray drying.

In this study, different wall materials consisting of maltodextrin, trehalose or in combination were used for spray drying nanoemulsions. The properties of the powders were characterised in terms of their moisture content, water activity, bulk density, particle density, particle size, particle morphology (microstructure) and encapsulation efficiency which are related to the powder quality and stability while wettability and dispersibility are related to the powder properties when reconstituted in water. From the results, an ideal wall material was selected to produce freeze dried powders. The aim of this study was to identify suitable wall materials for spray drying nanoemulsions with good powder properties and compare to those produced by freeze drying.

5.3 Materials and Methods

5.3.1 Materials

The wall materials used in encapsulation of nanoemulsions by spray drying or freeze drying were maltodextrin with DE of 17 – 20 derived from maize starch (AVONDEX 17, New Zealand Starch Ltd, New Zealand) and/or trehalose with purity of ≥98% (TREHA^{TM}, Hayashibara Co., Ltd, Japan). For a combination of wall mixture, maltodextrin and trehalose were used at a ratio of 1:1 in this study. Aqueous solutions of wall materials containing different concentrations (20, 40 and 60% w/w)

were prepared by dispersing the powders into Milli Q water (Millipore, 18.2 MΩ cm at 25°C) using a heavy duty laboratory mixer (Silverson Machines Ltd, England) at 5000 rpm for 5 minutes.

5.3.2 Preparation of nanoemulsions with wall solutions for spray drying

Nanoemulsion containing 2% (w/w) WPI and 1% (w/w) corn oil was prepared according to the method as described in Chapter 3 (Section 3.2.2). After preparation, nanoemulsion was mixed with an equal amount of wall solutions, resulting in a solid concentration of wall materials to be 10, 20 or 30% (w/w), excluding WPI, on a wet basis. The pH values of the mixtures were adjusted to 7 using 0.5 M HCl or NaOH solutions. Different combinations of wall materials and their respective composition are shown in Table 5.1.

Table 5.1 Formulations with different wall materials and their theoretical fat content in powders assuming removal of all moisture via evaporation during spray drying. MD and TRE represent maltodextrin and trehalose, respectively.

Formulation	Before spray drying					Theoretical amount of oil content after drying (g/100g powder)
	Dry matter (% w/w)					
	WPI	MD	TRE	Corn oil	Water	
10% MD	0.9	10	-	0.5	88.6	4.39
20% MD	0.9	20	-	0.5	78.6	2.34
30% MD	0.9	30	-	0.5	68.6	1.59
10% TRE	0.9	-	10	0.5	88.6	4.39
20% TRE	0.9	-	20	0.5	78.6	2.34
30% TRE	0.9	-	30	0.5	68.6	1.59
10% MD+TRE	0.9	5	5	0.5	88.6	4.39
20% MD+TRE	0.9	10	10	0.5	78.6	2.34
30% MD+TRE	0.9	15	15	0.5	68.6	1.59

5.3.3 Characterisation of nanoemulsions with wall materials before drying

5.3.3.1 Particle size and ζ- potential

The particle size and size distribution of nanoemulsions with wall materials before spray drying were measured by dynamic light scattering technique using a Malvern Zetasizer Nano ZS (Malvern Instruments Ltd, Worcestershire, UK). The electrical charge (ζ-potential) of nanoemulsions was also measured using a Malvern Zetasizer Nano ZS (Malvern Instruments Ltd, Worcestershire, UK). Prior to measurements, the emulsions were diluted using Milli Q at pH 7 to avoid multiple scattering effects. The mesurements were carried out in triplicates on two independent samples. Details of the characterisation techniques used in the determination of particle size and zeta potential are described in Chapter 3 (Section 3.3.1 and 3.3.2).

5.3.3.2 Viscosity

The viscosity of nanoemulsions containing various wall materials was measured using a Physica MCR 301 AR-G2 Rheometer (Anton Paar Gmbh, Graz, Austria). The measurements were made under controlled temperature of 25.0±0.1^{o}C using double gap geometry (17.5 mm rotor outer radius, 16 mm rotor inner radius, 15.1 mm stator inner radius, 53 mm cylinder immersed height, 2000 μm gap) and the shear rate applied ranged from 0.01 to100 s^{-1}. Measurements were made in duplicate on two individual samples.

5.3.4 Drying of nanoemulsions

5.3.4.1 Spray drying

Spray drying of nanoemulsions was carried out using a laboratory scale spray dryer (Mobile Minor^{TM} Spray Dryer, Niro A/S, Soeborg, Denmark) equipped with a fountain two-fluid nozzle and automated feeding system via a peristaltic pump. The feed solutions of liquid nanoemulsion mixed with their respective wall solutions were atomised to form small droplets by a vane atomiser wheel operating at a rotational speed of 17250 rpm. The feed and hot air in the drying chamber was directed in the manner of counter-current flow to increase drying efficiency. The nozzle air pressure was 300 kPa and the air inlet and outlet temperatures used were

150 ± 1°C and 65 ± 5°C, respectively. Dried powders were collected, placed in polyethylene bags and stored in airtight plastic containers at room temperature (20°C) for further analyses.

5.3.4.2 Freeze drying

Freeze drying was carried out using a freeze dryer (Cuddon, FD18LT ISLA, New Zealand) set at -30°C for overnight before use. Nanoemulsions mixed with wall solutions containing 20% (w/w) trehalose were poured into a metal pan and froze overnight at -30°C before transferring them to the freeze dryer. The vacuum pressure of the dryer was set at 1.8 mBar absolute and the freezing temperature started at -30°C for 3 hours, followed by increasing the temperature to -20°C in 1 hour and maintained at this temperature for 3 days. The dried product (or cake) was collected and milled into smaller particles using a food processor (Compact 3100, Magimix, France) for 30 seconds. The powders were placed in polyethylene bags and stored in airtight plastic containers at room temperature (20°C) for further analyses.

5.3.5 Analysis of dried nanoemulsion powders

5.3.5.1 Moisture content and water activity

The moisture content of powders was determined using an infrared moisture analyser (Sartorius, MA35, Goettingen, Germany) at 105°C with a drying rate of 1 mg per 30 seconds with fully automatic end-point determination. The water activity of powders was measured at 25°C using a water activity meter (Aqualab Dew Point Moisture Analyser, 4TE DUO, Washington, USA).

5.3.5.2 Particle size and size distribution

The particle size of powders was measured by light diffraction using a Mastersizer 2000 (Malvern Instruments Ltd, Worcestershire, UK) equipped with a dry powder dispersion unit (Scirocco 2000, Malvern Instruments Ltd, Worcestershire, UK). The powders were analysed in dry mode at 50% vibration feed rate with a compressed air pressure of 2.2 bar. A refractive index and an absorption index of 1.52 and 0.001, respectively was used. The results were calculated by general purpose model (Malvern Application, Version 5.60, Malvern Instruments Ltd, Worcestershire, UK).

5.3.5.3 Bulk density

The bulk density of powders was determined by measuring the ratio of mass and volume of powders occupied in a cylinder. The powders were placed into a 5 mL measuring cylinder up to the 5 mL mark by gently pouring them and then weighed. The bulk density was calculated by dividing the weight (mass) by the volume and expressed in g/mL.

5.3.5.4 Scanning electron microscope (SEM)

The morphological and microstructural features of powders were examined by SEM (FEI Quanta 200, Hillsboro, Oregon, USA) (FEI Electron Optics, Gindhoven, The Netherlands). The powders were also broken up with a metal spatula to examine the inner structures. The powders were placed onto aluminium stubs using a double sided tape and coated with a thin layer of gold by sputter coating (Bal-Tec SCD050 sputter coater, Scotia, New York, USA). The gold-coated samples were analysed using the SEM operating at an accelerating voltage of 12.5 to 20 kV.

5.3.5.5 Total and surface oil contents and encapsulation efficiency

The total oil content of powders was determined by the Mojonnier fat extraction method (American Association of Cereal Chemist, AACC 30-10). The surface oil of powders was determined by solvent extraction method based on GEA Niro Method No. A 10a (GEA Niro, 2005). Briefly, 10 g of powders was weighed and mixed with 50 mL of petroleum ether in an Erlenmeyer flask and placed in a laboratory shaker for 15 minutes for extraction of surface oil. After extraction, the mixture was filtered through a filter paper Whatman No 4 (Maidstone, UK) to separate the powder and solvent. A 25 mL of solvent was pipetted into a pre-weighed aluminium pan and left to evaporate in the fume hood. After evaporation, the aluminium pans were transferred to a laboratory drying oven (Model 2400, Contherm Scientific Company, Lower Hutt, New Zealand) at 108 ± 1^{o}C for 1 hour and cooled in a desiccator before weighing them.

The encapsulation efficiency (EE) of powders is defined as the amount of oil encapsulated in the powder particles (Jafari et al., 2008). It was calculated from the total oil and surface oil of powders using the following equation (5.1).

$$EE = \frac{TO-SO}{TO} \times 100 \qquad (5.1)$$

where *TO* is the total oil content and *SO* is the surface oil content

5.3.5.6 Wettability and dispersibility

Wettability and dispersibility of powders is associated with their ability to reconstitute in water. The wettability of powders is defined as the ability to absorb water and rehydrate without agitation while dispersibility is the ability of powders to disperse (separate out) in water without clumping (International Dairy Federation, 2011; Thiengnoi, Suphantharika & Wongkongkatep, 2012). Both are important parameters in measuring the properties of powders. In this study, the wettability of powders was determined by sprinkling 1 g of powders into 100 mL of Milli Q water at 25^{o}C in a 250 mL tall form glass beaker (Ø60 x H120 mm) and measuring the time taken for all the particles to penetrate through the surface of water (or turn wet).

The dispersibility of powders in water was determined using the method as described by Thiengnoi et al. (2012). Briefly, 1 g of powders was added into 10 mL of Milli Q water and the mixture was stirred uniformly with a teaspoon for 15 seconds. After stirring, the mixture was poured through a sieve with 180 µm mesh size and 1 mL of solution was transferred onto an aluminium pan and dried in a drying oven at 108 ± 1^{o}C for 4 hours. The dispersibility of powders in water was calculated using the equations as follow:

$$\%\ Dispersibility = \frac{(10+a)\times \%\ TS}{a \times \frac{100-b}{100}} \qquad (5.2)$$

where *a* is the amount of powder used, *b* is the moisture content in the powder and *% TS* is the dry matter in the reconstituted solution after passing through the sieve.

$$\%\ TS = \frac{dry\ matter\ after\ drying\ (g) \times 100}{solution\ used\ (g)} \qquad (5.3)$$

5.3.6 Reconstitution of nanoemulsions

Dried powders were reconstituted by dispersing the powders (2 – 9 g) into 20 g Milli Q water at 25^{o}C. The amount of powders added was to achieve the same solid content as the nanoemulsions mixed with different wall solutions by measuring the brix using a digital hand held refractometer (PAL-1, Atago Co. Ltd., Japan). After reconstitution, the nanoemulsions were adjusted to pH 7 using 0.5 M HCl or NaOH solutions. Details of the powders reconstituted in water (amount of powders used and brix) are shown in Table 5.6. The particle size and ζ-potential of reconstituted nanoemulsions were determined as mentioned above.

5.3.7 Data analysis

The results were statistically analysed using Minitab® 17.2.1 statistical software (Minitab, Inc., USA). The effect of wall solutions (i.e. type and concentration) on the properties of powders was determined by ANOVA using General Linear Model. All the measurements were performed at least twice for each sample from duplicate experiments. Differences between the mean values were further examined using the Tukey test at a significance level of $P < 0.05$.

5.4 Results and Discussion

5.4.1 Properties of nanoemulsions added with different wall materials

Nanoemulsions were first prepared and then added with different wall material solutions (either maltodextrin or trehalose or a combination of both at 1:1 ratio) at different solid concentrations (10, 20 and 30% w/w). All the nanoemulsions were similar in size with Z-Average around 80 nm in diameter and the particle size distribution was monomodal except those containing maltodextrin (bimodal) (Figure 5.1). The particle size and size distribution were also similar to those nanoemulsions prepared without the addition of wall materials (Chapter 4; Section 4.4.1). This indicates that the addition of wall materials did not affect the particle size of nanoemulsions and they were also physically stable.

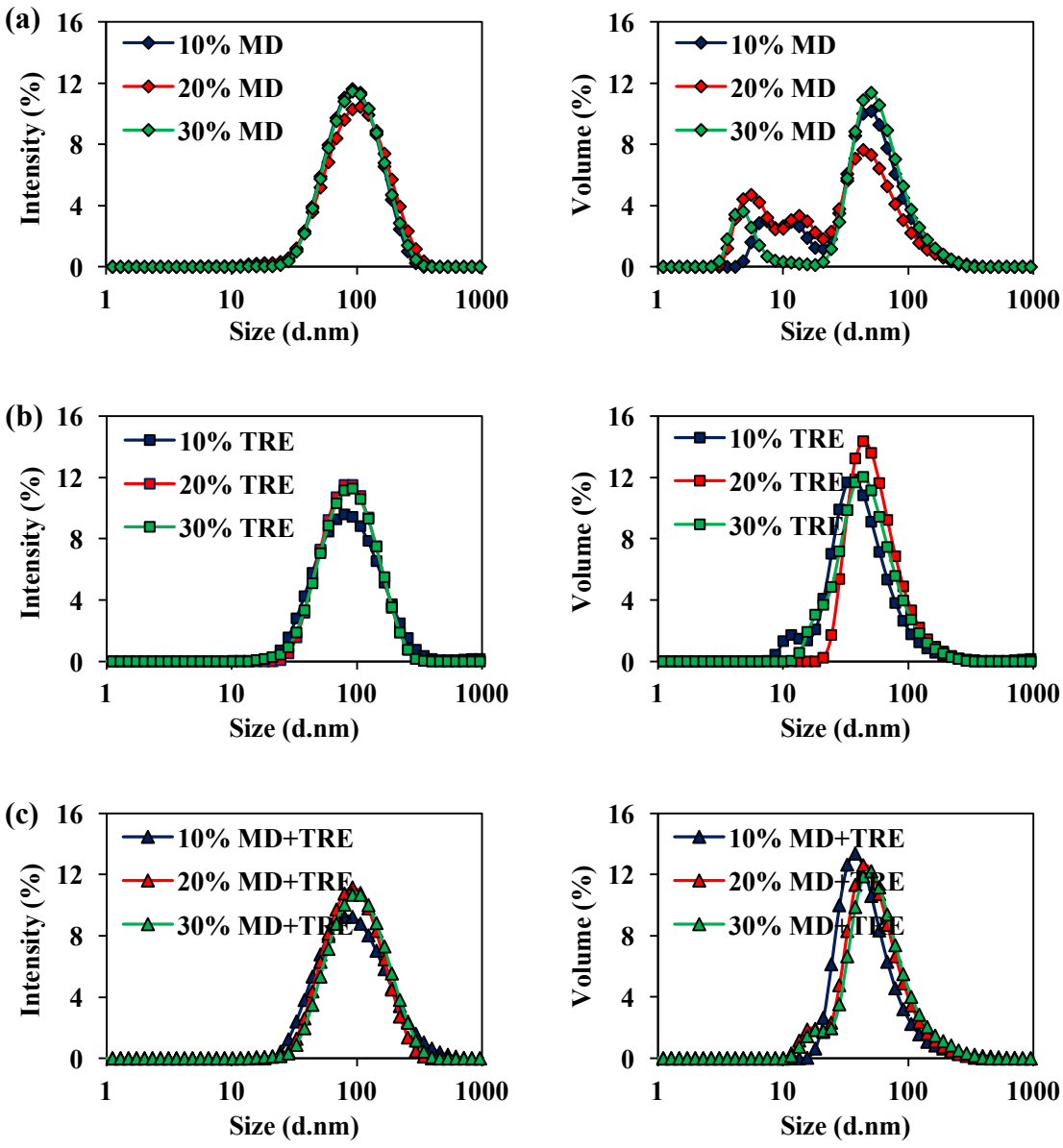

Figure 5.1 Particle size distributions (by intensity and volume) of WPI-stabilised nanoemulsions (0.5% w/w oil) mixed with (a) maltodextrin, (b) trehalose and (c) a 1:1 ratio of maltodextrin and trehalose at 10, 20 and 30% (w/w) before spray drying. MD and TRE represent maltodextrin and trehalose, respectively.

However, the viscosity of nanoemulsions was significantly affected by the wall materials used ($P < 0.05$). The nanoemulsions prepared with maltodextrin or in combination with trehalose (1:1 ratio) displayed higher viscosity than those containing only trehalose and there was also a slight increase in emulsion viscosity at a higher concentration of wall materials used (Figure 5.2). It has been reported that the viscosity of feed solution used for spray drying is important for the formation of small droplets on atomisation which in turn can affect the powder properties. Keogh,

Murray & O'Kennedy (2003) reported that spray drying of ultrafiltered whole milk concentrate with higher viscosity (43 – 550 mPa.s at 1 s^{-1}) increased the particle size ($D_{0.5}$ from 55.7 to 121 μm) and moisture content of dried milk powders (from 2.3 to 6.7%). Ng, Choong, Tan, Long & Nyam (2014) also found that spray drying of kenaf seed oil emulsions with higher concentration of maltodextrin (40% w/w total solid content) increased the emulsion viscosity (93.1 mPa.s at 1550.9 s^{-1}) and produced larger particle size ($D_{4,3}$ ~ 0.13 μm) in the dried microcapsules. In the following sections, the effects of different wall materials on the properties of the produced powders were further investigated.

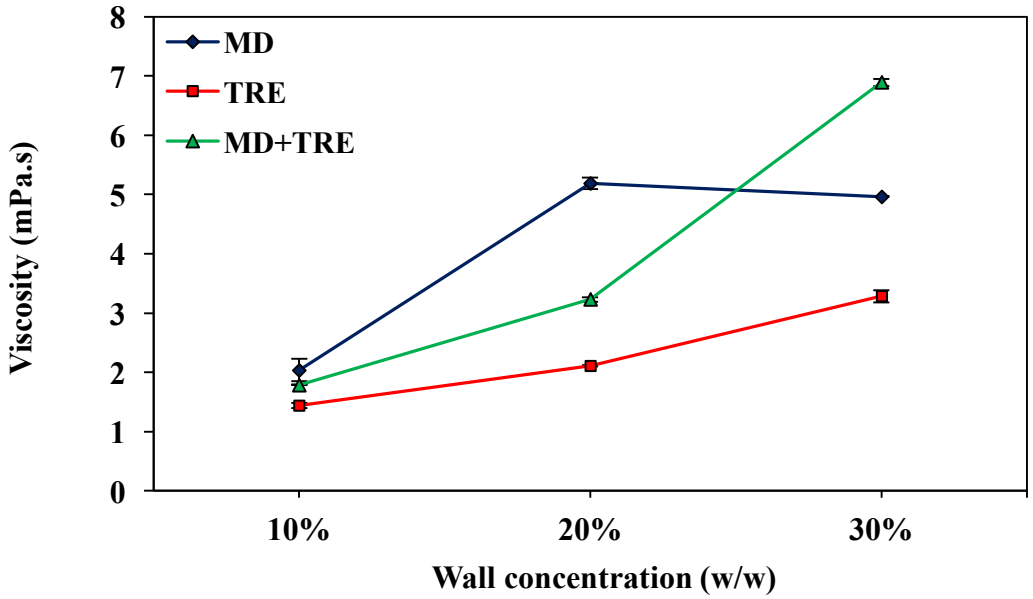

Figure 5.2 Viscosity of WPI-stabilised nanoemulsions (0.5% w/w oil) mixed with different wall materials (10, 20 and 30% w/w) before spray drying measured at shear rate 10s^{-1}. MD and TRE represent maltodextrin and trehalose, respectively. Data are presented as the mean of two independent measurements with triplicates (*n*=6) and error bars represent the standard deviation.

5.4.2 Properties of spray dried nanoemulsions with different wall materials

5.4.2.1 Moisture content and water activity of powders

Some physical properties of spray dried powders prepared with different types and concentrations of wall materials were analysed. The results are shown in Tables 5.2 and 5.3. The moisture content of powders ranged from 3.9 to 8.0% and water activity varied from 0.19 to 0.39 with a significant difference among the

different types of wall materials ($P < 0.05$) but no pronounced effect on their concentrations except for 20% maltodextrin sample (Table 5.2). The powders prepared with maltodextrin showed higher moisture content (5.8 – 8.0%) and water activity (0.23 – 0.39) than those of the powders produced with trehalose (3.9 – 4.6%; 0.19 – 0.24) or in combination of both wall materials (4.0 – 4.4%; 0.20 – 0.25). It has been reported in literature that changes in the composition of wall materials have little effect on the moisture content of powders (Carneiro et al., 2013; Botrel, Fernandes, Borges & Yoshia, 2014; Franceschinis, Salvatori, Sosa & Schebor, 2015). In particular, Franceschinis et al. (2015) observed that the moisture content (3.5 – 3.7%) and water activity (0.16 – 0.19) of blackberry juice powders prepared with either maltodextrin (DE 12) or a 1:1 ratio of maltodextrin and trehalose at 40% solid concentration spray dried at an inlet temperature of 175 ± 3^{o}C were not affected by the wall materials used. However, the moisture content and water activity of the spray dried powders in the present study were higher in maltodextrin powders than those produced with trehalose or a mixture of both wall materials. One of the possible reasons for a higher moisture content and water activity observed in the samples containing only maltodextrin is probably due to the fact that the maltodextrin with a high DE value of 17 – 20 is hygroscopic and may absorb moisture from the surrounding environment. In general, maltodextrins with higher DE are subjected to a greater extent of starch hydrolysis with more sugars produced which gave rise to a higher hydroscopicity than those of lower DE (Wang & Zhou, 2012).

According to Fang & Bhandari (2012), the drying temperatures used for spray drying have greater influence on the moisture content of the powders. In principle, the rate of heat transfer to the particles was increased at higher inlet air temperature with greater driving force for moisture evaporation, resulting in powders with lower moisture content and water activity (Fang & Bhandari, 2012). For instance, the moisture content and water activity of the spray dried powders containing black mulberry juice (8% maltodextrin DE9) was decreased from approximately 2.5 to 2% when the inlet air temperature was increased from 110 to 150^{o}C (Fazaeli, Emam-Djomeh, Ashtari & Omid, 2012). In the present study, the drying condition used was kept constant for all sample preparations with inlet and outlet air temperatures of 150^{o}C and 65^{o}C, respectively. Typically, the inlet air

temperature used for spray drying food ingredient ranges from 150 to 220°C and the outlet air temperature ranged from 50 to 80°C (Gharsallaoui et al, 2007; Fang & Bhandari, 2012). For most food powders, the recommended moisture content should be less than 5% and water activity below 0.2 (Bhandari, 2008).

Table 5.2 Mean moisture content and water activity of spray dried powders prepared with different wall materials containing 10, 20 or 30% (w/w) in feed solutions.

Wall materials	Moisture content (%)	Water activity
10% MD	7.96 ± 0.16^{a}	0.39 ± 0.01^{a}
20% MD	5.80 ± 0.27^{b}	0.23 ± 0.01^{b}
30% MD	7.42 ± 0.19^{a}	0.37 ± 0.01^{a}
10% TRE	3.86 ± 0.64^{d}	0.19 ± 0.05^{b}
20% TRE	4.61 ± 0.24^{c}	0.24 ± 0.03^{b}
30% TRE	$4.41 \pm 0.21^{c,d}$	0.22 ± 0.01^{b}
10% MD+TRE	$4.38 \pm 0.38^{c,d}$	0.25 ± 0.02^{b}
20% MD+TRE	3.95 ± 0.34^{d}	0.20 ± 0.01^{b}
30% MD+TRE	$4.15 \pm 0.41^{c,d}$	0.21 ± 0.03^{b}

Results for each sample are expressed as mean ± standard deviation of at least two measurements from duplicate experiments. Means with different letters within a column are significantly different at $P < 0.05$. MD: maltodextrin, TRE: trehalose.

5.4.2.2 Particle size and bulk density of powders

Spray drying of nanoemulsions produced fine powders with no apparent relation to particle size and bulk density that could be associated with the composition of the wall materials. The mean particle diameters ($D_{3,2}$ and $D_{4,3}$) and span values of powders prepared with different wall materials are shown in Table 5.3. All the powders exhibited similar particle size distribution with a single peak which means that the particle size were monodispersed (Figure 5.3) indicating the spray drying process was consistent throughout the experimental trials as would have been expected (Caparino, Tang, Nindo, Sablani, Powers & Fellman, 2012). The particle size of the nanoemulsion powders were within the size range of 10 – 100 μm like most spray dried powders (Thiengnoi et al., 2012). However, within the expected size range, the particle size of the powders varied significantly between the samples ($P < 0.05$; Table 5.3). At the same wall concentration, the powders produced from the mixture of nanoemulsions and wall materials containing maltodextrin had larger particles than samples containing nanoemulsions with only trehalose. No significant differences were observed between nanoemulsions with maltodextrin and those containing a mixture of maltodextrin and trehalose. It was also observed that the size

of particles genrally increase with increasing solid concentration (Table 5.3) which could be attributed to the viscosity of the feed solution as it was observed that there was an increase in viscosity at higher wall material concentration (Figure 5.2). This is so because larger droplets were formed during atomisation when spray drying emulsions with higher viscosity and resulted in the formation of powders with larger particle size (Turchiuli et al., 2014).

The results also showed increasing span values with increasing wall material concentration although the differences were not considerable. In general, spray dried powders with span value more than 2 are considered to be high. A high span value indicates a wide size distribution and a high polydispersity in the powders (Dubey & Parikh, 2004).

Table 5.3 Particle size and bulk density of spray dried powders prepared with different wall materials containing 10, 20 or 30% (w/w).

Wall materials	Particle diameter (µm)		Span	Bulk density (g/mL)
	$D_{3,2}$	$D_{4,3}$		
10% MD	5.66 ± 0.11^{c}	11.5 ± 2.09^{b}	1.85 ± 0.17^{b}	0.18 ± 0.01^{e}
20% MD	5.18 ± 0.11^{d}	7.05 ± 0.31^{c}	$1.55 \pm 0.09^{c,d}$	$0.26 \pm 0.02^{c,d}$
30% MD	7.20 ± 0.44^{a}	19.3 ± 1.30^{a}	2.51 ± 0.33^{a}	$0.25 \pm 0.02^{c,d}$
10% TRE	4.62 ± 0.38^{e}	6.84 ± 2.92^{c}	1.38 ± 0.13^{d}	$0.28 \pm 0.03^{c,d}$
20% TRE	5.72 ± 0.33^{c}	$9.77 \pm 2.85^{b,c}$	$1.62 \pm 0.15^{b,c,d}$	0.36 ± 0.03^{b}
30% TRE	6.01 ± 0.15^{c}	$10.0 \pm 1.97^{b,c}$	$1.70 \pm 0.10^{b,c}$	0.46 ± 0.03^{a}
10% MD+TRE	5.92 ± 0.07^{c}	$8.57 \pm 0.32^{b,c}$	$1.70 \pm 0.06^{b,c}$	$0.23 \pm 0.05^{d,e}$
20% MD+TRE	6.60 ± 0.08^{b}	$9.91 \pm 0.15^{b,c}$	$1.81 \pm 0.03^{b,c}$	0.29 ± 0.02^{c}
30% MD+TRE	$6.92 \pm 0.12^{a,b}$	11.7 ± 1.66^{b}	1.87 ± 0.04^{b}	0.46 ± 0.02^{a}

Results are expressed as mean ± standard deviation of at least two measurements from duplicate experiments. Means with different letters within a column indicate significant difference at $P < 0.05$. MD: maltodextrin, TRE: trehalose.

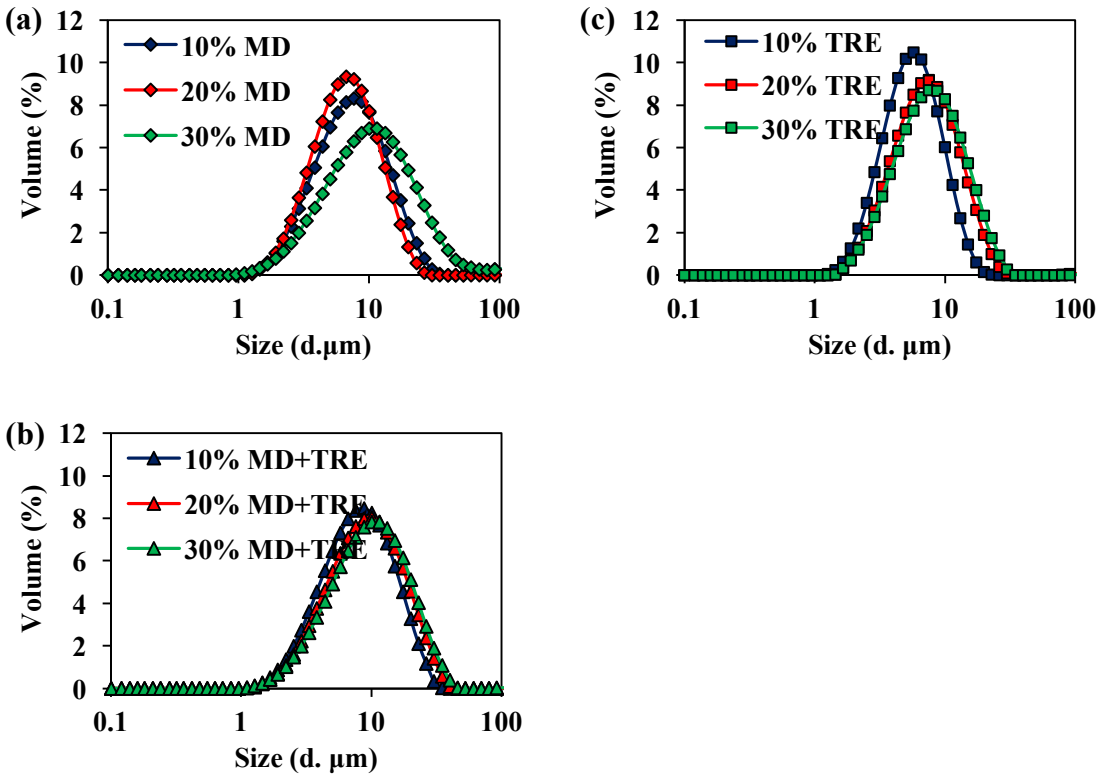

Figure 5.3 Particle size distribution (by volume) of spray dried powders prepared with (a) maltodextrin, (b) trehalose and (c) a 1:1 ratio of maltodextrin and trehalose at 10, 20 and 30% (w/w). MD and TRE represent maltodextrin and trehalose, respectively.

Bulk density is the mass of powders in a given volume of space whereby the bulk density is inversely related to the volume of powders, i.e. the higher the bulk density, the less volume occupied by the powders at a given mass (Bae & Lee, 2008). There are several factors affecting the bulk density of powders, including particle density, particle morphology (size and shape), degree of agglomeration and flowability. In the present study, the bulk density of powders varied from 0.18 to 0.46 g/mL (Table 5.3) and it was observed to vary significantly according to the wall materials and solid contents ($P < 0.05$).

Among different wall materials, powders produced with trehalose or a mixture of maltodextrin and trehalose (1:1 ratio) showed higher bulk densities (0.23 – 0.46 g/mL) than those powders produced with only maltodextrin (0.18 – 0.26 g/mL) which can be related to the particle size of the powders (Table 5.3). In general, particles with smaller size have higher bulk densities because they can penetrate between spaces and thus more particles can be packed tightly to obtain powders with

higher densities (Caparino et al., 2012). Powders with higher bulk densities are thought to be advantageous as more powders can be packed into smaller containers with less void spaces and air inclusion to minimise chemical reaction (oxidation) (Carneiro et al., 2013). The bulk densities of all the spray dried powders (0.18 – 0.46 g/mL) were within the range of dried milk products (0.21 to 0.56 g/mL) (FAO, 2012).

5.4.2.3 SEM microstructural features

The morphology of spray dried powders produced with different wall materials was examined by SEM (Figures 5.4 – 5.6). Most of the particles were spherical in shape but the powders containing maltodextrin exhibited surface collapse with indentations or dents on the surface of the particles (Figure 5.4). It was also observed that the particles produced with higher concentration of maltodextrin had higher degree of dents (Figures 5.4b & 5.4c) which were more distinct than 10% (w/w) maltodextrin (Figure 5.4a). Many previous studies have also shown the presence of surface dents in spray dried powders, depending on the wall materials used (Jafari et al., 2008; Botrel et al., 2014). In particular, Jafari et al. (2008) showed that fish oil encapsulated particles produced using maltodextrin in combination with either Hi-Cap (modified starch) or whey protein concentrate (40% w/w total dry matter) exhibited surface dents but there was a higher degree of dents in the particles containing Hi-cap. It was explained that the occurrence of surface dents is associated with a slow rate of crust formation and less elasticity of the wall matrix to resist structural collapse of the droplets during the drying process (Ré, 1998; Jafari et al., 2008).

As shown in Figure 5.4, the internal morphology of all the particles containing different concentrations of maltodextrin was similar. The particles were homogenous with a large hollow structure (or a central void) inside due to the quick expansion of particles during the drying process (Ré, 1998). The presence of a central void inside the particle was typical of all spray dried powders (Bae & Lee, 2008; Tonon et al., 2012; Chen et al., 2013). Similar internal morphology was also observed by Tonon et al. (2012) in spray dried powders containing 20% flaxseed oil using different wall materials (whey protein concentrate, gum Arabic and modified starch Hi-Cap 100). Further analysis on the morphology of the particles did not show any detectable pores as the oil droplets were embedded inside the wall matrix which is typical of spray dried powders as suggested by Carneiro et al. (2013). Taneja, Ye,

Jones, Archer & Singh (2013) studied the distribution of oil droplets in emulsion powders using confocal microscopy and showed that the oil droplets were evenly distributed inside the wall matrix.

(a) 10% (w/w) maltodextrin

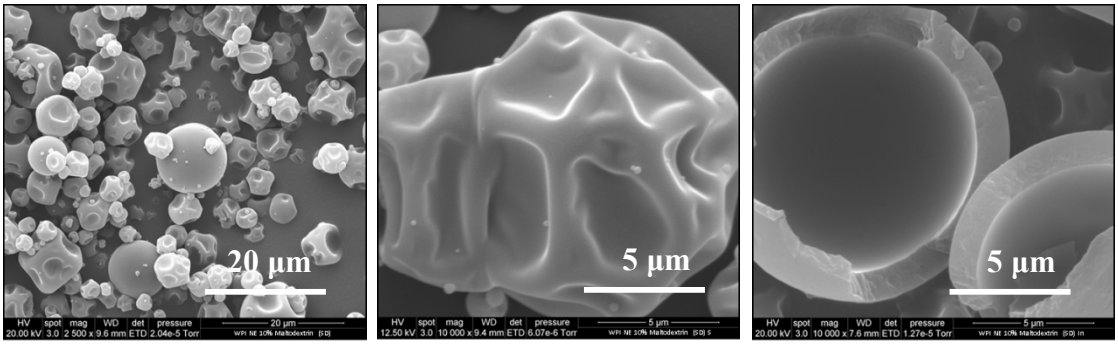

(b) 20% (w/w) maltodextrin

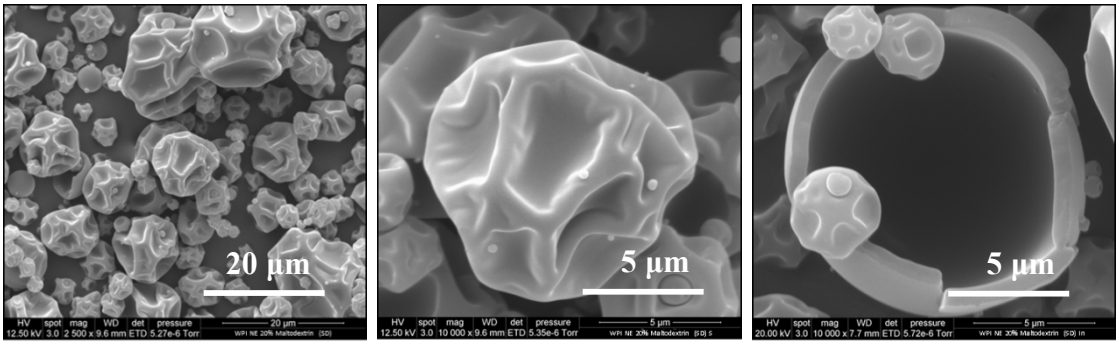

(c) 30% (w/w) maltodextrin

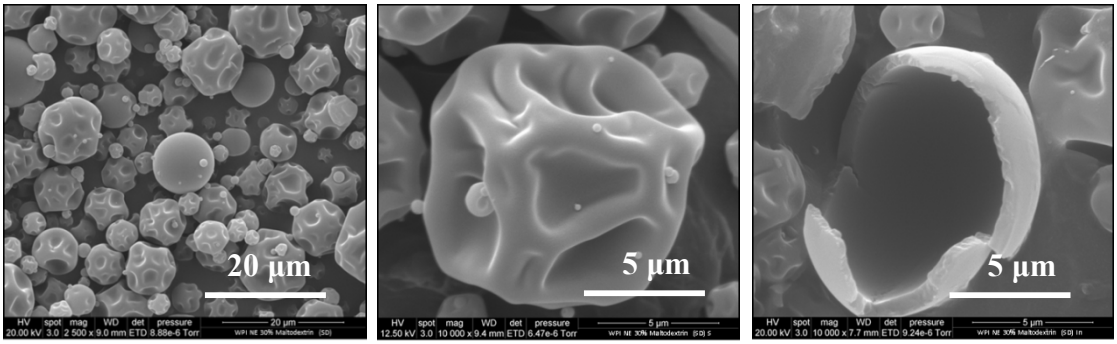

Figure 5.4 SEM images (outer and inner structures) of spray dried powders prepared with different concentrations of maltodextrin: (a) 10%, (b) 20% and (c) 30% (w/w).

Figure 5.5 shows the SEM images of spray dried powders containing trehalose as wall materials. The morphological shape of the powders appeared distinctly quite different from the powders made from maltodextrin (Figure 5.4). The results showed that the particles of trehalose containing 10% (w/w) appeared to be more agglomerated (Figure 5.5a) than the powders containing 20 and 30% (w/w) trehalose that were predominantly single particles (Figures 5.5b & c). Unlike

maltodextrin powders and irrespective of the concentration of wall material used, the outer structures of trehalose powders were smooth and did not exhibit any surface indentations (Figure 5.5). This may be due to a greater elasticity of the wall material (Jafari et al., 2008). It is known that trehalose is a kosmotrope which can interact strongly with water (Jain & Roy, 2009). During spray drying process, some water molecules may interact with trehalose in their amorphous form, presumably this may increase the viscoelasticity of the wall matrix to prevent the occurrence of shrinkage. The hydrostatic expansion of hot air inside the particles contributed to a spherical shaped particle when a viscoelastic wall material is used (Botrel et al., 2014). Drusch, Serfert, Van Den Heuvel & Schwarz (2006) also showed that spray dried microcapsules of 10% or 40% (wt) fish oil containing trehalose had less wrinkled surface than those samples containing glucose syrup (DE 38) at 40% solid load.

In other studies, low molecular weight sugars, mainly, glucose, lactose and sucrose were used for spray drying powders (Das, Wang & Langrish, 2014; Maher, Roos & Fenelon, 2014). These sugars have low viscosity and good glass forming properties which are useful for spray drying. However, spray drying of powders containing sugars (sucrose) is often associated with problems such as adhesion to surface of spray dryer and clogging of nozzle (due to stickiness and agglomeration of particles) as well as caking, structural collapse and crystallisation during storage (Gharsallaoui et al., 2007; Domian, Sułek, Cenkier & Kerschke, 2014). This is mainly due to the lower glass transition temperature of sucrose (65 – 75^{o}C) (Ohtake & Wang, 2010). Consequently, structures with amorphous sucrose collapse at temperature above the glass transition point (Booy, Ruiter & Meere, 1991; Ohtake & Wang, 2010). In this aspect, trehalose is a more suitable wall material as it has a relatively higher glass transition temperature of above 100^{o}C (110 – 120^{o}C) to remain in its glassy state over a wider range of temperature and humidity (Ohtake & Wang, 2010; Richards & Dexter, 2011).

As shown in Figure 5.5, the particles containing trehalose showed a central void internally similar to the maltodextrin samples. Also, it is observed that there were some cracks on the surface of particles produced with trehalose (Figure 5.5). The presence of surface cracks indicated that the wall material (trehalose) was prone to damage caused by the expansion of particles during spray drying process (Jafari et al., 2008). Domian et al. (2014) showed that sunflower oil microcapsules produced

by spray drying a mixture of 10% milk proteins and 34% trehalose (based on dry matter) as wall materials were smooth but did not report the presence of cracks on the surface of particles.

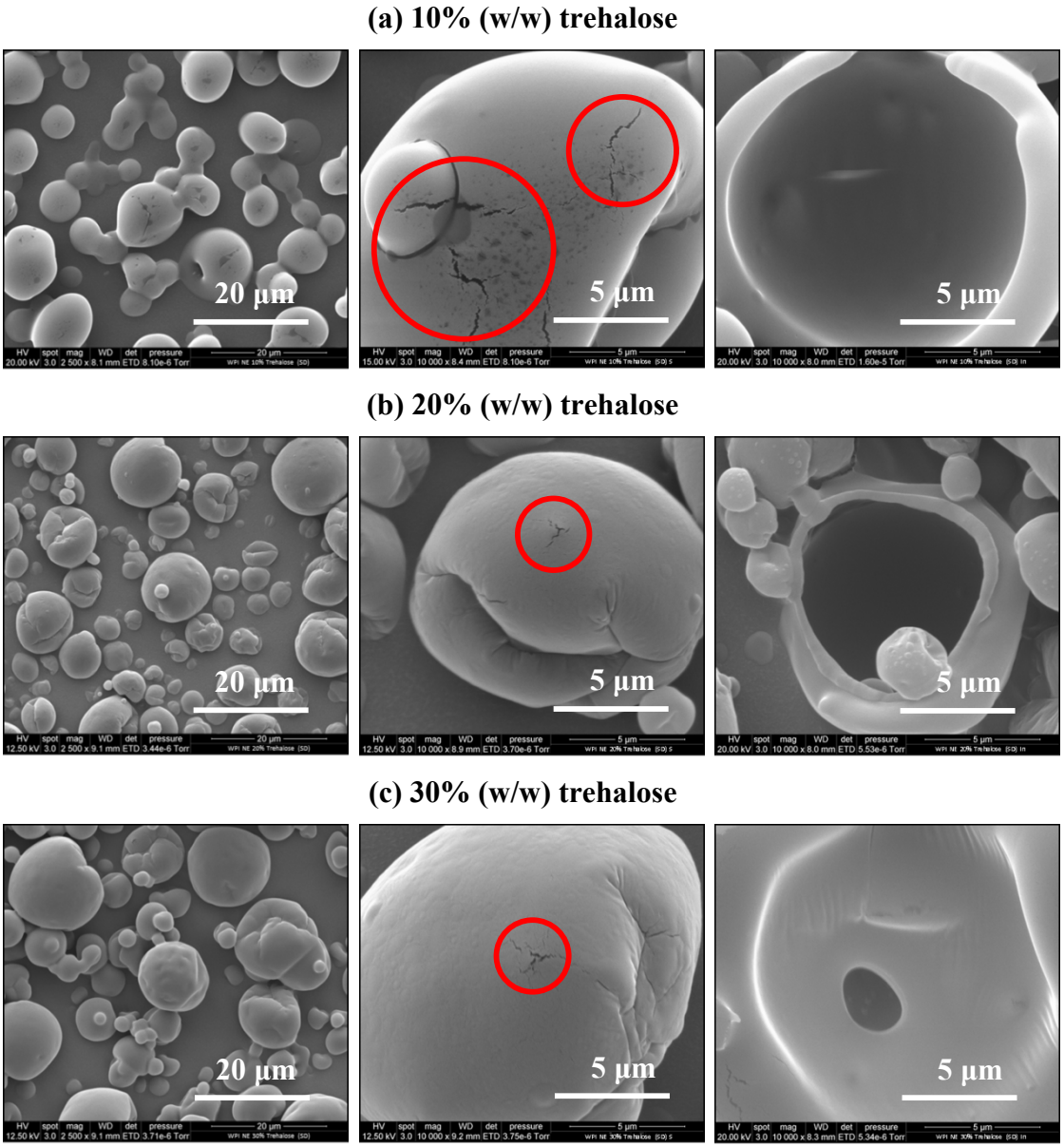

Figure 5.5 SEM images (outer and inner structures) of spray dried powders prepared with different concentration of trehalose: (a) 10%, (b) 20% and (c) 30% (w/w).

The particles of powders containing a mixture of maltodextrin and trehalose (1:1 ratio) were spherical with fewer surface indentations than the powders containing only maltodextrin, especially at higher concentrations (Figure 5.6). The powder particles produced with 30% of wall material were smoother with a less shrivelled surface (Figure 5.6c). It was hypothesised that the addition of trehalose improves the viscoelastic properties of the wall matrix and reduces the formation of

dents on the outer surfaces of particles. Similarly, particles with improved surfaces were formed when trehalose was used in combination with maltodextrin (40% w/w dry matter) in spray dried blackberry powders (Franceschinis et al., 2014). Domian et al. (2015) also showed that the addition of trehalose in conjunction with octenyl succinate starch (19.8% w/w) as the wall material produced particles containing rapeseed oil and linseed oil (13.2% w/w) with spherical shape and smoother surface. It was suggested that the trehalose helped to smoothen the surface of particles and thus prevent the formation of dents in the starch based particles. In addition, the surface cracks observed in the samples containing only trehalose (Figure 5.5) was not observed in the samples containing a combination of trehalose and maltodextrin (Figure 5.6). This suggested that the incorporation of maltodextrin helps to strengthen the wall material containing only trehalose and minimise the damage caused by expansion of particles during spray drying. Likewise, a central void was also observed in all the particles containing a mixture of maltodextrin and trehalose (Figure 5.6).

(a) 10% (w/w) 1:1 ratio of maltodextrin and trehalose

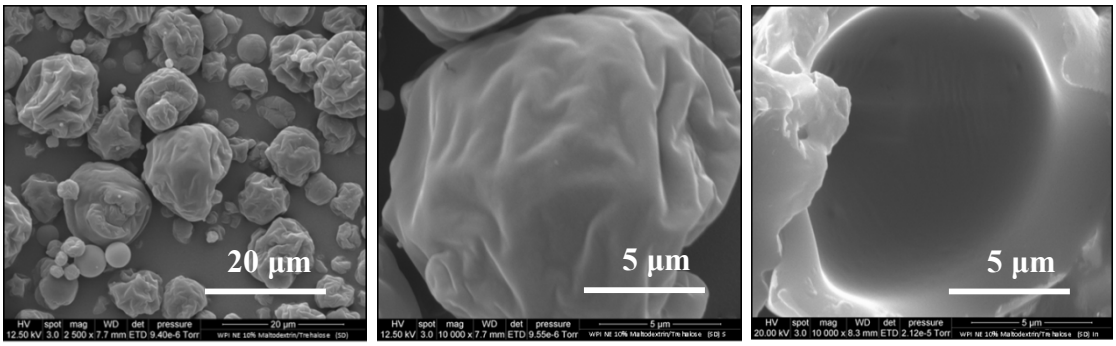

(b) 20% (w/w) 1:1 ratio of maltodextrin and trehalose

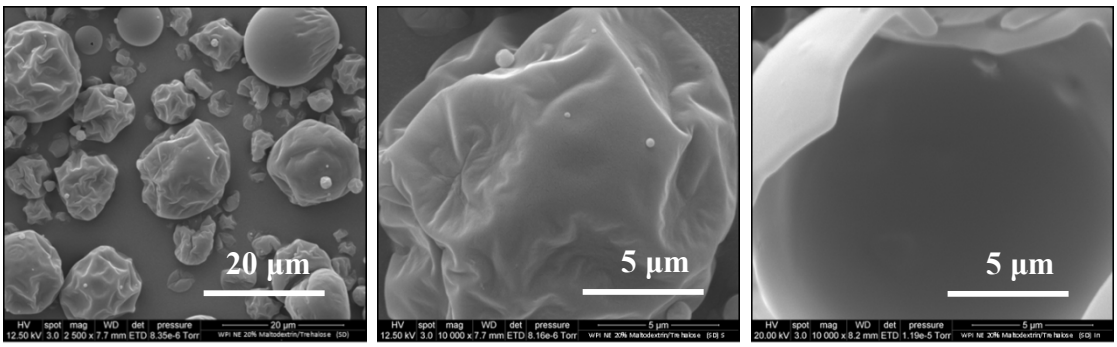

(c) 10% (w/w) 1:1 ratio of maltodextrin and trehalose

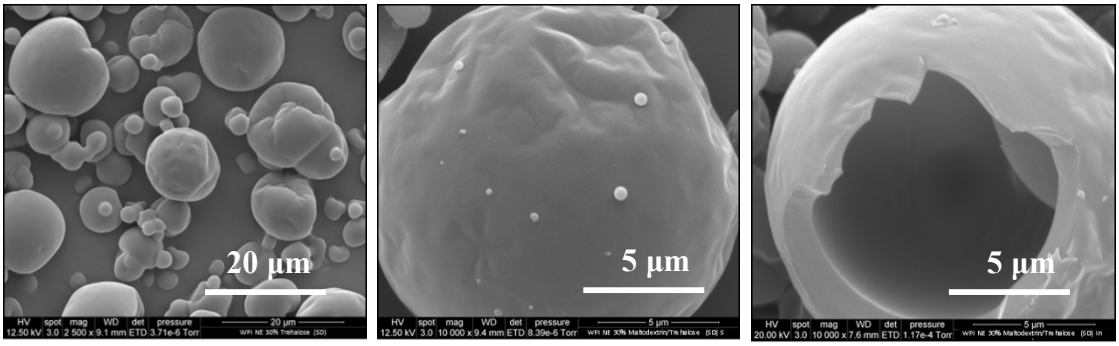

Figure 5.6 SEM images (outer and inner structures) of spray dried powders prepared with different concentration of a mixture of 1:1 ratio of maltodextrin and trehalose: (a) 10%, (b) 20% and (c) 30% (w/w).

5.4.2.4 Encapsulation efficiency

Encapsulation efficiency of powders is one of the important parameters for encapsulation of oils in spray dried powders. It determines the amount of oil encapsulated in the powder matrix by indirectly measuring the amount of surface oil in powders using solvent extraction (Jafari et al., 2008). The results obtained in this study indicated that the spray dried powders had high encapsulation efficiencies (97.1 – 99%) as the amount of surface oil extracted from the powders was generally low between 42.7 and 58.8 mg/100g powder (Table 5.4). This can be attributed to

the fact that nanoemulsions containing small oil droplets and low oil content of 0.5% (w/w) were surrounded by a relatively thick layer of wall materials with optimum efficiency to protect their core materials. Jafari et al. (2008) reported that the surface oil of fish oil (20% w/w) encapsulated powders using maltodextrin in combination with modified starch or whey protein concentrate (40% w/w) as wall materials was lower when the droplet size of emulsions was decreased using different emulsification systems. They found that emulsions with larger droplet size of $D_{4,3}$ of 4.6 – 5.9 μm were produced with Silverson increased the surface oil content (1270 – 2040 mg/100g powder) due to the instability of emulsion. On the other hand, smaller droplets of $D_{4,3}$ of 0.21 – 0.28 μm produced with Microfluidser (60 MPa; 1 cycle) had lower surface oil (170 – 690 mg/100g powder). Therefore, reducing the droplet size of emulsions is necessary to produce powders with lower surface oil and high encapsulation efficiency.

From the data, the surface oil of powders was found to be affected by the wall concentrations although it may seem there is no difference in the encapsulation efficiency between samples ($P > 0.05$; Table 5.4). The powders containing trehalose as the wall material had slightly higher surface oil content than other samples (Table 5.4). This may be related to the presence of some cracks at the surface of the particles (Figure 5.5) which would allow the solvent to penetrate more readily during solvent extraction and resulted in the extraction of more oil from the inside of the powder particles. Also, trechalose being a disaccharide is a smaller molecule than maltodextrin which could imply a more porous structure for the fat to be solubilised by the solvent used (Ohtake & Wang, 2011).

Table 5.4 Total, surface oil content and encapsulation efficiency of powders prepared with different wall materials containing 10, 20 and 30% (w/w) dry matter.

Wall materials	Total oil content (g/100g powder)	Surface oil content (mg/100g powder)	Encapsulation efficiency (%)
10% MD	4.00 ± 0.07^{c}	$46.3 \pm 7.2^{b,c}$	98.8 ± 0.2^{a}
20% MD	2.79 ± 0.44^{d}	$47.3 \pm 1.0^{b,c}$	$98.3 \pm 0.2^{b,c}$
30% MD	2.25 ± 0.05^{e}	42.7 ± 2.0^{c}	$98.1 \pm 0.1^{c,d}$
10% TRE	4.61 ± 0.05^{b}	58.8 ± 3.4^{a}	$98.7 \pm 0.1^{a,b}$
20% TRE	$2.51 \pm 0.04^{d,e}$	$55.7 \pm 5.0^{a,b}$	97.8 ± 0.2^{d}
30% TRE	1.71 ± 0.03^{f}	$48.8 \pm 7.3^{a,b,c}$	97.1 ± 0.5^{e}
10% MD+TRE	5.15 ± 0.15^{a}	$55.1 \pm 4.1^{a,b}$	98.9 ± 0.1^{a}
20% MD+TRE	$2.63 \pm 0.12^{d,e}$	$48.7 \pm 0.8^{a,b,c}$	$98.1 \pm 0.1^{c,d}$
30% MD+TRE	1.71 ± 0.14^{f}	$46.9 \pm 4.3^{b,c}$	97.3 ± 0.1^{e}

Results are expressed as mean ± standard deviation of at least two measurements from duplicate experiments. Means with different letters within a column indicate significant difference between samples at $P < 0.05$. MD: maltodextrin, TRE: trehalose.

5.4.2.5 Wettability and dispersibility

The ability of dried powders to reconstitute is important for their application in foods and this can be related to their wettability and dispersibility in water. Wettability is defined as the ability of powders to absorb water and become hydrated while dispersibility is the ability of powders to separate as individual particles without clumping in water (Thiengnoi et al., 2012). Therefore, wettability and dispersibility of powders are inter-related to each other. Powders with good dispersibility are easy to hydrate (good wettability) while powders with poor wettability are difficult to hydrate and contain clumps of particles (poor dispersibility).

In this study, wettability of powders varied between 3.9 and 27.6 minutes while dispersibility was between 40.2 and 81.7% (Table 5.5). The large discrepancy in the time taken to hydrate the powders suggested that the type of wall materials used can affect the wettability and dispersibility of the powders but are less affected by the concentration of wall materials used (Table 5.5). Powders produced with maltodextrin alone as wall materials had the highest wetting time required in the range of 22 to 27 minutes while wetting time was remarkably reduced to 4 to 5 minutes in powders made of trehalose alone (Table 5.5) although maltodextrin has a high solubility in water. According to Bhusari, Muzaffar & Kumar (2014), its larger molecular weight as wall materials can impede the rate of diffusion of water

molecules and will require a relatively longer time to hydrate when compared to trehalose which is a lower molecular weight sugar (Ohtake & Wang, 2011). Another possibility is that maltodextrin spray dried powders with high DE value are hydrophilic and can form clumps of particles in water with poor dispersibility (40 – 52%). This could result in prolonging the time for the powders to become hydrate during reconstitution. Moreover, the higher moisture content and water activity of the powders with only maltodextrin (Table 5.2) could indicate that the powders tended to be stickier with less surface area for contact with water and slower rehydration (Goula & Adamopoulos, 2008). In addition, the particle size of powders containing maltodextrin was the largest among the other samples (Table 5.3), therefore less surface area was available for water hydration and could have resulted in a higher wetting time.

Nevertheless, wettability and dispersibility were improved when powders containing maltodextrin were mixed with trehalose at a ratio of 1:1. The wetting time of powders containing a mixture of maltodextrin and trehalose was improved with wetting time ranging from 14 to 18 minutes and higher dispersibility values of 61 to 81% (Table 5.5).

Table 5.5 Wettability and dispersibility of spray dried powders prepared with different wall materials containing 10, 20 and 30% (w/w) dry matter.

Wall materials	Wettability (min)	Dispersibility (%)
10% MD	27.6 ± 5.02^{a}	40.2 ± 5.85^{d}
20% MD	25.8 ± 0.93^{a}	45.6 ± 1.00^{d}
30% MD	22.2 ± 1.45^{a}	51.9 ± 3.75^{c}
10% TRE	3.86 ± 0.62^{b}	61.8 ± 4.09^{b}
20% TRE	4.99 ± 0.60^{b}	81.7 ± 4.96^{a}
30% TRE	5.12 ± 1.32^{b}	76.7 ± 3.31^{a}
10% MD+TRE	14.7 ± 3.54^{c}	51.9 ± 4.82^{c}
20% MD+TRE	18.2 ± 1.32^{c}	60.3 ± 1.68^{b}
30% MD+TRE	14.3 ± 0.16^{c}	52.3 ± 0.62^{c}

Results are expressed as mean ± standard deviation of at least two measurements from duplicate experiments. Means with different letters within a column indicate significant difference between samples at $P < 0.05$. MD: maltodextrin, TRE: trehalose.

5.4.3 Reconstitution of spray dried nanoemulsions

Dried powders were reconstituted by dispersing the powders into a given amount of water. It should be noted that based on the moisture content of powders, different amounts of powders were used to reconstitute the emulsions to achieve the same solid content as their initial nanoemulsions with different wall material concentrations before spray drying. The brix readings of the nanoemulsions with different wall solutions ranged from 10 to 31%, depending on the wall concentrations (Table 5.6). The amount of powders added to reconstitute the emulsion dispersions were similar for the same concentration of wall materials used except the formulation made with 30% (w/w) maltodextrin (Table 5.6).

Table 5.6 Brix readings of nanoemulsions with wall solutions before and after spray drying process and the amount of powders added for reconstitution.

Wall materials	Brix (%)		Amount of powders added (g/mL water)
	Before spray drying	After spray drying	
10% MD	11.4 ± 0.0^{c}	11.5 ± 0.2^{c}	0.14 ± 0.00^{c}
20% MD	21.7 ± 0.1^{b}	21.1 ± 0.4^{b}	0.27 ± 0.00^{b}
30% MD	21.2 ± 0.0^{b}	21.5 ± 0.2^{b}	0.27 ± 0.01^{b}
10% TRE	10.0 ± 1.4^{c}	10.9 ± 1.3^{c}	0.13 ± 0.01^{c}
20% TRE	20.2 ± 0.0^{b}	20.5 ± 0.4^{b}	0.26 ± 0.01^{b}
30% TRE	29 ± 0.71^{a}	28.7 ± 0.6^{a}	0.41 ± 0.02^{a}
10% MD+TRE	11.5 ± 0.0^{c}	11.8 ± 0.1^{c}	0.14 ± 0.01^{c}
20% MD+TRE	21.0 ± 0.0^{b}	21.3 ± 0.1^{b}	0.27 ± 0.00^{b}
30% MD+TRE	30.6 ± 0.0^{a}	30.1 ± 0.1^{a}	0.43 ± 0.00^{a}

Results are expressed as mean ± standard deviation of at least two measurements. Means with different letters within a column indicate significant difference between samples at $P < 0.05$. MD: maltodextrin, TRE: trehalose.

The particle size and size distributions of reconstituted nanoemulsions containing different wall materials were similar to their initial nanoemulsions before spray drying. In all samples, small droplets with Z-Average around 80 nm were observed as shown in Table 5.7 and Figure 5.7. As expected, the ζ-potential of the reconstituted nanoemulsions at pH 7 was negatively charged between -31 and -47 mV (Table 5.7). This showed that the emulsion structure of nanoemulsions was not affected by spray drying. This is because some droplet coalescence may occur during spray drying due to the use of high shear stress that can force the droplets to come close together (Turchiuli et al., 2014). However, the fact that the droplet size of reconstituted nanoemulsions was similar as their initial nanoemulsions suggested

that spray drying did not affect the emulsion properties, possibly due to a relatively low amount of oil concentration coupled with very small droplet size, and can be used to produce dried powders to increase the storage stability. Similarly, Chen et al. (2013) observed the droplet size of reconstituted emulsions containing a mixture of fish oil, phytosterol esters and limonene (137 nm) to be similar to the droplet size of emulsions before spray drying (152 nm).

Table 5.7 Mean particle size (Z-Average) and ζ-potential of initial nanoemulsions and nanoemulsions after reconstitution prepared with different wall materials at pH 7.

Wall materials	Z-Average (d.nm)		ζ-potential (mV)	
	Initial	Reconstituted	Initial	Reconstituted
10% MD	79.3 ± 1.3^{a}	80.2 ± 1.5^{a}	$-38.2 \pm 1.4^{a,b}$	$-42.6 \pm 5.3^{c,d}$
20% MD	81.8 ± 1.3^{a}	$77.2 \pm 1.5^{a,b,c}$	$-40.6 \pm 3.2^{b,c}$	-42.0 ± 1.3^{c}
30% MD	79.4 ± 1.6^{a}	$79.9 \pm 1.5^{a,b}$	-34.0 ± 2.6^{a}	-31.5 ± 1.2^{a}
10% TRE	76.1 ± 3.7^{b}	73.0 ± 1.3^{c}	-34.7 ± 1.4^{a}	-47.0 ± 2.8^{d}
20% TRE	76.0 ± 0.4^{b}	$75.8 \pm 2.3^{a,b,c}$	$-39.8 \pm 3.5^{b,c}$	-37.2 ± 0.7^{b}
30% TRE	75.0 ± 2.2^{b}	$75.8 \pm 1.6^{a,b,c}$	$-38.2 \pm 2.0^{a,b,c}$	$-38.5 \pm 1.8^{b,c}$
10% MD+TRE	80.3 ± 10.3^{a}	$78.8 \pm 9.0^{a,b,c}$	$-41.5 \pm 4.0^{b,c}$	-37.3 ± 2.6^{b}
20% MD+TRE	78.8 ± 1.2^{a}	$73.6 \pm 2.2^{b,c}$	$-40.3 \pm 1.9^{b,c}$	-37.2 ± 0.6^{b}
30% MD+TRE	84.3 ± 1.5^{a}	$74.9 \pm 1.7^{a,b,c}$	-43.3 ± 3.0^{c}	$-40.4 \pm 1.8^{b,c}$

Results are expressed as mean ± standard deviation of at least two measurements from duplicate experiments. Means with different letters within a column indicate significant difference between samples at $P < 0.05$. MD: maltodextrin, TRE: trehalose.

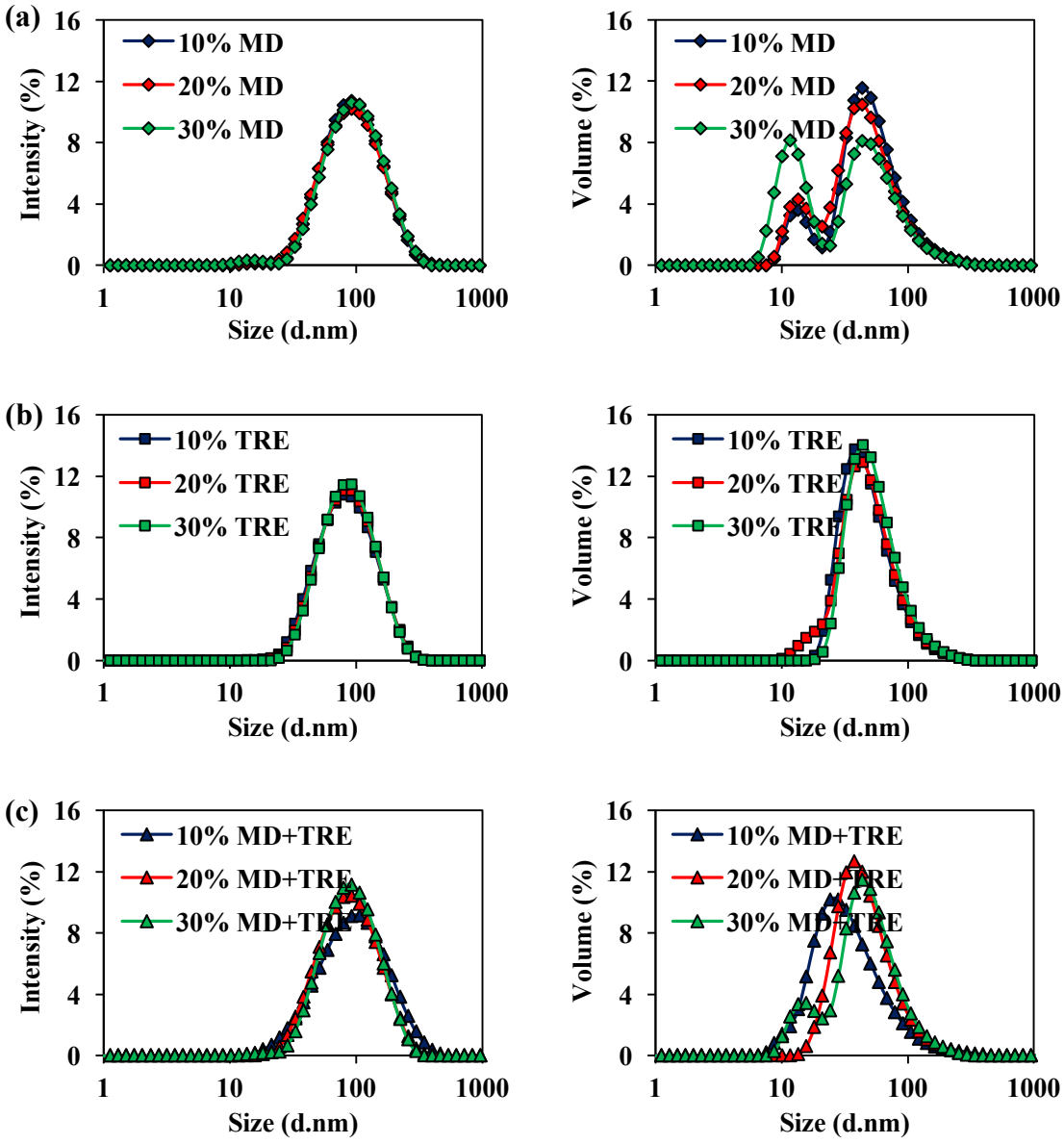

Figure 5.7 Particle size distributions (by intensity and volume) of reconstituted nanoemulsions prepared with (a) maltodextrin, (b) trehalose and (c) a 1:1 ratio of maltodextrin and trehalose at 10, 20 and 30% (w/w) dry matter. MD and TRE represent maltodextrin and trehalose, respectively.

5.4.4 Comparison of nanoemulsion powders produced by spray drying and freeze drying

In this section, the physicochemical properties of powders (20% (w/w) trehalose) produced by spray drying and freeze drying were examined. It should be mentioned that the results for spray dried powders were already presented in the previous section but they were included herein for comparison with respect to the freeze dried powders (Table 5.8). As shown in the table, spray dried powders had higher water content than freeze dried powders. The moisture content was 4.61 ± 0.24 and 1.50 ± 0.02% and water activity was 0.24 ± 0.03 and 0.04 ± 0.00, respectively, for spray dried and freeze dried powders. The difference in moisture content can be related to the drying process used. Many previous studies have shown that spray drying produced powders with lower moisture content than freeze dried powders (Franceschinis et al., 2015; Kuck & Noreña, 2016), presumably the high temperature of spray drying have a higher efficiency of heat transfer and could remove more water. However, Kuck & Noreña (2016) showed that encapsulation of grape phenolic extract by spray drying using gum Arabic, guar gum and polydextrose (10% solids) had lower moisture content and water activity (2.41 – 2.57%) than freeze drying (7.65 – 8.06%).

The particle size of powders was different as the freeze dried powders ($D_{4,3}$ ~ 203 μm) was much larger with a greater particle size distribution (i.e. a high span value) than the spray dried powders ($D_{4,3}$ ~ 10 μm) (Figure 5.8; Table 5.8). This can be attributed to the way the freeze dried sample was milled. In our case, only a simple food processor was used to obtain powder-like particles and no sieving was applied to obtain a certain particle size range. As a result, the powders showed a mixture of small and large particles with particle size ranging from 10.8 to 455.8 μm. From the results, the bulk density of freeze dried powders (1.12 g/mL) was much higher than that of spray dried powders (0.36 g/mL) The high polydispersity of the freeze dried sample could be caused by the smaller particles filling the void spaces among the the larger irregular shaped particles to achieve better packing which resulted in a higher bulk density. The SEM images showed that the freeze dried powders were irregularly shaped (as a result of the grinding) and the small particles were able to fill spaces between the large particles and packed densely as compared to spray dried sample (Figure 5.9). However, Franceschinis et al. (2014) reported

similar bulk density for both spray dried and freeze dried blackberry powders containing maltodextrin or a mixture of maltodextrin and trehalose (1:1 ratio) (0.34 – 0.46 g/mL). The lower bulk density of the spray dried powders in this study could be partly due to the void spaces within the spherical particles as observed in the SEM micrographs.

Table 5.8 Properties of spray dried and freeze dried nanoemulsion powders containing 20% (w/w) trehalose.

Properties	Spray dried powders	Freeze dried powders
Moisture content (%)	4.61 ± 0.24	1.50 ± 0.02
Water activity	0.24 ± 0.03	0.04 ± 0.00
Particle size		
- $D_{3,2}$ (µm)	5.72 ± 0.33	27.0 ± 1.63
- $D_{4,3}$ (µm)	9.77 ± 2.85	202.9 ± 13.4
Span	1.62 ± 0.15	4.13 ± 0.38
Bulk density (g/mL)	0.36 ± 0.03	1.12 ± 0.01
Surface oil (mg/100g powder)	55.7 ± 4.96	156.2 ± 20.7
Encapsulation efficiency (%)	97.8 ± 0.21	93.7 ± 0.87

Results for each sample are expressed as mean ± standard deviation of at least two measurements from duplicate experiments.

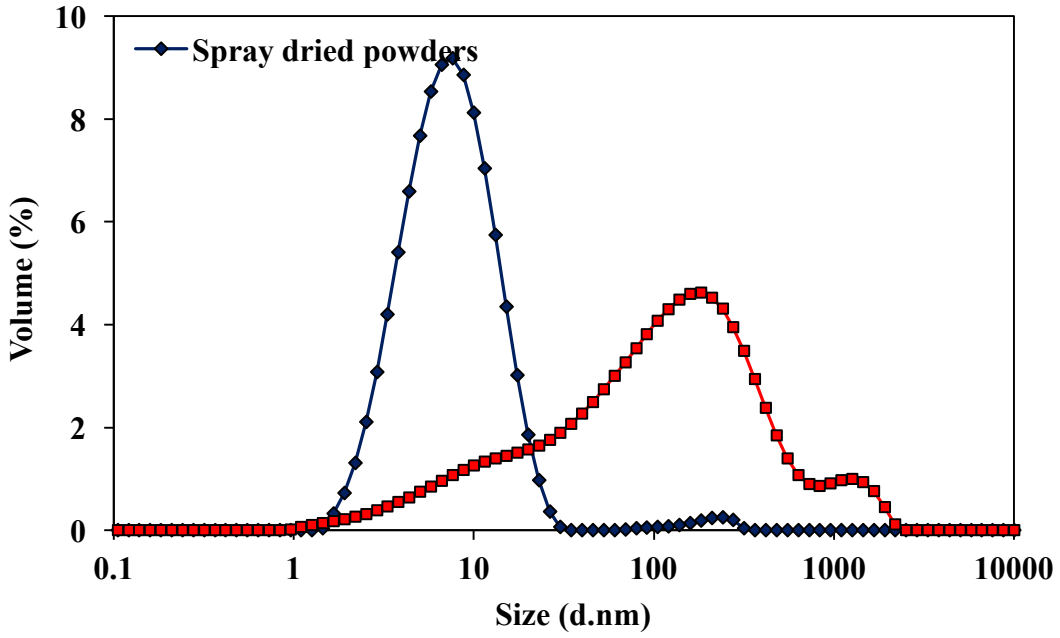

Figure 5.8 Particle size distributions of spray dried and freeze dried nanoemulsion powders containing 20% (w/w) trehalose.

Further analysis on the SEM images showed that the freeze dried powders were porous with some openings on the surface (Figure 5.9b). This would be the reason that freeze dried powders had higher surface oil and lower encapsulation efficiency (Table 5.8) as the solvent will be more likely to reach the interior of the particles and extract more oil through the openings at the surface of the particles. Certainly, this is also one of the disadvantages associated with freeze dried powders. The irregular shaped structure characteristics of freeze dried powders were similar to those observed by Franceschinis et al. (2014) and Kuck & Noreña (2016). More often, the formation of porous structure or cracked surfaces resulted in higher susceptibility of materials to chemical degradation (Kuck & Noreña, 2016).

(a) Spray drying of 20% (w/w) trehalose

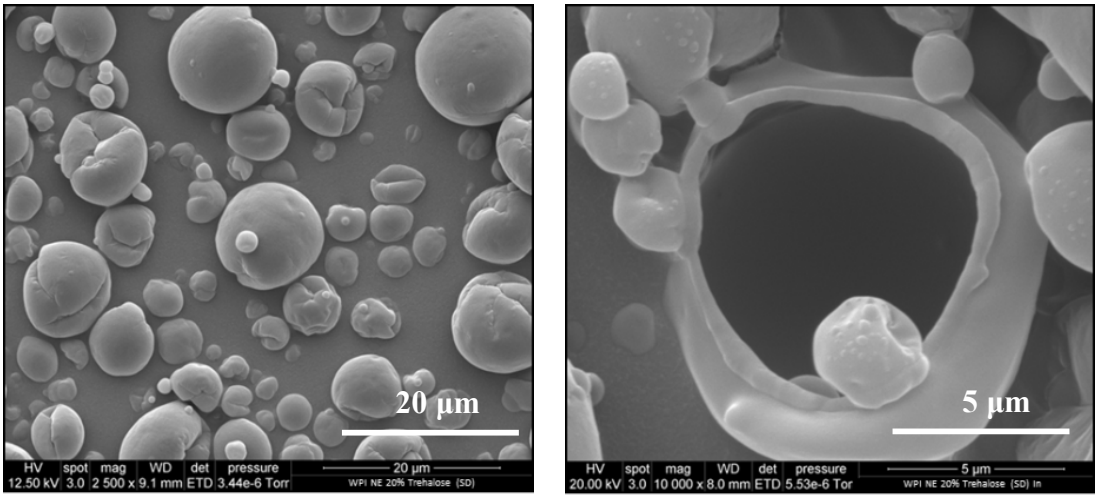

(b) Freeze drying of 20% (w/w) trehalose

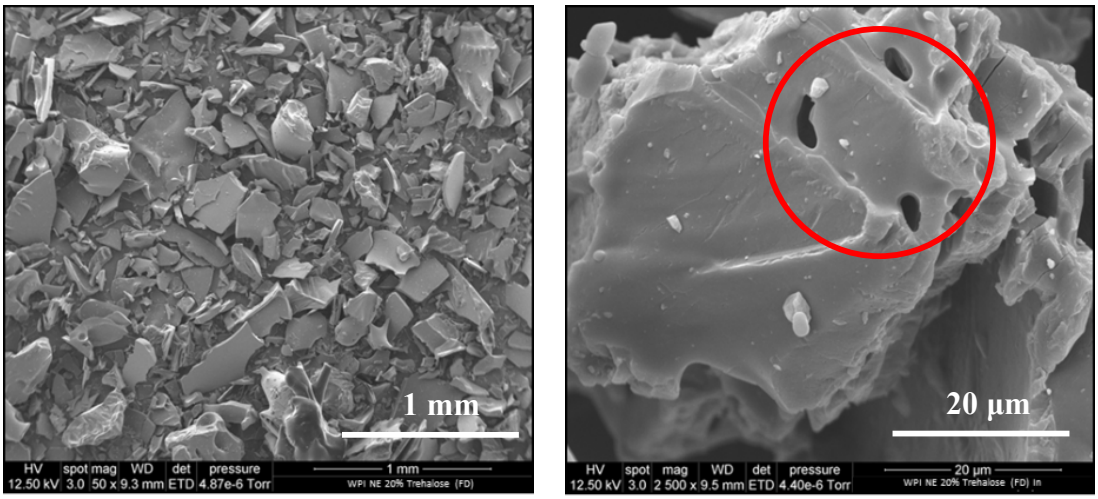

Figure 5.9 SEM images (outer and inner structures) of dried nanoemulsion powders containing 20% (w/w) trehalose produced by different methods: (a) spray drying and (b) freeze drying.

The wettability of freeze dried powders (3 seconds) was much faster than spray dried powders (5 minutes) (Table 5.9). The good wetting ability of freeze dried powders as compared to spray dried powders can be attributed to the fact that the freeze dried powder particles contained more porous structure that can absorb water more easily. Furthermore, freeze dried powders contained large particles with no internal hollow structure that could allow water to pass through and enter the pores of particles to increase their wettability. Also, the larger particles of freeze dried powders were higher in density (heavier) and tended to sink in water faster which would make their wetting and reconstitution easier. Similarly, the freeze dried powders displayed good dispersibility in water with a high value of 96.2% while the spray dried powders had a value of 81.7%. In general, powders with good dispersibility are desired as the powders are readily dispersed in water and do not form clumps of particles.

Table 5.9 Wettability and dispersibility of spray dried and freeze dried nanoemulsion powders containing 20% (w/w) trehalose.

Properties	Spray dried powders	Freeze dried powders
Wettability (minutes)	4.99 ± 0.60	0.05 ± 0.00
Dispersibility (%)	81.7 ± 4.96	96.2 ± 5.02

Results are expressed as mean ± standard deviation of at least two measurements from duplicate experiments.

The spray dried and freeze dried powders were reconstituted by dispersing the powders in water. As shown in Table 5.10, the properties of the reconstituted nanoemulsions were similar to their initial nanoemulsions with wall solutions before spray drying. The drying methods did not have any effect on the properties of the nanoemulsions as they contained small droplets less than 80 nm in diameter with ζ-potential value of around -40 mV at pH 7. The particle size distributions showed that the reconstituted emulsions were monodispersed (Figure 5.10a) except the volume distribution of freeze dried emulsions (Figure 5.10b).

Table 5.10 Mean particle size (Z-Average) and ζ-potential of initial nanoemulsions and nanoemulsions after reconstitution at pH 7.

Drying methods	Z-Average (d.nm)		ζ-potential (mV)	
	Initial	Reconstituted	Initial	Reconstituted
Spray drying	76.0 ± 0.4	75.8 ± 2.3	-39.8 ± 3.5	-37.2 ± 0.7
Freeze drying		78.3 ± 2.3		-43.9 ± 1.3

Results are expressed as mean ± standard deviation of at least two measurements from duplicate experiments.

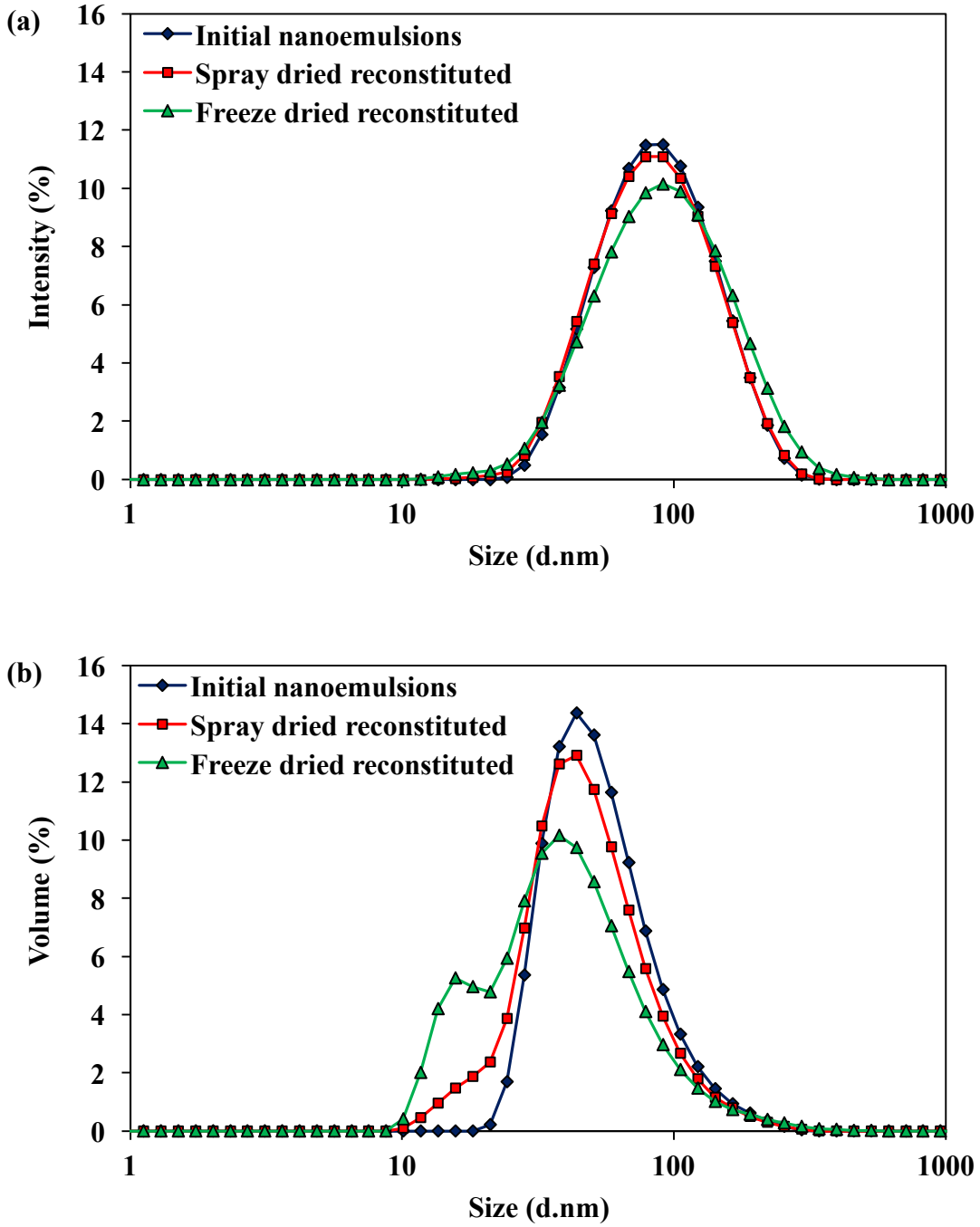

Figure 5.10 Particle size distributions by (a) intensity and (b) volume of initial nanoemulsions and reconstituted nanoemulsions containing 20% (w/w) trehalose produced by spray drying or freeze drying.

5.5 Conclusions

In this work, nanoemulsions containing 10, 20 and 30% (w/w) maltodextrin, trehalose or in combination of both materials were spray dried. Spray drying of the nanoemulsions produced fine particles with high encapsulation efficiencies. However, the properties of the powders were dependent on the wall materials used. Inspite of their differences in powder properties, dried powders with different wall materials showed no change in nanoemulsions properties when reconstituted in water. In terms of drying method, freeze drying produced powders with better physical properties but they were not superior to spray drying with slightly lower encapsulation efficiencies. This study indicated that drying of nanoemulsions with suitable wall materials would produce dried powders to improve shelf stability, ease of handling and increased its application in many food systems.

Chapter Six:

Interactions between WPI and Lactoferrin in Aqueous Solution and Interfacial Structures monitored by QCM-D

6.1 Abstract

In this work, the interactions between two oppositely charged proteins in solution, namely WPI and lactoferrin were investigated for uses in the design of multilayer nanoemulsions. The results of ζ-potential and turbidity measurements indicated that these two proteins interact strongly via electrostatic attraction at pH 6. Quartz crystal microbalance with dissipation (QCM-D) was employed to study the adsorption behaviour and the formation of different interfacial structures of these two proteins onto a model hydrophobic surface that mimics the oil-water interface in emulsion droplets. Sequential addition of WPI and lactoferrin (or vice versa) formed thin and rigid protein bi-layers (8 – 10 nm). However, a viscous and thick surface layer (101 nm) was formed by the protein complex using a mixture of WPI and lactoferrin (1:1 ratio). The current study is the starting point for understanding the formation of emulsions with different interfacial structures made of WPI and lactoferrin that are oppositely charged protein molecules.

6.2 Introduction

Like conventional emulsions, the structure and composition of the oil-water interface of nanoemulsions can be manipulated to form emulsions with better performance and novel functionalities as microencapsulation systems for bioactive compounds (Skirtach, Yashchenok & Möhwald, 2011; Trojer, Nordstierna, Nordin, Nydén & Holmberg, 2013; Trojer, Nordstierna, Bergek, Blanck, Holmberg & Nydén, 2015). This can be achieved by depositing oppositely charged biopolymers at the interface of oil droplets using an electrostatic LBL deposition method to form multilayer emulsions (Sukhorukov, Caruso, Davis & Möhwald, 1998; Guzey & McClements, 2006; Bouyer, Mekhloufi, Rosilio, Grossiord & Agnely, 2012). Alternatively, electrostatic complexes of two oppositely charged biopolymers can be used to form mixed layer emulsions (Bouyer et al., 2012; Tokle et al., 2012).

Examples of multilayer and mixed layer emulsions have been reported in the literatures, e.g. caseinate/sodium alginate multilayer emulsions (Pallandre, Decker & McClements, 2007); β-lactoglobulin/lactoferrin multilayer emulsions (Ye & Singh, 2007); β-lactoglobulin/lactoferrin multilayer and mixed layer emulsions (Tokle et al., 2012) and WPI/pectin mixed layer emulsions (Mao, Boiteux, Roos & Miao, 2014).

These studies have shown that modification of interfacial properties can influence the stability of emulsions under environmental stresses (such as pH, ionic strength and temperature) and affect the chemical and oxidative stability of encapsulated components in the oil droplets. However, the majority of these studies have been focused on conventional emulsions containing relatively large droplet size and the mechanism underlying the complex formation and the interfacial structure of small oil droplets has not been fully understood. This is interesting because the interfacial characteristic of nanoemulsions is different from conventional emulsions. The small oil droplets of nanoemulsions are being surrounded by a thicker interfacial layer whereas conventional emulsions have a thinner interfacial layer relative to their respective droplet size (McClements & Rao, 2011). As a result, the interfacial properties of nanoemulsions have a greater influence on the overall particle characteristics such as physical stability, particle interactions and stability and digestibility of emulsions.

Formation of multilayer interfaces involves species (e.g. polyelectrolytes) having different pI in a pH dependent process driven by electrostatic interactions (Guzey & McClements, 2006; Ye & Singh, 2007). In the case of micron sized emulsions, the composition and structure of the biomolecules (e.g. proteins) adsorbed at the droplet surface can be determined by centrifugation, followed by gel electrophoresis of the cream layer (Ye & Singh, 2007; Sarkar, Goh, Singh & Singh, 2009). However, such protocol cannot be easily employed with nanoemulsions which are characterised by kinetically stable small oil droplets that cannot be readily separated by centrifugal forces. The interfacial structures of nanoemulsions can be studied through indirect techniques such as surface plasmon resonance (SPR), QCM-D, atomic force microscopy, ellipsometry, dual polarisation interferometry, optical tensiometry and dilatational rheoloy (Boddohi, Almodóvar, Zhang, Johnson & Kipper, 2010; Lundin, Elofsson, Blomberg & Rutland, 2010; Krivosheeva, Dėdinaite & Claesson, 2012; Trojer, Mohamed & Eastoe, 2013; Berendsen, Güell, Henry &

Ferrando, 2014). For example, Berendsen et al. (2014) used SPR technique to study the formation of multilayer emulsions with different interfacial structures, e.g. mono-layer, bi-layer and complex layer.

Interestingly, QCM-D has not been well used to study the interfacial structures of protein layers in emulsions. Particularly, QCM-D is well-suited to measure surface adsorption and structural properties of adsorbed layers. This technique enables simultaneous measurement of the resonance frequency of an oscillating sensor and decay of the oscillation (i.e. dissipation) which are related to the amount of adsorbed layer and its viscoelastic properties, respectively (Höök, Kasemo, Nylander, Fant, Sott & Elwing, 2001; Liu & Kim, 2009; Lundin et al., 2010). This surface characterisation technique has been successfully used to study adsorption of proteins and formation of multilayers on different surfaces for biomedical and other applications (Lundin et al., 2010; Craig, Bordes & Holmberg, 2012; Chandrasekaran, Dimartino & Fee, 2013). Still, QCM-D has not been employed as a complementary technique to study protein adsorption at the O/W interface for emulsion systems.

In this study, the interactions of WPI and/or lactoferrin at an oil-water interface were studied in a model system by depositing aqueous protein solutions to a gold hydrophobic surface using QCM-D technique. This model system was used to simulate the adsorption of proteins on the hydrophobic surface of oil droplets in aqueous solution, allowing the monitoring of the adsorption of different layers and their resulting structural characteristics on surfaces.

6.3 Materials and Methods

6.3.1 Materials

The proteins (WPI and lactoferrin) used are as listed in Chapter 3 (Section 3.1). 1-hexadecanethiol (≥ 95% GC) was purchased from Sigma Chemical Co. (St. Louis, MO, USA). Ammonia (25%) and hydrogen peroxide (30%) were purchased from Sigma Aldrich (Sydney, Australia). All the chemicals used were of analytical grade.

6.3.2 Preparation of protein solutions

Protein solutions containing 1% (w/w) WPI or lactoferrin were prepared in Milli Q water (Millipore, 18.2 MΩ cm at 25°C) under gentle stirring for at least 3 hours at room temperature. The pH of protein solutions was adjusted with HCl or NaOH solutions to the pH value required in the experiment (ranging from 2 to 10). A mixture of WPI and lactoferrin (1:1 ratio) was also prepared by mixing equal volumes of both protein solutions at pH 6.

6.3.3 Analysis of protein solutions

The ζ-potential of protein solutions and protein mixtures was determined in disposable folded capillary cells (Model DTS1070) using a Malvern Zetasizer Nano ZS (Malvern Instruments, Worcestershire, UK). The samples were analysed at 25^{o}C without further dilution. The mesurements were carried out in triplicates on two independent samples. The details of ζ-potential measurements are described in Chapter 3 (Section 3.3.2). The optical density (O.D.) of individual protein solutions and protein mixtures of WPI and lactoferrin was measured at 600 nm using a UV-visible spectrophotometer (SPECTROstar^{Nano}, BMG LABTECH GmbH, Ortenberg, Germany) in a 1 cm path length optical cell against a water reference.

6.3.4 Quartz crystal microbalance with dissipation (QCM-D) measurements

6.3.4.1 Preparation of hydrophobic gold surfaces

AT-cut piezoelectric quartz crystals (Q-Sense, ATA Scientific, Tarren Point, NSW, Australia) coated with gold and having a fundamental frequency of 4.95 Hz were used. The gold sensors were cleaned with "Piranha" solution (a mixture of 5:1:1 ratio of Milli Q water, 25% ammonia and 30% hydrogen peroxide) at 75^{o}C for 10 min and rinsed with hot Milli Q water. The sensors were dried with nitrogen gas and placed in a UV/ozone chamber (BioForce Nanosciences, USA) for 10 minutes. After cleaning and drying the sensors, the gold surface was rendered hydrophobic by introducing a self-assembled monolayer (SAM) as per the protocol reported by Lebec, Landoulsi, Boujday, Poleunis, Pradier & Delcorte (2013) and Mivehi, Bordes & Holmberg (2013). Briefly, the cleaned gold surface was immersed overnight in a solution of 2 mM hexadecanethiol in ethanol and then rinsed thoroughly with ethanol to remove unadsorbed hexadecanethiol. The contact angle of the modified

sensor surface was measured using the drop analysis in Image J (Version 1.47, National Institutes of Health, USA).

6.3.4.2 QCM-D experiment

Protein adsorption on the SAM hydrophobic surfaces was carried out using a QCM-D system (Q-Sense E4 system, Q-Sense, ATA Scientific, Tarren Point, NSW, Australia) equipped with a temperature controlled measuring chamber and a peristaltic pump (ISMATEC® IPC High Precision Multi channel Dispenser, IDEX Health & Science, Germany). Each QCM-D experiment started with pre-equilibration with Milli Q water to obtain a signal baseline before addition of protein solutions. The test solutions were then fed to the SAM hydrophobic QCM-D sensors at a flow rate of 0.1 mL/min. All the experiments were measured at 22 ± 2^{o}C.

Protein bi-layers were obtained at a given pH in the range of 2 to 10 by successive addition of the individual protein solution until equilibrium, i.e. when stable frequency and dissipation signals were reached. Poorly adsorbed or unadsorbed proteins were removed by intermediate rinsing steps with Milli Q water at the same pH as protein solution. The adsorption of protein complex was studied at pH 6 by feeding the protein mixture until equilibrium, followed by a rinse with Milli Q water.

6.3.4.3 Data analysis of QCM-D results

In the QCM-D experiments, the changes in the resonance frequency and dissipation were recorded at several overtones and analysed to calculate the mass adsorbed using the Sauerbrey or the Kevin-Voigt model using Q-Tools™ software (version 3.0.12, Biolin Scientific AB, Sweden). In the simplest case of a thin, homogeneous and rigidly adsorbed layer, the frequency shift of the oscillating quartz crystal is linearly related to the mass adsorbed on the crystal surface according to the Sauerbrey model (Sauerbrey, 1959):

$$\Delta m = -C\frac{\Delta f}{n} \qquad (6.1)$$

where Δm is the adsorbed mass, Δf is the frequency shift at the overtone number, n and C is the mass sensitivity constant of the quartz crystal. For the 4.95 MHz sensor used in this study, the constant (C) is equal to 17.7 ng/cm^2 Hz (Malmström, Agheli, Kingshott & Sutherland, 2007).

The thickness of the adsorbed layer, h_{eff}, can be calculated from the following equation:

$$h_{eff} = \frac{\Delta m}{\rho_{eff}} \qquad (6.2)$$

where ρ_{eff} is the effective surface density of adsorbed protein layer.

However, when the adsorbed film displays strong viscoelastic properties, the Sauerbrey equation underestimates the actual mass adsorbed (Liu & Kim, 2009). In this case, the frequency and dissipation data collected at different overtones are modelled using the software based on the Kevin-Voigt model (Voinova, Rohahl, Jonson & Kasemo, 1999). According to this model, the viscoelastic properties of the adsorbed protein layer and the QCM-D responses (Δf and ΔD) can be expressed using the equations as follows (Liu & Kim, 2009):

$$\Delta f \approx -\frac{1}{2\pi\rho_0 h_0}\left\{\frac{\eta_3}{\delta_3} + h_1\rho_1\omega - 2h_1\left(\frac{\eta_3}{\delta_3}\right)^2 \frac{\eta_1\omega^2}{\mu_1^2+\omega^2\eta_1^2}\right\} \qquad (6.3)$$

$$\Delta D \approx \frac{1}{\pi f\rho_0 h_0}\left\{\frac{\eta_3}{\delta_3} + 2h_1\left(\frac{\eta_3}{\delta_3}\right)^2 \frac{\eta_1\omega^2}{\mu_1^2+\omega^2\eta_1^2}\right\} \qquad (6.4)$$

where ρ_0 and h_0 are the density and thickness of the quartz crystal, η_3 and ρ_3 are the viscosity and density of the bulk fluid, respectively, δ_3 is the viscous penetration depth of the shear wave in the bulk fluid and ω is the angular frequency of the oscillation. The density, viscosity, shear elastic modulus and thickness of the adsorbed protein layer, i.e. ρ_1, η_1, μ_1 and h_1, respectively, were fit to the experimental values of Δf (frequency shift) and ΔD (dissipation shift) at three different overtones (5^{th}, 7^{th} & 9^{th}). The fluid viscosity (η_3) and fluid density (ρ_3) were assumed to be 0.001 kg/m.s and 1000 kg/m^3, respectively (Liu & Kim, 2009).

6.3.5 Data analysis

All experiments were carried out at least in duplicates using freshly prepared samples. All statistical analysis was done using MS-Excel 2010 package. The results are reported as means and standard deviations.

6.4 Results and Discussion

6.4.1 Characteristics of individual protein solutions and their mixture

The knowledge of the characteristics of aqueous solutions containing the proteins under investigation (i.e. WPI and lactoferrin) is fundamentally important to elucidate the structure of the resulting interfacial layer at the oil-water interface of nanoemulsions. The ζ-potential of proteins was measured at different pH values ranging from 2 to 10. As reasonably expected the ζ-potential of WPI was positive at acidic pH and turned negative at basic pH (Figure 6.1). The results obtained in this study were similar to a study on the effect of pH on the ζ-potential of protein solutions (e.g. β-lactoglobulin and/or lactoferrin) reported by Tokle et al. (2012). The point of zero charge (or pI) for WPI was 4.9, a value matching previous results reported in the literatures (Salminen & Weiss, 2013; Berendsen et al., 2014). An increase in the turbidity of protein solutions containing WPI related to protein aggregation was apparent at pH close to the pI (pH 4.5 – 5.5) due to loss of electrostatic repulsion (Figure 6.2).

On the other hand, the pI of lactoferrin molecules was around 8.8 because of its high concentration of basic amino acids (Steijns & van Hooijdonk, 2000; Baker & Baker, 2005). The lactoferrin molecules were however stable to aggregation across the pH range studied with no noticeable change in solution turbidity even at the pI of the molecules (Figure 6.2). It is known that lactoferrin contains amphiphilic moieties and exists as a mixture of positively charged monomers and negatively charged aggregates in the bulk solution (Mela, Aumaitre, Williamson & Yakubov, 2010). At pH below the pI, lactoferrin is dominated by the monomers and are positively charged. As the pH approaches the pI, the monomers decrease and the aggregates increase. However, because the aggregates are negatively charged there are intra-molecular repulsive forces for the lactoferrin solution to remain clear which explained why lactoferrin solution is clear at the pI.

When the solution pH is at the intermediate range between the pI for WPI and lactoferrin, the two proteins possess opposite charge and will interact with each other through electrostatic forces. To assess the pH at which the two proteins would interact strongly, the ζ-potential of a mixture of WPI and lactoferrin was measured across the same pH range (Figure 6.1). The results clearly indicated that the point of

zero net charge for the protein mixture was approximately between pH 5.5 and 6 which corresponds to the pH at which the charge difference between the two individual proteins was the highest. Under these conditions, strong electrostatic interactions between the oppositely charged proteins were expected. Interactions of the two oppositely charged proteins led to the formation of complexes as evidenced by an increase in turbidity observed at pH 5.5 and 6 (Figure 6.2). This corroborated with previous findings that complex coacervation of β-lactoglobulin and lactoferrin occurred in the pH range of 5.7 to 6.2 (Yan, Kizilay, Seeman, Flanagan, Dubin, Bovetto, Donato & Schmitt, 2013). Based on the results, all protein samples considered henceforth in this work were prepared at pH 6 to maximise the electrostatic interactions between WPI and lactoferrin.

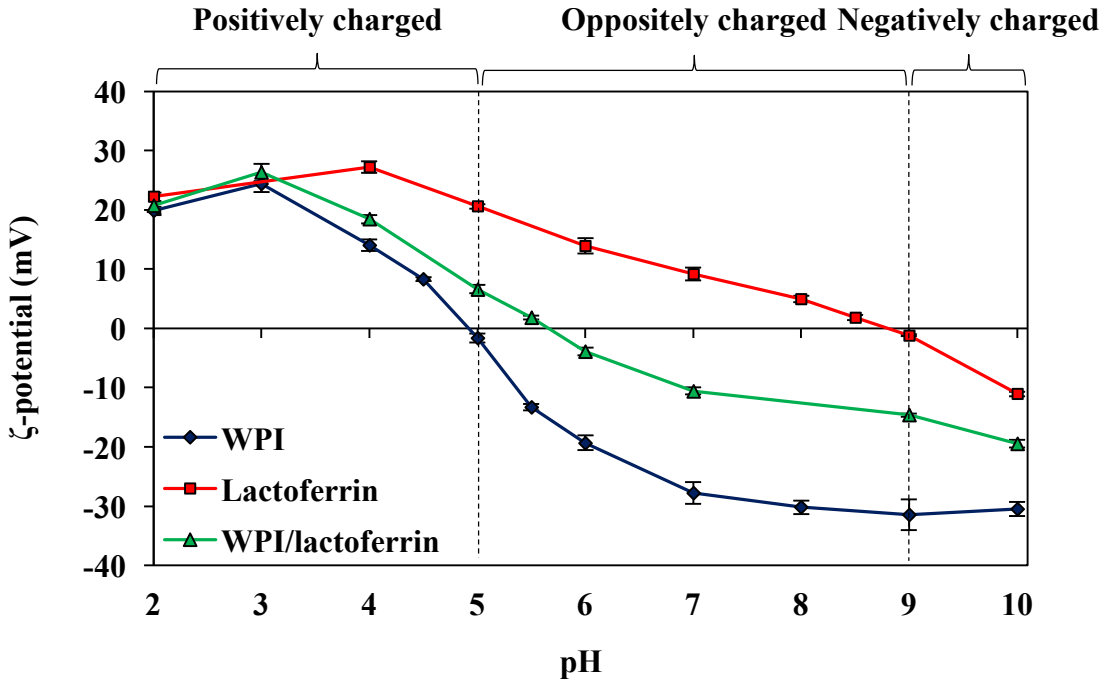

Figure 6.1 Mean ζ-potential of 1% (w/w) protein solutions of WPI and lactoferrin and 1% (w/w) of protein mixtures of WPI and lactoferrin (1:1 ratio) at different pH values. Data are presented as the mean of two independent measurements with triplicate (n=6) and error bars represent the standard deviation.

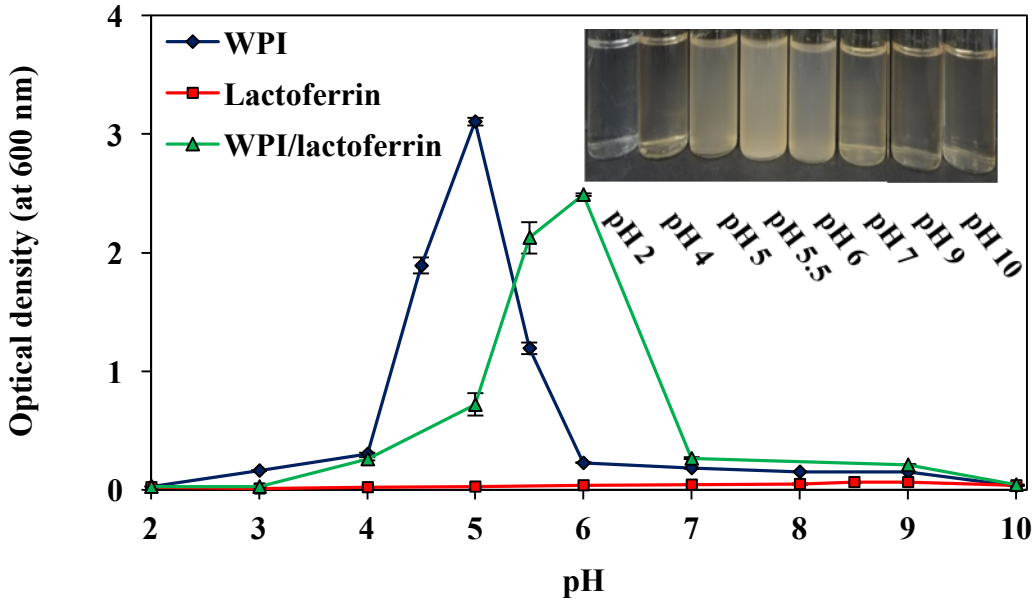

Figure 6.2 Mean optical density (at 600 nm) of 1% (w/w) protein solutions of WPI and lactoferrin and 1% (w/w) protein mixtures of WPI and lactoferrin (1:1 ratio) at different pH values, including a photograph of the protein mixtures. Data are presented as the mean of two independent measurements with triplicate (n=6) and error bars represent the standard deviation.

6.4.2 Adsorption of protein bi-layers on hydrophobic surface

Since WPI and lactoferrin are capable of electrostatic interactions under a certain pH range, they can assemble a variety of different emulsion interfacial structures such as single layer, bi-layer and mixed layer as described in Section 2.4 (Chapter 2). Until now, few works have reported the characteristics of protein coatings at the oil-water interface, which constitute important data for the design of interfacial structures and allow manipulation of the functionality of nanoemulsions.

As a first step, the surface adsorption and structure of protein layers on surfaces was studied by QCM-D to indirectly obtain information about the behaviour of proteins at the oil-water interface that may occur in emulsions. The gold coated quartz crystals used in the QCM-D experiments were modified using an alkanethiol molecule (1-hexadecanethiol) to create a hydrophobic layer which can be used to mimic the oil-water interface in real emulsions. This molecule has been used in the formation of a SAM hydrophobic surface and contains a thiol group $(CH_3CH_2)_{14}CH_2SH$ that can be immobilised onto gold surfaces through a covalent bond (Ito, Arai, Hara & Noh, 2009; Nováková, Oriňáková, Oriňák, Hvizdoš & Fedorková, 2014). It has been shown that the formation of SAM of alkyl thiols containing CH_3 terminated groups is hydrophobic and that protein adsorption on the modified surfaces is driven by hydrophobic interactions (Lebec et al., 2013). In this study, a SAM hydrophobic layer to mimic the oil-water interface in real emulsions was formed on gold surfaces. The measured contact angle of the SAM modified QCM-D sensors was 107.1 ± 0.5^o indicating a hydrophobic layer was formed (contact angle of unmodified gold surface was 21.2 ± 2.3^o).

The protein solutions were prepared and used in pH conditions in which they were oppositely charged. At pH 6, WPI has a negative charge of -19.3 ± 1.2 mV while the ζ-potential of lactoferrin is +14.0 ± 1.3 mV (Figure 6.1). The two proteins can thus interact with each other via electrostatic interactions. The individual protein solutions were adsorbed to the gold surface to form a mono-layer and the bi-layer was formed by adding the other oppositely charged protein solution. Based on the order of protein addition, the positively charged lactoferrin molecules were adsorbed to a negatively charged WPI layer denoted as "WPI-LF" or the negatively charged WPI molecules were adsorbed to a positively charged lactoferrin layer denoted as "LF-WPI" in the experiment.

Using QCM-D technique, the adsorption of proteins on the modified hydrophobic surface was monitored and the frequency and dissipation shifts were recorded as a function of time. Figure 6.3 reports the QCM-D results for the sequential adsorption of WPI and lactoferrin (WPI-LF sample) while Figure 6.4 reports the analogous data where lactoferrin and WPI were instead sequentially adsorbed (LF-WPI sample). The qualitative trend of the two experiments was very similar, regardless of the sequence of protein loading to the QCM-D. When the first protein was fed, a rapid decrease in the frequency signal mirrored by a simultaneous dissipation increase was observed. This result is consistent with rapid adsorption of the protein molecules to the bare hydrophobic surface of the quartz sensor. Protein adsorption continued to occur at a slower rate until adsorption-desorption equilibrium was reached, as indicated by a corresponding plateau in the frequency and dissipation signals. During the first washing step with water, the frequency slightly increased while the dissipation returned back to the baseline. This condition is clearly associated with the removal of loosely bound proteins at the surface (Messina, Satriano & Marletta, 2009). The remaining adsorbed layer consisted of protein molecules rigidly and irreversibly bound to the hydrophobic surface of the QCM-D sensor. This layer constituted a priming layer for subsequent adsorption of the oppositely charged protein. Similar phenomena was observed when the second protein solution was added and subsequently washed, i.e. an initial frequency decrease and dissipation increase during protein loading (formation of second protein layer) followed by partial frequency regain and dissipation going to zero during washing (removal of loosely viscoelastic layer of proteins and formation of a rigid irreversible layer).

The energy dissipation can be defined as the energy loss of adsorbed layer during oscillation and provides information about the viscoelastic properties of the adsorbed layer (Liu & Kim, 2009; Craig et al., 2012). It is suggested that little energy dissipation is associated to a thin, rigid film but higher energy is dissipated for a viscoelastic layer (Liu & Kim, 2009; Reviakine, Johannsmann & Richter, 2011). While the protein solutions were initially fed into the QCM-D sensors, a relatively high dissipation signal was apparent, indicating that the adsorbed layer had a viscous component. However, this viscous layer was loosely bound and removed during rinsing, thus exposing a layer of rigidly adsorbed protein. This observation holds true

for both the first and the second layer of proteins, irrespective of the order in which the proteins were fed to the sensor. Mivehi et al. (2013) proposed a trade-off of 1 x 10^{-6} in the dissipation signal to distinguish between rigid and viscoelastic layers, while Reviakine et al. (2011) stated that the adsorbed layer can be assumed rigid when $\Delta D/(-\Delta f/n)$ << 4 x 10^{-7} Hz^{-1}. Both conditions were satisfied for the residual protein layers following water wash, therefore the protein films were considered rigid and the adsorbed mass was calculated using the Sauerbrey model given in equation (6.1).

The layer thickness of the individual proteins of WPI and lactoferrin was 4.95 and 6.97 nm, respectively (Table 6.1) and they are consistent with the dimensions of the proteins reported in the literatures. It has been reported that whey proteins have a rigid, compact structure and β-lactoglobulin (which represents a majority of whey proteins) exists as dimers at neutral pH with a diameter of 4.8 nm based on light and X-ray scattering measurements (Jost, 1993; Baldini, Beretta, Chirlco, Franz, Maccioni, Mariani & Spinozzi, 1999). On the other hand, the dimensions of lactoferrin based on lattice cell parameter data are ~ 4 x 5.1 x 7.1 nm (Mela et al., 2010). The obtained value of lactoferrin layer (6.97 nm) corresponds well to the longest axis of lactoferrin molecule, indicating that a well-formed mono-layer was adsorbed on the hydrophobic surface of the QCM-D sensor.

QCM-D results for the formation of the secondary layer were significantly different for the two bi-layers considered in this study. For WPI-LF bi-layer, a large frequency shift occurred following lactoferrin adsorption (Figure 6.3), suggesting that lactoferrin molecules were deposited on the WPI-coated surface. The thickness of this secondary layer was of 5.12 nm, consistent with the size of lactoferrin molecules, leading to a bi-layer having total thickness of 10.1 nm (Table 6.1). In contrast, addition of WPI solution to the LF-WPI sample displayed a relatively small frequency shift, with an additional layer of 1.49 nm deposited following loading of the WPI solution. According to Trojer, Holmberg & Nydén (2012), desorption can occur when electrostatic interactions between the adsorbed layers are weaker than hydrophobic interactions between the surface and first layer. In this case, WPI competes for the adsorption onto the hydrophobic SAM and partially displaces the previously adsorbed lactoferrin molecules, with the formation of a mixed proteinaceous layer. Similar results have been observed by Wahlgren, Arnebrant &

Paulsson (1993) using *in situ* ellipsometry at pH 7 for the sequential adsorption of lactoferrin and β-lactoglobulin (one of the main proteins in WPI) on silica surfaces. The authors in fact reported that a large amount of lactoferrin was deposited on pre-adsorbed β-lactoglobulin, but detected a decrease in the adsorbed mass when β-lactoglobulin was reversely added to a lactoferrin adsorbed layer.

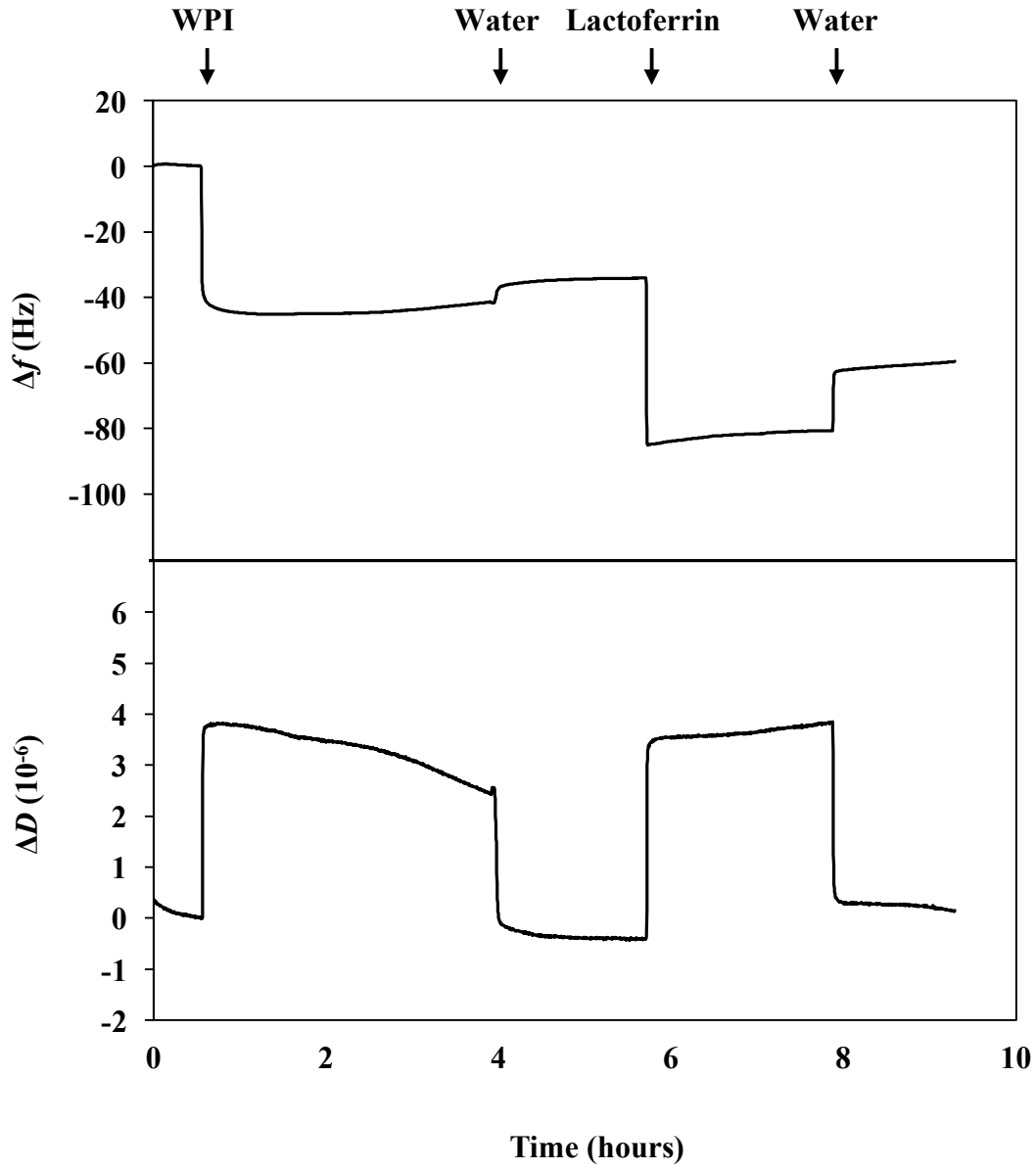

Figure 6.3 Frequency and dissipation shift versus time at 7th overtone for the sequential adsorption of WPI first and then lactoferrin on the quartz crystal surface with alternate rinse intervals with water at pH 6.

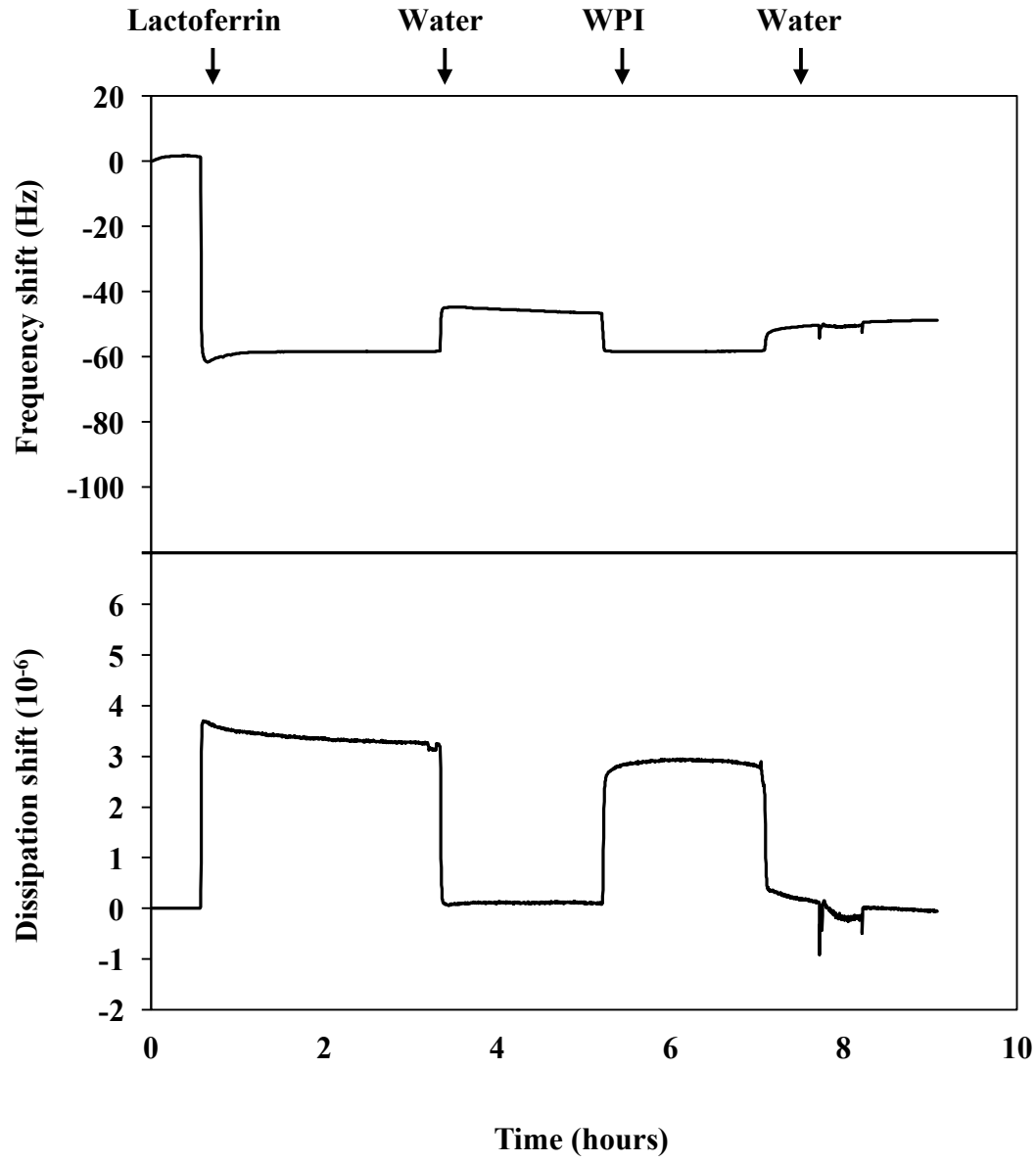

Figure 6.4 Frequency and dissipation shift versus time at 7th overtone for the sequential adsorption of lactoferrin first and then WPI on the quartz crystal surface with alternate rinse intervals with water at pH 6.

Table 6.1 Thickness of different interfacial structures of WPI and lactoferrin adsorbed on SAM modified hydrophobic gold surface at pH 6. Data are presented as the mean and standard deviation of two independent measurements.

Structure	1st layer		2nd layer		Total thickness (nm)
	Protein type	Thickness (nm)	Protein type	Thickness (nm)	
Bi-layer	WPI	4.95 ± 1.60	LF	5.12 ± 0.21	10.1 ± 1.40
	LF	6.97 ± 1.26	WPI	1.49 ± 0.21	8.46 ± 1.05
Mixed layer	WPI/LF	101* ± 33	-	-	101 ± 33

*Thickness achieved after loading the protein mixture for 5 hours and water rinse.

6.4.3 Effect of pH on the adsorption of WPI and lactoferrin bi-layer

The stable bi-layer formed by lactoferrin molecules when deposited on WPI-coated surface was further investigated under different pH conditions. The pH of the individual proteins was precisely adjusted in the range from 2 to 10, hence spanning across the different combinations of both positively charged proteins (below pH 5), oppositely charged (between pH 5 and 9), and both negatively charged proteins (above pH 9). WPI was fed first to the QCM-D sensors, followed by an intermediate rinsing step with water (Figure 6.5a), then lactoferrin was loaded and the run was completed with a final water wash (Figure 6.5b). All the solutions used in this experiment were at same pH conditions. Figure 6.5b shows the frequency and dissipation shifts for the adsorption of lactoferrin on the WPI-coated surface at different pH values, while Figure 6.6 presents the thickness of the second layer obtained after lactoferrin absorption.

As the investigated range of pH spanned from acidic to basic conditions, the individual protein molecules are expected to undergo some structural changes which will affect their interaction and adsorption on surfaces. Under the adsorption conditions employed, there was a larger decrease in frequency corresponding to higher protein adsorption after the addition of WPI (first layer) at pH 4 and 6 which is intermediate to the pI of WPI around 4.9 (Figure 6.5b). This corresponds well with the literatures on the adsorption of proteins on surfaces which in general exhibited pH dependency with a higher adsorption rate near to its pI (Belegrinou et al., 2008; Ma, Wu & Zhang, 2013). The dominance of hydrophobic attraction is strongest at its pI with little changes in conformational structure of protein which will favour their interactions on hydrophobic gold surfaces. On the other hand, a relatively smaller

decrease in frequency shift was observed in particular at pH 2 (Figure 6.5a), indicating WPI adsorption was lower. This is interesting because β-lactoglobulin (a major component of whey proteins) exists as a dimer at neutral pH but can dissociate into monomers under acidic conditions (pH < 3) which can then expose hydrophobic groups (Hunt and Dalgleish, 1994; Liu & Kim, 2009). Therefore, it may be expected that hydrophobic interaction between WPI molecules and hydrophobic surface to increase at very low pH. However, WPI adsorption on the surface at pH 2 was reduced compared to at other pH levels. This can be attributed to the fact that WPI molecules were highly positive charged and electrostatic repulsion between the protein molecules was strong enough to overcome their hydrophobic attraction at the interface which can potentially reduce their alignment and intermolecular interaction on surfaces, thus less adsorption to form a less dense protein layer. This may also be related to some changes in the conformation and quaternary structure of whey protein due to pH change. For example, in a study by Zhang, Dalgleish & Goff (2004) that reported protein adsorption to air/water interfaces in aqueous foam, β-lactoglobulin is described to be less competitive to interfacial adsorption at pH 3 due to its becoming more rigid and thermodynamically stable at low pH.

In the second stage of the adsorption, lactoferrin molecules were added to the WPI-coated surface under the same pH conditions. At pH 2 and 4, the frequency remained practically at the baseline of WPI (Figure 6.5b), indicating that there was no adsorption of lactoferrin on the WPI layer, mainly because of charge repulsion between the two positively charged proteins. At pH 6 or higher, the frequency shift was significant, indicating the adsorption of lactoferrin molecules on top of the WPI-coated surface. Interestingly, the thickness of this secondary layer of lactoferrin slightly decreased as the pH further increased above pH 6 (Figure 6.6). This result is consistent with the large but opposite charge densities on the two proteins studied at pH 6 (Figure 6.1), with electrostatic interactions playing the strongest role at this pH. Interestingly, there was still a considerable amount of lactoferrin adsorbing to the WPI-coated surfaces at pH equal or higher than 9 (Figure 6.6). Lactoferrin is a large globular protein which displays a bipolar charge distribution (Mantel, Miyazawa & Broxmeyer, 1994). Therefore, the protein presents positively charged patches even at the pI or above (Iafisco, Foggia, Bonora, Prat & Roveri, 2011; Müller, 2014). In addition, the interactions between lactoferrin and WPI can be enhanced by other

interaction forces such as hydrophobic attractions and hydrogen bonds which tend to dominate near the pI (McClements, 1999). This result is consistent with the study on adsorption of lactoferrin on negatively charged adsorbents at different pH and salt concentrations (Du, Lin, Wang & Yao, 2014). The authors reported that there was substantial amount of lactoferrin adsorbed even at pH near the pI of lactoferrin.

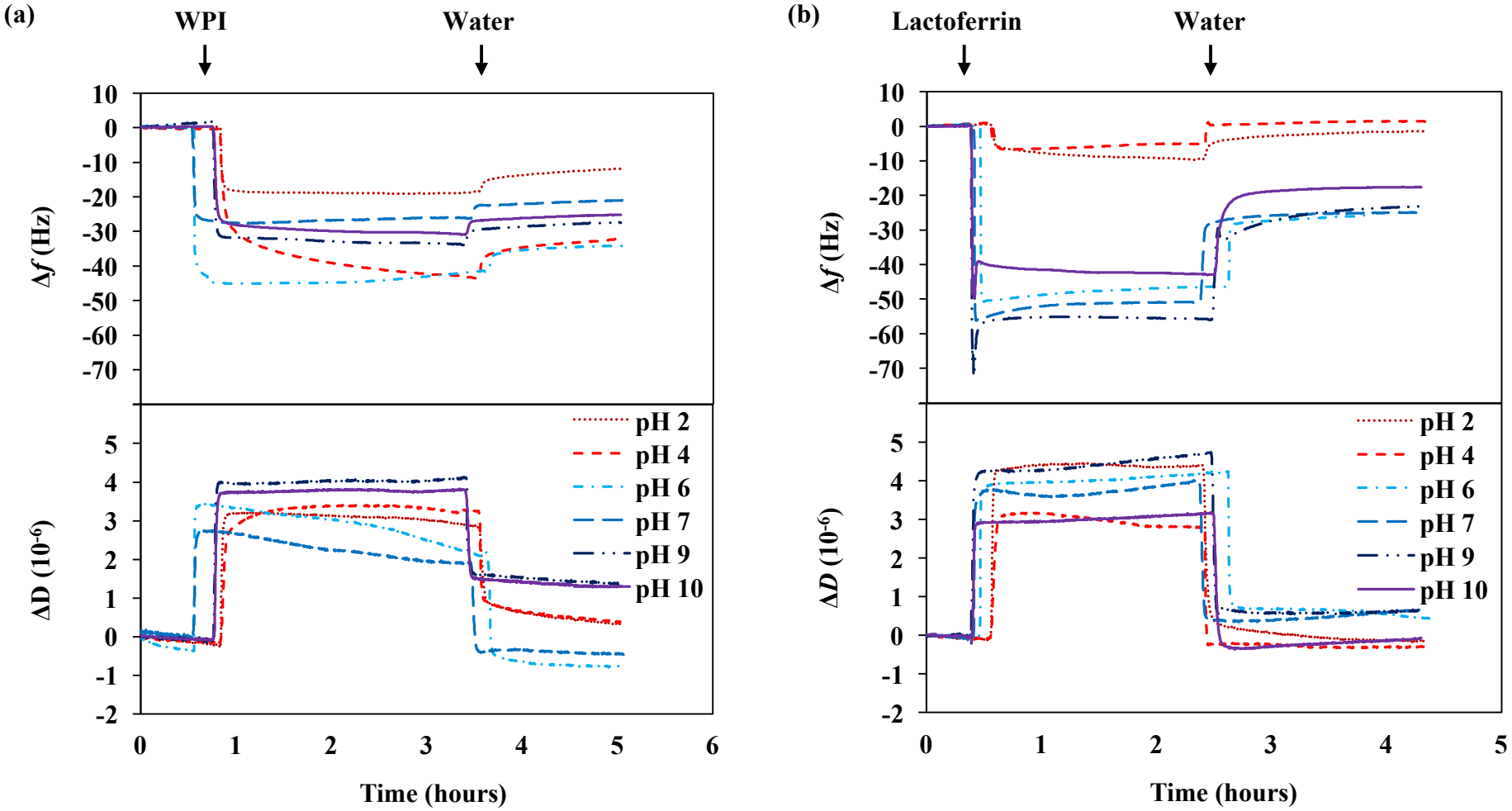

Figure 6.5 Frequency and dissipation shift versus time at 7th overtone for (a) the adsorption of WPI on the quartz crystal surface (first layer) and (b) the adsorption of lactoferrin on the WPI-coated quartz crystal surface (second layer) at various pHs.

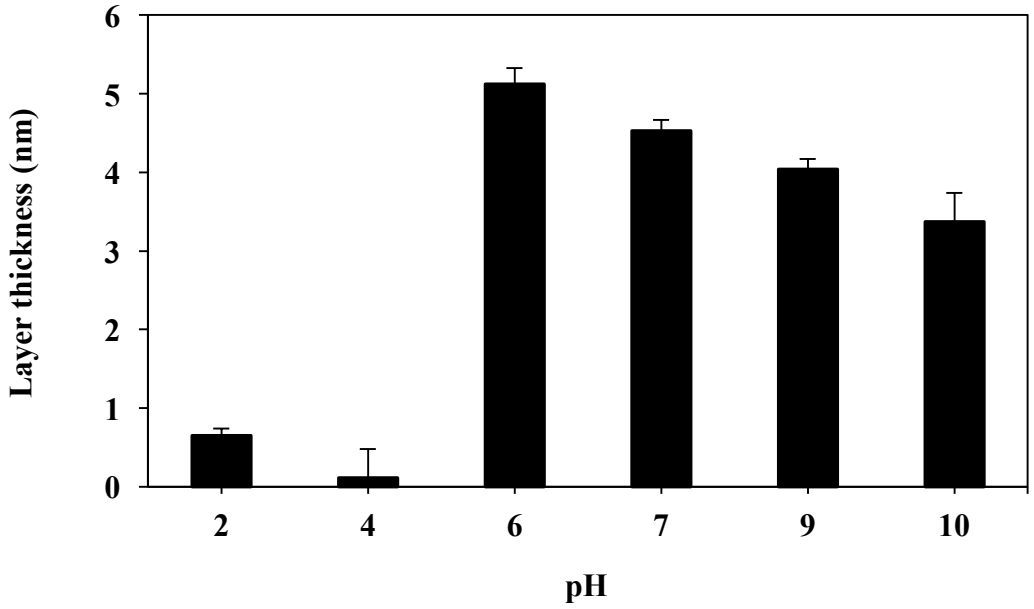

Figure 6.6 Thickness of secondary layer after adsorption of lactoferrin on the WPI-coated surface at different pH from 2 to 10 using the Sauerbrey model. Data are presented as the mean of two independent measurements and error bars represent the standard deviation.

6.4.4 Adsorption of protein complex on hydrophobic surface

The adsorption behaviour of a protein mixture of WPI and lactoferrin was very different to that previously observed with sequential adsorption of the two proteins. The adhered layers displayed relatively large frequency and dissipation shifts and showed no trend of reaching saturation or equilibrium after 5 hours exposure to the protein mixture (Figure 6.7). This could be due possibly to a feature of continuous sedimentation associated with large aggregates of protein complex of WPI and lactoferrin at pH 6 as indicated in Table 6.1 and Figure 6.2. The layer formed was however stable against rinsing with water, indicating relatively strong cohesive interactions.

According to the high dissipation value measured for the adsorption of protein complex, the Kevin-Voigt model was used to estimate the thickness of the adsorbed film at the end of the experiment (Table 6.1). This thickness is to be considered an indicative measure only, because of the limitations of the Voigt model to describe such thick layers, and also because the layer did not reach an equilibrium value. The formed layer had a thickness of 101 μm, much larger than what was obtained when sequentially loading the two pure proteins in bi-layers, and potentially

could have further increased after continuous loading of the protein mixture. This observation, together with the negligible desorption of proteins during the rinsing step, additionally indicates the formation of a strong cohesive adsorbed layer with the two proteins mutually interacting. The complex proteinaceous layer was formed by a mixture of WPI and lactoferrin at pH 6, where the opposite electrical charges on the proteins are fostering a strong durable layer. The consequent aggregation and unfolding of the two proteins lead to establishment of additional hydrophobic, hydrogen bonding as well as some dipole-dipole and charge-dipole interactions, with the consequent formation of stable electrically neutral adsorbed layer of proteins (Ye, 2008). These non-electrostatic attractive forces can act in concert offering a large driving force for the continued adsorption of the protein complex on the sensor surface and formed a thick layer.

To gain more information on the adsorption behaviour, dissipation shift was plotted as a function of frequency shift (Figure 6.8). In such a plot, a relatively small slope (i.e. small dissipation gain for a given frequency shift) characterises rigidly adsorbed layers, while a larger slope (i.e. high dissipation for a given frequency shift) is representative of a soft viscous layer (Belegrinou et al., 2008). Based on the results reported in Figure 6.7, the mixed protein layer initially deposited onto the sensor was rigidly coupled to the hydrophobic surface, but progressive deposition produced a softer second layer having more viscous structure which might be expected due to retention of water as the protein film was continuously deposited on the surface. It should also be mentioned that there is the possibility that the secondary adsorption observed (line 2 in Figure 6.8) could also be possibly related to continuous sedimentation of large aggregates of the mixed proteins described above.

The thickness of this mixed protein layer was 10 times larger than the one measured for the protein bi-layer. It is worth noticing that the layer thickness of the protein bi-layers approximately corresponded to the sum of the two stacked mono-layers for the individual proteins, whereas the mixture of proteins formed a thick multilayer of protein complex. Preliminary results confirmed that the thickness of the bi-layer can be further increased by sequential addition of the oppositely charged proteins, leading to film with larger thicknesses than the simple bi-layer.

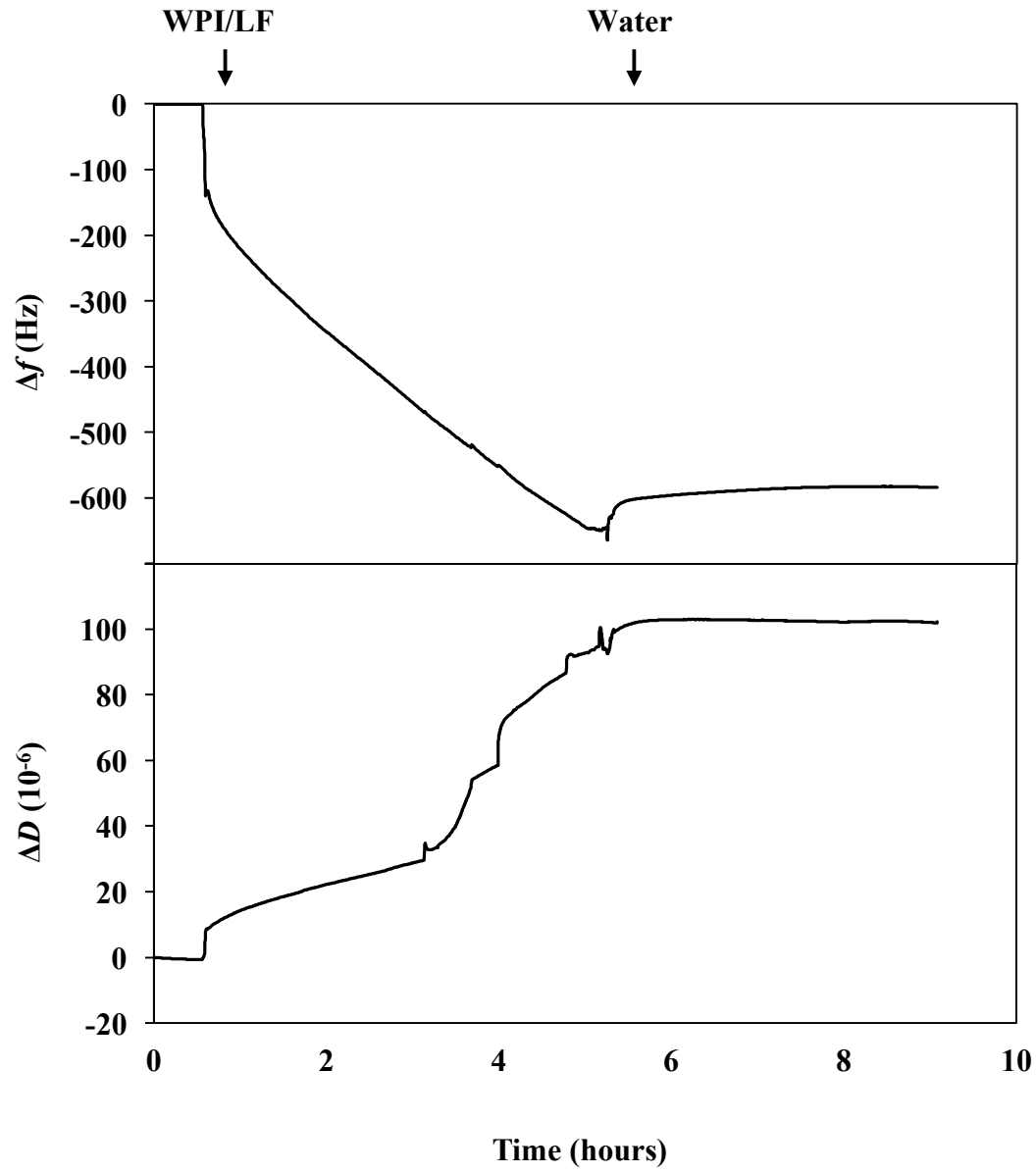

Figure 6.7 Frequency and dissipation shift versus time at 7th overtone for the adsorption of protein complex of WPI and lactoferrin on the quartz crystal surface with water rinse after 5 h at pH 6.

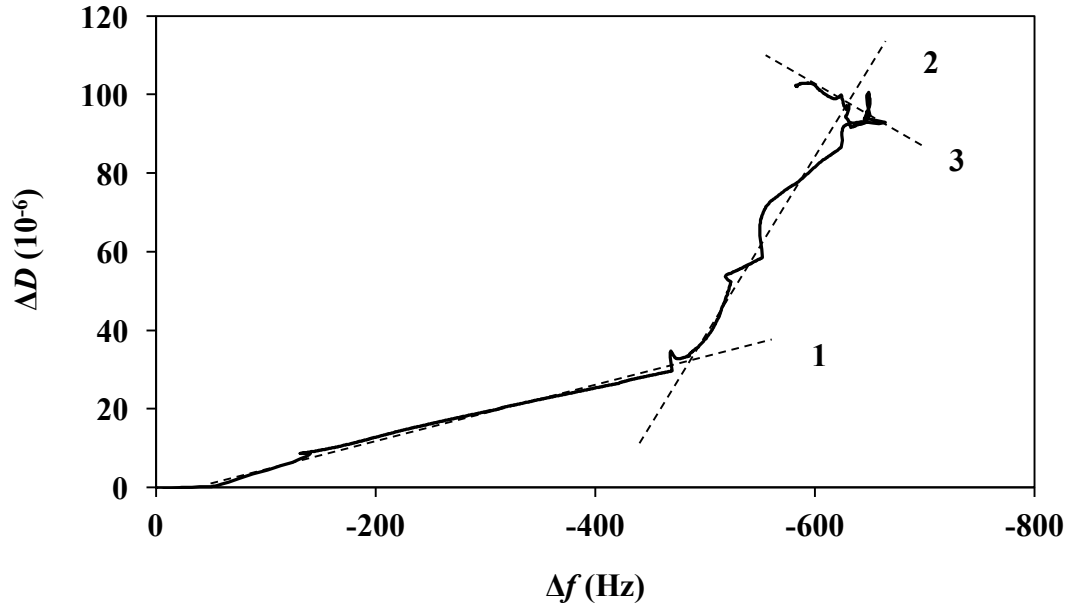

Figure 6.8 Dissipation shift versus frequency shift plot at 7th overtone during the adsorption of protein complex of WPI and lactoferrin at pH 6. Line 1: trend line during adsorption of initial layer. Line 2: trend line during formation of secondary soft layer. Line 3: rinse step with water.

6.5 Conclusions

The formation of different interfacial structures of proteins on a modified hydrophobic surface was able to be investigated using two proteins (WPI and lactoferrin) by OCM-D. The QCM-D results showed that there was protein adsorption when the protein layers were added to a surface pre-coated by another protein to form a thin layer via electrostatic interactions. However, the protein complex formed a thick, viscous layer that was strongly attached to the surfaces. This study builds the foundation for investigating the formation of different interfacial structures of WPI and lactoferrin in emulsions.

Chapter Seven:

Physicochemical Properties and *In vitro* Gastrointestinal Digestion of Nanoemulsions Stabilised by WPI and/or Lactoferrin

7.1 Abstract

In this chapter, electrostatic deposition of lactoferrin on the stability of nanoemulsions stabilised by WPI was investigated as a function of pH (2 – 10) and lactoferrin concentration (0.25 – 5% w/w). The nanoemulsions were prepared by emulsification and solvent evaporation method as described in Chapter 4 and then diluted with different concentrations of lactoferrin solutions to form a series of bi-layer emulsions. At pH 2, 4 and 5, lactoferrin molecules were weakly adsorbed at the droplet surface of WPI nanoemulsions due to strong electrostatic repulsion between the protein molecules as both WPI and lactoferrin were positively charged. The bi-layer nanoemulsions remained stable at pH 2 and 4 but the emulsions were unstable to droplet aggregation at pH 5 which is near to the pI of WPI. At pH 6, electrostatic interactions between the protein molecules were favoured for the deposition of lactoferrin onto the surfaces of WPI-coated droplets. However, the emulsions were prone to droplet aggregation at low concentration of lactoferrin (0.5 – 1% w/w), presumably due to bridging flocculation as there was insufficient lactoferrin molecules at the oil droplet interface. Thus, a sufficiently high level of lactoferrin (3% w/w) was necessary to produce stable emulsions in bi-layer emulsions at pH 6. At pH 7, 8, 9 and 10, there is sufficient electrostatic attraction between the protein molecules to form WPI-Lf bi-layer at the droplet surface and the nanoemulsions were stable. The environmental stability (namely, temperature, pH and ionic strength) on selected nanoemulsions was also tested. The single layer nanoemulsions of WPI was stable to heat treatment (30 – 90^{o}C) but was found to become unstable to pH changes (near the pI around pH 5) and salt addition (above 5 mM $CaCl_2$ at pH 6). The incorporation of lactoferrin in bi-layer emulsions improved the stability of single layer emulsions over a wide range of pH (2 – 12) and salt addition (0 – 500 mM NaCl or 0 – 90 mM $CaCl_2$) but the bi-layer emulsions were susceptible to droplet aggregation at temperatures above 60^{o}C. The *in vitro* digestion of the nanoemulsions under simulated gastric and intestinal conditions in sequence demonstrated that the

addition of lactoferrin did not alter the digestion process and the majority of protein digestion took place in the intestinal phase. This study showed the potential benefits of having of a lactoferrin layer to improve the stability of WPI-stabilised nanoemulsions.

7.2 Introduction

As described in Chapter 4, nanoemulsions were successfully prepared by emulsification and solvent evaporation method but they are still thermodynamically unstable to certain environmental conditions such as temperature changes, pH changes and salt addition. It is therefore important to improve the environmental stability of nanoemulsions. This can be achieved by controlling the characteristics of the interfacial coatings around the small oil droplets. Specifically, the interfacial layer can be designed to contain one or more biopolymers around oil droplets using a LBL electrostatic deposition method (Guzey & McClements, 2006; McClements, 2010). This can be achieved by depositing oppositely charged biopolymers onto the surfaces of electrically charged oil droplets through electrostatic interactions. This procedure can be repeated several times to form multilayer emulsions with two or more biopolymers.

Many previous studies have already reported the assembly of multilayer emulsions by proteins and/or polysaccharides, e.g. β-lactoglobulin, caseinate, lactoferrin, sodium alginate, pectin and etc. (Lesmes et al., 2010; Schmelz, Lesmes, Weiss & McClements, 2011; Salminen & Weiss, 2013; Fioramonti, Martinez, Pilosof, Rubiolo & Santiago, 2015). However, few studies have been carried out on the formation of multilayer emulsions at a nanometric scale using WPI and lactoferrin. In particular, lactoferrin is an iron-binding glycoprotein and contains high concentrations of positive charges that can interact with other milk proteins that are negatively charged (Ye & Singh, 2007). The pIs of most whey proteins and lactoferrin have been reported to be around pH 5 and 9, respectively (Shimazaki, 2000; Salminen & Weiss, 2013). It can be expected that they are oppositely charged and can interact electrostatically when the solution conditions are favourable such as at pH values between their pI. Furthermore, QCM-D data in Chapter 6 indicated that

WPI and lactoferrin molecules could be deposited successively to form protein bi-layers on surfaces.

However, one of the challenges in producing a stable emulsion containing two or more layers is due to droplet aggregation (Guzey & McClements, 2006; Pallandre et al., 2007). In this case, the biopolymer concentration used must be sufficient to cover the droplet surface to prevent bridging flocculation and not excessive to promote depletion flocculation (Guzey & McClements, 2006; Fioramonti et al., 2015). Although several studies have been carried out to produce multilayer emulsions and investigate their physicochemical stability, few have investigated thoroughly on the effects of pH and biopolymer concentration. These have important implications on the physicochemical properties of the interfacial layer formed on the droplets.

The objective of this work was therefore to study the effects of pH and lactoferrin concentration in order to determine the optimum conditions to produce stable bi-layer nanoemulsions containing WPI and lactoferrin. The stability of nanoemulsions to environmental stresses and *in vitro* gastrointestinal digestion were also studied. This research aimed to provide insight into the design of nanoemulsions with customised interfacial structure for encapsulation and delivery of high value food ingredients.

7.3 Materials and Methods

7.3.1 Materials

The materials used for making nanoemulsions are as listed in the previous chapter (Chapter 3; Section 3.1). Pepsin from porcine gastric mucosa (P7125-100g, Lot #030M15711V), pancreatin from porcine pancreas (P-1750-100g, Lot #31K1838) and bile extract from porcine (B8631-100g, Lot #100M0192V) were from Sigma Aldrich Chemical Company (St. Louis, MO, USA). Potassium dihydrogen orthophosphate (K_2HPO_4) was from BDH Chemicals (Poole, England). For SDS-PAGE analysis, acrylamide/bis premixed powder (37.5:1 mixture of 99.9% pure acrylamide and bis-acrylamide powder), N,N,N',N'-tetramethylethylene diamine (TEMED) (Catalog #161-0800), bromophenol blue (Catalog #161-0404) and SDS-

PAGE Molecular Weight Standards, Broad Range unstained standards (Catalog #161-0317) were purchased from Bio-Rad Laboratories (Hercules, CA, USA). The molecular weight standards contained a mixture of nine proteins in the molecular range of 6.5 – 200 kDa (6.5, 14.4, 21.5, 31, 45, 66.2, 97.4, 116.25 & 200 kDa). Bromophenol blue was used a tracking dye. Ammonium persulphate (APS) (≥ 98% purity) was purchased from Sigma Aldrich Chemical Company (St. Louis, MO, USA). TEMED was used with a solution of APS as catalysts for polymerisation of polyacrylamide gels. Tris-(hydroxymethyl) aminomethane), glycerol, 2-mercaptoethanol (98%) and glacial acetic acid (100%) were purchased from BDH Chemicals (Poole, England). Sodium dodecyl sulphate (SDS) (99%) and 2-propanol (certified ACS, HPLC grade) were purchased from Fisher Scientific (New Jersey, USA). Coomassie Brillant Blue (Catalog #1610406) was purchased from Bio-Rad Laboratories (Hercules, CA, USA) and used in the staining solution. Isopropanol and glacial acetic acid were used in the preparation of staining and de-staining solutions.

7.3.3 Preparation of bi-layer naneomulsions

Two types of nanoemulsions consisting of a single layer emulsion and a bi-layer emulsion were prepared and studied. The nanoemulsions were prepared uing emulsification and solvent displacement method as described in Section 3.2.2 of Chapter 3. The nanoemulsions were prepared with 2% (w/w) WPI solution and then diluted with an equal amount of lactoferrin solution (1:1 ratio) at different concentrations (0, 0.5, 1, 1.5, 2, 4, 6, 8 and 10%) and pH values (2, 4, 5, 6, 7, 8. 9 and 10) as shown in Table 7.1. The single layer emulsion was stabilised by a single protein (i.e. WPI) while the bi-layer emulsion was formed by depositing lactoferrin molecules on the surfaces of WPI-coated droplets to form bi-layer as illustrated in Figure 7.1

Table 7.1 Composition of bi-layer nanoemulsions formed by mixing WPI-stabilised nanoemulsions (2% WPI, 1% w/w oil) with an equal amount of lactoferrin solution (1:1 ratio) at different concentrations.

Before mixing			After mixing		
WPI nanoemulsions		**Lactoferrin solution**	**Bi-layer emulsions**		
% WPI	% Oil	% LF	% WPI	% LF	% Oil
2	1	0	1	0	0.5
2	1	0.5	1	0.25	0.5
2	1	1	1	0.5	0.5
2	1	1.5	1	0.75	0.5
2	1	2	1	1	0.5
2	1	4	1	2	0.5
2	1	6	1	3	0.5
2	1	8	1	4	0.5
2	1	10	1	5	0.5

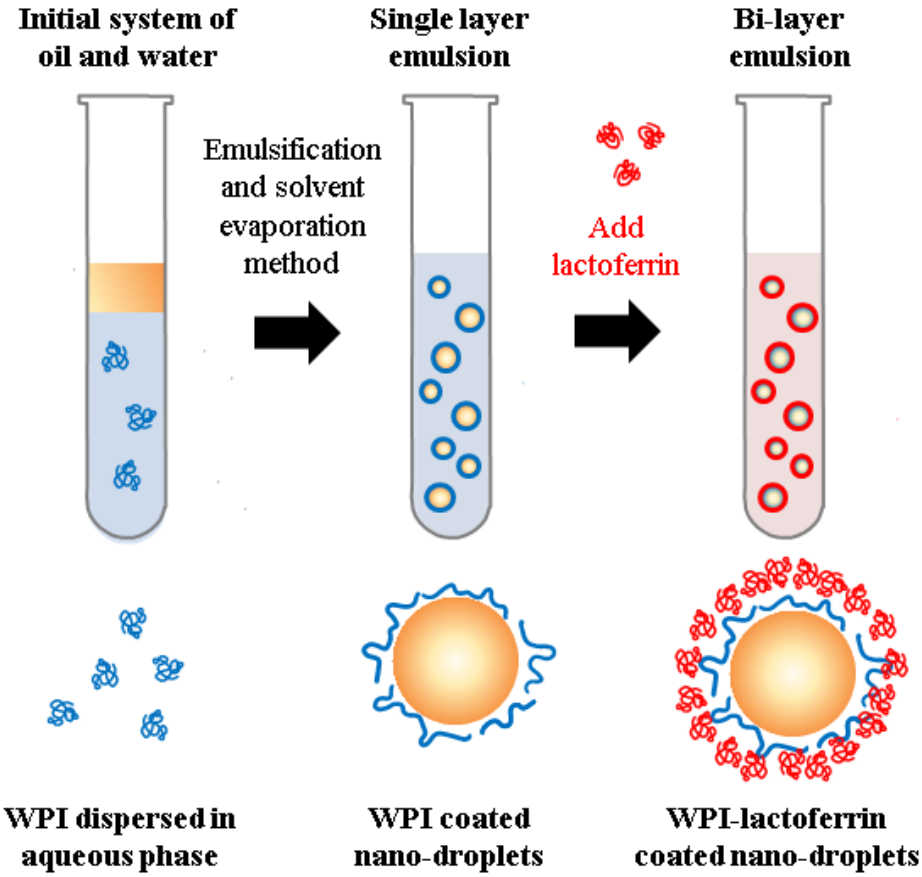

Figure 7.1 Schematic illustration of interfacial deposition of lactoferrin molecules on WPI-coated oil droplets to produce bi-layer nanoemulsions.

7.3.4 Effect of environmental conditions on nanoemulsions

The physical stability of the single layer and bi-layer emulsions to environmental stresses including the effects of temperature (30 – 90^{o}C), pH (2 – 12) and ionic strength (0 – 500 mM NaCl or 0 – 90 mM $CaCl_2$) was carried out as described in Chapter 4 (Section 4.3.3). In this study, single layer emulsion containing 0.5% (w/w) corn oil and 1% (w/w) WPI and bi-layer emulsion containing 0.5% (w/w) corn oil, 1% (w/w) WPI and 3% (w/w) lactoferrin at pH 6 were used.

7.3.5 Characterisation of nanoemulsions

The particle size and size distribution of nanoemulsions were measured by dynamic light scattering technique using a Malvern Zetasizer Nano ZS (Malvern Instruments Ltd, Worcestershire, UK). The emulsion samples were measured without further dilution during the size measurement. For those aggregated samples (particularly, single layer emulsions at pH 5 and 5.5 and salt concentrations above 5 mM $CaCl_2$), they were measured using a Mastersizer instrument (Mastersizer 2000 Hydro MU, Malvern Instruments Ltd, Worcestershire, UK). The ζ-potential of nanoemulsions was measured using a Malvern Zetasizer Nano ZS (Malvern Instruments Ltd, Worcestershire, UK) and disposable ζ-potential cells ("Size & Zeta" folded capillary cell; DTS1070). The samples were used without further dilution during the measurement. The mesurements were carried out in triplicates on two independent samples. Details of the particles size analysis and ζ-potential measurements are described in Chapter 3 (Sections 3.3.1 and 3.3.2). The microstructure of selected nanoemulsions was determined by TEM using resin embedding method as described in Section 3.3.3 of Chapter 3.

7.3.5 *In vitro* gastrointestinal digestion

A two-step simulated gastrointestinal model that consisted of a gastric phase and a small intestinal phase was used to understand the behaviour of nanoemulsions under physiological conditions. The simulated gastric fluid (SGF) and simulated intestinal fluid (SIF) were prepared according to the United States Pharmacopeial Convention (2002). Briefly, SGF was prepared by adding 0.2 g of NaCl, 700 µL of HCl and 0.32 g of pepsin in 80 ml water and diluted to 100 mL with pH adjusted to 1.2 using 1 M HCl. SIF was prepared by adding 0.68 g of K_2HPO_4 in 25 mL of water, 77 µL of 0.2 M NaOH, 50 mL of water and 1 g of pancreatin and diluted to 100 mL

with pH adjustment to 6.8. Bile extract was added at a concentration of 5 mg/mL and 30 mM $CaCl_2$ was added to simulate actual physiological conditions.

The *in vitro* digestion was performed by subjecting the nanoemulsions to SGF and SIF in sequence. Briefly, an equal amount of pre-incubated nanoemulsions (15 mL) was mixed with 15 mL SGF (1:1 ratio) in a glass beaker and the pH was adjusted to 1.2. The mixture was incubated for 1 hour at 37^{o}C under continuous stirring at 100 rpm in a temperature controlled water bath. During the digestion process, aliquots (250 μL) of samples were withdrawn at different time intervals (0, 5, 15, 30 and 60 minutes) for SDS-PAGE analysis. The samples were immediately treated with 750 μL of sample buffer (containing Tris-HCl buffer at pH 6.8, glycerol, SDS, bromophenol blue, 2-mercaptoethanol), raised to the pH to near neutral using 0.2 M $NaHCO_3$ to terminate proteolysis (inactivate pepsin) and heated to 95^{o}C for 5 minutes.

After gastric digestion, the sample was removed and mixed with SIF at the same ratio of 1:1 and the mixture was adjusted to pH 6.8 by adding NaOH. The mixture was incubated for 2 hours at 37 ^{o}C under continuous stirring at 100 rpm in a temperature controlled water bath. Aliquots of samples were also collected during the digestion process at different time intervals (continuing from 65, 75, 90 and 120 minutes) for SDS-PAGE analysis and immediately treated with the sample buffer and heated to 95^{o}C for 5 minutes. At the end of incubation, samples were also collected at each phase and immediately characterised by measuring the emulsion particle size and ζ-potential.

7.3.5.1 Sodium dodecyl sulfate polyacrylamide gel electrophoresis (SDS-PAGE)

10 μL of each sample were loaded on a pre-prepared acrylamide gel consisting of 16% resolving gel (1.5 M Tris-HCl buffer, pH 8.8, 10% SDS, TEMED and 10% APS) and 4% stacking gel (0.5 M Tris-HCl buffer, pH 6.8, 10% SDS, TEMED and 10% APS). The molecular weight standard was diluted in the sample buffer and heatd for 5 minutes at 95^{o}C and then loaded into the well (5 μL). The gels were run on a Mini-protean® 3 cell (Bio-rad Laboratories, Richmond, CA, USA) at 200 V for 30 to 40 minutes or until the bands reached the bottom of gels. The gels were carefully removed from the glass plates and transferred into a plastic container

for staining and de-staining. The gels were stained with 0.3% (w/v) Coomassie Brilliant Blue R solution with 10% (v/v) isopropanol and 10% (v/v) glacial acetic acid for 30 minutes and then de-stained with a solution of 10% (v/v) isopropanol and 10% (w/v) glacial acetic acid. The de-staining solution was replaced 2 to 3 times with fresh solution until the background of gel was clear. After which, the gels were scanned using Molecular Imager® Gel Doc XR (Bio-rad Laboratories, Richmond, CA, USA) to obtain images of the gels.

7.4 Results and discussion

7.4.1 Effects of pH and lactoferrin concentration on the adsorption at the droplet surface of WPI nanoemulsions

The interfacial characteristics of emulsions can be modified by surface deposition of oppositely charged biopolymers to form bi-layer emulsions via electrostatic interactions as discussed in the literature review (Chapter 2; Section 2.4). The nanoemulsions stabilised by WPI as the primary emulsifier were mixed with different concentrations of lactoferrin solutions at the same pH. Figure 7.2 shows that in the absence of lactoferrin, WPI-coated droplets in single layer nanoemulsions were positively charged (around +30 mV) at pH below 4 and the samples were negatively charged (around -40 mV) when the pH was above 7. The emulsions were stable containing small droplets around 80 – 90 nm in diameter (Z-Average) (Figure 7.3) as they were predominantly stabilised by electrostatic repulsion (Tokle et al., 2012). At pH 5, the ζ-potential was close to zero which corresponds with the pI of whey proteins (Gbassi, Yolou, Sarr, Atheba, Amin & Ake, 2012; Salminen & Weiss, 2013). This resulted in extensive droplet aggregation ($D_{4,3}$ > 10 μm) (Figure 7.3), indicating that the stability of the WPI single layer nanoemulsions was sensitive to pH when the net charge was brought close to zero at around pH 5 and 5.5.

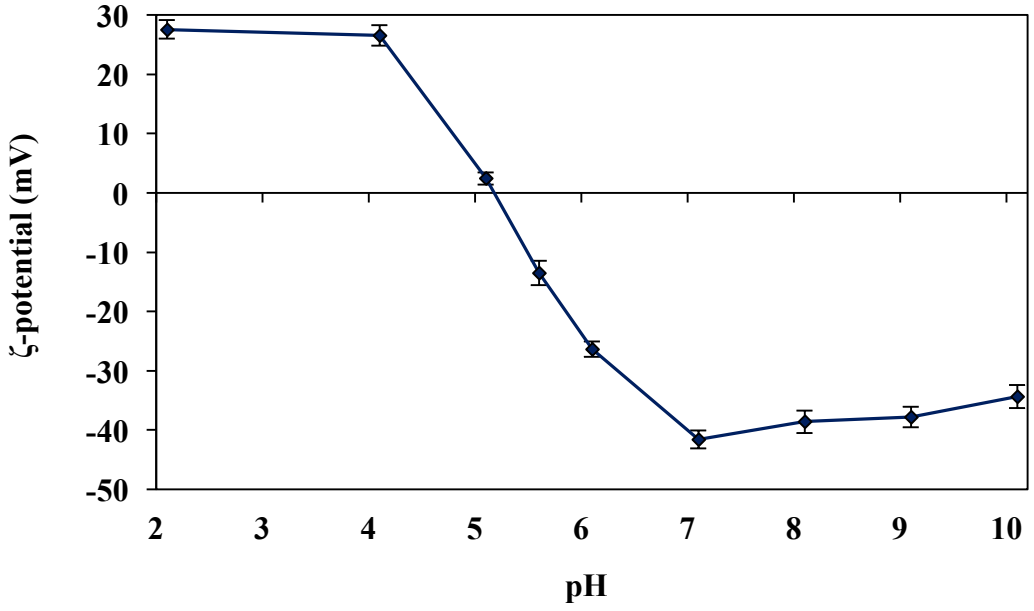

Figure 7.2 Mean ζ-potential of droplets in single layer emulsions (0.5% w/w oil and 1.0% WPI) prepared at different pH values (pH 2 to 10). Data are presented as the mean of two independent measurements with triplicates (*n*=6) and error bars represent the standard deviation.

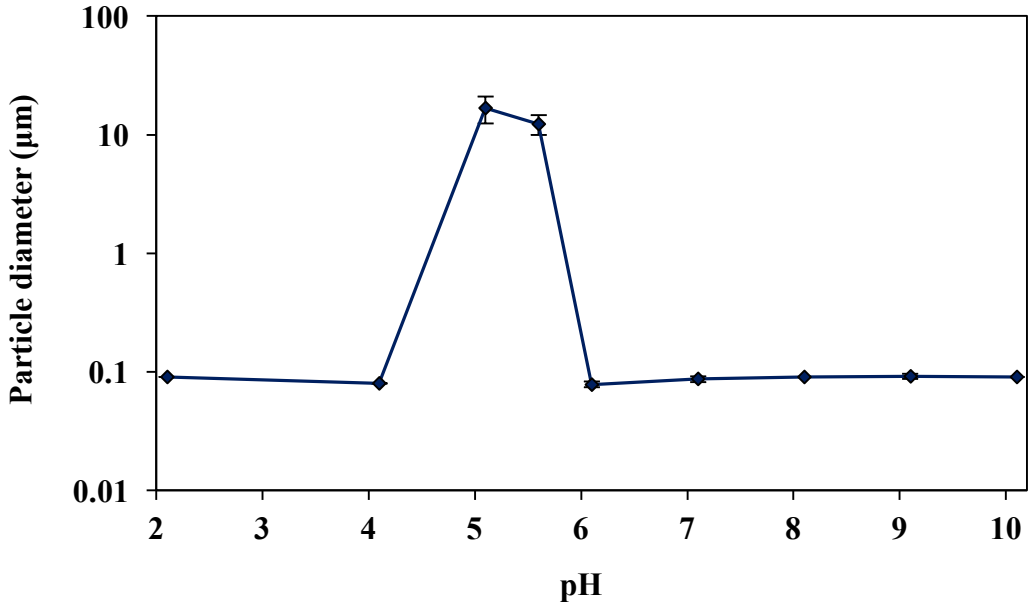

Figure 7.3 Mean particle diameter (Z-Average) of droplets in single layer emulsions (0.5% w/w oil and 1.0% WPI) prepared at different pH values (pH 2 to 10) measured using a Zetasizer Nano ZS. Particle size of WPI emulsion at pH 5 and 5.5 is reported as the $D_{4,3}$ measured using a Mastersizer 2000. Data are presented as the mean of two independent measurements with triplicates (*n*=6) and error bars represent the standard deviation.

The effect of lactoferrin concentrations on the characteristics of droplets in bi-layer emulsions as a function of pH was studied. Figure 7.4 shows photographs of bi-layer emulsions mixed with different concentrations of lactoferrin solutions prepared at their respective pH (2, 4, 5, 6, 7, 8, 9 and 10).

At pH 2 and 4, the ζ-potential values of the nanoemulsions in the presence of lactoferrin were positive (> +20 mV). There was no increase in the ζ-potential with increasing lactoferrin concentrations (Figure 7.5). It is postulated that lactoferrin molecules did not adsorb to the WPI-coated droplets as both WPI droplets and lactoferrin molecules are positively charged to mutually repel each other. This is in agreement with the QCM-D results which indicate that there was no adsorption of lactoferrin molecules on the WPI-coated surface at pH 2 and 4 (Chapter 6; Section 6.4.3). A slight decreasing ζ-potential was observed at higher lactoferrin concentrations (Figure 7.5). This could be due to an electrical charge screening effect associated with an increase in ionic strength at higher protein concentrations as discussed previously (Chapter 4; Section 4.4.3). Since there was no adsorption of lactoferrin molecules on the droplet surfaces at pH 2 and 4, the particle size of the emulsions was relatively small (< 100 nm) and similar to the single layer emulsions without the addition of lactoferrin (Figure 7.6). It was also noted that the color of the nanoemulsions at pH 2 and 4 (especially at higher lactoferrin concentrations) appeared less reddish as compared to other samples at pH 5, 6, 7, 8, 9 and 10 (Figure 7.4). It is known that lactoferrin has a strong affinity to bind iron ($K_D \sim 10^{-20}$ M) which results in the reddish pink colouration (Baker & Baker, 2004). However, iron is relased from the N-lobe of bovine lactoferrin at a pH of around 4, followed by the C-lobe albeit at a lower pH (Troost, Steijns, Saris & Brummer, 2001; Baker & Baker, 2004). Thus, the release of iron (Fe^{2+}) from lactoferrin at lower pH could explain the loss of reddishness in the emulsions containing lactoferrin at pH 2.

At pH 5, there was a slight increase in the ζ-potential from +2.5 to +6.4 mV as lactoferrin concentration was increased from 0 to 0.25% (w/w) but ζ-potential remained constant thereafter without a further increase in lactoferrin concentration (Figure 7.5). At pH 5 near to the pI of WPI, the charge for WPI approached zero but lactoferrin remained positively charged (+20.6 mV) as shown in Chapter 6 (Section 6.4.1; Figure 6.1). Therefore, at this pH with almost zero net surface charge (in the case of WPI), there was limited interaction between WPI and lactoferrin molecules

at the droplet interface. It was also expected that the lactoferrin molecules remained in the aqueous phase of the emulsions. This probably explained the slightly positive net charge in the presence of lactoferrin. As described earlier, it was noted that at pH 5, the particle size was markedly large (> 10 μm) indicating droplet aggregation due to weak electrostatic repulsion (i.e. only a slight adsorption of lactoferrin to overcome the attractive forces). As a result, there was extensive phase instability in the emulsions as shown in the photographs (Figure 7.4c).

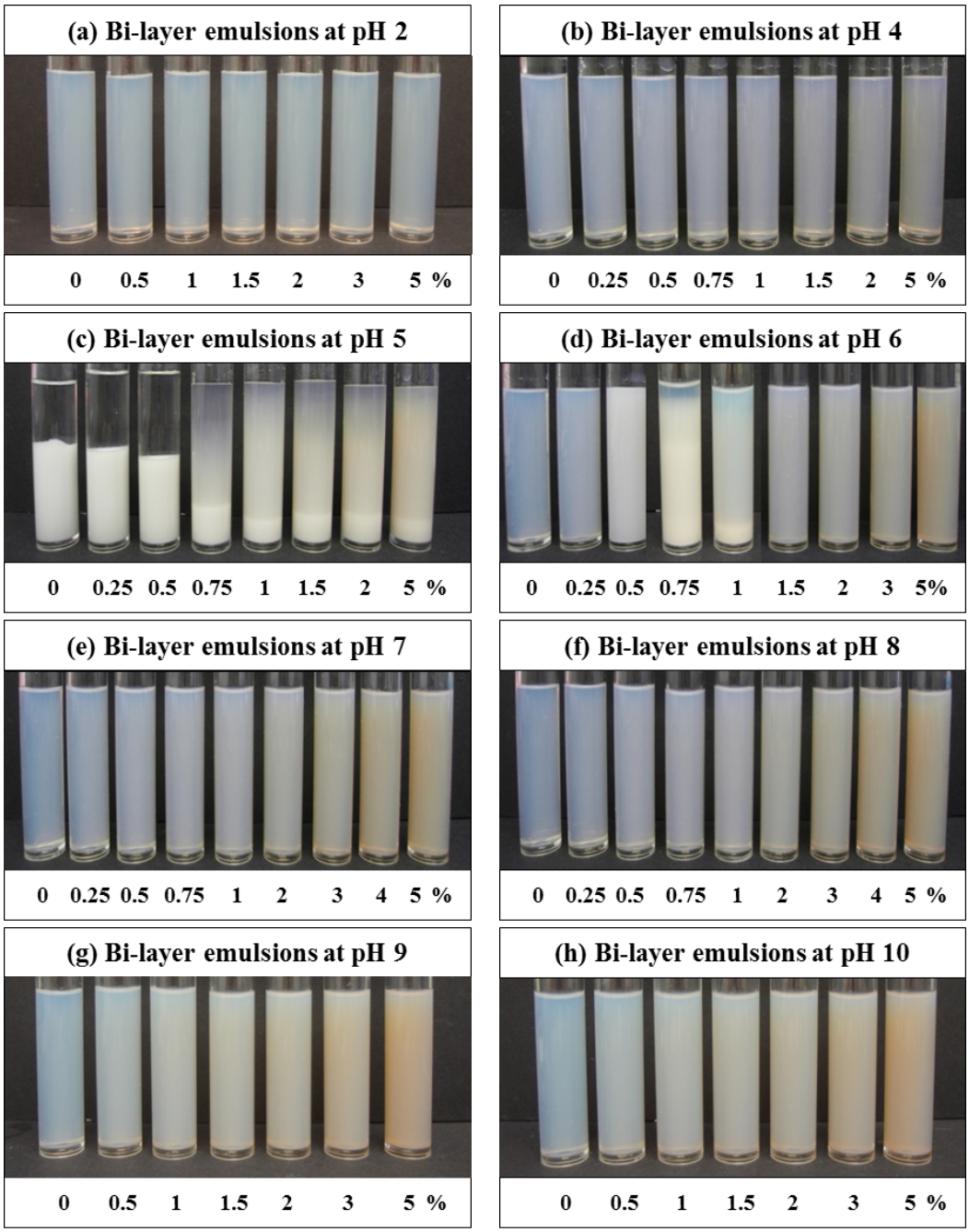

Figure 7.4 Photographs of bi-layer emulsions (0.5% w/w oil, 1.0% w/w WPI and 0.0 to 5.0% w/w LF) at different pH values: (a) pH 2, (b) pH 4 (c) pH 5, (d) pH 6, (e) pH 7, (f) pH 8, (g) pH 9 and (h) pH 10.

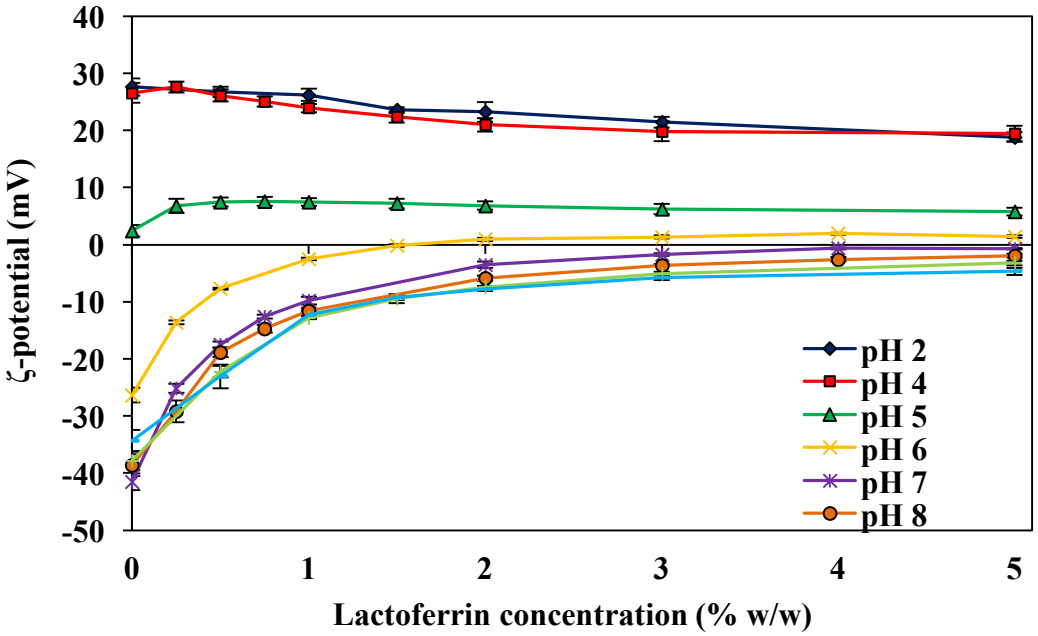

Figure 7.5 Mean ζ-potential of droplets in bi-layer emulsions with increasing lactoferrin concentrations (0 – 5% w/w) prepared at different solution pH from 2 to 10. Data are presented as the mean of two independent measurements with triplicates (n=6) and error bars represent the standard deviation.

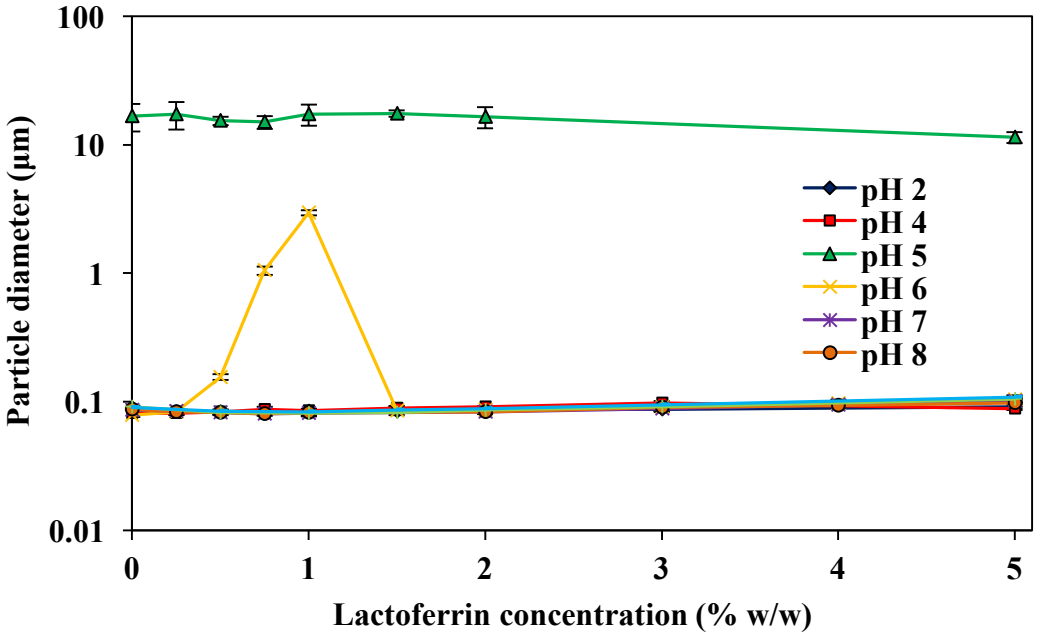

Figure 7.6 Mean particle diameter (Z Average) of droplets in bi-layer emulsions with increasing lactoferrin concentrations (0 – 5% w/w) prepared at different solution pH from 2 to 10 measured using a Zetasizer Nano ZS. Particle size of emulsion samples prepared at pH 5 is reported as the $D_{4,3}$ measured using a Mastersizer 2000. Data are presented as the mean of two independent measurements with triplicates (n=6) and error bars represent the standard deviation.

At higher pH values above the pI of WPI between 6 and 10, the droplets were negatively charged (from -26 to -41 mV) (Figure 7.2). The ζ-potential of the nanoemulsions decreased with increasing lactoferrin concentrations until a plateau was reached (Figure 7.5). This indicated the adsorption of lactoferrin molecules on the droplet surface and a bi-layer was formed on the droplets. This was evidenced by examination of the microstructure of emulsions under TEM as the micrographs showed that the oil droplets in the single layer emulsions were mostly spherical (Figure 7.7a) but a dense outer layer engulfing the oil droplets was observed in the bi-layer emulsions prepared at pH 6, 7 and 10 (Figure 7.7b). The emulsions at pH 2 and 4 appeared to be spherical with less proteinaceous material around the droplets while those of pH 5 were surrounded by large protein aggregates (Figure 7.7b).

(a) Single layer emulsions stabilised by WPI at pH 6

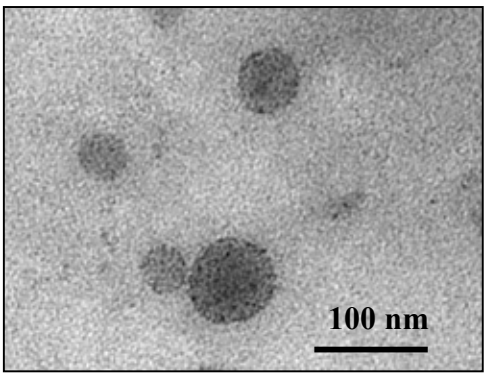

(b) Bi-layer emulsions containing WPI and lactoferrin at pH 2, 4, 5, 6, 7 and 10

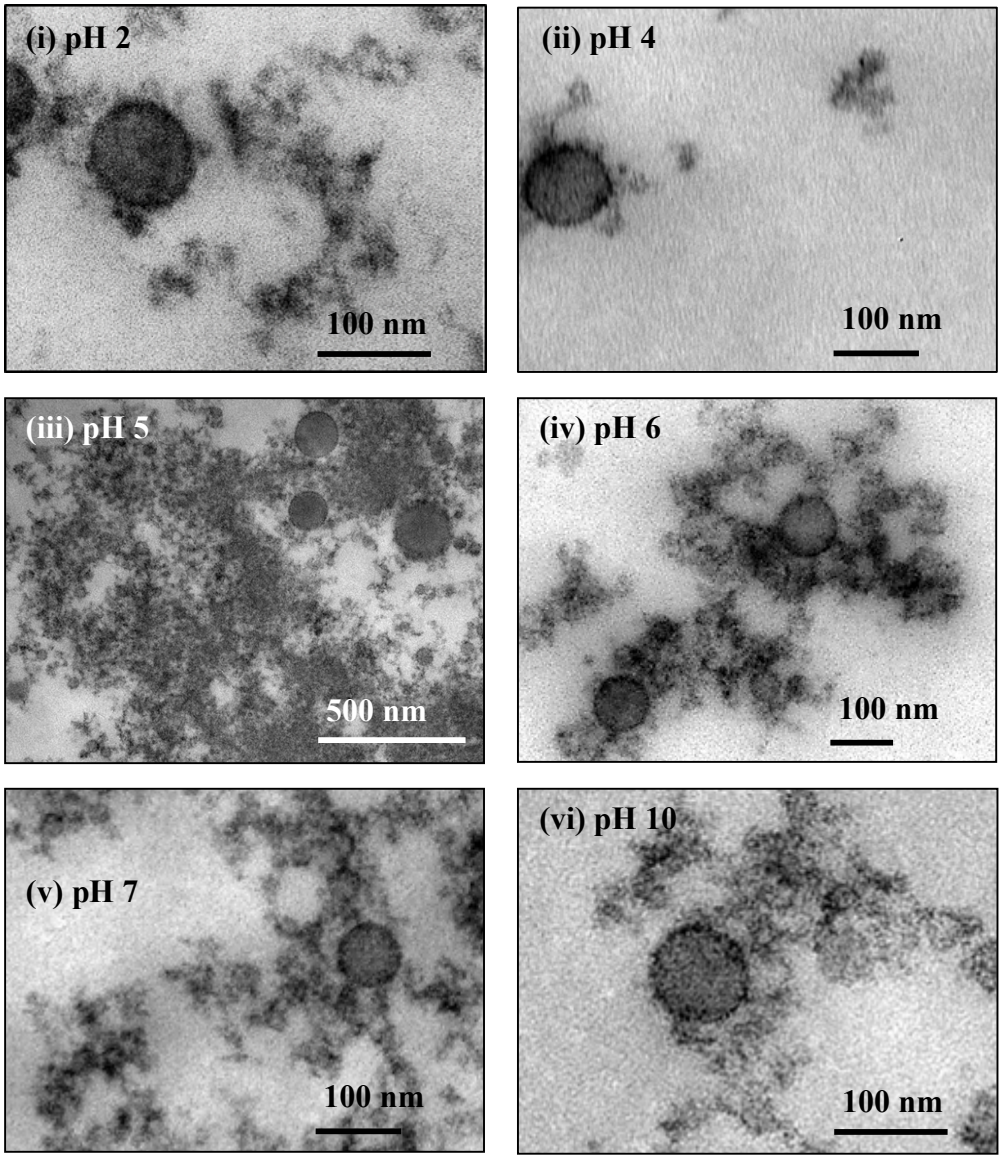

Figure 7.7 TEM images of (a) nanoemulsions containing 1% (w/w) WPI (single layer) at pH 6 and (b) those nanoemulsions containing 1% (w/w) WPI and 3% (w/w) lactoferrin (bi-layer) adjusted to 0.5% (w/w) oil at different pH of 2, 4, 5, 6, 7 and 10.

The adsorption of lactoferrin was also confirmed by modelling the curves of the ζ-potential versus lactoferrin concentrations using the equation proposed by Pallandre et al. (2007). However, this model cannot be used for emulsions at pH 2, 4 and 5 because there was no or little adsorption of lactoferrin molecules.

$$\frac{\zeta(C)-\zeta_{Sat}}{\zeta_0-\zeta_{Sat}} = exp\left(-\frac{3C}{C_{Sat}}\right) \qquad (7.1)$$

where $\zeta(C)$ is the ζ-potential of the emulsion droplets at lactoferrin concentration C, ζ_0 is the ζ-potential in the absence of lactoferrin, ζ_{Sat} is the ζ-potential when the droplets are saturated with lactoferrin and C_{Sat} is the minimum amount of lactoferrin required to completely cover the surface of droplets when saturation. Therefore, the extent of adsorption of lactoferrin to the droplet surface can be characterised by the ζ-potential and the saturation concentration using the above equation. Based on the model, the curves shown in Figure 7.8 demonstrate a good fit ($R^2 > 0.99$) when the predicted ζ-potential values (red line) were plotted with the experimental data at the respective pH (6, 7, 8, 9 and 10). The obtained ζ_0, ζ_{Sat}, C_{Sat} and R^2 values are as shown in Table 7.2. The amount of lactoferrin molecules to saturate the droplets was higher as the pH increased. At pH 6, only 1.35% was needed whereas at pH 10, C_{Sat} was 2.53%. This is in an agreement with the ζ-potential data shown in Figure 7.5. This can be attributed to the fact that the droplets were more negatively charged at higher pH and could correspondingly attract more lactoferrin molecules.

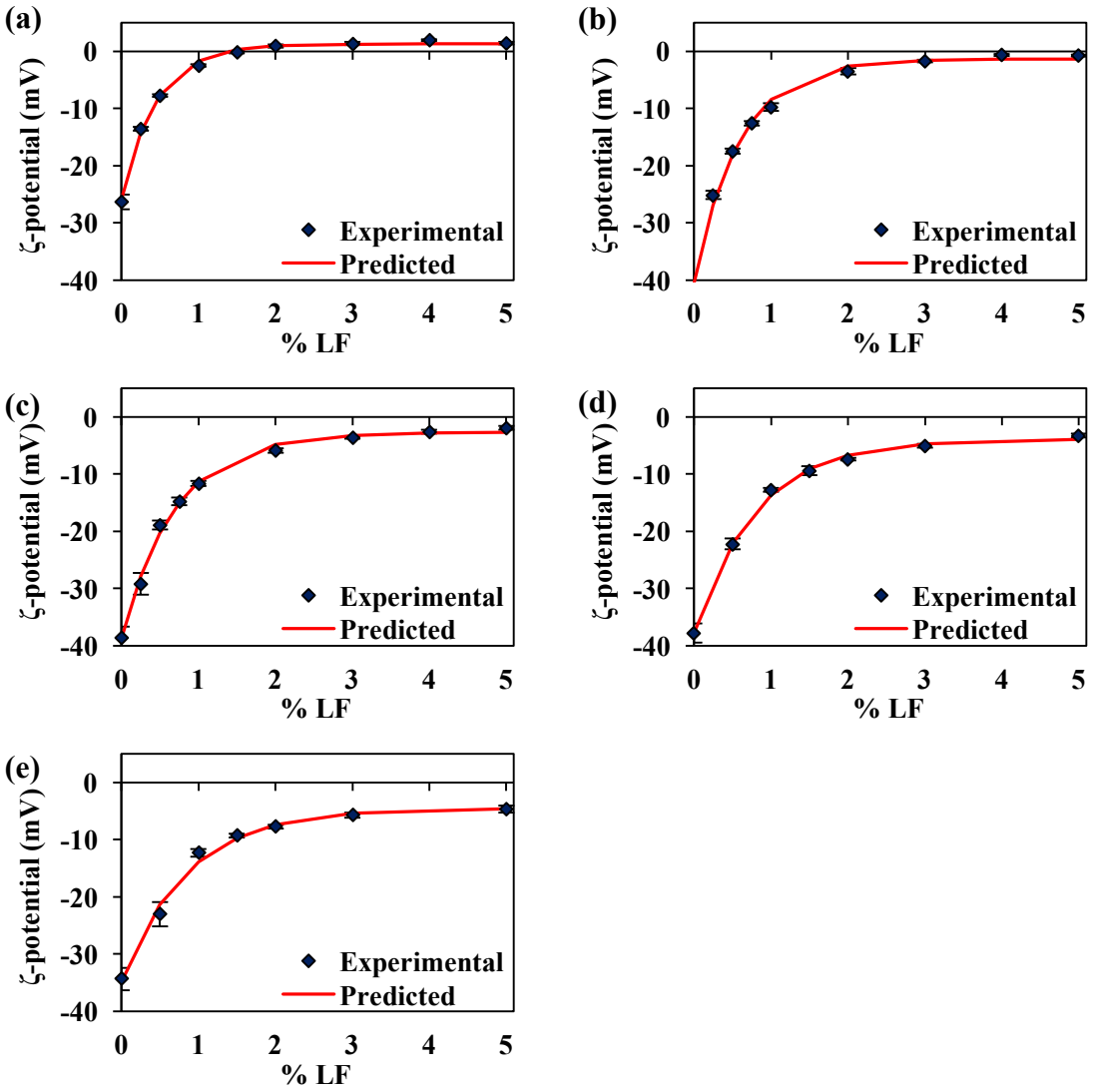

Figure 7.8 Mean ζ-potential versus lactoferrin concentration of bi-layer nanoemulsions at different pH values: (a) pH 6, (b) pH 7, (c) pH 8, (d) pH 9 and (e) pH 10. The curve (red) shows the predicted values of ζ-potential modelled using equation 7.1.

Table 7.2 Values of ζ_0, ζ_{Sat}, C_{Sat} and R^2 obtained by fitting the equation 7.1 to the experimental values and lactoferrin concentration.

	pH				
	6	**7**	**8**	**9**	**10**
ζ_0 (mV)	-26.0	-40.6	-38.8	-37.7	-34.8
ζ_{Sat} (mV)	1.27	-1.40	-2.74	-3.91	-4.58
C_{Sat} (%)	1.35	1.74	2.09	2.41	2.53
R^2	0.997	0.995	0.995	0.998	0.992

It is clear from this study that the adsorption of lactoferrin molecules to the surface of droplets had not had a significant adverse impact on the stability of nanoemulsions against droplet aggregation at all pH levels except for pH 6. At pH 6, the WPI-stabilised nanoemulsions were negatively charged (-26.3 ± 1.3 mV) in the absence of lactoferrin and the particle size measurements indicated that the nanoemulsion was relatively stable (around 80 nm) due to electrostatic repulsion between the droplets. However, nanoemulsions containing lactoferrin (bi-layer emulsions) exhibited some droplet aggregation as there was a large increase in the particle size from around 80 to 2950 nm at lactoferrin concentrations between 0.5 and 1% (w/w) (Figure 7.6). As a consequence, the samples exhibited precipitation, especially at 0.75 and 1% of lactoferrin concentration as shown in Figure 7.4d. The drastic increase in particle size was attributed to the adsorption of the positively charged lactoferrin molecules onto the droplet surface with negative charges via electrostatic interactions. However, when there was insufficient lactoferrin molecules (0.5 to 1% w/w) to completely cover the droplet surface, bridging flocculation could result. Similar observation has been reported by (Pallandre et al., 2007; Fioramonti et al., 2015). Pallandre et al. (2007) studied the adsorption of sodium alginate (pK_a ~ 3.5) on sodium caseinate stabilised emulsions (pI of sodium caseinate ~ 4.6) (0.15% wt sodium caseinate; 1% wt corn oil) at pH 3.5. The ζ-potential of the emulsions changed from positive to negative when different concentrations of alginate solutions (0.05 – 1% wt) was added. Extensive droplet aggregation was observed at low alginate concentrations (0.025 – 0.05% wt) as there was insufficient alginate molecules to cover the droplet surface and resulted in bridging flocculation to occur. The particle size of the emulsions decreased when increasing the alginate concentrations (0.1 to 0.4% wt). Likewise, the particle size decreased when the lactoferrin concentration was increased above 1.5% which corresponds to C_{Sat} (Figure 7.6).

In contrast, the particle size of the nanoemulsions was relatively stable (around 80 nm) over a wide concentrations of lactoferrin (0.25 – 5% w/w) at pH 7, 8, 9 and 10 (Figure 7.6). At these pH values, WPI-coated droplets were highly negative charged (around -34 to -41 mV) (Figure 7.2) while lactoferrin molecules were slightly positive charged at these pH levels except at pH 9 and 10 (Chapter 6; Figure 6.1) for them to interact electrostatically. This implies that it is likely that the

lactoferrin molecules also adsorb to the surface of more than one droplet at concentration below saturation as described in the above as pH 6 but the negative charges on the emulsion droplets might be sufficient to repel each other. As pH falls towards the protein pI, the net positive charge of lactoferrin decreases, becomes zero and eventually become negative charge (Chapter 6; Figure 6.1), it would be expected that lactoferrin molecules did not adsorb to the droplet surfaces at pH 9 and 10. However, it may be still possible for lactoferrin molecules to interact with WPI under these conditions. This is so because lactoferrin is a bi-polar protein molecule with uneven charge distribution (Mantel et al., 1994). Therefore, the negatively charged WPI-coated droplets could interact with the positively charged "patches" on the lactoferrin surface. Besides, the emulsions were stable containing small droplets (80 to 100 nm; Figure 7.6) with an overall slight net negative charge (Figure 7.5). This is supported by the QCM-D results that showed the adsorption of lactoferrin molecules on the surface coated by WPI at pH 9 and 10 (Chapter 6; Section 6.4.3).

The mechanism for the observed phenomenon during the adsorption of lactoferrin molecules at different pH was proposed and summarised as illustrated in Figure 7.9. There was no or little adsorption of lactoferrin molecules on the droplet surface at pH 2 and 4 due to the positive net charges of both WPI and lactoferrin (weak electrostatic interactions). There was also limited interaction between WPI droplets and lactoferrin molecules at pH 5 as the net charge of WPI near zero around its pI. At pH 6, lactoferrin molecules can adsorb onto the surfaces of the droplets to produce a stable emulsion at sufficiently high concentration above 1.5% (w/w). At higher pH (7, 8, 9 & 10), a similar behaviour of the adsorption of lactoferrin onto the WPI droplets was observed.

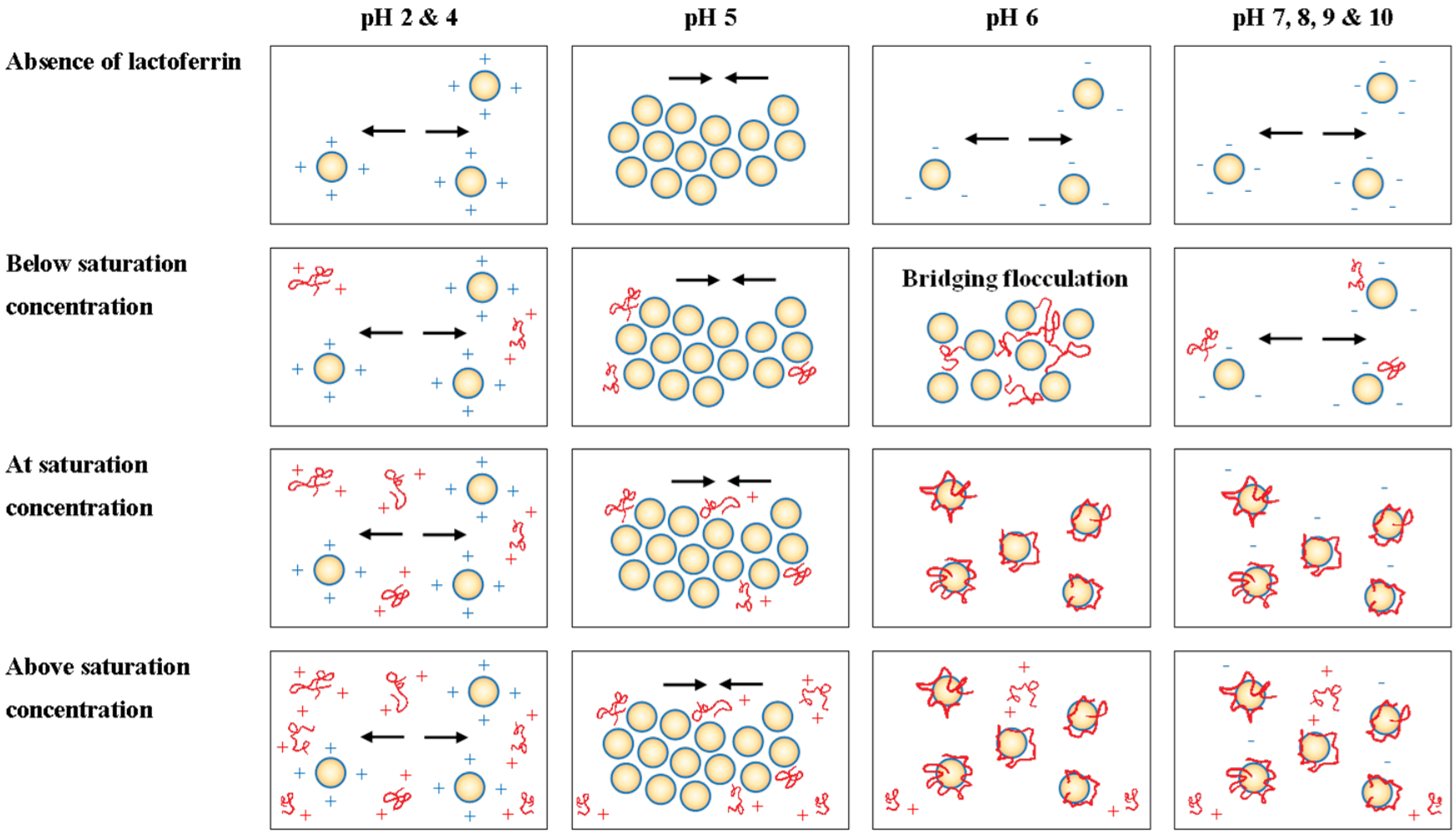

Figure 7.9 Schematic illustrations of interactions between WPI-coated droplets and lactoferrin molecules in bi-layer emulsions at different lactoferrin concentrations and solution pH (not drawn to scale).

7.4.2 Environmental stability of nanoemulsions

7.4.2.1 Effect of heat treatment

The effect of heat treatment on the stability of single layer (1% w/w WPI) and bi-layer emulsions (1% w/w WPI and 3% w/w lactoferrin) prepared at pH 6 was determined by heating them in water baths at different temperatures ranging from 30 to 90^{o}C for 15 minutes and cooling them down in ice-water bath before measurements. From the particle size data, the single layer emulsions containing WPI-coated droplets were relatively stable with no droplet aggregation at the temperature range used since the particle size remained fairly constant at around 80 nm (Figure 7.10). This result was similar to those of heat treated WPI nanoemulsions as shown in Section 4.4.7.1 of Chapter 4. However, droplet aggregation occurred in the bi-layer emulsions as there was an appreciable increase in their particle size from 90 to 230 nm when the temperature was increased from 50 to 90^{o}C with a significant increase in droplet size at 60^{o}C (Figure 7.10). The increased in particle size was attributed to the thermal denaturation of lactoferrin resulting in the globular protein to unfold and increase in hydrophobic attraction between the droplets (Tokle & McClements, 2011; Tokle et al., 2012). It has been reported that lactoferrin has two thermal denaturation temperatures at 61 and 93^{o}C due to two structural lobes with different heat sensitivities (Bengoechea et al., 2011; Bokkhim, Bansal, Grondhal & Bhandari, 2013). Previous studies have also reported that some lactoferrin emulsions exhibited droplet aggregation when heated above 60^{o}C (and up to 90^{o}C) (Tokle & McClements, 2011; Tokle et al., 2012). Therefore, the adsorption of lactoferrin at the droplet surface in bi-layer emulsions had led to an increased droplet aggregation at elevated temperatures.

Interestingly, droplet aggregation as a result of thermal denaturation was not observed in single layer nanoemulsions stabilised by lactoferrin in Chapter 4 (Section 4.4.7.1; Figure 4.16). This could be due to the fact that the concentration of lactoferrin used in the two emulsion systems was different. As mentioned earlier, the bi-layer emulsions was formed by mixing 3% (w/w) lactoferrin to ensure there are sufficient lactoferrin molecules adsorbed to the droplet surface to prevent bridging flocculation. As a result, there could be a sufficiently large amount of free proteins available in the bi-layer emulsions. In contrast, the lactoferrin (1% w/w) used in the

single layer emulsions (Chapter 4; Section 4.4.7.1) was mainly to form and stabilise the emulsions therefore there was not much free protein available in the serum phase.

As shown in Figure 7.11, there were some appreciable changes in the droplet charge of both single layer and bi-layer nanoemulsions with increasing temperature. The ζ-potential measurements showed that the single layer emulsions became more negatively charged as the temperature was increased from 30 to 90^{o}C with ζ-potential values ranging from -25.4 ± 0.8 to -34.3 ± 0.6 mV. A significant increase was also observed especially when the temperature was above 70^{o}C which is near to denaturation temperature of most whey proteins (Anema, 2008). Likewise, the bi-layer emulsions became more positively charged (+1.70 ± 0.30 to +7.21 ± 0.97 mV) with increasing temperature. These results indicated that the adsorbed proteins had probably undergone some structural changes at the droplet surface during heating, exposing the charged groups which might have resulted in an increase in the ζ-potential of the nanoemulsions. However, the relatively shorter heating duration of emulsions used in this experiment (15 minutes) did not cause considerable changes to the structure of whey proteins for extensive droplet aggregation to occur. It is known that the denaturation of whey proteins is also dependent on the heating time as mentioned in Section 4.4.7.1 of Chapter 4.

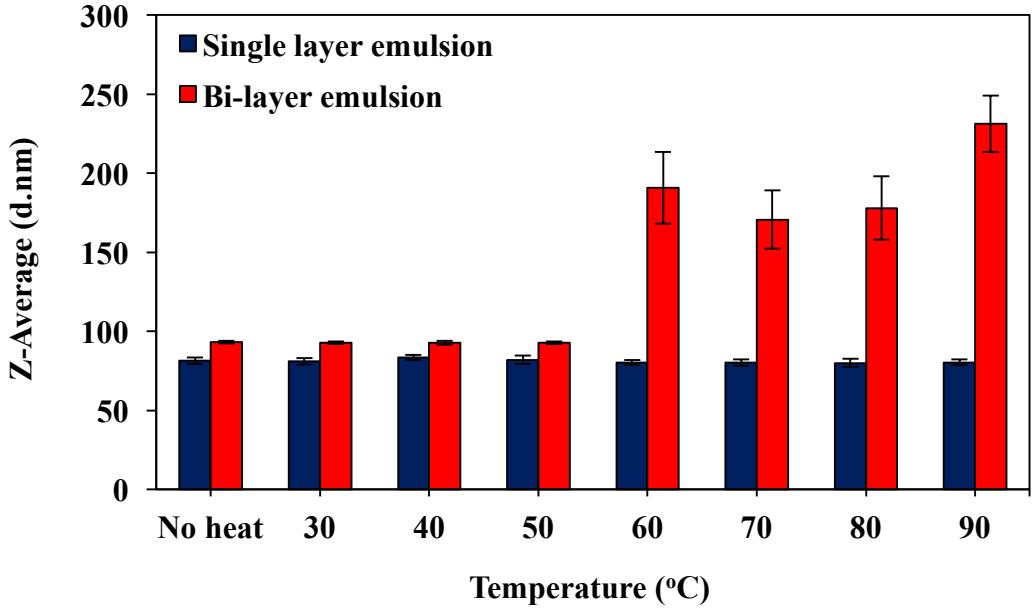

Figure 7.10 Influence of heating temperatures at different temperatures for 15 minutes on the mean particle diameter (Z-Average) of single layer and bi-layer emulsions. Data are presented as the mean of two independent measurements with triplicate (n=6) and error bars represent the standard deviation.

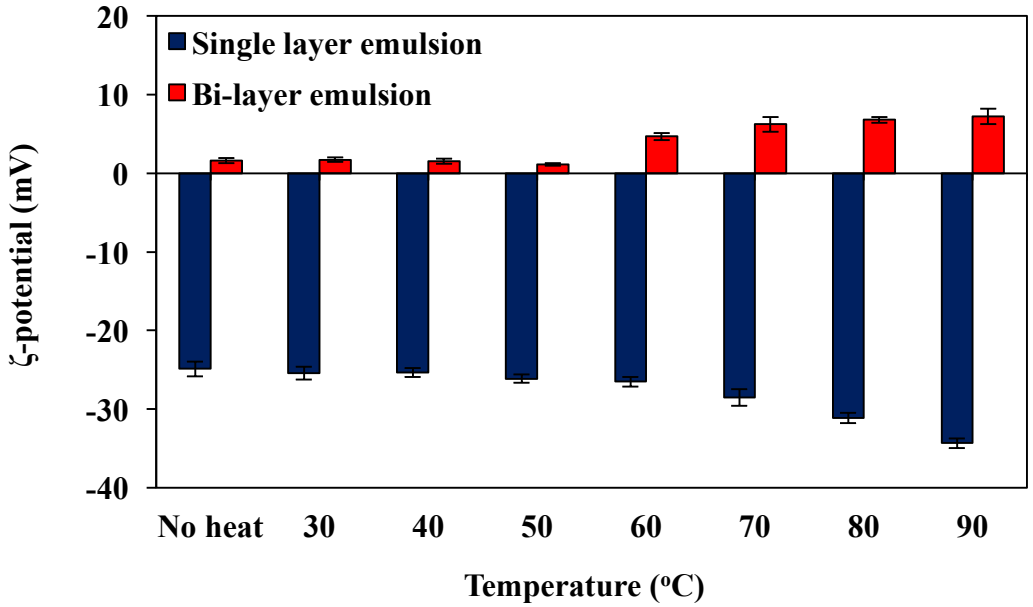

Figure 7.11 Influence of heat treatment at different temperatures for 15 minutes on the mean ζ-potential of single layer and bi-layer emulsions. Data are presented as the mean of two independent measurements with triplicate (n=6) and error bars represent the standard deviation.

7.4.2.2 Effect of pH changes

Single layer emulsions containing 1% (w/w) WPI and bi-layer emulsions containing 1% (w/w) WPI and 3% (w/w) lactoferrin were both prepared at pH 6 and then adjusted to different pH values (2, 3, 4, 5, 6, 7, 8, 9, 10, 11 and 12) to study the effect of pH changes on the stability of emulsions. The particle size and ζ-potential of the respective emulsions after pH adjustment are given in Figures 7.12 and 7.13, respectively. Initially, the single layer emulsions were negatively charged at pH 6 (-24.7 ± 1.8 mV) and they were stable to droplet aggregation mainly due to electrostatic repulsion forces. The emulsions remained stable around 80 nm when the pH was increased from 6 to 12 (Figure 7.12) and the droplets become more negatively charged (> -30 mV) (Figure 7.13). However, the emulsions were prone to extensive droplet aggregation (> 10 μm) when the pH was reduced near to the pI of whey proteins (Figure 7.12). At pH 5 near to the pI, the adsorbed proteins on the droplets contained few electrical charges and the electrostatic repulsion was insufficient to overcome the attractive forces for protein aggregation via hydrophobic interaction to occur (Kulmyrzaev et al., 2000; McClements, 2004). This accounts for the large increase in the particle size at pH 5. When the pH was reduced at lower pH values of 2, 3 and 4, the droplets become positively charged (> +30 mV) as expected and the emulsions appeared to be stable (due to electrostatic repulsion) and their particle size was around 80 nm (Figure 7.12).

In contrast, the bi-layer emulsions did not exhibit any droplet aggregation when the pH was increased or decreased above or below pH 5 (Figure 7.12). This indicated that the adsorption of lactoferrin to the surfaces of WPI-coated droplets can improve the emulsion stability at pH near to the pI of whey proteins. The fact that the bi-layer emulsions was neutrally charged or slightly charged at pH above 5 (Figure 7.13) suggested that the lactoferrin molecules could improve the pH stability by providing a strong steric repulsion. However, in the earlier study described in Section 7.4.1, there was no or little adsorption of lactoferrin to the droplet surface at lower pH values of 2 and 4. Under these conditions, one might expect that the lactoferrin molecules do not interact with the free or adsorbed WPI molecules on the droplet surface due to both molecules with the same charges (positive). Both the electrical charge of the droplets in single layer and bi-layer emulsions was highly positive although the bi-layer emulsions had a slightly lower ζ-potential value of

around +20 mV (Figure 7.13). A slight decrease in the ζ-potential may be due to the neutralisation of positive charges of WPI by some anionic salts derived from when lactoferrin was added. Although iron is released from lactoferrin at around pH 4, it is expected that the iron released from lactoferrin does not interact with the WPI droplets as both are positively charged to mutually repel each other.

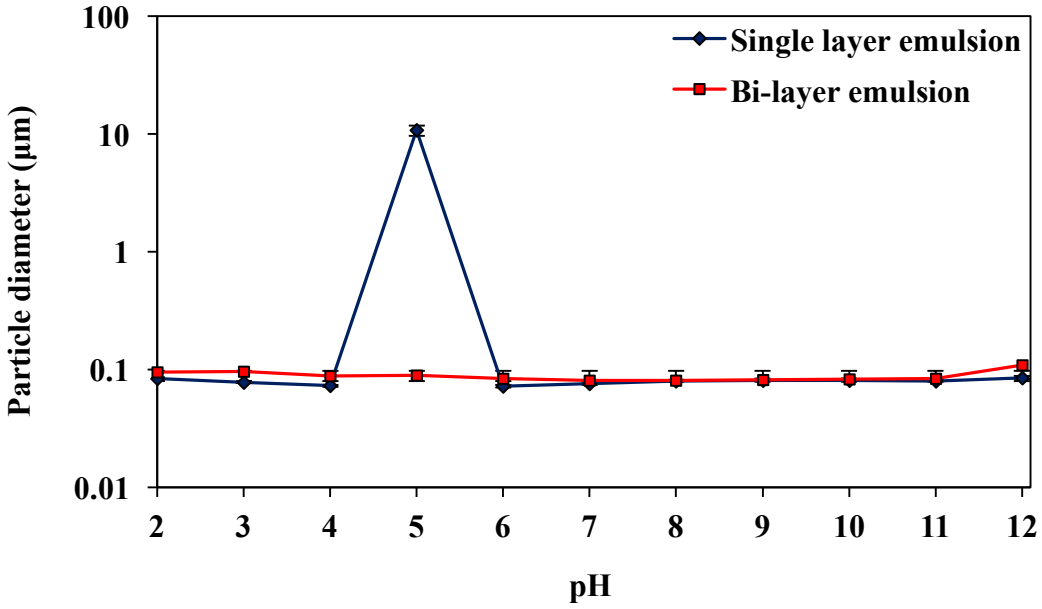

Figure 7.12 Influence of pH changes on the mean particle diameter (Z-Average) of single layer and bi-layer emulsions measured using a Zetasizer Nano ZS. Particle size of single layer emulsion at pH 5 is reported as the $D_{4,3}$ measured using a Mastersizer 2000. Data are presented as the mean of two independent measurements with triplicate (n=6) and error bars represent the standard deviation.

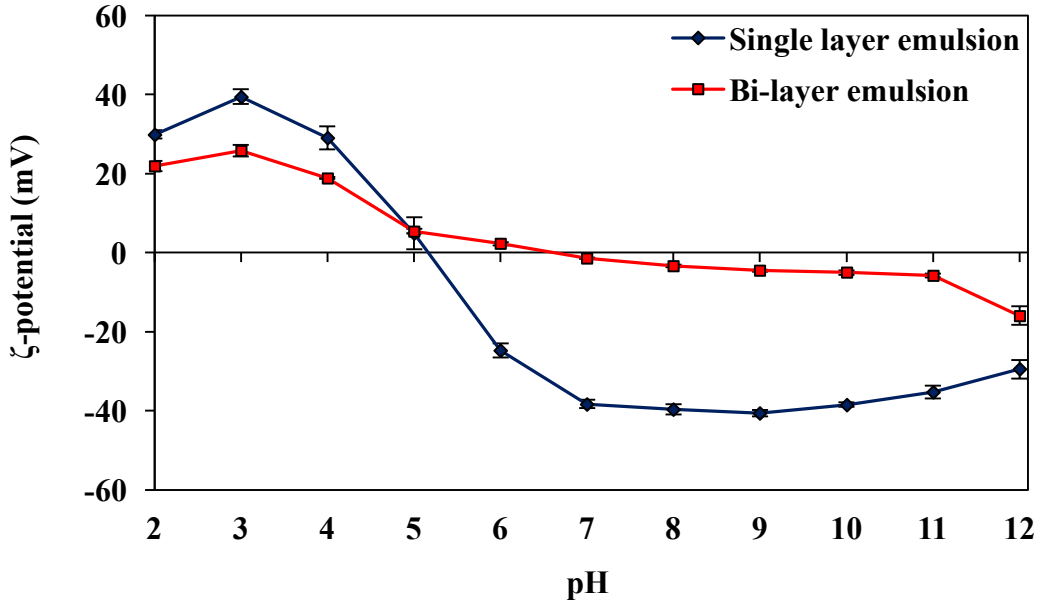

Figure 7.13 Influence of pH changes on the mean ζ-potential of single layer and bi-layer emulsions. Data are presented as the mean of two independent measurements with triplicate (n=6) and error bars represent the standard deviation.

7.4.2.3 Effects of type and concentration of salts

The stability of the single layer (1% w/w WPI) and bi-layer nanoemulsions (1% w/w WPI and 3% w/w lactoferrin) to salt addition (0 – 500 mM NaCl or 0 – 90 mM $CaCl_2$) was determined at pH 6. All of the nanoemulsions appeared to be stable to NaCl addition as there were no drastic changes in the particle size with increasing salt concentration (Figure 7.14), presumably due to good steric repulsion between the droplets in nanoemulsions as discussed in Chapter 4 (Section 4.4.7). It was also observed that there was a decrease in electrical charge of the droplets in all the nanoemulsions with increasing NaCl concentration (Figure 7.15) due to the ability of the counter-ions (Na^+ or Cl^-) present that influences the droplet charge. The ζ-potential of the single layer emulsions decreased from around -20 to -7 mV while the bi-layer emulsions changed from around +1.8 to -3.6 mV (Figure 7.15).

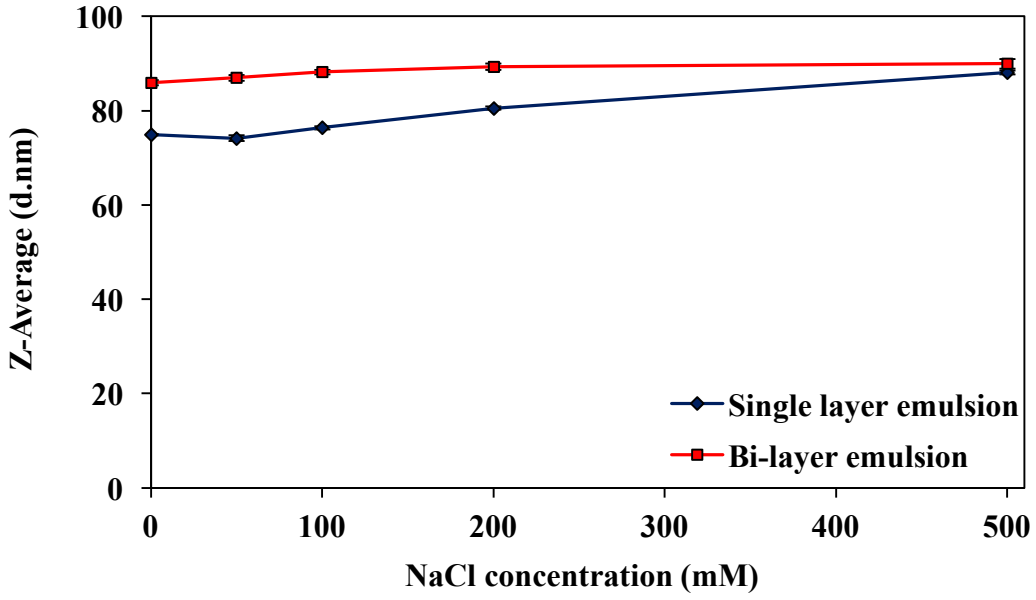

Figure 7.14 Influence of NaCl concentrations on the mean particle diameter (Z-Average) of single layer and bi-layer emulsions. Data are presented as the mean of two independent measurements with triplicate (n=6) and error bars represent the standard deviation.

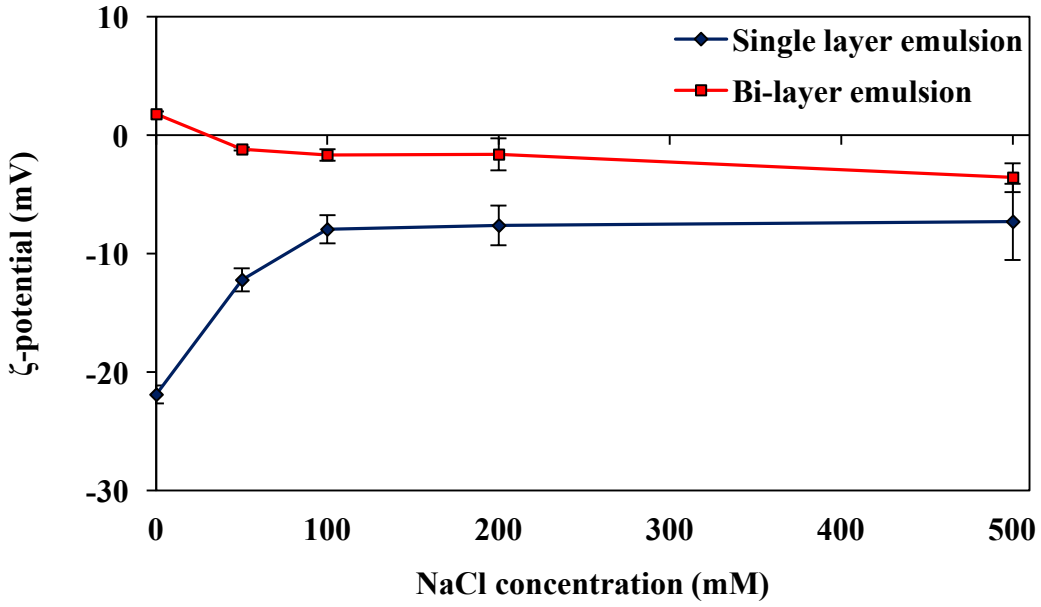

Figure 7.15 Influence of NaCl concentrations on the mean ζ-potential of single layer and bi-layer emulsions. Data are presented as the mean of two independent measurements with triplicate (*n*=6) and error bars represent the standard deviation.

However, there was a clear difference in the stability of the single layer and bi-layer emulsions to $CaCl_2$ addition. There was a large decrease in the ζ-potential of the droplets in single layer emulsions (from around -26 to -9 mV) (Figure 7.16) with the occurrence of droplet aggregation (Figure 7.17). Droplet aggregation was attributed to the binding of Ca^{2+} ions to the negatively charged droplets in the single layer emulsions and resulted in the formation of calcium bridging between the droplets for extensive droplet aggregation to occur (Ye et al., 2012; Degner et al., 2014). However, the bi-layer emulsions were stable to $CaCl_2$ as there was no change in the ζ-potential (Figure 7.16) as well as the particle size with increasing salt concentration (Figure 7.17). This effect could be explained by the positively charged lactoferrin at the droplet interface which are not affected by the like charge of the Ca^{2+} ions.

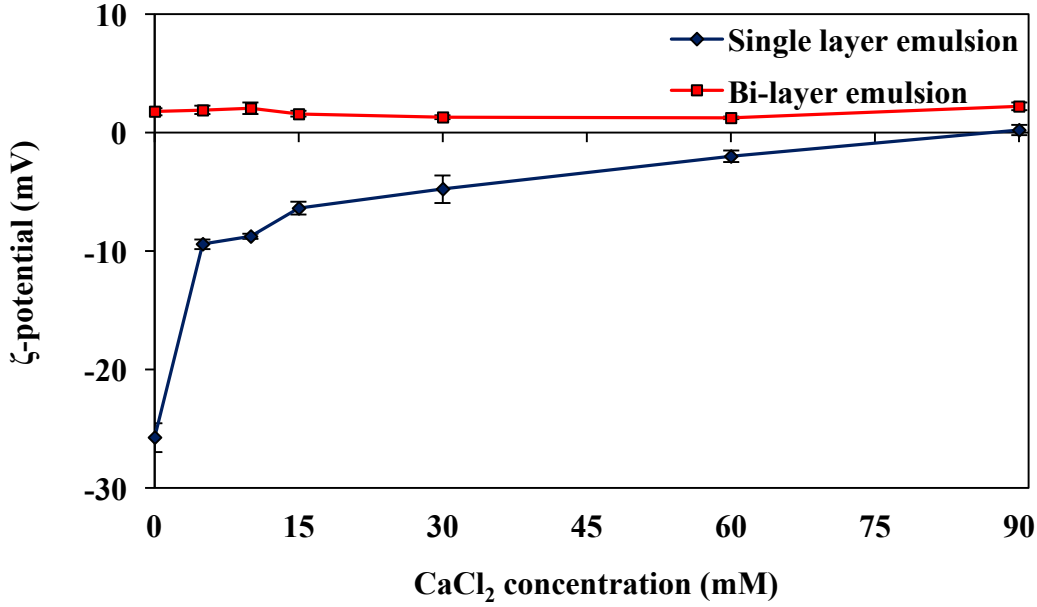

Figure 7.16 Influence of $CaCl_2$ concentrations on the mean ζ-potential of single layer and bi-layer emulsions. Data are presented as the mean of two independent measurements with triplicate (n=6) and error bars represent the standard deviation.

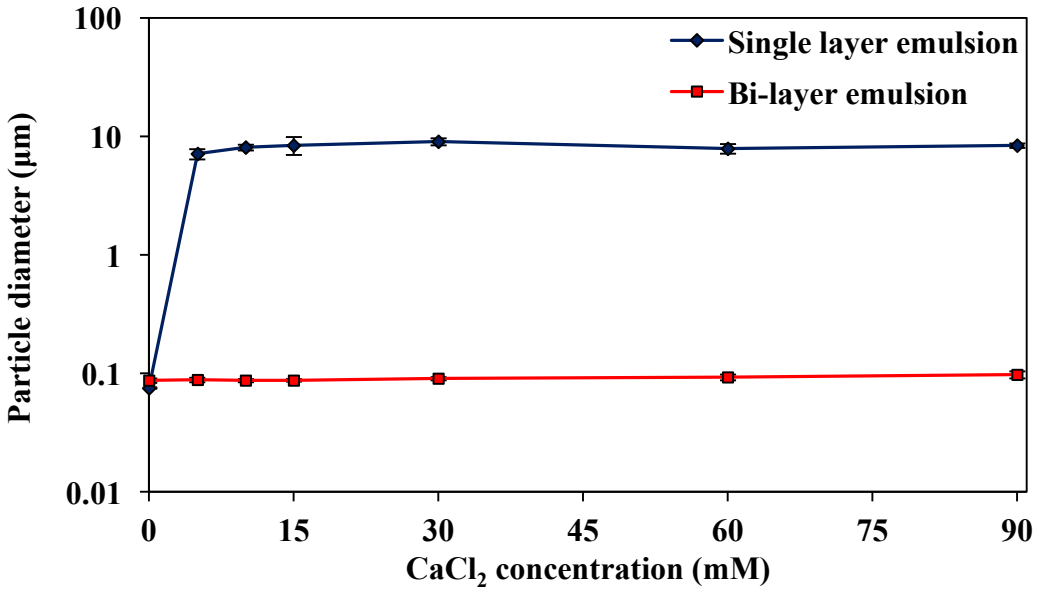

Figure 7.17 Influence of $CaCl_2$ concentrations on the mean particle diameter (Z-Average) of single layer and bi-layer emulsions measured using a Zetasizer Nano ZS. Particle size of single layer emulsions at salt concentration above 5 mM $CaCl_2$ is reported as the $D_{4,3}$ measured using a Mastersizer 2000. Data are presented as the mean of two independent measurements with triplicate (n=6) and error bars represent the standard deviation.

7.4.3 Protein hydrolysis of nanoemulsions using *in vitro* gastrointestinal model

The rate of protein hydrolysis during *in vitro* digestion of nanoemulsions under simulated gastric and intestinal conditions was monitored by SDS-PAGE. As shown in Figure 7.18a, the major proteins in WPI, namely β-lactoglobulin (β-lg) and α-lactalbumin (α-lac), were present in single layer emulsions stabilised by whey proteins. Similarly, β-lg and α-lac bands were present in the corresponding SDS-PAGE gel containing protein solution of 1% WPI (Figure 7.18i). In Lane E in Figure 7.18b, the bi-layer emulsions before digestion contained lactoferrin as well as β-lg and α-lac. It should be mentioned that the bi-layer emulsions were diluted to a same total protein concentration of 1% (w/w) with Milli Q water as the single layer emulsions before mixing with SGF in order to obtain clear bands for SDS-PAGE. This explains why the intensities of β-lg and α-lac bands in the bi-layer emulsions were notably lower than in single layer emulsions.

As shown in Figure 7.18a, it was observed that the intensity of β-lg band had decreased slightly when the single layer emulsions were incubated with SGF while the band of α-lac disappeared at longer incubation time (≥ 30 minutes) during the gastric phase. This was attributed to β-lg being more resistant than α-lac to pepsin digestion (Guo, Fox, Flynn & Kindstedt, 1995). The side chains of aromatic amino acids (hydrophobic) in native β-lg were buried inside the globular protein structure but the β-lg adsorbed on the emulsions was susceptible to proteolysis due to the conformation changes of β-lg structure during emulsification process which exposes some aromatic residues (Reddy, Kella & Kinsella, 1988; Nik, Wright & Corredig, 2010). It is known that the cleavage of pepsin is the most efficient on peptides with hydrophobic and aromatic residues such as phenylalanine, tyrosine, tryptophan and leucine in position P1 or P1' (Keil, 1992). However, a clear band of β-lg was still present in the single layer emulsions at the end of gastric phase after 60 minutes of incubation (Figure 7.18a) which is similar to those of 1% WPI solution (Figure 7.18i). One possible explanation could be a portion of whey proteins in the nanoemulsions was present in the native form as it was not possible to separate the oil droplets (cream phase) and serum phase in nanoemulsions due to the low oil concentration (0.5% w/w) used in the formulation. As such, some fractions of β-lg was present in the SDS-PAGE gel of single layer nanoemulsions after incubation

with SGF as the native protein (β-lg) in the emulsions was resistant to hydrolysis. However, the band of pepsin (35 kDa) was not detected in the SDS-PAGE gel due to the low concentration used in the experiment.

The digestion pattern of the bi-layer emulsions was very similar to the single layer emulsions. It was observed that the lactoferrin band present in the emulsion (Lane E) disappeared immediately after gastric incubation at 0 minute (Figure 7.18b) while the β-lg band decreased and α-lac disappeared as digestion continues which was similar to the single layer emulsions. In fact, all the lactoferrin was hydrolysed in the SDS-PAGE gel loaded with 1% lactoferrin solution upon incubation with SGF (Figure 7.18ii). This is because lactoferrin is very susceptible to gastric proteolysis (Shimoni, Levi, Tal & Lesmes, 2013) and therefore the majority of lactoferrin present in the system was hydrolysed and different fractions of peptides with lower molecular weights (6.5 to 21.5 kDa) were observed in the gel (Figure 7.18b). The gastrointestinal hydrolysis of lactoferrin has been reported by several other researchers (Brock, Arzabe, Lampreave & Piñeiro, 1976; Troost et al., 2001). According to Troost et al. (2001), lactoferrin become susceptible to pepsin degradation when iron is released from the protein molecule at pH less than 4. Contrary to the literature that states that the lactoferrin molecule is resistant to proteolysis by pepsin due to the two structural lobes (C- and N-lobe), the lactoferrin in these emulsions were quickly hydrolysed into small fragments (Figure 7.18b). It was mentioned in the literature that incubation of lactoferrin with pepsin (~ pH 2.5) produced a fragment at 39.5 kDa due to the ability of the C-lobe to bind iron at low pH (Troost et al., 2001). However, in our study, small lactoferrin fragments were immediately formed after gastric incubation, presumably due to the low pH used (around 1.2) which resulted in the rapid release of iron from the lactoferrin molecule, making the protein susceptible to digestion by pepsin.

The subsequent incubation of nanoemulsions with SIF (containing pancreatin) showed that the protein bands of β-lg and other peptides present in the emulsions soon disappeared after mixing with SIF (Figure 7.18). This indicates that the protein was completely hydrolysed during the intestinal phase of *in vitro* digestion and any encapsulated components in the oil droplets can be released for absorption by the intestinal epithelial cells. It is evident that several other bands present in the SDS-PAGE gels were produced by pancreatin during incubation of the intestinal phase.

As known, pancreatin is a mixture of digestive enzymes containing proteases, amylases and lipases which hydrolyses proteins, starches and fats, respectively. From Figure 7.18, a prominent band at the vicinity of 45 and 66.2 kDa (amylase (AMS) and lipase (L)) with another four minor bands around 31 kDa (trypsin (TR), ribonuclease (RNase) and protease) soon appeared after intestinal incubation (from 65 minutes onwards). Similarly, Bokkhim, Bansal, Grøndhal & Bhandari (2016) also reported the presence of these bands in SDS-PAGE of pancreatin.

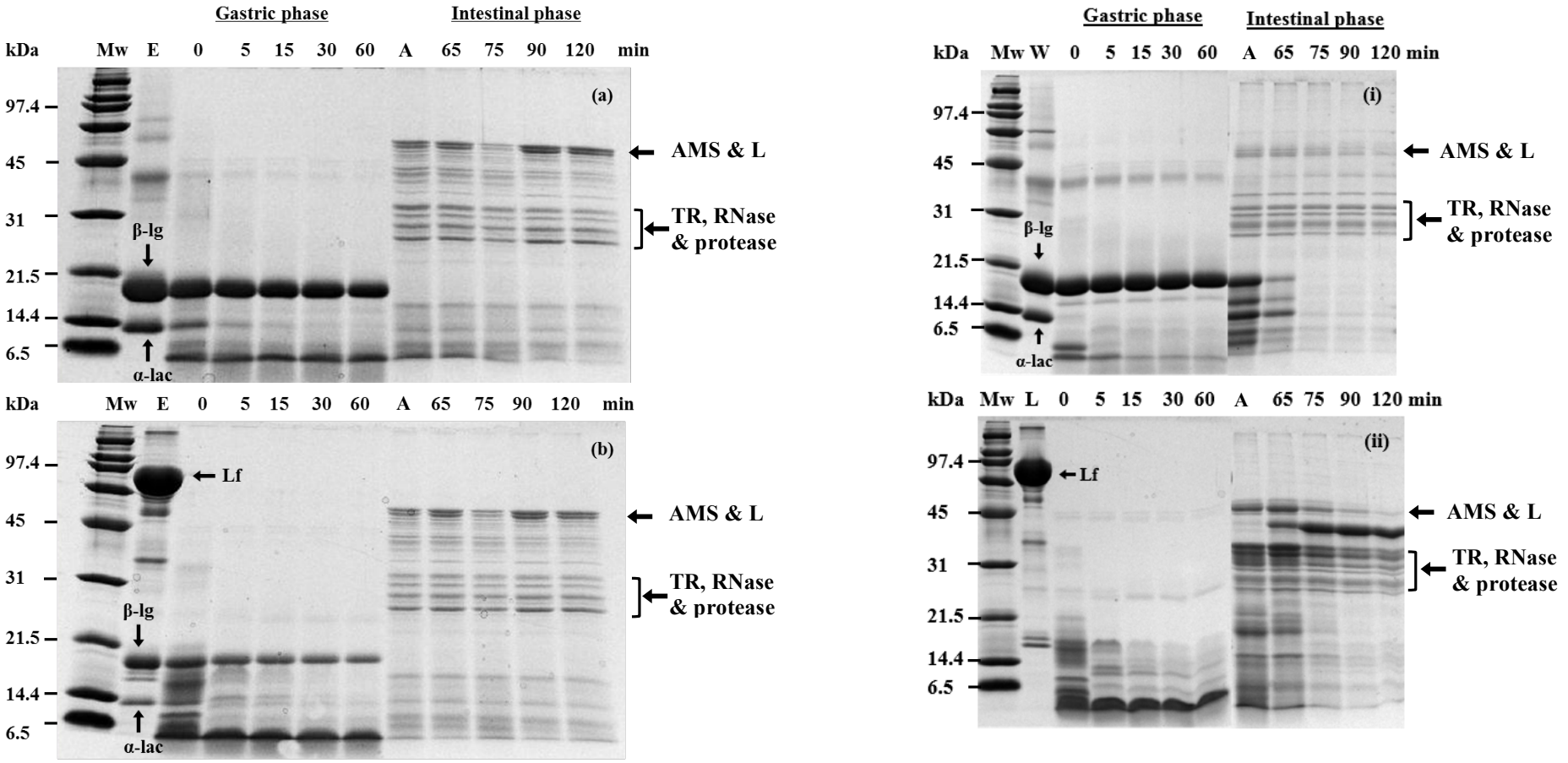

Figure 7.18 SDS-PAGE analysis of nanoemulsions containing (a) 1% (w/w) WPI (single layer emulsion) and (b) those containing 1% (w/w) WPI and 3% (w/w) lactoferrin (bi-layer emulsion) diluted to the same protein concentration as the WPI emulsions during *in vitro* digestion when mixed with SGF and SIF in sequence at different time intervals (0, 5, 15, 30, 60, 65, 75, 90 and 120 minutes). Mw: molecular weight standards; E: original emulsion; A: mixing of emulsion/ protein solution after gastric phase with SIF. SDS-PAGE analysis of 1% protein solution of (i) WPI or (ii) lactoferrin subjected to the same digestion conditions.

The particle sizes of the emulsions before and after incubation with SGF and SIF are shown in Figure 7.19. As expected, the nanoemulsions containing WPI (single layer emulsions) and those with the addition of lactoferrin (bi-layer emulsions) were relatively stable and contained small oil droplets less than 90 nm in diameter (Z-Average). At pH 6, the WPI-coated droplets in single layer emulsions were negatively charged (-21.9 ± 0.7 mV) because the adsorbed whey proteins were above their pI (around 4.9) whereas the bi-layer emulsions containing WPI droplets coated by lactoferrin were slightly positive charged (+1.8 ± 0.2mV) (Figure 7.20).

There was no major change in the particle size of both nanoemulsions after incubation with SGF (Figure 7.19) but the ζ-potential of both nanoemulsions become highly positive charged as the pH was drastically reduced from close to neutral at pH 6 to highly acidic in the gastric phase at pH 1.2 (Figure 7.20). The single layer emulsion changed from being negative (-21.9 mV) to positive (+23.5 mV) and the bi-layer emulsion became more positively charged (from +1.8 to +20.7 mV). Not surprisingly, the nanoemulsions were stable against the conditions used in the gastric phase. The positive charges on the droplets suggested that there is a strong electrostatic repulsion between them.

In contrast, large particles ($D_{4,3}$ > 60 μm) were formed in the particle size of both nanoemulsions after subsequent incubation under intestinal conditions (Figure 7.19). The ζ-potential also changed from being positive to negative (less than -10 mV) after incubation with SIF (Figure 7.20), presumably due to the adsorption of anionic components from bile salt or other components generated during the digestion process (Lesmes et al., 2010; Li et al., 2011) as well as the increase in pH value of the intestinal phase at pH 6.8. Previous studies have shown that protein-stabilised emulsions undergo extensive droplet flocculation and coalescence on exposure to SIF due to proteolysis of the interfacial layer by trypsin, along with some displacement of protein layer by bile salt (Nik, Wright & Corredig, 2011; Tokle et al., 2012). Consequently, changes in the interfacial composition may affect the emulsion stability, making them more susceptible to droplet aggregation. The presence of $CaCl_2$ in the SIF could also promote flocculation of the droplets as shown in the environmental study. In addition, the reduction in ζ-potentials observed in both nanoemulsions after digestion (Figure 7.20) meant a reduction in electrostatic repulsion and therefore led to an increase in droplet aggregation.

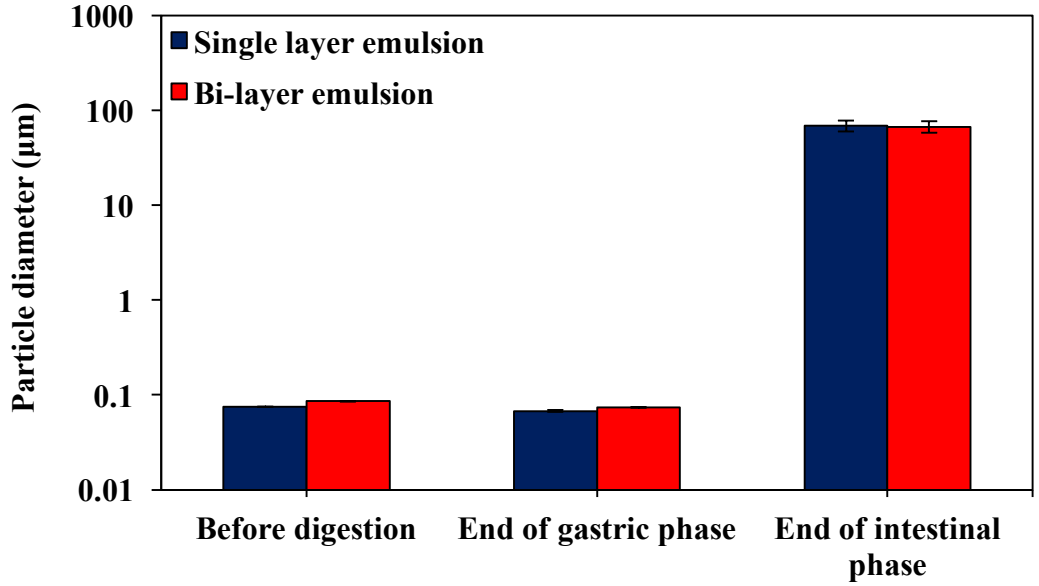

Figure 7.19 Influence of simulated gastrointestinal tract conditions on the mean particle diameter (Z-Average) of single layer and bi-layer emulsions measured using a Zetasizer Nano ZS. Particle size of emulsion at end of intestinal phase is reported as the $D_{4,3}$ measured using a Mastersizer 2000. Data are presented as the mean of two independent measurements with triplicate (n=6) and error bars represent the standard deviation.

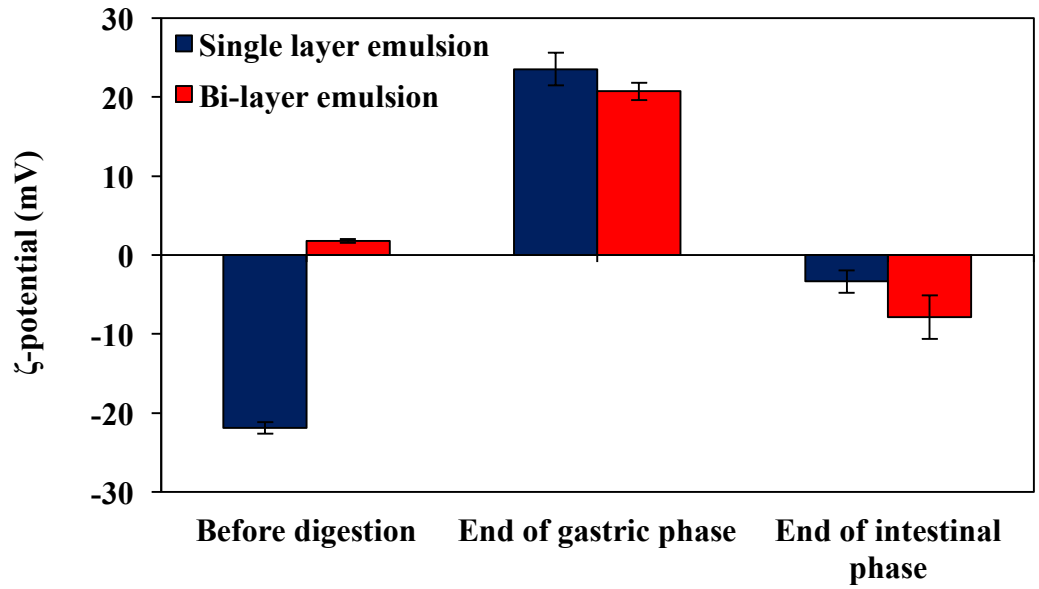

Figure 7.20 Influence of simulated gastrointestinal tract conditions on the mean ζ-potential of single layer and bi-layer emulsions. Data are presented as the mean of two independent measurements with triplicate (n=6) and error bars represent the standard deviation.

7.5 Conclusions

This study has demonstrated that nanoemulsions containing multiple layers of proteins can be formed by depositing lactoferrin molecules onto the surface of droplets stabilised by WPI. However, the stability of emulsions was dependent on the solution pH and lactoferrin concentration. At pH 2 and 4, lactoferrin did not adsorb to the droplet surface due to strong electrostatic repulsion and there was only a slight adsorption of lactoferrin to the droplets at pH 5. At higher pH above 6, there was an electrostatic attraction between lactoferrin molecules and WPI to form a bi-layer around the droplets. However, the emulsions were prone to droplet aggregation by bridging flocculation in the presence of insufficient lactoferrin molecules. Consequently, a sufficiently high level of lactoferrin was required to obtain a stable bi-layer emulsion containing 1% (w/w) WPI and 3% (w/w) lactoferrin at pH 6. In the environmental study, the bi-layer emulsions were susceptible to thermal degradation at temperatures above 60^{o}C but exhibited good stability to pH changes and salt addition. During *in vitro* digestion, bi-layer emulsions containing lactoferrin did not affect the digestion process and all the protein layers were completely hydrolysed at the end of the digestion process. This study provided insight into the design and use of emulsions composed of WPI and lactoferrin to improve emulsion stability to some environmental stresses.

Chapter Eight:

Encapsulation and Stability of Lutein in Protein-stabilised Nanoemulsions and Cytotoxicity using Caco-2 cell line

8.1 Abstract

With the use of emulsification and solvent evaporation method, the potential application of nanoemulsions is to encapsulate bioactive compounds as a delivery system for their incorporation in foods or beverages. In this study, nanoemulsions stabilised by a single layer of WPI or a sequential bi-layer of WPI and lactoferrin were loaded with lutein using the mentioned method. The physicochemical properties, storage stability and *in vitro* cytotoxicity of nanoemulsions and cellular uptake of lutein by the gut enterocyte cell line Caco-2 were measured and compared to a WPI-stabilised conventional emulsion containing lutein prepared under the same conditions but without the use of an organic solvent (ethyl acetate). Nanoemulsions containing lutein produced small droplets (70 – 80 nm) while larger droplets (147 nm) were formed in conventional emulsions. The encapsulation efficiencies of lutein in conventional emulsions and nanoemulsions were 86% and 81%, respectively. The storage stability study showed that all the emulsions were physically stable as the particle size did not change during 28 days of storage at different temperatures of 5, 20 and 40^{o}C. However, the emulsion colour was observed to become lighter (less redness and yellowness) in samples stored at higher temperatures due to degradation of lutein. The lutein content was found to decrease during storage especially at higher temperature of 40^{o}C. The degradation of lutein in emulsions was fitted to a first order kinetic and the rate constant was found to increase with increasing temperatures especially in WPI-stabilised single layer nanoemulsions. The temperature dependence of lutein degradation in the emulsions was also determined by the Arrhenius equation. The activation energies of lutein in conventional emulsions (38.0 ± 12.0 kJ/mol) and bi-layer nanoemulsions (37.3 ± 1.0 kJ/mol) were lower than single layer nanoemulsions (45.4 ± 8.5 kJ/mol) with higher retention of lutein in conventional emulsions and bi-layer nanoemulsions after 28 days of storage. The possible toxicity of lutein nanoemulsions was also investigated using MTT assay on Caco-2 cells. All the nanoemulsions did not show more toxicity than the

conventional emulsions as the cell viability of all the emulsions was more than 80% at 10 times or more dilution after 24 hours of incubation. The uptake of lutein was higher in bi-layer nanoemulsions than single layer conventional emulsions and nanoemulsions. The results of this study indicated that nanoemulsions can be used as delivery system to encapsulate bioactive materials and the stability and cellular uptake of lutein can be enhanced using a combination of WPI and lactoferrin in bi-layer nanoemulsions.

8.2 Introduction

In previous chapters, the making of nanoemulsions with different composition and interfacial structures was investigated using emulsification and solvent evaporation method. The nanoemulsions were translucent and contained small oil droplets with high surface area to volume ratio that can potentially improve absorption of encapsulated bioactive materials in the GI tract. In addition, the water dispersible nanoemulsions displayed good physical stability under different environmental conditions (Chapter 4; Section 4.4.7). The functionality of nanoemulsions was further improved by depositing oppositely charged biopolymers (i.e. lactoferrin) on the surface of WPI-coated droplets to form bi-layer nanoemulsions (Chapter 7). Therefore, there is an increasing interest to use water dispersible nanoemulsions as a potential delivery system for encapsulating bioactive compounds to overcome some limitations associated with their poor water solubility and high susceptibility to degradation.

A variety of bioactive compounds can be added to functionalise foods and beverages to improve health and well-being. Lutein is one of these bioactive compounds which have health benefits associated with a lower risk of eye diseases such as AMD and cataracts when consumed at reasonable amounts (Alves-Rodrigues & Shao, 2004; Shegokar & Mitri, 2012). An increased intake of 6 mg lutein per day has been shown to reduce the risk of AMD (Seddon et al., 1994; Krinsky et al., 2003). However, dietary intake of lutein remained low in today's diet as it is not realistic to consume a large proportion of leafy vegetables rich in lutein (e.g. kale, spinach) which is equivalent to having 1 – 2 large salad bowls to meet the recommendations. Hence, it is more desirable to fortify foods with lutein. However,

lutein has poor water solubility with a log octanol/water partition coefficient (P_{oct}) of 14.8 (Reboul, Abou, Mika, Ghiringhelli, André, Portugal, Jourdheuil-Rahmani, Amiot, Lairon & Borel, 2005) and is only soluble in fats or organic solvents (Craft & Soares, 1992; Shegokar & Mitri, 2012). As a consequence, nanoemulsions prepared by solvent evaporation is a suitable method for incorporating lutein into water-based formulation with high loading capacity. The use of organic solvent in this method is advantageous over traditional oil carriers which can improve the solubility of lipophilic compound in the dispersed phase, yet making these compounds dispersible in water.

Although the materials used in making nanoemulsions are food grade and are considered as generally recognised as safe (GRAS), the possible toxicological effect of smaller particles in the nanometric range is a concern. In particular, some studies have shown that 15 μM curcumin microemulsions with small particle size of 30 nm exhibited more cytotoxic effect than particles of 80 nm on the hepatocellular (HepG2) cell line (Lin et al., 2014). On the other hand, Yu & Huang (2013) reported that nanoemulsions (10% w/w MCT) made with 5% (w/w) modified starch, Tween 20 or WPI (155 – 173 nm) did not show any differences in toxicity (no toxic) from their micro-sized emulsions (5.7 – 10.3 μm) in Caco-2 cells but exhibited hepatic toxicity in HepG2 cells.

Meanwhile, the use of nanometric size delivery systems (below 200 nm) was found to improve cell absorption and uptake of encapsulated bioactive components (Choi et al., 2014; Li, Liu & Yu, 2015). According to Xiao & McClements (2012), the small droplet size of nanoemulsions may be transported directly across the epithelium cell layer by passive transport for absorption in the small intestine. Furthermore, modifying the particle characteristics in bi-layer nanoemulsions may affect their interactions with the cells. Caco-2 cells derived from human colon cancers can be used to mimic the small intestine epithelium to study the absorption of bioactive compounds *in vitro*. Caco-2 cells were used because they can differentiate into polarised cell monolayers with the formation of microvilli and tight junctions which is similar to those found in the human enterocytes (Balimane & Chong, 2005). Furthermore, this cell line has been repeatedly used to study the transport and uptake of several nutrients. For example, Qhattal, Wang, Salihima, Srivastava & Liu (2011) studied the transport of benzyl isothiocyanate in

nanoemulsions (< 300 nm) across Caco-2 cells. Zhang, Field, Vine & Chen (2015) studied the effect of particle size on the uptake and transport of Vitamin B_{12} nanoparticles (30 – 180 nm) in Caco-2 cells. To the best of our knowledge, the possible toxicity and *in vitro* cellular uptake of lutein nanoemulsions with different interfacial structures on Caco-2 cells have not been addressed.

The objective of this study was therefore to encapsulate lutein into nanoemulsions using emulsification and solvent evaporation method. The physicochemical properties and stability of lutein during storage at different temperatures (5, 20 and 40^{o}C) were studied and compared to a conventional emulsion. The *in vitro* cytotoxicity and cellular uptake of lutein in emulsions on Caco-2 cells were also investigated. This study is useful for the incorporation of bioactive compounds in nanoemulsions for applications in foods.

8.3 Materials and Methods

8.3.1 Materials

The materials used for making nanoemulsions are as listed in the previous chapter (Chapter 3; Section 3.1). Lutein powder (≥90% purity) and lutein standard was purchased from Shaanxi Sciphar Biotechnology Co., Ltd. (China). (±)-α-Tocopherol (synthetic, ≥96% HPLC) was purchased from Sigma Aldrich (St. Louis, MO, USA).

HPLC grade methanol and ethyl acetate were purchased from Fisher Scientific, Leicestershire, UK. Potassium hydroxide, butylated hydroxyl toluene (BHT), dichloromethane and acetic acid were from BDH Chemicals (BDH Ltd, Poole, England). n-Hexane for liquid chromatography and acetonitrile gradient grade for liquid chromatography were from EMD Millipore Corporation, Billerica MA, USA.

Dulbecco's modified eagle medium (DMEM) (1X), fetal calf serum, non-essential amino acids solution (100X), penicillin streptomycin glutamine (100X), sodium bicarbonate (7.5% solution) and trypsin-EDTA (0.05%) were from Gibco Life Technologies (New York, USA). Thiazolyl blue tetrazolium bromide (98% TLC) and dimethyl sulfoxide (DMSO) were from Sigma Aldrich (St. Louis, MO, USA).

8.3.2 Preparation of lutein conventional emulsion and nanoemulsion

Nanoemulsions were prepared according to the method as described in Chapter 3 (Section 3.2.2). For conventional emulsions, they were prepared under the same conditions but without the addition of ethyl acetate. Lutein was first dissolved in the organic phase containing corn oil or a mixture of 10% (w/w) corn oil and 90% (w/w) ethyl acetate. 0.001% (w/w) α-tocopherol was added as an antioxidant to minimise degradation of lutein during the preparation of emulsions. The organic phase was mixed with the aqueous phase containing 2% (w/w) WPI at a ratio of 10:90 and they were subjected to high pressure homogenisation for 4 cycles at 80 MPa (12000 psi). Ethyl acetate was removed from the nanoemulsions by rotatory evaporation under reduced pressure at 50^{o}C for around 20 minutes.

Nanoemulsions containing bi-layer structure were formed by mixing WPI-stabilised nanoemulsions with an equal amount of 6% (w/w) lactoferrin solution at pH 6. For single-layer emulsions, they were mixed with Milli Q water so that the respective emulsion systems contained the same concentration of oil (0.5% w/w). The details of the composition of lutein loaded conventional emulsions and nanoemulsions are shown in Table 8.1.

Table 8.1 Composition of lutein loaded conventional emulsion and nanoemulsion.

	Conventional emulsion			**Nanoemulsion**		
	Before evaporation	**After evaporation**	**Final**	**Before evaporation**	**After evaporation**	**Final**
Aqueous phase						
WPI	1.79	1.79	0.09	1.80	1.80	0.90
Water	87.8	87.8	4.39	88.2	97.2	48.6
Organic phase						
Corn oil	9.96	9.96	0.50	1.00	1.00	0.50
Ethyl acetate	-	-	-	9.00	0.00	0.00
Lutein	0.448	0.448	0.022	0.045	0.045	0.023
α-tocopherol	0.001	0.001	0.000	0.001	0.001	0.001
Adjust to 0.5% oil level						
Water or lactoferrin solution	-	-	95.0	-	-	50.0
Total	100.0	100.0	100.0	100.0	100.0	100.0

After preparation, the conventional emulsions and nanoemulsions were stored in the absence of light at different temperatures of 5, 20 and 40^{o}C for 28 days and the samples were taken periodically (0, 7, 14, 21 and 28th day) for analysis.

8.3.3 Characterisation of lutein nanoemulsions

The particle size, ζ-potential and microstructures of the lutein emulsions were determined as described in Chapter 3 (Section 3.3). The colour of emulsions during storage at different temperatures (5, 20 and 40^{o}C) was observed visually and measured using a pre-calibrated colour measuring instrument (Minolta CR-410 Chroma Meter, Minolta Co., Japan). The emulsion samples were gently stirred before measurement, then poured into the measurement cup and covered with a white tile. The colour of samples was measured according to the colour parameters *L*, *a** and *b** which are used by the International Commission on Illumination (CIE). The *L* value corresponds to the lightness of colour with values ranging from 0 (black) to 100 (white). The *a** and *b** values are colour coordinates expressed numerically where *a** represents red or green colour and *b** represents yellow or blue colour. The total colour difference (*ΔE**) was calculated using the following equation:

$$\Delta E^* = \sqrt{[(L^* - L_0^*)^2 + (a^* - a_0^*)^2 + (b^* - b_0^*)^2]} \quad (8.1)$$

where L^*, a^* and b^* are the measured colour coordinates of the emulsions at a certain storage time and L_0^*, a_0^* and b_0^* are the initial colour coordinates at zero time before storage.

8.3.4 Analysis of lutein content in nanoemulsions using HPLC

Lutein content was determined by extracting lutein from the emulsions and analysed using high performance liquid chromatography (HPLC) based on the procedures in the previous studies reported by Lim et al. (2014). Briefly, 2 mL of lutein emulsions was mixed with 3.9 mL of 1:1 ratio (v/v) of methanol and ethyl acetate containing 0.2% BHT, followed by 1 mL of saturated potassium hydroxide in methanol to separate lutein from the oil carrier. 1 mL of dichloromethane was added to dissolve lutein in the organic phase and the separation of organic phase was enhanced by the addition of 3.9 mL of hexane. The organic phase (which contains lutein) was removed using a glass Pasteur pipet, filtered through a 0.2 μm nylon membrane filter (Sartorius Stedim Biotech GmbH, Goettingen, Germany) and

collected in amber glass vials for HPLC analysis. The extraction process was carried out under dimmed light to minimise degradation of lutein.

HPLC analysis was carried out using the Shimadzu Nexera liquid chromatograph system (LC-20AT) equipped with SIL-20AC autosampler, CTO-20A column oven and SPD-M20A photodiode-array detector (Nakagyo-ku, Japan). Lutein in the samples was analysed using a C_{30} reverse phase analytical column (250 x 4.6 mm i.d.) (Develosil RP Aqueous-AR-5) along with a cartridge column (10 x 4 mm i.d.) (Nomura Chemical Co., Ltd, Seto, Japan). The mobile phases used consisted of A: acetonitrile, B: 1:1 (v/v) of methanol and ethyl acetate and C: 0.5% of 200 mmol acetic acid in water. The elution was carried out using a gradient profile of 84.5% A, 15% B and 0.5% C for 0 to 2 minutes, changed to 64.5% A, 35% B and 0.5% C in 10 minutes and returned to 84.5% A, 15% B and 0.5% C. The injection volume of samples used was 10 µL with a flow rate of 1 mL/min at room temperature and lutein was detected at 450 nm wavelength.

The retention time and peak area were compared to a lutein standard using LCsolution software Version 1.25 SP5 (Lab Solutions, Shimadzu Corporation, Japan) to identify the lutein present in the samples. The lutein peak identified in this study was considered to be all-*trans*-lutein. Examples of the HPLC chromatograms of a lutein standard dissolved in ethyl acetate (100 µg/mL) and the lutein recovered from the emulsions at Day 0 are shown in the Appendix (Figure 1). The retention time of lutein recovered from the emulsions was similar to the lutein standard with retention time varying between 10 and 12 minutes. To quantify the amount of lutein present in the extracted samples, different concentrations of lutein were prepared by diluting a stock solution of lutein in ethyl acetate to create a calibration curve (Appendix; Figure 2). The calibration curve was linear in the concentration range of 6 to 384 µg/mL with R^2 value of 0.9972.

8.3.5 Cell cultures

Caco-2 cell line was obtained from American Type Culture Collection (Rockville, MD, USA). Caco-2 cells were grown and maintained in DMEM (Gibco-Invitrogen) supplemented with 10% (v/v) fetal calf serum, 1% (v/v) non-essential amino acids, 1% (v/v) penicillin and streptomycin and 1% (v/v) sodium bicarbonate ("growth medium") in a humidified incubator at 37^{o}C with 5% CO_2 (Thermo

Scientific Forma® Direct Heat CO_2 Incubator, Thermo Fisher Scientific Inc., USA). The cells were grown until 80 – 90% confluent and the growth media was changed and replaced every 2 – 3 days. After which, the cells were harvested with trypsin-EDTA, washed and passaged into new flasks or into multi-well plates for MTT assay. The cells used were between passages 26 and 31.

8.3.6 *In vitro* cytotoxicity of lutein nanoemulsions

The *in vitro* cytotoxicity of conventional emulsions and nanoemulsions containing lutein was determined by measuring the cell viability of Caco-2 cells using the MTT assay as described elsewhere (Stephenson, Wolber, Plieger & Harding, 2016). The MTT assay is a colorimetric assay for measuring cell proliferation based on tetrazolium reduction to formazan (insoluble) (Fotakis & Timbrell, 2006). The cells were harvested and seeded on a 96-well plate at a density of 1 x 10^5 cells per well with 200 μL of growth medium and incubated at 37°C with 5% CO_2 for 24 hours. The growth medium was decanted and 150 μL of lutein nanoemulsions diluted with growth medium were added to the wells. The emulsion samples were diluted at different dilution concentrations ranging from 10^{-1} to 10^{-3} times. Cells treated with growth medium alone were used as a negative control group. After incubation for 24 and 72 hours, 10 μL of MTT in phosphate buffer saline (5 mg/mL) were added to each well and incubated for 4 hours. The growth medium was decanted and 100 μL of 100% DMSO was added into each well to dissolve the formazan crystals. The plates were analysed with a microplate reader (ELx808 Ultra Microplate Reader, Bio-Tek Instruments Inc., Winooski, VT, USA) at 550 nm wavelength. The number of viable cells present was expressed as a percentage relative to the control group, which was normalised to 100%.

The cytotoxicity of lutein loaded emulsions was tested on two independent samples with duplicate for each dilution on the culture plates (0.225, 2.25 and 22.5 μg/mL lutein). The cytotoxicity of blank emulsions without the addition of lutein was also tested as mentioned. In this way, the oil content for all emulsion systems was 0.0005, 0.005 and 0.05% (w/w) for each dilution on the culture plates but the total protein emulsifier varied from 0.0001 to 0.4% (w/w). For preliminary study on the individual components, three replicates on one sample for each dilution on the culture plates were carried out.

8.3.7 Cellular uptake of lutein from nanoemulsions

The uptake of lutein by Caco-2 cell monolayers incubated with the emulsions was measured. The cells were seeded on a 6-well plate at a density of 1 x 10^5 cells per well with 2 mL of growth medium and incubated at 37^{o}C with 5% CO_2 until the cells reached about 90% confluence. The growth medium was removed and the respective emulsions diluted in growth medium (10^{-1} dilution) were added to the wells and incubated for 24 hours. After incubation, the growth medium was removed and the cell monolayers were washed twice with cold phosphate buffer solution at pH 6.8 to stop lutein uptake on the cell surface. The cell monolayers were scraped and suspended in 1 mL of phosphate buffer. A portion of cell suspensions was used for extraction of lutein and also for determination of protein content in the cells using the bicinchoninic acid (BCA) protein assay kit (Sigma Aldrich, St. Louis, MO, USA).

Lutein in the Caco-2 cell monolayers was extracted with solvents and analysed by HPLC as mentioned above (Section 8.3.4). Briefly, 0.5 mL of cell suspension was mixed with 0.5 mL of dichloromethane, followed by 1 mL of hexane and vortexed for 1 minute. The extraction process was repeated and the organic fractions were combined and evaporated to dryness. The extract was dissolved in 1 mL of methanol and ethyl acetate (1:1 v/v) for HPLC analysis.

The protein content of Caco-2 cells in the cell suspensions was determined using BCA assay in 96-well plate according to the manufacturer instructions. 200 μL of BCA working reagent was added to 25 μL of cell suspensions in each well and incubated at 37^{o}C for 30 minutes. After incubation, the plate was analysed at a wavelength of 550 nm. The protein content of each sample was determined from a standard curve with different concentrations of bovine serum albumin solutions (200 – 1000 μg/mL).

Results of cellular uptake of lutein are the average and standard deviation of two independent experiments with duplicate. The data were analysed using Minitab® 17.2.1 statistical software (Minitab, Inc, USA) by ANOVA followed by a Tukey test ($P < 0.05$).

8.4 Results and Discussion

8.4.1 Physicochemical properties of lutein loaded conventional emulsions and nanoemulsions

The particle size distributions of lutein loaded conventional emulsions and nanoemulsions stabilised by a single layer of WPI or a sequential bi-layer of WPI and lactoferrin are shown in Figure 8.1. All of the samples showed a monomodal distribution that was narrow with PDI value of less than 0.2 (Table 8.2). The mean Z-Average size of lutein nanoemulsions (70 – 80 nm in diameter) was smaller than conventional emulsions (150 nm). Furthermore, the TEM images showed that the droplets in the emulsions were uniform and spherically shaped (Figure 8.2). This suggested that the lutein was well encapsulated inside the oil droplets by the protein emulsifiers.

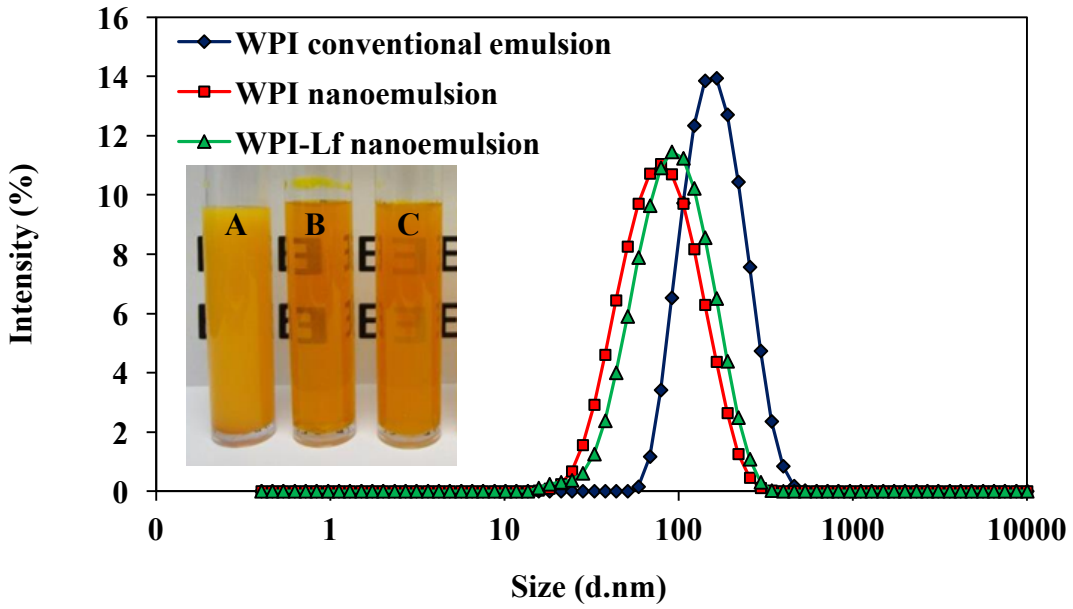

Figure 8.1 Particle size distributions and photographs of lutein conventional emulsions and nanoemulsions: (a) WPI-stabilised conventional emulsion, (b) WPI-stabilised nanoemulsions and (c) WPI-lactoferrin stabilised nanoemulsions.

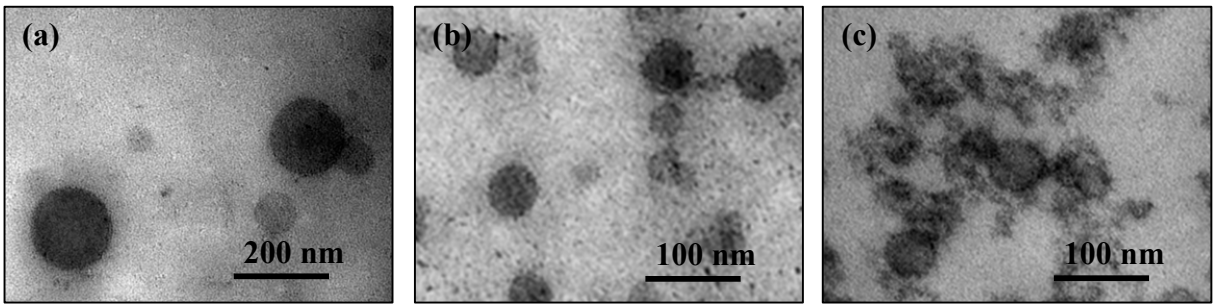

Figure 8.2 TEM images of lutein loaded conventional emulsions and nanoemulsions: (a) WPI-stabilised conventional emulsion, (b) WPI-stabilised nanoemulsions and (c) WPI-lactoferrin stabilised nanoemulsions.

As observed, the particle size of bi-layer nanoemulsions was slightly larger than single layer nanoemulsions (Figure 8.1). This can be attributed to the formation of lactoferrin layer on the droplet surface as the previous QCM-D data showed that lactoferrin molecules formed a layer thickness of 5.12 nm on WPI pre-adsorbed gold surfaces (Chapter 6; Section 6.4.2; Table 6.1) which also corresponds to the increase in particle size of bi-layer nanoemulsions. In addition, the TEM images showed that the nanoemulsions stabilised by WPI and lactoferrin were surrounded by a more contrasting dense layer (presumably proteinaceous material) whereas the ones stabilised by WPI alone did not show any dense layer on the surface of droplets (Figure 8.2). Nevertheless, the particle size of single layer and bi-layer nanoemulsions was relatively small (less than 80 nm) for them to be optically translucent (Figure 8.1). In comparison, the conventional emulsions (150 nm) were twice the size of nanoemulsions (70 – 80 nm) and appeared opaque as large particles do scatter light strongly (McClements, 1999).

The WPI-stabilised conventional emulsions (-36.2 ± 1.1 mV) and nanoemulsions (-28.7 ± 1.1 mV) were negatively charged at pH 6 (Table 8.2) as they were stabilised by WPI. This was expected because the droplets were negatively charged at pH above the pI of the adsorbed proteins. On the other hand, the droplets stabilised by a sequential bi-layer of WPI and lactoferrin were neutrally charged (+0.79 ± 0.12 mV) at pH 6 (Table 8.2).

Table 8.2 Particle characteristics of lutein loaded conventional emulsions and nanoemulsions at pH 6. Data are presented as the mean and standard deviation of two independent measurements in triplicate (n=6).

	Mean ± S.D.			
	Z-Average (nm)	**PDI**	**ζ-potential (mV)**	**Encapsulation efficiency (%)**
WPI conventional emulsion	147.3 ± 0.6	0.13 ± 0.02	-36.2 ± 1.1	86.3 ± 0.3
WPI nanoemulsion	68.8 ± 0.3	0.20 ± 0.02	-28.7 ± 1.1	80.7 ± 0.8
WPI-lactoferrin nanoemulsion	79.6 ± 0.9	0.21 ± 0.01	+0.79 ± 0.12	81.8 ± 1.3

The encapsulation efficiency of lutein for conventional emulsions and nanoemulsions was 80.7 – 86.3% (Table 8.2). This indicates that a reasonable amount of lutein was incorporated into the emulsions but there was some loss of lutein. Like other carotenoids, lutein is susceptible to degradation due to light, oxygen and heat (Li, Song & Liu, 2014; Kuang, Zhang, Bajaj, Yuan, Tang, Chen & Sablani, 2015). Therefore, lutein in the emulsions can degrade during preparation when exposed to light and oxygen and rise in temperature (heat generation) during homogenisation and evaporation process. Tan & Nakajima (2005b) pointed out that cavitation forces generated within the homogeniser induce the formation of free radicals in the emulsions. The formation of free radicals is a series of auto catalytic reactions including hydroxylation and oxidation which could result in degradation or loss of activity of the carotenoids (Boon, McClements, Weiss & Decker, 2010). In addition, the oil carrier used is corn oil which is highly polyunsaturated (70% linoleic acid) and can contribute to the formation of free radicals (Yi et al., 2014). The loss of lutein in the samples during preparation is in agreement with the findings of astaxanthin loss in nanodispersions using emulsification-evaporation technique due to the exposure to heat, light and oxygen (Anarjan, Mirhosseini, Baharin & Tan, 2011; Anarjan, Nehdi & Tan, 2013). The authors also found that there was a greater loss of astaxanthin using higher pressure (90 MPa) and evaporation temperature (66^{o}C).

Although there was some lutein loss during processing of emulsions, the conventional emulsions had slightly higher encapsulation efficiency (86.3%) than the nanoemulsions (80.7 – 81.8%). This may be related to the particle size of the

emulsions as smaller particles in the nanoemulsions have a larger surface area to volume ratio, resulting in greater exposure for lutein degradation. This agrees with several studies that small droplets are more susceptible to chemical degradation than large droplets due to an increased surface area (Tan & Nakajima, 2005b; Jo & Kwon, 2014).

8.4.2 Stability of lutein nanoemulsions during storage

The physical stability of emulsions during storage is important for their use in foods. Therefore, the particle size of emulsions during storage was measured. In general, there was no distinct change in the particle size of conventional emulsions and nanoemulsions during storage for 28 days at 5, 20 and 40^{o}C (Figure 8.3). This indicates that the emulsions were relatively stable, probably due to strong repulsion forces. It is well known that the major mechanism in preventing droplet aggregation in protein-stabilised emulsions is due to a combination of steric and electrostatic repulsions (McClements, 1999). The conventional emulsions and single layer nanoemulsions stabilised by WPI were more negatively charged with ζ-potential values of -36.2 and -28.7 mV, respectively (Table 8.2). Whilst the bi-layer nanoemulsions stabilised by WPI and lactoferrin were less electrically charged with low ζ-potential value of +0.8 mV but the nanoemulsions remained stable during storage, presumably due to a strong steric repulsion arising from the sugar moiety on the lactoferrin molecules (Tokle et al., 2012).

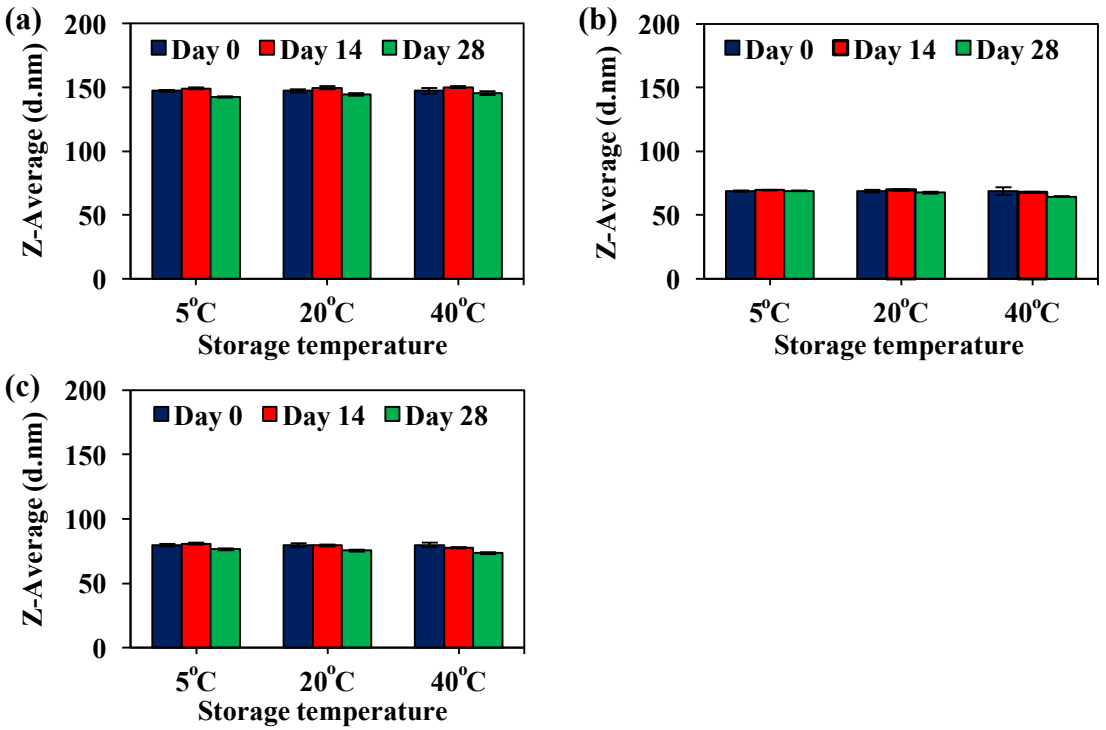

Figure 8.3 Mean particle size (Z-Average) of lutein loaded conventional emulsions and nanoemulsions during storage at different temperatures (5, 20 & 40°C) for 28 days: (a) WPI-stabilised conventional emulsion, (b) WPI-stabilised nanoemulsions and (c) WPI-lactoferrin stabilised nanoemulsions. Data are presented as the mean of two independent measurements in triplicate (n=6) and error bars represent the standard deviation.

Although the emulsions were physically stable during storage, it was observed that the colour of all the emulsions faded slightly over time and became lighter especially at higher temperature of 40°C (Figure 8.4). Initially, the emulsions were orange in colour as lutein is a colour pigment with an intense yellow-orange (depending on the concentration) but the colour intensity of emulsions became lighter due to chemical degradation of lutein. Indeed, the L value of emulsions increased while the colour parameters were found to decrease during storage at higher temperatures (Table 8.3). The L value measures lightness and an increase in L value indicate colour fading of emulsions during storage (Qian, Decker, Xiao & McClements, 2012). A decrease in positive a value indicates a decrease in the redness of the emulsions while a decrease in positive b value indicates a decrease in the yellowness (Qian et al., 2012). Therefore, the colour measurements indicate some loss or change of colour in the emulsions during storage, also indicating the degradation of lutein.

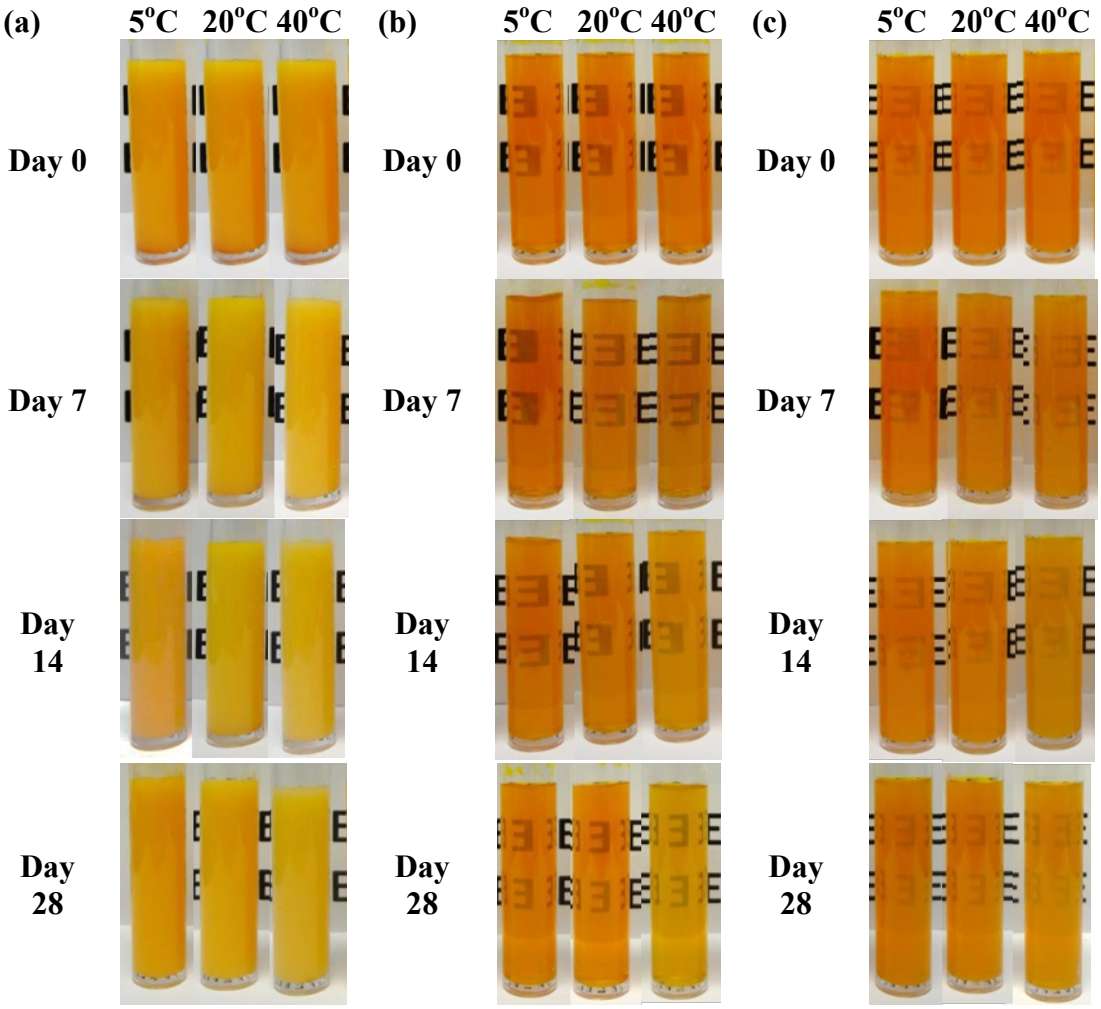

Figure 8.4 Photographs of lutein conventional emulsions and nanoemulsions during storage at different temperatures (5, 20 & 40°C) for 28 days: (a) WPI-stabilised conventional emulsion, (b) WPI-stabilised nanoemulsions and (c) WPI-lactoferrin stabilised nanoemulsions.

Table 8.3 Change in colour parameters of lutein loaded conventional emulsions and nanoemulsions during storage at different temperatures.

Storage	5°C			20°C			40°C		
days	L	+a	+b	L	+a	+b	L	+a	+b
Conventional emulsions									
0	55.6 ± 0.4	9.66 ± 0.1	34.7 ± 0.5	55.6 ± 0.4	9.66 ± 0.1	34.7 ± 0.5	55.6 ± 0.4	9.66 ± 0.1	34.7 ± 0.5
3	55.4 ± 0.2	9.57 ± 0.1	34.3 ± 0.2	55.4 ± 0.2	9.48 ± 0.2	33.4 ± 0.2	55.9 ± 0.3	8.51 ± 0.2	30.5 ± 0.2
7	55.4 ± 0.3	9.50 ± 0.1	33.4 ± 0.2	55.5 ± 0.3	9.06 ± 0.2	32.0 ± 0.1	56.4 ± 0.4	7.57 ± 0.1	28.2 ± 0.3
14	55.3 ± 0.2	9.11 ± 0.1	32.7 ± 0.1	55.6 ± 0.3	8.27 ± 0.1	30.6 ± 0.1	57.1 ± 0.5	6.40 ± 0.1	27.0 ± 0.5
21	55.3 ± 0.4	9.21 ± 0.3	32.4 ± 0.3	55.7 ± 0.3	7.84 ± 0.4	29.9 ± 0.5	57.9 ± 0.4	5.42 ± 0.3	26.0 ± 0.3
28	55.3 ± 0.3	8.80 ± 0.1	32.0 ± 0.1	55.8 ± 0.3	6.93 ± 0.1	29.3 ± 0.3	59.1 ± 0.7	4.24 ± 0.2	24.8 ± 0.6
Single layer nanoemulsions									
0	36.5 ± 0.1	13.3 ± 0.3	21.7 ± 0.3	36.5 ± 0.1	13.3 ± 0.3	21.7 ± 0.3	36.5 ± 0.1	13.3 ± 0.3	21.7 ± 0.3
3	36.3 ± 0.1	13.1 ± 0.2	21.3 ± 0.2	35.9 ± 0.1	12.5 ± 0.1	20.7 ± 0.2	35.0 ± 0.1	10.9 ± 0.1	18.7 ± 0.3
7	36.2 ± 0.1	12.9 ± 0.8	20.1 ± 0.2	35.4 ± 0.1	11.8 ± 0.1	19.3 ± 0.1	34.2 ± 0.2	9.29 ± 0.1	16.2 ± 0.1
14	35.7 ± 0.0	12.6 ± 0.1	19.9 ± 0.1	34.7 ± 0.1	10.8 ± 0.1	17.9 ± 0.2	33.9 ± 0.4	7.60 ± 0.4	14.0 ± 0.2
21	35.6 ± 0.1	12.2 ± 0.2	19.8 ± 0.2	34.4 ± 0.1	10.5 ± 0.1	17.0 ± 0.1	37.0 ± 0.8	7.78 ± 0.1	13.6 ± 0.2
28	35.5 ± 0.1	12.1 ± 0.2	19.6 ± 0.2	34.4 ± 0.1	10.3 ± 0.1	17.0 ± 0.1	35.1 ± 0.6	7.69 ± 0.1	13.3 ± 0.2
Bi-layer nanoemulsions									
0	39.5 ± 0.4	8.64 ± 0.1	26.1 ± 0.5	39.5 ± 0.4	8.64 ± 0.1	26.1 ± 0.5	39.5 ± 0.4	8.64 ± 0.1	26.1 ± 0.5
3	39.4 ± 0.2	8.48 ± 0.2	25.8 ± 0.3	39.2 ± 0.2	8.12 ± 0.2	25.6 ± 0.3	38.7 ± 0.3	6.55 ± 0.2	25.0 ± 0.5
7	39.4 ± 0.1	8.65 ± 0.2	25.6 ± 0.3	39.1 ± 0.2	8.00 ± 0.2	24.9 ± 0.4	38.5 ± 0.5	5.47 ± 0.4	22.1 ± 0.7
14	39.2 ± 0.3	8.36 ± 0.3	25.3 ± 0.6	38.8 ± 0.2	7.54 ± 0.2	24.3 ± 0.5	39.5 ± 0.1	3.75 ± 0.1	19.3 ± 0.2
21	39.1 ± 0.1	8.45 ± 0.1	24.9 ± 0.3	38.6 ± 0.2	6.94 ± 0.5	23.1 ± 0.9	40.0 ± 0.9	3.35 ± 0.1	15.9 ± 0.3
28	39.2 ± 0.2	8.23 ± 0.1	24.7 ± 0.2	38.5 ± 0.2	6.22 ± 0.3	22.1 ± 0.6	40.8 ± 0.0	3.51 ± 0.0	13.7 ± 0.1

More often, colour degradation in emulsions was compared by calculating the total colour difference (ΔE^*) from the measured coordinates. Figure 8.5 shows that the colour changes for all the emulsions were greater at 40°C than at 5 and 20°C. This is not surprising as previous studies have also found a rapid colour loss of β-carotene at elevated temperatures (Qian et al., 2012; Yi et al., 2014). For instance, Qian et al. (2012) found that there was greater loss of colour in β-carotene nanoemulsions at 37 and 55°C than at 5 and 20°C.

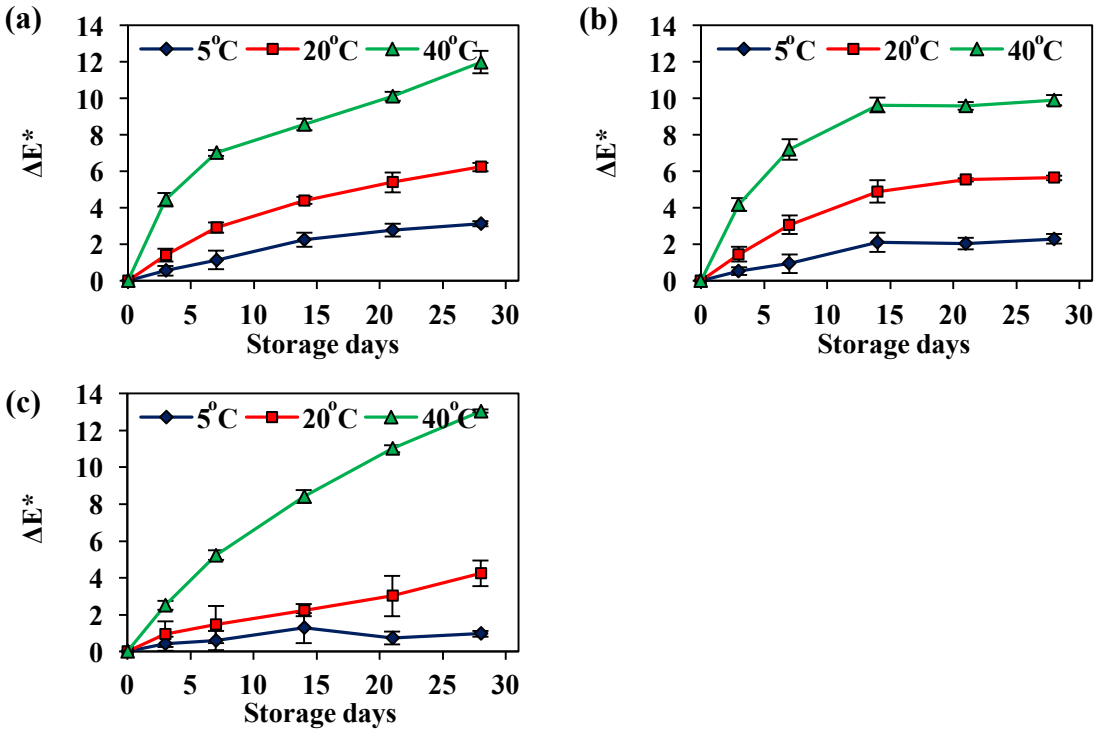

Figure 8.5 Total colour changes (ΔE^*) of lutein conventional emulsions and nanoemulsions during storage at different temperatures (5, 20 & 40°C) for 28 days: (a) WPI-stabilised conventional emulsion, (b) WPI-stabilised nanoemulsions and (c) WPI-lactoferrin stabilised nanoemulsions. Data are presented as the mean of two independent measurements in triplicate (n=6) and error bars represent the standard deviation.

Apart from colour measurements, the lutein content in the emulsions during storage was determined by solvent extraction method using HPLC analysis. The degradation of lutein in the emulsions was determined and expressed as relative lutein concentration, C_t/C_0 where the lutein concentration during storage at time, Ct was divided by the initial lutein concentration, C_0. As shown in Figure 8.6, there was a decrease in lutein concentration after storage for up to 28 days. There was also a higher degree of degradation of lutein in the emulsions at 40°C than at 5 and 20°C.

Unlike other carotenoids, lutein is a xanthophyll with two hydroxyl groups. This makes lutein more polar for them to assemble at the oil-water interface and become exposed to oxygen which results in degradation of lutein (Pérez-Gálvez & Mínguez-Mosquera, 2005). There are several mechanisms accounting for the degradation of carotenoids in foods due to oxidation and isomerisation when exposed to oxygen, light and heat. The oxidation of carotenoids is a chain of reactions involving the formation of several compounds such as epoxides and apocarotenoids (Boon et al., 2011; Silva et al., 2011). Lin & Chen (2004) reported that the degradation and isomerisation of carotenoids in tomato juice produced *cis*-isomers during storage under various conditions. The isomers identified from all-*trans*-lutein were 9-*cis*- and 13-*cis*-lutein. In the study, they found that both all-*trans* and *cis* forms of lutein decreased more during storage of tomato juice at 35°C than 4 and 25°C under dark conditions.

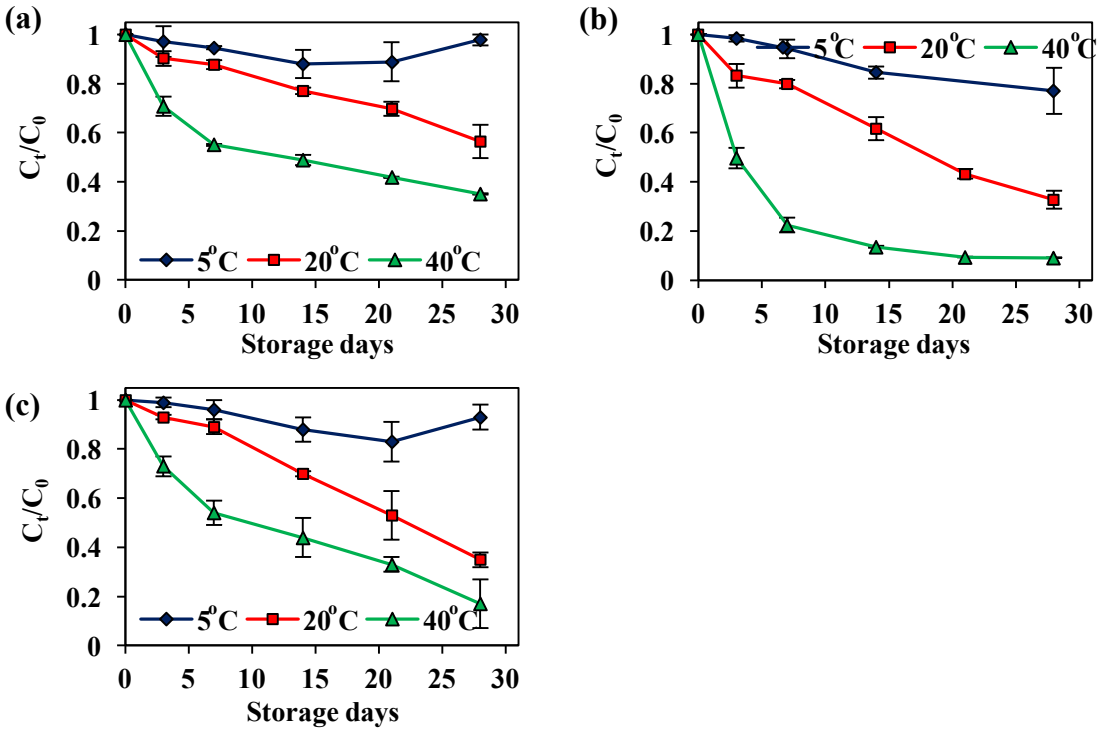

Figure 8.6 Relative content of lutein conventional emulsions and nanoemulsions during storage at different temperatures (5, 20 & 40°C) for 28 days: (a) WPI-stabilised conventional emulsion, (b) WPI-stabilised nanoemulsions and (c) WPI-lactoferrin stabilised nanoemulsions. Data are presented as the mean of two independent measurements in duplicate (n=4) and error bars represent the standard deviation.

Interestingly, lutein degradation was the highest in WPI nanoemulsions, followed by bi-layer nanoemulsions and WPI conventional emulsions. This was not expected because nanoemulsions are thought to have better stability towards lutein degradation as they contain more proteins to protect emulsions from degradation. At the same oil concentration of 0.5% (w/w), the nanoemulsions contained 0.9% (w/w) WPI whereas the conventional emulsions contained 0.09% (w/w) proteins (Table 8.1). It was therefore hypothesised that the small droplets in nanoemulsions were surrounded by a thicker interfacial layer of protein with better protection against degradation. One possible explanation is the observed differences in the droplet size among the various emulsion systems. As described above, the reduction in droplet size to a nanometre level resulted in an increase in the surface area to volume ratio with greater exposure to the surrounding environment for a more rapid degradation of lutein. As a result, nanoemulsions containing smaller droplets showed a higher loss of lutein during storage than conventional emulsions. It is worthwhile noticing that the degradation of lutein in nanoemulsions was improved when lactoferrin was incorporated in bi-layer nanoemulsions. This can be attributed to the metal chelating ability of lactoferrin as well as an increase in the interfacial layer (Lesmes et al., 2010). There was a sharp decrease in lutein content from Day 0 to Day 7 for single layer nanoemulsion (Figure 8.6b) but the degradation of lutein in bi-layer nanoemulsions was slower at all the temperatures (Figure 8.6c).

The decrease in lutein concentration during storage was fitted to a first order kinetic model i.e. $lnC_t = lnC_0 - kt$ as described previously (Mizrahi, 2011). It is evident that lutein degradation is a typical first order reaction as a plot of $ln(C_t/C_0)$ against time produced a straight line with regression coefficient ranging from 0.63 to 0.98 (Table 8.4). The rate of lutein degradation was found to increase with increasing storage temperature from 5 to 40^{o}C for all the emulsions.

The temperature dependence of lutein degradation in emulsions was also determined by the Arrhenius equation. The Arrhenius plots for all the emulsions were linear (Figure 8.7) and this confirmed that lutein degradation in the emulsions is a first order kinetic. Previous studies have also shown that degradation of lutein follows a first order reaction (Tang & Chen, 2000; Li et al., 2014). The activation energies were calculated based on the Arrhenius plot of the emulsions. The activation energy of WPI single layer nanoemulsions was higher (45.4 ± 8.5 kJ/mol)

than conventional emulsions (38.0 ± 12.0 kJ/mol) and bi-layer nanoemulsions (37.3 ± 1.0 kJ/mol). A higher activation energy indicated that the sample is more heat sensitive (Li et al., 2014; Lim et al., 2014). In a similar study, Lim et al. (2014) also found that the activation energy of all-*trans*-lutein in freeze-dried emulsions was higher in single layer emulsion coated with WPI (58.9 kJ/mol) compared to layer by layer emulsion coated with WPI and gum arabic (45.9 kJ/mol). The single layer emulsion coated with WPI showed a faster degradation of lutein.

The half-life ($t_{½}$) of lutein at which the time required to decrease the lutein concentration by 50% was calculated by the equation: $t_{1/2} = -\ln(2)/k$ and is shown in Table 8.4. The estimated $t_{½}$ for conventional emulsions was higher (19 to 147 days), depending on storage temperatures, which indicates that lutein in conventional emulsions was more stable than nanoemulsions (8 to 79 days). Nevertheless, $t_{½}$ of lutein in all the emulsions was much higher at 5°C than those stored at 20 or 40°C. In this way, nanoemulsions can still be used to incorporate materials for transparent liquid foods for relatively short term cold storage (e.g. 2 – 3 months) compared to conventional emulsions which tend to make beverages appear turbid.

Table 8.4 Rate constant, coefficient and activation energy of lutein conventional emulsions and nanoemulsions at different temperatures of 5, 20 and 40°C. Data are presented as the mean and standard deviation of two independent measurements with replicate (*n*=4).

	Rate constant, *k* (day^{-1})	**Coefficient, R^2**	**Activation energy, *Ea* (kJ/mol)**	**Half-life, $t_{½}$ (day)**
WPI conventional emulsions				
5°C	0.006 ± 0.004	0.634 ± 0.246	38.0 ± 12.0	147 ± 84
20°C	0.019 ± 0.003	0.971 ± 0.023		37 ± 6
40°C	0.035 ± 0.001	0.937 ± 0.010		19 ± 1
WPI single layer nanoemulsions				
5°C	0.010 ± 0.004	0.809 ± 0.180	45.4 ± 8.5	79 ± 33
20°C	0.039 ± 0.001	0.976 ± 0.002		17 ± 1
40°C	0.086 ± 0.001	0.939 ± 0.009		8 ± 1
WPI-lactoferrin bi-layer nanoemulsions				
5°C	0.010 ± 0.003	0.726 ± 0.167	37.3 ± 1.0	77 ± 21
20°C	0.037 ± 0.001	0.930 ± 0.037		18 ± 1
40°C	0.059 ± 0.016	0.891 ± 0.024		12 ± 3

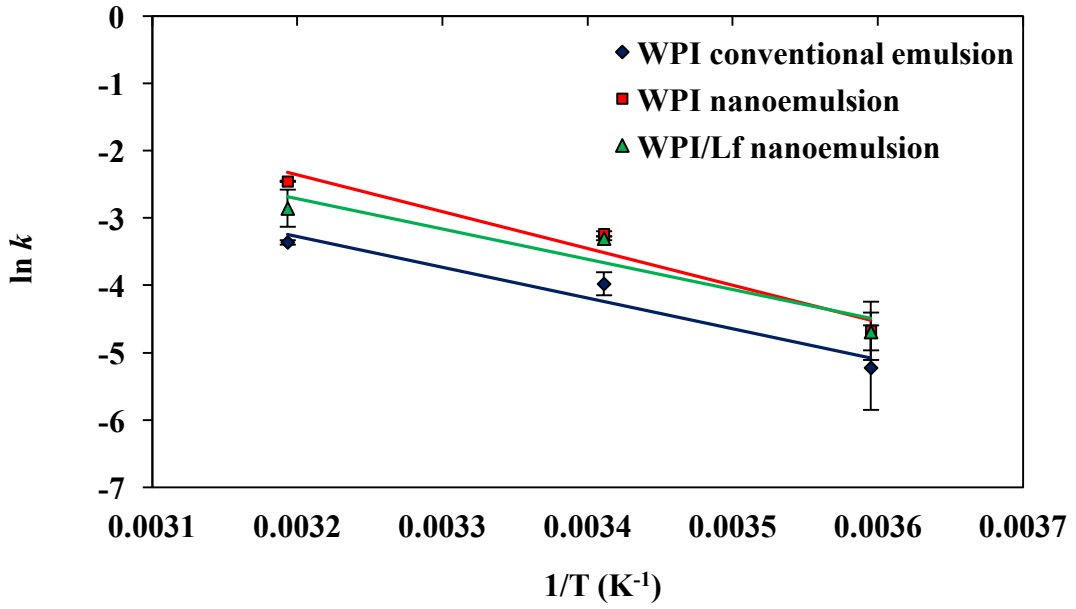

Figure 8.7 Arrhenius plot of lutein conventional emulsions and nanoemulsions stored at 5, 20 and 40°C. Data are presented as the mean of two independent measurements with replicate (n=4) and error bars represent the standard deviation.

This study showed that chemical degradation of lutein resulted in a loss of colour and lutein content of emulsions during storage. Even so, lutein degradation in WPI nanoemulsions can be improved (especially at higher temperature) by adding lactoferrin to form bi-layer.

8.4.3 *In vitro* cytotoxicity of lutein nanoemulsions

The *in vitro* cytotoxicity of lutein loaded conventional emulsions and nanoemulsions on Caco-2 cell monolayers was evaluated by MTT assay. As mentioned, MTT assay is a colorimetric method that measures the cell metabolic activity in viable cells by reducing the tetrazolium dye in MTT into purple formazan crystals (Fotakis & Timbrell, 2006). The optical density of the wells is measured with the values directly corresponding to the number of viable cells present in a linear fashion.

A preliminary study was conducted to consider any possibilities that the individual components used to make the emulsions were toxic to the cells. For comparison, a 1% (w/w) emulsifier level was used to prepare the individual protein solution consisting of either WPI or lactoferrin. The protein solutions were then diluted with growth medium at different dilution concentration ranging from 10^{-1} to

10^{-3} times on the culture plates. Due to its poor solubility in water, 0.023% (w/w) lutein was dissolved in corn oil, ethyl acetate or in combination. The lutein concentration used was the same as the amount present in lutein loaded emulsions. They were also diluted with growth medium at different dilution concentration on the culture plates.

No cytotoxicity was observed among the individual components after incubation for 24 hours (Figure 8.8a) and they were biocompatible to make the emulsions. In another experiment, blank emulsions (without lutein) were used in order to determine whether the emulsion formulations have any adverse effect on the cells (Figure 8.8b). The high viabilities of cells incubated with the emulsions (> 80%) ensured that the formulations were non-toxic and could be used safely as delivery system for encapsulation of bioactive compounds.

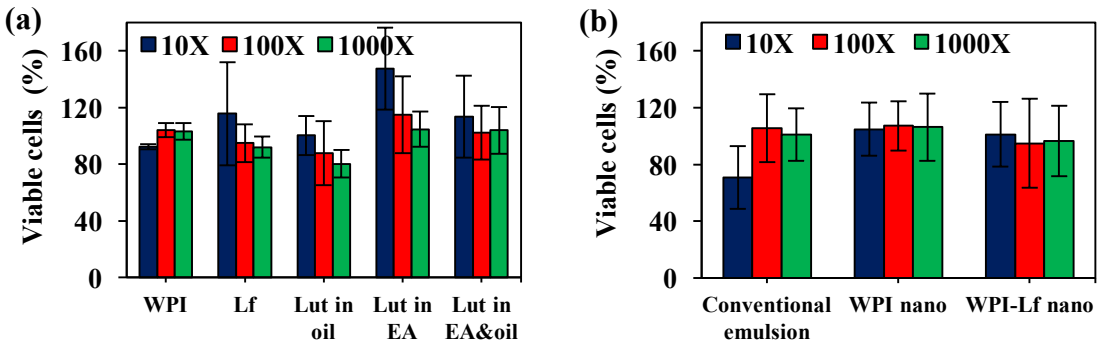

Figure 8.8 Viability of Caco-2 cells as determined by MTT assay after incubation for 24 hours with (a) individual components and (b) blank emulsions stabilised by WPI and/or lactoferrin at different dilution time from 10 to 1000. The composition of the individual components used were 1% (w/w) WPI, 1% (w/w) lactoferrin (Lf), 0.0225% (w/w) lutein dissolved in corn oil and/or ethyl acetate. For emulsion samples, the oil concentration was 0.5% (w/w) and the total amount of protein emulsifiers varied from 0.1 to 4% (w/w). The samples were then diluted from 10 to 1000 times in growth medium before their addition to the cells. Data are presented as the mean of three measurements and error bars represent the standard deviation.

Lutein loaded emulsions were also prepared and evaluated for their cytotoxicity after dilution with the growth medium. As shown in Figure 8.9a, the number of viable cells present after treatment with different emulsions after incubation for 24 hours was more than 80% of control. This indicates that the emulsions were non-toxic to the cells at the dilution concentration and time used. At the same time, nanoemulsions did not show any difference in their toxicity from the conventional emulsions which are generally being accepted as safe and not toxic to

the human body. However, nanoemulsions have small particle size which means that they have larger surface area to volume ratio for them to be digested more rapidly than conventional emulsions. It is also possible for these nanoemulsions to remain intact and be transported directly across the epithelium layer via passive transport to the liver (McClements & Xiao, 2012). But in reality, nanoemulsions undergo some physicochemical changes in their particle size and surface charge during digestion as shown in Chapter 7. Thus, there is little chance for the nanoemulsions to reach the small intestine epithelium intact.

Previous studies have also found no toxicity on Caco-2 cells treated with 1% (w/w) β-carotene nanoparticles (78 – 372 nm) stabilised by various food proteins (1% w/w WPI, sodium caseinate or soy protein) using homogenisation and evaporation method (Yi et al. 2014). He et al. (2011) reported high cell viability (> 85%) in food proteins stabilised nanoemulsions (3 mg/mL) (< 300 nm) but there was a decrease in cell viability with lecithin and other synthetic surfactants.

However, the number of viable cells was reduced when they were incubated with the emulsions for 72 hours ($P < 0.05$) (Figure 8.9b). This effect was more pronounced with the conventional emulsion when present at the highest concentration. This could indicate that the incubation of cells with the emulsions over a prolonged period can slow the proliferation of cells, or alternatively may induce an increase in necrosis or apoptosis. It has been reported that whey proteins and lactoferrin displayed anti-proliferative activity (Sah, Vasiljevic, McKechnie & Donkor, 2015) which may interfere with the growth of Caco-2 cells. Many previous studies have also demonstrated that whey proteins reduce the growth of several cancer cells such as mammary cancer cells and colorectal cancer cells (Eason, Velarde, Chatman, Till, Geng, Ferguson, Badger & Simmen, 2004; Xiao, Badger & Simmen, 2005). Lactoferrin was also shown to reduce the growth of tumour cells in mice (Bezault, Bhimani, Wiprovnick & Furmanski, 1994).

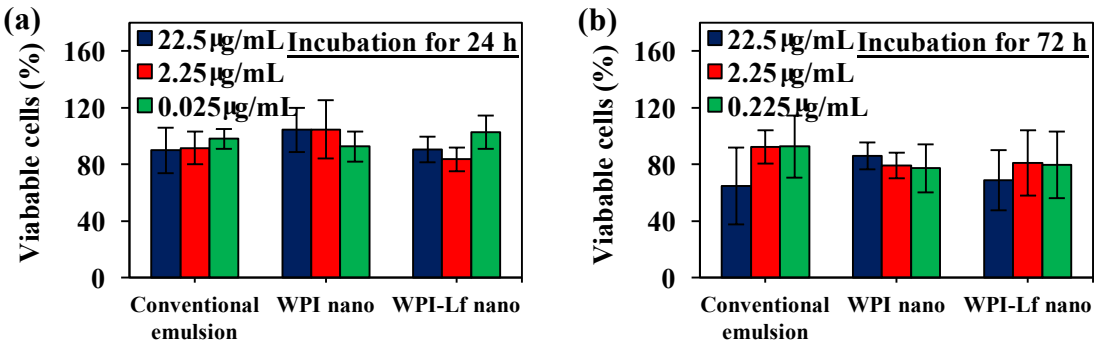

Figure 8.9 Viability of Caco-2 cells as determined by MTT assay after incubation with lutein loaded emulsions for (a) 24 hours and (b) 72 hours at different dilution time from 10 to 1000. The samples were diluted in growth medium before their addition to the cells. The amount of lutein presented in the cells for each concentration were 0.225, 2.25 and 22.5 µg/mL. Data are presented as the mean of two independent measurements with replicate (n=4) and error bars represent the standard deviation.

8.4.4 Cellular uptake of lutein from nanoemulsions

As shown in earlier study, the emulsions were non-toxic and suitable as delivery system of lutein, therefore, the cellular uptake of lutein from emulsions in Caco-2 cells was further investigated. Based on the literature, absorption of lutein and other carotenoids in the small intestine is facilitated by a non-specific transporter protein, mainly SR-B1 and other proteins (e.g. niemann-pick C1-like, cluster determinant 36) or they may be absorbed by passive diffusion (Reboul, 2013). In particular, SR-B1 receptor has been shown to play an important role in the uptake of lutein in Caco-2 cells (Reboul et al., 2005). For this reason, the Caco-2 cell line was selected to study the transport of lutein *in vitro* to mimic the exposure of nanoemulsions to the small intestine in the digestive tract.

The cellular uptake of lutein in conventional emulsions and nanoemulsions was significantly different ($P < 0.05$) with higher values observed in WPI-lactoferrin nanoemulsions (Figure 8.10). The uptake of lutein in conventional emulsions and nanoemulsions was 323 and 873 – 1304 pmol/mg protein, respectively. The differences in lutein uptake may be related to the particle size of emulsions. Previous studies have reported that nanoparticles less than 200 nm in diameter (or up to 500 nm) were transported by passive transport through the epithelium layer (Luo, Chen, Ren, Zhao & Qin, 2006; McClements & Xiao, 2012). It is possible that the smaller particle size of nanoemulsions was able to permeate through the cell membrane more

efficiently than conventional emulsions despite their droplet sizes being less than 200 nm. In addition, small particles have larger surface area to volume ratio, resulting in higher cell absorption. Moreover, Zhang et al. (2015) found that soy protein isolate nanoparticles with particle size of 100 nm have higher cellular uptake of vitamin B12 in Caco-2 cells than particles of 30 and 180 nm. It was suggested that higher driving force and more energy are required for the internalisation of larger nanoparticles into the cells therefore there is a decrease in uptake when increasing the particle size from 100 to 180 nm. On the other hand, it was mentioned that smaller particles have lower cellular uptake because the particles were not internalised by the cells but instead could pass through the cell membranes via paracellular spaces.

Apart from the particle size, other particle characteristics such as shape, surface charge, functional groups and hydrophilicity may also affect the uptake and cell adsorption (Kettler, Veltman, van de Meent, van Wezel & Hendriks, 2014). In particular, the formation of bi-layer nanoemulsions using a combination of WPI and lactoferrin improved cell absorption of lutein compared with single layer nanoemulsions stabilised by WPI alone. Both single layer and bi-layer nanoemulsions were similar in size (70 – 80 nm) but the surface charge (ζ-potential) of the emulsions was different (Table 8.2). The single layer nanoemulsions was negatively charged (-28.7 ± 1.1 mV) while the bi-layer nanoemulsions was +0.79 ± 0.12 mV. As a result of the slightly positive charges, the bi-layer nanoemulsions may be more easily adsorbed to the surface of Caco-2 cells which is coated with a negatively charged mucin layer. Similarly, Yi et al. (2014) reported that the surface charge of β-carotene loaded nanoparticles (stabilised by sodium caseinate, whey proteins or soy proteins) affect the uptake of β-carotene in Caco-2 cells. It was found that whey proteins nanoparticles with a lower ζ-potential value of -30 mV have a higher uptake of β-carotene (891 pmol/mg protein) than those of soy proteins with a ζ-potential value of -38 mV (452 pmol/mg protein). Furthermore, it has been reported the presence of lactoferrin specific receptors in the brush border membrane of enterocytes (Lönnerdal, 1994) which could possibly enhance the uptake of bi-layer nanoemulsions coated with lactoferrin.

The results of this study indicated that particle characteristics is an important factor in their interaction with the cells and consequently, cell absorption. It was

demonstrated that smaller particle size (< 100 nm) in nanoemulsions and lower surface charge in bi-layer nanoemulsions improved their uptake and efficacy in the cells compared to conventional emulsions. Nevertheless, further investigation after absorption in the small intestine is required for *in vivo* assessment to understand the metabolism and other possible toxicity of nanoemulsions.

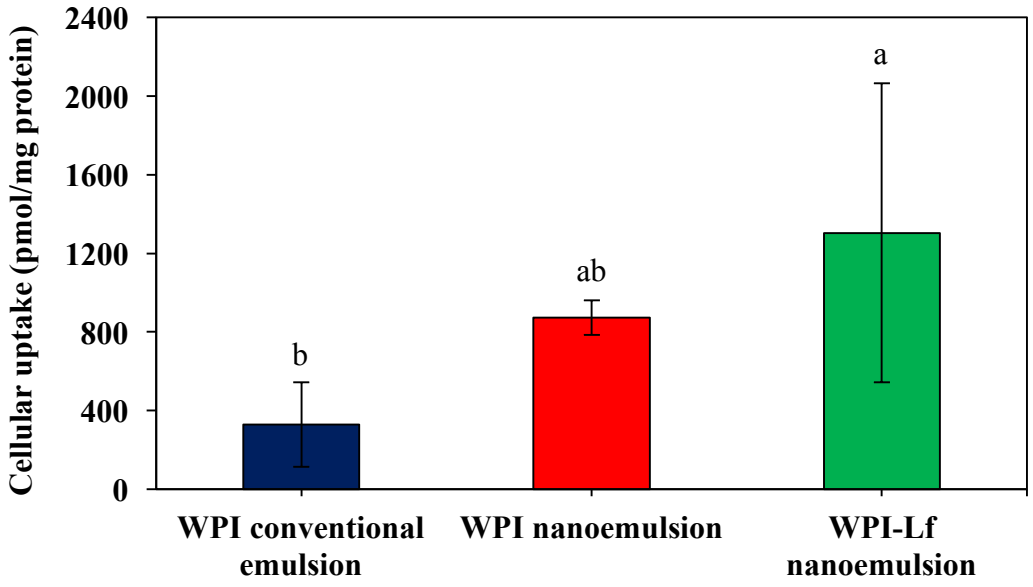

Figure 8.10 Cellular uptake of lutein by Caco-2 cell monolayers incubated with lutein loaded conventional emulsions and nanoemulsions with single or bi-layer interfacial layer. Means with the same letter are not significantly different from each other; n=4, Tukey test, P > 0.05.

8.5 Conclusions

The encapsulation of lutein in nanoemulsions was successfully prepared using emulsification and solvent evaporation method. WPI-stabilised nanoemulsions contained small droplets but they were less chemically stable to lutein degradation during storage especially at elevated temperatures as compared to the conventional ones. However, the chemical degradation of lutein in nanoemulsions during storage was improved by forming a bi-layer of lactoferrin around the WPI-coated droplets. All the nanoemulsions did not show apparent cytotoxicity on Caco-2 cells. Besides, the cellular uptake of lutein was higher as compared to the conventional emulsions. The study highlights the possibility of utilising nanoemulsion based delivery system to encapsulate and deliver bioactive compounds in foods.

Chapter Nine:

Overall Conclusions & Recommendations

Nanoemulsions containing small droplets were successfully formulated by emulsification and solvent evaporation method using food-grade materials. The optimal processing conditions for producing nanoemulsions with small droplet size and narrow size distribution using this method were determined to be 80 MPa for 4 cycles at an organic phase ratio of 10:90. The droplet size of nanoemulsions decreased from around 120 to 80 nm with a PDI of 0.2 when increasing the homogenisation pressures and number of cycles through the microfluidiser. Corn oil or coconut oil was more effective to produce stable nanoemulsions with small droplet size (80 nm) when compared to lemon oil (890 nm). Among the emulsifiers used, WPI or lactoferrin produced smaller emulsion droplets (70 – 110 nm) than those produced with Tween 20 (120 – 450 nm). The protein-stabilised nanoemulsions were shown to be more stable to heating temperatures ranging from 30 to 90^{o}C for 15 minutes except Tween 20. The nanoemulsions stabilised by lactoferrin or Tween 20 displayed good stability to pH changes (2 to 12) and salt addition (0 to 500 mM NaCl or 0 to 90 mM $CaCl_2$). However, the WPI-stabilised nanoemulsions were unstable to droplet aggregation at pH values near to the pI of the adsorbed whey proteins (around 4.5 – 5) and in the presence of salt addition at concentration above 30 mM $CaCl_2$. The results indicate that the formulation of nanoemulsions as delivery systems is promising for their applications in foods with careful selection of emulsifier and oil types.

The liquid nanoemulsions were converted into dried powders by spray drying or freeze drying. The type and concentration of wall materials were studied to determine the most suitable wall materials to produce dried emulsion powders with desired properties. The wall materials used include maltodextrin, trehalose or a mixture of 1:1 ratio of maltodextrin and trehalose with a solid concentration of 10, 20 or 30% (w/w). The results showed that the powders containing 20% (w/w) trehalose were superior as they contained lower moisture content (3.9 – 4.4%) and water activity (0.19 – 0.22), higher bulk density (0.28 – 0.46 g/mL) and better

wettability (3.9 – 5.1 minutes) and dispersibility in water (62 – 82%) than other wall materials used. All the powders displayed good reconstitution ability as they formed emulsion droplets with similar size as the original nanoemulsions with wall solutions before spray drying.

Despite achieving the smallest droplet size, WPI-stabilised nanoemulsions displayed poor stability to pH changes and salt addition. Therefore, nanoemulsions with modified interfacial structures were studied to improve their environmental stability and functionality. The interfacial structures of nanoemulsions were studied using WPI and lactoferrin. Consequently, the interactions between these two proteins and their adsorption on a modified hydrophobic surface were investigated for better understanding of the designated nanoemulsions. The ζ-potential and turbidity measurements indicated that both proteins can interact more strongly with each other via electrostatic interactions at pH 6. The QCM-D study on the adsorption behaviour of proteins showed that a thin and rigid protein bi-layer (8 – 10 nm) was formed when the individual protein solutions of WPI and lactoferrin was added sequentially regardless of the order of addition. However, the protein complex of a mixture of WPI and lactoferrin formed a thick and viscous layer (101 nm) on the surface. This study on the structural features of interfacial layers consisting of WPI and lactoferrin pointed to the design of nanoemulsions with modified interfacial structures. Of which, the formulation of bi-layer nanoemulsions was investigated as described below.

The effects of emulsion pH (2 – 10) and lactoferrin concentration (0.25 – 5% w/w) were studied to determine the best conditions for the formation of a stable, bi-layer nanoemulsion. The emulsion pH and lactoferrin concentration were found to affect the stability of the nanoemulsions. At pH values between 2 and 5, the lactoferrin molecules were weakly adsorbed at the droplet interface of WPI-stabilised nanoemulsions due to electrostatic repulsion. All the emulsions were unstable and exhibited phase separation at pH 5 which is close to the pI of whey proteins. The emulsions were also unstable at low concentration between 0.5 and 1% (w/w) at pH 6 but the stability of emulsions was improved when a sufficiently high level of lactoferrin (3% w/w) was used. The nanoemulsions were stable at pH 7 to 10 as there is sufficient electrostatic attraction between lactoferrin molecules and WPI to form bi-layer at the droplet surface. The stability of the nanoemulsions to various

environmental stresses and *in vitro* digestion under simulated gastrointestinal conditions was tested and compared to nanoemulsions without the addition of lactoferrin (single layer emulsion). Results showed that the bi-layer emulsions had good stability to pH changes and salt addition but they were susceptible to thermal degradation at temperatures above 60^{o}C. The lactoferrin layers in bi-layer emulsions had little impact on the digestion profile as the proteins were hydrolysed at the end of the digestion process.

Lutein was incorporated into the nanoemulsions with encapsulation efficiency of ≥ 80%. The droplet size of nanoemulsions containing lutein was around 70 – 80 nm with PDI of 0.2. The lutein loaded nanoemulsions displayed excellent physical stability and were stable for 28 days at different storage temperatures of 5, 20 and 40^{o}C. However, the lutein content of all the nanoemulsions decreased during storage especially at higher temperature (40^{o}C). Based on the results, it was apparent that the bi-layer nanoemulsions have better stability to lutein degradation. The *in vitro* cell toxicity on Caco-2 cells using MTT assay showed that all the nanoemulsions did not show more toxicity than the conventional emulsions without the use of organic solvent. The cellular uptake of lutein in bi-layer nanoemulsions (1304 pmol/mg protein) was higher than single layer nanoemulsions (873 pmol/mg protein).

In this research, the development of nanoemulsions is a promising approach to incorporate lutein as a bioactive compound for application in foods. This study has shown that a substantial amount of lutein can be incorporated into nanoemulsions (225 mg/L). The amount of lutein presents in the nanoemulsions is considered to be sufficient to meet the recommended daily intake of 6 to 10 mg of lutein in order to have health benefits. By calculation, there would be approximately 9 mg of lutein in a 200 ml beverage when the nanoemulsions are diluted 5 times. Future work is to explore the feasibility of the designated nanoemulsions in food systems such as fruit beverages or dairy products. In reality, these food systems are a complex matrix comprising of several food ingredients such as sugars and dietary fats and varying environmental conditions such as pH and ionic strength which can affect the quality and bioavailability of the encapsulated components in nanoemulsions. Currently, few commercial products of nanoemulsions are available in the market though nanoemulsions have been shown to be advantageous over

conventional emulsions. Thus, the next tranche of the research is to provide information on the application of nanoemulsions to food products. Additionally, *in vivo* assessment of nanoemulsions is another important study area to understand the metabolism and other possible toxicity of nanoemulsions to ensure their safety for oral consumption.

REFERENCES

Adlerova, L., Bartoskova, A. & Faldyna, M. (2008). Lactoferrin: a review. *Veterinarni Medicina*, 53(9), 457-468.

Ahmed, K., Li, Y., McClements, D. J. & Xiao, H. (2012). Nanoemulsion- and emulsion-based delivery systems for curcumin: encapsulation and release properties. *Food Chemistry*, 132(2), 799-807.

Alves-Rodrigues, A. & Shao, A. (2004). The science behind lutein. *Toxicology Letters*, 150(1), 57-83.

AACC International. Approved Methods of Analysis. (11th Ed). Method 30-10.01. Crude Fat in Flour, Bread, and Baked Cereal Products Not Containing Fruit. AACC International, St. Paul, MN, USA.

Anarjan, N., Mirhosseini, H., Baharin, B. S. & Tan, C. P. (2011). Effect of processing conditions on physicochemical properties of sodium caseinate-stabilized astaxanthin nanodispersions. *LWT - Food Science and Technology*, 44(7), 1658-1665.

Anarjan, N., Nehdi, I. A. & Tan, C. P. (2013). Influence of astaxanthin, emulsifier and organic phase concentration on physicochemical properties of astaxanthin nanodispersions. *Chemistry Central Journal*, 7(1), 127.

Anema, S. G. (2008). Chapter 8 – The whey proteins in milk, thermal denaturation, physical interactions and effects on the functional properties of milk. In Thompson, A., Boland, M. & Singh, H. (Eds.), *Milk Proteins From to Food* (239-281). Academic Press.

Anton, N. & Vandamme, T. F. (2009). The universality of low-energy nano-emulsification. *International Journal of Pharmaceutics,* 377(1-2), 142-147.

Anton, N., Benoit, J. & Saulnier, P. (2008). Design and production of nanoparticles formulated from nano-emulsion templates – A review. *Journal of Controlled Release*, 128(3), 185-199.

Anton, N., Gayer, P., Benoit, J. & Saulnier, P. (2007). Nano-emulsions and nanocapsules by the PIT method: An investigation on the role of the temperature cycling on the emulsion phase inversion. *International Journal of Pharmaceutics*, 344(1-2), 44-52.

Artursson, P., Palm, K. & Luthman, K. (2001). Caco-2 monolayers in experimental and theoretical predictions of drug transport. *Advanced Drug Delivery Reviews*, 46(1-3), 27-43.

Aryee, F. N. A. & Nickerson, M. T. (2012). Formation of electrostatic complexes involving mixtures of lentil protein isolates and gum Arabic polysaccharides. *Food Research International,* 48(2), 520-527.

Bae, E. K. & Lee, S. J. (2008). Microencapsulation of avocado oil by spray drying using whey protein and maltodextrin. *Journal of Microencapsulation*, 25(8), 549-560.

Baker, E. N. & Baker, H. M. (2005). Molecular structure, binding properties and dynamics of lactoferrin. *Cellular and Molecular Life Sciences*, 62(22), 2531-2539.

Baker, H. M. & Baker, E. N. (2004). Lactoferrin and iron: structural and dynamic aspects of binding and release. *Biometals*. 17(3), 209-216.

Baldini, G., Beretta, S., Chirlco, G., Franz, H., Maccioni, E., Mariani, P. & Spinozzi, F. (1999). Salt-induced association of β-lactoglobulin by light and X-ray scattering. *Macromolecules*, 32(19), 6128-6138.

Balimane, P. V. & Chong, S. (2005). Cell culture-based models for intestinal permeability: a critique. *Drug Discovery Today*, 10(5), 335-343.

Barbosa-Cánovas, G. V., Ortega-Rivas, E., Juliano, P. & Yan, H. (2005). *Food Powders Physical Properties, Processing, and Functionality*. Kluwer Academic/ Plenum Publishers, New York.

BBC Research. (2011). *The Global Market for Carotenoids*. Retrieved on 7 January 2016 from http://www.companiesandmarkets.com/Market/Food-and-Drink/Market-Research/The-Global-Market-for-Carotenoids/RPT988273.

Bengoechea, C., Peinado, I. & McClements, D. J. (2011). Formation of protein nanoparticles by controlled heat treatment of lactoferrin: Factors affecting particle characteristics. *Food Hydrocolloids*, *25*(5), 1354-1360.

Berendsen, R., Güell, C., Henry, O. & Ferrando, M. (2014). Premix membrane emulsification to produce oil-in-water emulsions stabilized with various interfacial structures of whey protein and carboxymethyl cellulose. *Food Hydrocolloids*, 38, 1-10.

Bezault, J., Bhimani, R., Wiprovnick, J. & Furmanski, P. (1994). Human lactoferrin inhibits growth of solid tumors and development of experiment metastases in mice. *Cancer Research*, 54(9), 2310-2312.

Bhandari, B. R., Patel, K. C. & Chen, X. D. (2008). Spray drying of food materials – process and product characteristics, In Chen, X. D. & Mujumdar, A. S. (Eds.), *Drying Technologies in Food Processing* (113-159). John Wiley & Sons.

Bhusari, S. N., Muzaffar, K. & Kumar, P. (2014). Effect of carrier agents on physical and microstructural properties of spray dried tamarind pulp powder. *Powder Technology*, 266, 354-364.

Boddohi, S., Almodóvar, J., Zhang, H., Johnson, P. A. & Kipper, M. J. (2010). Layer-by-layer assembly of polysaccharide-based nanostructured surfaces containing polyelectrolyte complex nanoparticles. *Colloids and Surfaces B: Biointerfaces*, 77(1), 60-68.

Bokkhim, H., Bansal, N., Grøndhal, L. & Bhandari, B. (2013). Physico-chemical properties of different forms of bovine lactoferrin. *Food Chemistry,* 141(3), 3007-3013.

Bokkhim, H., Bansal, N., Grøndhal, L. & Bhandari, B. (2016). In-vitro digestion of different forms of bovine lactoferrin encapsulated in alginate micro-gel particles. *Food Hydrocolloids*, 52, 231-242.

Boon, C. S., McClements, D. J., Weiss, J. & Decker, E. A. (2010). Factors influencing the chemical stability of carotenoids in foods. *Critical Reviews in Food Science and Nutrition*, 50(6), 515-532.

Booy, M. P. W. M., Ruiter, R. A. & Meere, A. L. J. (1991). Evaluation of the physical stability of freeze dried sucrose-containing formulations by differential scanning calorimetry. *Pharmaceutical Research*, 9(1), 109-114.

Botrel, D. A., Fernandes, R. V. B., Borges, S. V. & Yoshida, (2014). Influence of wall matrix systems on the properties of spray-dried microparticles containing fish oil. *Food Research International*, 62, 344-352.

Bouwmeester, H. & Marvin, H. J. P. (2010). Potential Risks of Nanofood to Consumers. In Chaudhry, Q., Castle, L. & Watkins.(Eds), *Nanotechnologies in Food* (134-149). Cambridge, The Royal Science of Chemistry.

Bouyer, E., Mekhloufi, G., Rosilio, V., Grossiord, J. L. & Agnely, F. (2012). Proteins, polysaccharides, and their complexes used as stabilizers for emulsions: alternatives to synthetic surfactants in the pharmaceutical field? *International Journal of Pharmaceutics*, 436(1-2), 359-378.

Brock, J. H., Arzabe, F., Lampreave, F. & Piñeiro, A. (1976). The effect of trypsin on bovine transferrin and lactoferrin. *Biochimica et Biophysica Acta*, 446(1), 214-215.

Caparino, O. A., Tang, J., Nindo, C. I., Sablani, S. S., Powers, J. R. & Fellman, J. K. (2012). Effect of drying methods on the physical properties and microstructures of mango (Philippine 'carabo' var) powder. *Journal of Food Engineering*, 111(1), 135-148.

Carneiro, H. C. F., Tonon, R. V., Grosso, C. R. F. & Hubinger, M. D. (2013). Encapsulation efficiency and oxidative stability of flaxseed oil microencapsulated by spray drying using different combinations of wall materials. *Journal of Food Engineering*, 115, 443-451.

Cerón, M. C., Campos, I., Sánchez, J. F., Acién, F. G., Molina, E. & Fernández-Sevilla, J.M. (2008). Recovery of lutein from microalgae biomass: development of a process for scenedesmus almeriensis biomass. *Journal of Agricultural and Food Chemistry*, 56(24), 11761-11766.

Chalothorn, K. & Warisnoicharoen, W. (2012). Ultrasonic emulsification of whey protein isolate-stabilized nanoemulsions containing omega-3 oil from plant seed. *American Journal of Food Technology,* 7(9), 532-541.

Chandrasekaran, N., Dimartino, S. & Fee, C. (2013). Study of the adsorption of proteins on stainless steel surfaces using QCM-D. *Chemical Engineering Research and Design*, 91(9), 1674-1683.

Chaudhry, Q., Watkins, R. & Castle, L. (2010). Nanotechnologies in the Food Arena: New Opportunities, New Questions, New Concerns. *Nanotechnologies in Food* (1-17). Cambridge, The Royal Science of Chemistry.

Chen, Q., Zhong, F., Wen, J., McGillivray, D. & Quek, Y. Q. (2014). Properties and stability of spray-dried and freeze-dried microcapsules co-encapsulated with fish oil, phytosterol esters, and limonene. *Drying Technology*, 31(6), 707-716.

Cheong, J. N., Tan, C. P., Man, Y. B. C. & Misran, M. (2008). α-tocopherol nanodispersions: preparation, characterization and stability evaluation. *Journal of Food Engineering,* 89(2), 204-209.

Cheuk, S. Y., Shih, F. F., Champagne, E. T., Daigle, K. W., Patindol, J. A., Mattison, C. P. & Boue, S. M. (2015). Nano-encapsulation of coenzyme Q_{10} using octenyl succinic anhydride modified starch. *Food Chemistry*, 174, 585-590.

Choi, A. J., Kim, C. J., Cho, Y. J., Hwang, J. K. & Kim, C. T. (2011). Characterization of capsaicin-loaded nanoemulsions stabilized with alginate and chitosan by self-assembly. *Food Bioprocess Technology,* 4(6), 1119-1126.

Chopra, H. K. & Panesar, P. S. (2010). *Food Chemistry.* Oxford, Alpha Science International Ltd.

Chu, B., Ichikawa, S., Kanafusa, S. & Nakajima, M. (2007). Preparation of protein-stabilized β-carotene nanodispersions by emulsification-evaporation method. *Journal American Oil Society*, 84(11), 1053-1062.

Chu, B., Ichikawa, S., Kanafusa, S. & Nakajima, M. (2008). Stability of protein-stabilised β-carotene nanodispersions against heating, salts and pH. *Journal of the Science of Food and Agriculture*, 88(10), 1764-1769.

Cornacchia, L. & Roos, Y. H. (2011). Stability of β-carotene in protein-stabilized oil-in-water delivery systems. *Journal of Agricultural and Food Chemistry*, *59*(13), 7013-7020.

Craft, N. E. & Soares, J. H. (1992). Relative solubility, stability and absorptivity of lutein and β-carotene in organic solvents. *Journal of Agricultural and Food Chemistry*, 40(3), 431-434.

Craig, M., Bordes, R. & Holmberg, K. (2012). Polypeptide multilayer self-assembly and enzymatic degradation on tailored gold surfaces studied by QCM-D. *Soft Matter*, 8(17), 4788-4794.

Dalgleish, D. G. (2004). Food Emulsions: Their Structures and Properties. In Friberg, S. E., Larsson, K. and Sjohlom, J. (Eds.), *Food Emulsions* (1-44). 4th ed. New York, Marcel Dekker, Inc.

Dalgleish, D. G. & Corredig, M. (2012). The structure of the casein micelle of milk and its changes during processing. *Annual Review of Food Science and Technology*, 3(1), 449-467.

Das, D., Wang, E. & Langrish, T. A. G. (2014). Solid-phase crystallization of spray-dried glucose powders: a perspective and comparison with lactose and sucrose. *Advanced Powder Technology*, 25(4), 1234-1239.

de Kruif, C. G., Huppertz, T., Urban, V. S. & Petukhov, A. V. (2012). Casein micelles and their internal structure. *Advances in Colloid and Interface Science*, 171-172, 36-52.

Degner, B. M., Chung, C., Schlegel, V., Hutkins, R. & McClements, D. J. (2014). Factors influencing the freeze-thaw stability of emulsion-based foods. *Comprehensive Reviews in Food Science and Food Safety*, *13*(2), 98-113.

Deshmukh, A. S., Setty, C. M., Badiger, A. M. & Muralikrishna, K. S. (2012). Gum ghatti: a promising polysaccharide for pharmaceutical applications. *Carbohydrate Polymers,* 87(2), 980-986.

Dickinson, E. (2003). Hydrocolloids at interfaces and the influence on the properties of dispersed systems. *Food Hydrocolloids,* 17(1), 25-39.

Dickinson, E. (2009). Hydrocolloids as emulsifiers and emulsion stabilizers. *Food Hydrocolloids,* 23(6), 1473-1482.

Domian, E., Brynda-Kopytowska, A., Cenkier, J. & Świrydow, E. (2015). Selected properties of microencapsulated oil powders with commercial preparations of maize OSA starch and trehalose. *Journal of Food Engineering*, 152, 72-84.

Domian, E., Sułek, A., Cenkier, J. & Kerschke, A. (2014). Influence of agglomeration on physical characteristics and oxidative stability of spray-dried oil powder with milk protein and trehalose wall material. *Journal of Food Engineering*, 125, 34-43.

Donhowe, E. G., Flores, F. P., Kerr, W. L., Wicker, L. & Kong, F. (2014). Characterization and in vitro bioavailability of β-carotene: effects of microencapsulation method and food matrix. *LWT - Food Science and Technology*, 57(1), 42-48.

Drusch, S., Serfert, Y., Van Den Heuvel, A. & Schwarz, K. (2006). Physicochemical characterization and oxidative stability of fish oil encapsulated in an amorphous matrix containing trehalose. *Food Research International*, 39(7), 807-815.

Du, Q., Lin, D., Wang, R. & Yao, S. (2014). Mechanistic analysis of effects of pH and salt concentration on lactoferrin adsorption onto adsorbents with sulfonic ligand. *Chemical Industry and Engineering Society of China*, 65(2), 593-598.

Dubey, R. R. & Parikh, R. H. (2004). Studies of PLGA microspheres. *Pharmaceutical Technology Europe*, 16, 23-24.

Dwyer, J. H., Navab, M., Dwyer, K. M., Hassan, K., Sun, P., Shircore, A., Hama-Levy, S., Hough, G., Wang, X., Drake, T., Merz, N. B. & Fogelman, A. M. (2001). Oxygenated carotenoid lutein and progression of early atherosclerosis: the Los Angeles atherosclerosis study. *Circulation*, 103(24), 2922-2927.

Eason, R. R., Velarde, M. C., Chatman, L., Till, S. R., Geng, Y., Ferguson, M., Badger, T. M. & Simmen, R. C. M. (2004). Dietary exposure to whey proteins alters rat mammary gland proliferation, apoptosis, and gene expression during postnatal development. *The Journal of Nutrition*, 134(12), 3370-3377.

Ee, S. L., Duan, X., Liew, J. & Nguyen, Q. D. (2008). Droplet size and stability of nano-emulsions produced by the temperature phase inversion method. *Chemical Engineering Journal,* 140(1-3), 626-631.

Fang, Z. & Bhandari, B. (2012). Spray drying, freeze drying and related processes for food ingredient and nutraceutical applications. In Garti, N. & McClements, D. J. (Eds.), *Encapsulation Technologies and Delivery Systems for Food Ingredients and Nutraceuticals* (73-109). Woodhead Publishing.

Food and Agriculture Organization. (2012). *FAO/INFOODS Density Database Version 2.0*. Retrieved from http://www.fao.org/docrep/017/ap815e/ap815e.pdf.

Fazaeli, M., Emam-Djomeh, Z., Ashtari, A. K. & Omid, M. (2012). Effect of spray drying conditions and feed composition on the physical properties of black mulberry juice powder. *Food and Bioproducts Processing*, 90(4), 667-675.

Fernandez, P., André, V., Rieger, J. & Kühnie, A. (2004). Nano-emulsion formation by emulsion phase inversion. *Colloids and Surfaces A: Physicochem. Eng. Aspects.* 251(1-3), 53-58.

Fernández-Sevilla, J. M. & Fernández, F. G. A. (2010). Biotechnological production of lutein and its applications. *Applied Microbiology Biotechnology*, 86, 27-40.

Fioramonti, S. A., Martinez, M. J., Pilosof, A. M. R., Rubiolo, A. C. & Santiago, L. G. (2015). Multilayer emulsions as a strategy for linseed oil microencapsulation: effect of pH and alginate concentration. *Food Hydrocolloids*, 43, 8-17.

Fotakis, G. & Timbrell, J. A. (2006). In vitro cytotoxicity assays: comparison of LDH, neutral red, MTT and protein assay in hepatoma cell lines following exposure to cadium chloride. *Toxicology Letters*, 160(2), 171-177.

Fox, P. F. (2011). Bovine milk. *Encyclopedia of Dairy Sciences*. 2nd ed. Academic Press.

Franceschinis, L., Salvatori, D. M., Sosa, N. & Schebor, C. (2015). Physical and functional properties of blackberry freeze- and spray-dried powders. *Drying Technology*, 32 (2), 197-2014.

Frede, K., Henze, A., Khalil, M., Baldermann, S., Schweigert, F. J. & Rawel, H. (2014). Stability and cellular uptake of lutein-loaded emulsions. *Journal of Functional Foods*, 8(1), 118-127.

Gallier, S., Tate, H. & Singh, H. (2013). In vitro gastric and intestinal digestion of a walnut oil body dispersion. *Journal of Agricultural and Food Chemistry*, 61(2), 410-417.

Gbassi, G. K., Yolou, F. S., Sarr, S. O., Atheba, P. G., Amin, C. N. & Ake, M. (2012). Whey proteins analysis in aqueous medium and in artificial gastric and intestinal fluids. *International Journal of Biological and Chemical Sciences*, 6(4), 1828-1837.

GEA Niro. GEA Niro Research Laboratory. Method No. A 10a. Surface Free Fat of a Powder. Revised September 2011. GEA Process Engineering, Søborg, Denmark.

Gharsallaoui, A., Roudaut, G., Chambin, O., Voilley, A. & Saurel, R, (2007). Applications of spray-drying in microencapsulation of food ingredients: an overview. *Food Research International*, 40(9), 1107-1121.

Ghosh, V., Mukherjee, A. & Chandrasekaran, N. (2012). Ultrasonic emulsification of food-grade nanoemulsion formulation and evaluation of its bactericidal activity. *Ultrasonics Sonochemistry,* 20(1), 338-344.

Golding, M. & Wooster, T. J. (2010). The influence of emulsion structure and stability on lipid digestion. *Current Opinion in Colloid & Interface Science*, 15(1-2), 90-101.

Goula, A. M. & Adamopoulos, K. G. (2008). Effect of maltodextrin addition during spray drying of tomato pulp in dehumidified air: i. drying kinetics and product recovery. *Drying Technology*, 26(6), 714-725.

Guo, M. R., Fox, P. F., Flynn, A. & Kindstedt, P. S. (1995). Susceptibility of beta-lactoglobulin and sodium caseinate to proteolysis by pepsin and trypsin. *Journal of Dairy Science*, 78(11), 2336-2344.

Guttoff, M., Saberi, A. H. & McClements, D. J. (2015). Formation of vitamin D nanoemulsions-based delivery systems by spontaneous emulsification: factors affecting particle size and stability. *Food Chemistry*, 171, 117-122.

Guzey, D. & McClements, D. J. (2006). Formation, stability and properties of multilayer emulsions for application in the food industry. *Advances in Colloid and Interface Science*, 128-130, 227-248.

Hasenhuettl, G. L. (2008). Synthesis and commercial preparation of food emulsifiers. In Hasenhuettl, G. L. & Hartel, R. W. (Eds.), *Food Emulsifiers and Their* Applications (11-37). 2nd ed. New York, Springer Science + Business Media, LLC.

He, W., Tan, Y., Tian, Z., Chen, L., Hu, F. & Wu, W. (2011). Food protein-stabilized nanoemulsions as potential delivery systems for poorly water-soluble drugs: preparation, in vitro characterization, and pharmacokinetics in rats. *International Journal of Nanomedicine*, 6, 521-533.

Henry, J. V. L., Fryer, P. J., Frith, W. J. & Norton, I. T. (2009). Emulsification mechanism and storage instabilities of hydrocarbon-in-water sub-micron

emulsions stabilised with Tweens (20 and 80), Brij 96v and sucrose monoesters. *Journal of Colloid and Interface Science,* 338(1), 201-206.

Höök, F., Kasemo, B., Nylander, T., Fant, C., Sott, K. & Elwing, H. (2001). Variations in coupled water, viscoelastic properties, and film thickness of a Mefp-1 protein film during adsorption and cross-linking: a quartz crystal microbalance with dissipation monitoring, ellipsometry, and surface plasmon resonance study. *Analytical Chemistry*, 73(24), 5796-5804.

Horne, D. S. (2011). Analytical Methods Light Scattering Techniques. *Encyclopaedia of Dairy Sciences.* 2nd ed. Academic Press.

Horvath, H. (2009). Gustav Mie and the scattering and absorption of light by particles: Historic developments and basics. *Journal of Quantitative Spectroscopy and Radiative Transfer,* 10(11), 787-799.

Hosseinpour, S., Izadi, M., Aminlari, M., Ramezani, R. & Tavana, M. (2011). Changes in the solubility and SDS-PAGE profile of whey proteins during storage at different temperatures: A kinetic study. *Journal of Food and Agriculture Science,* 1(1), 15-21.

Hu, L., Mao, Z. & Gao, C. (2009). Colloidal particles for cellular uptake and delivery. *Journal of Materials Chemistry,* 19(20), 3108-3115

Hunt, J. A & Dalgleish, D. G. (1994). Effect of pH on the stability and surface composition of emulsions made with whey protein isolate. *Journal of Agricultural and Food Chemistry*, 42(10), 2131-2135.

Iafisco, M., Foggia, M. D., Bonora, S., Prat, M. & Roveri, N. (2011). Adsorption and spectroscopic characterization of lactoferrin on hydroxyapatite nanocrystals. *Dalton Transactions*, 40(4), 820-827.

Imeson, A., Helgerud, T., Gåserød, Fiaereide, T., Anderson, P. O. & Larsen, C. K. (2009). Chapter 4. Alginates, In Imeson, A. (52-72)., *Food Stabilisers, Thickeners and Gelling Agents* (eds). Wiley-Blackwell Publishing Ltd.

International Dairy Federation. Determination of the dispersibility and wettability of instant dried milk. Brussels.

Ito, E., Arai, T., Hara, M. & Noh, J. (2009). Surface potential change depending on molecular orientation of hexadecanethiol self-assembled monolayers on AU(111). *Bulletin of the Korean Chemical Society*, 30(6), 1309-1312.

Jafari, S. M., Assadpoor, E., Bhandari, B. & He, Y. (2008). Nano-particle encapsulation of fish oil by spray drying. *Food Research International*, 41(2), 172-183.

Jafari, S. M., Assadpoor, E., He, Y. & Bhandari, B. (2008). Encapsulation efficiency of food flavours and oils during spray drying. *Drying Technology*, 26(7), 816-835.

Jafari, S. M., He, Y. & Bhandari, B. (2007). Optimization of nano-emulsions production by microfluidisation. *European Food Research Technology,* 225(5-6), 733-741.

Jain, N. K. & Roy, I. (2009). Effect of trehalose on protein structure. *Protein Science*, 18(1), 24-36.

Jo, Y. J. & Kwon, Y. J. (2014). Characterization of β-carotene nanoemulsions prepared by microfluidisation technique. *Food Science Biotechnology*, *23*(1), 107-114.

Jost, R. (1993). Functional characteristics of dairy proteins. *Trends in Food Science and Technology*, 4(9), 283-288.

Kang, J., Cui, S. W., Chen, J., Philips, G. O., Wu, Y. & Wang, Q. (2011). New studies on gum ghatti (*Anogeissus latifolia*) part I. fractionation, chemical and physical characterization of the gum. *Food Hydrocolloids,* 25(8), 1984-1990.

Keil, B. (1992). *Specificity of proteolysis*. Berlin-Heidelberg-New York, Springer-Verlag.

Kentish, S., Wooster, T. J., Ashokkumar, M., Balachandran, S., Mawson, R. & Simons, L. (2008). The use of ultrasonics for nanoemulsion preparation. *Innovative Food Science and Emerging Technologies,* 9(2), 170-175.

Keogh, M. K., Murray, C. & O'Kennedy, B. T. (2003). Effects of ultrafiltration of whole milk on some properties of spray-dried milk powders. *International Dairy Journal*, 13(12), 995-1002.

Kettler, K., Veltman, K., Meent, D., Wezel, A. & Hendriks, A. J. (2013). Cellular uptake of nanoparticles as determined by particle properties, experimental conditions, and cell type. *Environmental Toxicology and Chemistry*, 33(3), 481-492.

Khalil, M., Raila, J., Ali, M., Islam, K. M. S., Schenk, R., Krause, J., Schweigert, F. J. & Rawei, H. (2012). Stability and bioavailability of lutein ester supplements from Tagetes flower prepared under food processing conditions. *Journal of Functional Foods*, 4(3), 602-610.

Kijlstra, A., Tian, Y., Kelly, E. R. & Berendschot, T. T. J. M. (2012). Lutein: more than just a filter for blue light. *Progress in Retinal and Eye Research*, 31(4), 303-315.

Kim, S. O., Ha, T. V. A., Choi, Y. J. & Ko, S. (2014). Optimization of homogenization-evaporation process for lycopene nanoemulsion production and its beverage applications. *Journal of Food Science*, 79(8), N1604-N1610.

Kinsella, J. E. & Whitehead, D. M. (1989). Proteins in whey: chemical, physical, and functional properties. In Kinsella, J. E. (Eds.), *Advances in Food and Nutrition Research* (343-438). Academic Press, Inc.

Klang, V., Matsko, N. B., Valenta, C. & Hofer, F. (2012). Electron microscopy of nanoemulsions: an essential tool for characterisation and stability assessment. *Micron*, 43(2-3), 85-103.

Krinsky, N. I., Landrum, J. T. & Bone, R. A. (2003). Biologic mechanisms of the protective role of lutein and zeaxanthin in the eye. *Annual Review of Nutrition*, 23, 171-201.

Krivosheeva, O., Dėdinaitė, A. & Claesson, P. M. (2012). Adsorption of Mefp-1: Influence of pH adsorption kinetics and adsorbed amount. *Journal of Colloid and Interface Science*, 379(1), 107-113.

Kuang, P., Zhang, H., Bajaj, P. R., Yuan, Q., Tang, J., Chen, S. & Sablani, S. (2015). Physicochemical properties and storage stability of lutein microcapsules prepared with maltodextrins and sucrose by spray drying. *Journal of Food Science*, 80(2), E359-E369.

Kuck, L. S. & Noreña, C. P. Z. (2016). Microencapsulation of grape (vitis labrusca var. bordo) skin phenolic extract using gum Arabic, polydextrose, and partially hydrolysed guar gum as encapsulating agents. *Food Chemistry*, 194,569-576.

Kulmyrzaev, A., Chanamai, R. & McClements, D. J. (2000). Influence of pH and $CaCl_2$ on the stability of dilute whey protein stabilized emulsions. *Food Research International,* 33(1), 15-20.

Lapshova, M. S., Deineka, V. I., Deineka, L. A., Blinova, I. P. & Tret'yakov, M.Y. (2013). Identification of xanthophylls in a marigold petal extract. *Journal of Analytical Chemistry*, 68(11), 1014-1019.

Lebec, V., Landoulsi, J., Boujday, S., Poleunis, C., Pradier, C.-M. & Delcorte, A. (2013). Probing the orientation of β-lactoglobulin on gold surfaces modified by alkyl thiol self-assembled monolayers. *The Journal of Physical Chemistry*, 117(22), 11569-11577.

Lee, S. J. & McClements, D. J. (2010). Fabrication of protein-stabilized nanoemulsions using a combined homogenization and amphiphilic solvent dissolution/evaporation approach. *Food Hydrocolloids*, 24(6-7), 560-569.

Lee, S. J., Choi, S. J., Li, Y., Decker, E. A. & McClements, D. J. (2011). Protein-stabilized nanoemulsions and emulsions: comparison of physicochemical stability, lipid oxidation, and lipase digestibility. *Journal of Agricultural and Food Chemistry*, 59(1), 415-427.

Leong, W. F., Lai, O. M., Long, K., Man, Y. B. C., Misran, M. & Tan, C. P. (2011). Preparation and characterisation of water-soluble phytosterol and nanodispersions. *Food Chemistry*, 129(1), 77-83.

Lesmes, U., Baudot, P. & McClements, D. J. (2010). Impact of interfacial composition on physical stability and in vitro lipase digestibility of triacylglycerol oil droplets coated with lactoferrin and/ or caseinate. *Journal of Agricultural and Food Chemistry*, 58(13), 7962-7969.

Lesmes, U., Sandra, S., Decker, E. A. & McClements, D. J. (2010). Impact of surface deposition of lactoferrin on physical and chemical stability of omega-3 rich lipid droplets stabilised by caseinate. *Food Chemistry*, 123(1), 99-106.

Li, Y., Hu, M., Du, Y. & McClements, D. J. (2011). Controlling lipid nanoemulsion digestion using nanolaminated biopolymer coatings. *Journal of Microencapsulation*, 28(3), 166-175.

Li, Q., Liu, C. G. & Yu, Y. (2015). Separation of monodisperse alginate nanoparticles and effect of particle size on transport of vitamin E. *Carbohydrate Polymers*, 124, 274-279.

Li, D. J., Song, J. F. & Liu, C. Q. (2014). Kinetic stability of lutein in freeze-dried sweet corn powder stored under different conditions. *Food Science and Technology Research*, 20(1), 65-70.

Li, Y., Zheng, J., Xiao, H. & McClements, D. J. (2012). Nanoemulsion-based delivery systems for poorly water-soluble bioactive compounds: Influence of formation parameters on polymethoxyflavone crystallization. *Food Hydrocollods,* 27(2), 517-528.

Lim, A. S. L., Griffin, C. & Roos, Y. H. (2014). Stability and loss kinetics of lutein and β-carotene encapsulated in freeze-dried emulsions with layered interface and trehalose as glass former. *Food Research International*, 62, 403-409.

Lin, C. H. & Chen, B. H. (2005). Stability of carotenoids in tomato juice during storage. *Food Chemistry*, 90(4), 837-846.

Liu, S. X. & Kim, J. T. (2009). Application of Kevin-Voigt model in quantifying whey protein adsorption on polyethersulfone using QCM-D. *Journal of Laboratory Automation*, 14(4), 213-220.

Livney, Y. D. (2010). Milk proteins as vehicles for bioactives. *Current Opinion in Colloid & Interface Science,* 15(1-2), 73-83.

Lönnerdal, B. (1994). Lactoferrin receptors in intestinal brush border membranes. In Hutchens, T. W., Rumball, S. V. & Lönnerdal, B. (Eds.), *Lactoferrin: Structure and Function* (171-175). New York and London, Plenum Press.

Lundin, M., Elofsson, U. M., Blomberg, E. & Rutland, M. W. (2010). Adsorption of lysozyme, β-casein and their layer-by-layer formation on hydrophilic surfaces: effect of ionic strength. *Colloids and Surfaces B: Biointerfaces*, 77(1), 1-11.

Luo, Y., Chen, D., Ren, L., Zhao, X. & Qin, J. (2006). Solid lipid nanoparticles for enhancing vinpocetine's oral bioavailability. *Journal of Controlled Release*, 114(1), 53-59.

Ma, C., Wu, B. & Zhang, G. (2013). Protein-protein resistance investigated by quartz crystal microbalance. *Colloids and Surface B: Biointerfaces*, 104, 5-10.

Mahajan, R. K., Chawla, J. & Bakshi, M. S. (2004). Depression in the cloud point of Tween in the presence of glycol additives and triblock polymers. *Colloid and Polymer Science*, *282*(10), 1165-1168.

Mahdi, E. S., Sakeena, M. H. F., Abdulkarim, M. F., Abdullah, G. Z., Sattar, M. A. & Noor, A. M. (2011). Effect of surfactant and surfactant blends on pseudoternary phase diagram behaviour of newly synthesized palm kernel oil esters. *Drug Design, Development and Therapy,* 5, 311-323.

Maher, P. G., Roos, Y. H. & Fenelon, M. A. (2014). Physicochemical properties of spray dried nanoemulsions with varying final water and sugar contents. *Journal of Food Engineering*, 126, 113-119.

Malmström, J., Agheli, H., Kingshott, P. & Sutherland, D. S. (2007). Viscoelastic modelling of highly hydrated laminin layers at homogenous and nanostructured surfaces: quantification of protein layer properties using QCM-D and SPR. *Langmuir*, 23(19), 9760-9768.

Malvern Instruments Limited. (2014). Zeta Potential An Introduction in 30 Minutes. Retrieved from http://www3.nd.edu/~rroeder/ame60647/slides/zeta.pdf.

Mantel, C., Miyazawa, K. & Broxmeyer, H. E. (1994). Physical characteristics and polymerization during iron saturation of lactoferrin, a myelopietic regulatory molecule with suppressor activity. *Advance in Experimental Medicine and Biology*, 357, 121-132.

Mao, L., Boiteux, L., Roos, Y. H. & Miao, S. (2014). Evaluation of volatile characteristics in whey protein isolate-pectin mixed layer emulsions under different environmental conditions. *Food Hydrocolloids*, 41, 79-85.

Mao, Y., Dubot, M., Xiao, H. & McClements, D. J. (2013). Interfacial engineering using mixed protein systems: emulsion-based delivery systems for encapsulation and stabilisation of β-carotene. *Journal of Agricultural and Food Chemistry*, *61*(21), 5163-5169.

Mela, I., Aumaitrem E., Williamson, A. & Yakubov, G. E. (2010). Charge reversal by salt-induced aggregation in aqueous lactoferrin solutions. *Colloids and Surafces B: Biointerfaces*, 78(1), 53-60.

Messina, G. M. L., Satriano, C. & Marletta, G. (2009). A multitechnique study of preferential protein adsorption on hydrophobic and hydrophilic plasma-modified polymer surfaces. *Colloids and Surfaces B: Biointerfaces*. 70(1), 76-83.

McClements, D. J. (1999). *Food Emulsions Principles, Practices, and Techniques*. Boca Raton, FL, CRC Press.

McClements, D. J. (2007). Critical review of techniques and methodologies for characterization of emulsion stability. *Critical Reviews in Food Science and Nutrition,* 47(7), 611-649.

McClements, D. J. (2010). Emulsion design to improve the delivery of functional lipophilic components. *The Annual Review of Food Science and Technology*, 1(1), 241-269.

McClements, D. J. (2012). Nanoemulsions *versus* microemulsions: terminology, differences, and similarities. *Soft Matter,* 8(6), 1719-1729.

McClements, D. J. & Rao, J. (2011). Food-grade nanoemulsions: formulation, fabrication, properties, performance, biological fate, and potential toxicity. *Critical Reviews in Food Science and Nutrition,* 51(4), 285-330.

McClements, D. J. & Xiao, H. (2012). Potential biological fate of ingested nanoemulsions: influence of particle characteristics. *Food & Function,* 3(3), 202-220.

Mivehi, L., Bordes, R. & Holmberg, K. (2013). Adsorption of cationic gemini surfactants at solid surfaces studied by QCM-D and SPR-effect of the presence of hydroxyl groups in the spacer. *Colloids and Surfaces A: Physicochemical and Engineering Aspects*, 419, 21-27.

Mizrahi, S. (2011). Accelerated shelf life testing of foods, in *Food and Beverage Stability and Life* (eds Kilcast, D. & Subramaniam, P.). Woodhead Publishing Limited, Cambridge, 482-506

Müller, M. (2014). Polyelectrolyte Complexes in the Dispersed and Solid State II: Application Aspects. Springer-Verlag Berlin Heidelberg.

Mun, S., McClements, D. J. & Surh, J. (2010). Influence of maltodextrin type and multi-layer formation on the freeze-thaw stability of model beverage emulsions stabilized with β-lactoglobulin. *Food Science Biotechnology*, 19(1), 7-17.

National Science and Technology Council. (2006). *The National Nanotechnology Initiative Environmental, Health, and Safety Research Needs for Engineered Nanoscale Materials.* Retrieved from http://www.nano.gov/sites/default/files/pub_resource/nni_ehs_research_needs.pdf?q=NNI_EHS_research_needs.pdf.

Ng, S. K., Choong, Y. H., Tan, C. P., Long, K. & Nyam, K. L. (2014). Effect of total solids content in feed emulsion on the physical properties and oxidative stability of microencapsulated kenaf seed oil. *LWT - Food Science and Technology*, 58(2), 627-632.

Niamprem, P., Rujivipat, S. & Tiyaboonchai, W. (2014). Development and characterization of lutein-loaded SNEDDS for enhanced absorption in Caco-2 cells. *Pharmaceutical Development and Technology*, 19(6), 735-742.

Nik, A. M., Wright, A. J. & Corredig, M. (2010). Surface adsorption alters the susceptibility of whey proteins to pepsin-digestion. *Journal of Colloid and Interface Science*, 344(2), 372-281.

Nik, A. M., Wright, A. J. & Corredig, M. (2011). Impact of interfacial composition on emulsion digestion and rate of lipid hydrolysis using *in vitro* digestion models. *Colloids and Surfaces B: Biointerfaces*, 83(2), 321-320.

Nováková, Z., Oriňáková, R., Oriňák, A., Hvizdoš, P. & Fedorková, A. S. (2014). Elimination voltammetry as a new method for studying the SAM formation. *Internal Journal of Electrochemical Science*, 9(7), 3846-3863.

Ohtake, S. & Wang, Y. J. (2011). Trehalose: current use and future applications. *Journal of Pharmaceutical Sciences*, 100(6), 2020-2052.

Pal, S. J., Jana, U., Manna, P. K., Mohanta, G. P. & Manavalan, R. (2011). Nanoparticle: an overview of preparation and characterization. *Journal of Applied Pharmaceutical Science*, 1(6), 228-234.

Pallandre, S., Decker, E. A. & McClements, D. J. (2007). Improvement of stability of oil-in-water emulsions containing caseinate-coated droplets by addition of sodium alginate. *Journal of Food Science*, 72(9), E518-524.

Pegg, R. B. & Shahidi, F. (2007). Encapsulation, stabilization, and controlled of food ingredients and bioactives. In Rahman, M. S. (Eds.), *Handbook of Food Preservation* (509-568). 2nd ed. CRC Press.

Pérez-Gálvez, A. & Mínguez-Mosquera, M. I. (2005). Esterification of xanthophylls and its effect on chemical behavior and bioavailability of carotenoids in the human. *Nutrition Research*, 25(7), 631-640.

Pierce, A., Colavizza, D., Benaissa, M., Maes, P., Tartar, A., Montreuil, J. & Spik, G. (1991). Molecular cloning and sequence analysis of bovine lactotransferrin. *European Journal of Biochemistry,* 196(1), 177-184.

Pourashouri, P., Shabanpour, B., Razavi, S. H., Jafari, S. M., Shabani, A. & Aubourg, S. P. (2014). Impact of wall materials on physicochemical properties of microencapsulated fish oil by spray drying. *Food Bioprocess Technology*, 7(8), 2354-2365.

Qhattal, H. S. S., Wang, S., Salihima, T., Srivastava, S. K. & Liu, X. (2011). Nanoemulsions of cancer chemopreventive agent benzyl isothiocyanate display enhanced solubility, dissolution, and permeability. *Journal of Agricultural and Food Chemistry*, 59(23), 12396-12404.

Qian, C., Decker, E. A., Xiao, H. & McClements, D. J. (2012). Physical and chemical stability of β-carotene-enriched nanoemulsions: influence of pH, ionic strength, temperature, and emulsifier type. *Food Chemistry*, 132(3), 1221-1229.

Qian, C. & McClements, D. J. (2011). Formation of nanoemulsions stabilized by model food-grade emulsifiers using high pressure homogenizations: factors affecting particle size. *Food Hydrocolloids*, 25(5), 1000-1008.

Ré, M. I. (1998). Microencapsulation by spray drying. *Drying Technology*, 16(6), 1195-1236.

Reboul, E. (2013). Absorption of vitamin A and carotenoids by the enterocyte: focus on transport proteins. *Nutrients*, 5(9), 3563-3581.

Reboul, E., Abou, L., Mika, C., Ghiringhelli, O., André, M., Portugal, H., Jourdheuil-Rahmani, D., Amiot, M., Lairon, D. & Borel, P. (2005). Lutein transport by Caco-2 TC-7 cells occurs partly by a facilitated process involving the scavenger receptor class B type 1 (SR-B1). *Biochemical Society*, 387(2), 455-461.

Reddy, M., Kella, N. K. D. & Kinsella, J. E. (1988). Structural and conformational basis of the resistance of β-lactoglobulin to peptic and chymotryptic digestion. *Journal of Agricultural and Food Chemistry*, 36(4), 737-741.

Reichardt, C. & Welton, T. (2010). Appendix A. Properties, Purification, and Use of Organic Solvents, In Reichardt, C. & Welton, T. (549-586)., *Solvents and Solvent Effects in Organic Chemistry* (eds) (4th ed.). Wiley-VCH Verlag GmbH & Co. KGaA.

Reviakine, I., Johannsmann, D. & Richter, R. P. (2011). Hearing what you cannot see and visualizing what you hear: interpreting quartz crystal microbalance data from solvated interfaces. *Analytical Chemistry*, 83(23), 8838-8848.

Ribaya-Mercado, J. D. & Blumberg, J. B. (2004). Lutein and zeaxanthin and their potential roles in disease prevention. *Journal of the American College of Nutrition*, 23(6), 567S-587S.

Richards, A. B. & Dexter, L. B. (2011). Trehalose. In O'Brien-Nabors, L. (Eds.), *Alternative Sweeteners* (439-470). 4th ed. CRC Press.

Rocha, G. A., Fávaro-Trindade, C. S. & Grosso, C. R. F. (2012). Microencapsulation of lycopene by spray drying: characterization, stability and application of microcapsules. *Food and Bioproducts Processing*, 90(1), 37-42.

Sah, B. N. P., Vasiljevic,T., McKechnie, S. & Donkor, O. N. (2015). Identification of anticancer peptides from bovine milk proteins and their potential roles in management of cancer: a critical review. *Comprehensive Reviews in Food Science and Food Safety*, 14(2), 123-138.

Sahin, S. & Sumnu, S. G. (2006). *Physical Properties of Foods.* New York, Springer Science + Business Media.

Salminen, H. & Weiss, J. (2013). Effect of pectin type on association and pH stability of whey protein-pectin complexes. *Food Biophysics*, 9(1), 29-38.

Salvia-Trujillo, L., Rojas-Graü, M. A., Soliva-Fortuny, R. & Martín-Belloso, O. (2013). Effect of processing parameters on physiochemical and characteristics of microfluidised lemongrass essential oil-alginate nanoemulsions. *Food Hydrocolloids,* 30(1), 401-407.

Sarkar, A., Goh, K. K. T., Singh, R. P. & Singh, H. (2009). Behaviour of an oil-in-water emulsion stabilized by β-lactoglobulin in an in vitro gastric model. *Food Hydrocolloids*, 23(6), 1563-1569.

Sato, Y., Kobayashi, M., Itagaki, S., Hirano, T., Noda, T., Mizuno, S., Sugawara, M. & Iseki, K. (2011). Pharmacokinetic properties of lutein emulsion after oral administration to rats and effect of food intake on plasma concentration of lutein. *Biopharmaceutics & Drug Disposition*, 32(3), 151-158.

Sauerbrey, G. (1959). The use of quartz crystals for weighing thin layers and for microweighing. *Zeitschrift für Physik*, 155(2), 206-222.

Schmelz, T., Lesmes, U., Weiss, J. & McClements, D. J. (2011).Modulation of physicochemical properties of lipid droplets using β-lactoglobulin and/or lactoferrin interfacial coatings. *Food Hydrocolloids*, 25(5), 1181-1189.

Seddon, J. M., Ajani, U. A., Sperduto, R. D., Hiller, R., Blair, N., Burton, T. C., Farber, M. D., Gragoudas, E. S., Haller, J. & Miller, D. T. (1994). Dietary carotenoids, vitamins A, C, and E, and advanced age-related macular degeneration. Eye disease case-control study group. *Journal of the American Medical Association*, 272(18), 1413-1420.

Shah, P., Jogani, V., Bagchi, T. & Misra, A. (2006). Role of caco-2 cell monolayers in prediction of intestinal drug absorption. *Biotechnology Progress*, 22(1), 186-198.

Shegokar, R. & Mitri, K. (2012). Carotenoid lutein: a promising candidate for pharmaceutical and nutraceutical applications. *Journal of Dietary Supplements*, 9(3), 183-210.

Shimazaki, K. (2000). Lactoferrin: A marvelous protein in milk? *Animal Science Journal,* 71(4), 329-347.

Shimoni, G., Levi, S., Tal, L. & Lesmes, U. (2013). Emulsions stabilization by lactoferrin nano-particles under *in vitro* digestion conditions. *Food Hydrocolloids*, 33(2), 264-272.

Shinoda, K. & Arai, H. (1964). The correlation between phase inversion temperature in emulsion and cloud point in solution of nonionic emulsifier. *The Journal of Physical Chemistry*, 68(12), 3485-3490.

Silva, H. D., Cerqueira, M. A., Souza, B. W. S., Ribeiro, C., Avides, M. C., Quintas, M. A. C., Coimbra, J. S. R., Carneiro-da-Cunha, M. G. & Vicente, A. A. (2011). Nanoemulsions of β-carotene using a high-energy emulsification-evaporation technique. *Journal of Food Engineering,* 102(2), 130-135.

Skirtach, A. G., Yashchenok, A. M. & Möhwald, H. (2011). Encapsulation, release and applications of LBL polyelectrolyte multilayer capsules. *Chemical Communications*, 47(48), 12736-12746.

Singh, H. (2011). Milk protein products functional properties of milk proteins. *Encyclopaedia of Dairy Sciences*. 2nd ed. Academic Press.

Singh, H. & Sarkar, A. (2011). Behaviour of protein-stabilised emulsions under various physiological conditions. *Advances in Colloid and Interface Science*, 165(1), 47-57.

Skirtach, A. G., Yashchenok, A. M. & Möhwald, H. (2011). Encapsulation, release and applications of LBL polyelectrolyte multilayer capsules. *Chemical Communications*, 47, 12736-12746.

Smallwood, I. M. (1996). *Handbook of Organic Solvent Properties*. New York, Halsted Press.

Solans, C., Izquierdo, P., Nolla, J., Azemar, N. A. & Garcia-Celma, M. J. (2005). Nano-emulsions. *Current Opinion in Colloid and Interface Science*, 10(3-4), 102-110.

Solans, C. & Solè, I. (2012). Nano-emulsions: Formation by low-energy methods. *Current Opinion in Colloid & Interface Science,* 17(5), 246-254.

Sosa, N., Schebor, C. & Pérez, O. E. (2014). Encapsulation of citral in formulations containing sucrose or trehalose: emulsions properties and stability. *Food and Bioproducts Processing*, 92(3), 266-274.

Sukhorukov, B., Caruso, F., Davis, S. A. & Möhwald, H. (1998). Novel hollow polymer shells by colloid-templated assembly of polyelectrolytes. *Angewandte Chemie International Edition*, 37(16), 2201-2205.

Steijjns, J. M. & Hooijonk, A. C. M. (2000). Occurrence, structure, biochemical properties and technological characteristics of lactoferrin. *British Journal of Nutrition*, 84(1), S11-S17.

Stephenson, R. J., Wolber, F., Plieger, P. G., & Harding, D. R. K. (2016). Synthesis and characterization of bradykinin derivatives based on a beta-cyclodextrin core. *Australian Journal of Chemistry*, 69(3), 328-335.

Stone, A. K. & Nickerson, M. T. (2012). Formation and functionality of whey protein isolate-(kappa-, iota and lamda-type) carrageenan electrostatic complexes. *Food Hydrocolloids,* 27(2), 271-277.

Sun, C., Gunasekaran, S. & Richards, M. P. (2007). Effect of xanthan gum on physiochemical properties of whey protein isolate stabilised oil-in-water emulsions. *Food Hydrocolloids,* 21(4), 555-564.

Tadros, T., Izquierdo, R., Esquena, J. & Solans, C. (2004). Formation and stability of nano-emulsions. *Advance Colloid Interface Science*, 108-109, 303-318.

Takeiti, C. Y., Koechbusch, T. G. & Collares-Queiroz, F. P. (2010). Morphological and physicochemical characterization of commercial maltodextrins with different

degrees of dextrose-equivalent. *International Journal of Food Properties*, 13(2), 411-425.

Taneja, A., Ye, A., Jones, J. R., Archer, R. & Singh, H. (2013). Behaviour of oil droplets during spray drying of milk-protein-stabilised oil-in-water emulsions. *International Dairy Journal*, 28(1), 15-23.

Tan, C. P. & Nakajima, M. (2005a). Effect of polyglycerol esters of fatty acids on physicochemical properties and stability of β-carotene nanodispersions prepared by emulsification/ evaporation method. *Journal of the Science of Food and Agriculture*, 85(1), 121-126.

Tan, C. P. & Nakajima, M. (2005b). β-Carotene nanodispersions: preparation, characterization and stability evaluation. *Food Chemistry*, 92(4), 661-671.

Tang, Y. C. & Chen, B. H. (2000). Pigment change of freeze-dried carotenoid powder during storage. *Food Chemistry*, 69(1), 11-17.

Tang, S. Y., Shridharan, P. & Sivakumar, M. (2012). Impact of process parameters in the generation of novel aspirin nanoemulsions - comparative studies between ultrasound cavitation and microfluidiser. *Ultrasonics Sonochemistry,* 20(1), 485-497.

Thiengnoi, P., Suphantharika, M. & Wongkongkatep, P. (2012). Influence of binder type and concentration on physical properties of agglomerated, spray-dried, and high oil loaded microcapsules. *Journal of Food, Agriculture & Environment*, 10(3 & 4), 141-150.

Tiwari, R. & Takhistove, P. (2012). Nanotechnology-enabled delivery systems for food functionalization and fortification. In Padua, G.W. & Wang, Q. (Eds.), *Nanotechnology Research Methods for Foods and Bioproducts* (55-101). John Wiley & Sons, Inc.

Tokle, T. & McClements, D. J. (2011). Physicochemical properties of lactoferrin stabilized oil-in-water emulsions: effects of pH, salt and heating. *Food Hydrocolloids*, 25(5), 976-982.

Tokle, T., Decker, E. A. & McClements, D. J. (2012). Utilization of interfacial engineering to produce novel emulsion properties: pre-mixed lactoferrin/β-lactoglobulin protein emulsifiers. *Food Research International*, 49(1), 46-52.

Tonon, R. V., Pedro, R. B., Grosso, C. R. F. & Hubinger, M. D. (2012). Microencapsulation of flaxseed oil by spray drying: effect of oil load and type of wall material. *Drying Technology*, 30(13), 1491-1501.

Trojer, M. A., Holmberg, K. & Nydén, M. (2012). The importance of proper anchoring of an amphiphilic dispersant for colloidal stability. *Langmuir*, 28(9), 4047-4050.

Trojer, M. A., Mohamed, A. & Eastoe J. (2013). A highly hydrophobic anionic surfactant at oil–water, water–polymer and oil–polymer interfaces: Implications for spreading coefficients, polymer interactions and microencapsulation via internal phase separation. *Colloids and Surfaces A: Physicochemical and Engineering Aspects*, 436, 1048-1059.

Trojer, M. A., Nordstierna, L., Bergek, J., Blanck, H., Holmberg, K. & Nydén, M. (2015). Use of microcapsules as controlled release devices for coatings. *Advances in Colloid and Interface Science*, 222, 18-43.

Trojer, M. A., Nordstiema,L., Nordin, M., Nydén, M. & Holmberg, K. (2013). Encapsulation of actives for sustained release. *Physical Chemistry Chemical Physics*, 15(41), 17727-17741.

Troost, F. J., Steijns, J., Saris, W. H. M. & Brummer, R. M. (2001). Gastric digestion of bovine lactoferrin in vivo in adults. *American Society for Nutritional Science*, 131(8), 2101-2104.

Turchiuli, C., Munguia, M. T. J., Sanchez, M. H., Ferre, H. C. & Dumoulin, E. (2014). Use of different supports for oil encapsulation in powder by spray drying. *Powder Technology,* 255, 103-108.

United States Pharmacopeial Convention. (2002). *The Official Compendia of Standards*. Toronto, Ontario, Canada, Webcom Limited.

Voinova, M. V., Rohahl, M., Jonson, M. & Kasemo, B. (1999). Viscoelastic acoustic response of layered polymer films at fluid solid interfaces: Continuum mechanics approach. *Physica Scripta*, 59(5), 391-396.

Wahlgren, M. C., Arnebrant, T. & Paulsson, M. A. (1993). The adsorption from solutions of β-lactoglobulin mixed with lactoferrin or lysozyme onto silica and methylated silica surfaces. *Journal of Colloid and Interface Science*, 158(1), 46-53.

Walstra, P. & Vliet, T. (2008). Dispersed systems: basic considerations. In Damodaran, S., Parkin, K. & Fennema, O. R. (Eds). *Fennema's Food Chemistry*. 4th ed. CRC Press.

Wang, W. & Zhou, W. (2012). Characterization of spray-dried soy sauce powders using maltodextrins as carrier. *Journal of Food Engineering*, 109(3), 399-405.

Weinbreck, F., Vries, R., Schrooyen, P. & Kruif, C. G. (2003). Complex coacervation of whey proteins and gum Arabic. *Biomacromolecules,* 4(2), 293-303.

Weiss, J., Gaysinsky, S., Davidson, P. M. & McClements, D. J. (2009). Nanostructured encapsulation systems: food antimicrobials. In Barbosa-Canovas, G., Mortimer, A., Lineback, D., Spiess, W., Buckle, K. & Colonna, P. (Eds), *Global Issues in Food Science and Technology* (435-479). Academic Press.

Weiss, J. & McClements, D. J. (2000). Influence of Ostwald ripening on rheology of oil-in-water emulsions containing electrostatically stabilized droplets. *Langmuir*, 16(5), 2145-2150.

Willart, de Gusseme, A., Hemon, S., Descamps, M., Leveiller, F. & Rameau, A. (2002).Vitrification and polymorphism of trehalose induced by dehydration of trehalose dehydrate. *Journal of Physical Chemistry B*, 106(13), 3365-3370.

Wooster, T. J., Golding, M. & Sanguansri, P. (2008). Impact of oil type on nanoemulsion formation and Ostwald ripening stability. *Langmuir,* 24(22), 12758-12765.

Xiao, R., Badger, T. M., Simmen, F. A. (2005). Dietary exposure to soy or whey proteins alters colonic global gene expression profiles during rat colon tumorigenesis. *Molecular Cancer*, 4, 1-17.

Xin, H. L. & Mujumdar, A. S. (2009). Spray drying and its application in food processing. In Passos, M.L. & Ribeiro, C.P. (Eds.), *Innovation in Food Engineering New Techniques and Products* (303-329). CRC Press.

Yan, Y., Kizilay, E., Seeman, D., Flanagan, S., Dubin, P. L., Bovetto, L., Donato, L. & Schmitt, C. (2013). Heteroprotein complex coacervation: bovine β-lactoglobulin and lactoferrin. *Langmuir*, 29(50), 15614-15623.

Yang, Y., Leser, M. E., Sher, A. & McClements, D. J. (2013). Formation and stability of emulsions using a natural small molecule surfactant: Quillaja saponin (Q-Naturale®). *Food Hydrocolloids*, 30(2), 589-596.

Yang, Y., Marshall-Breton, C., Leser, M. E., Sher, A. A. & McClements, D. J. (2012). Fabrication of ultrafine edible emulsions: comparison of high-energy and low-energy homogenization methods. *Food Hydrocolloids,* 29(2), 398-406.

Ye, A. (2008). Complexation between milk proteins and polysaccharides via electrostatic interaction: principles and application - a review. *International Journal of Food Science and Technology*, 43(3), 406-415.

Ye, A., Flanagan, J. & Singh, H. (2006). Formation of stable nanoparticles via electrostatic complexation between sodium caseinate and gum Arabic. *Biopolymers,* 8(2), 121-133.

Ye, A, Lo, J. & Singh, H. (2012). Formation of interfacial milk protein complexation to stabilize oil-in-water emulsions against calcium. *Journal of Colloid and Interface Science*, *378*(1), 184-190.

Ye, A. & Singh, H. (2006).Adsorption behaviour of lactoferrin in oil-in-water emulsions as influenced by interactions with β-lactoglobulin. *Journal of Colloid and Interface Science*, *295*(1), 249-254.

Ye, A. & Singh, H. (2007). Formation of multilayers at the interface of oil-in-water emulsion via interactions between lactoferrin and β-lactoglobulin. *Food Biophysics*, 2(4), 125-132.

Yi, J., Lam, T. I., Yokoyama, W., Cheng, L. W. & Zhong, F. (2014). Cellular uptake of β-carotene from protein stabilized solid lipid nanoparticles prepared by homogenization-evaporation method. *Journal of Agricultural and Food Chemistry*, 62(5), 1096-1104.

Yin, L. J., Chu, B. S., Kobayashi, I. & Nakajima, M. (2009). Performance of selected emulsifiers and their combinations in the preparation of β-carotene nanodispersions. *Food Hydrocolloids,* 23(6), 1617-1622.

Yonekura, L. & Nagao, A. (2007). Intestinal absorption of dietary carotenoids. *Molecular Nutrition and Food Research*, 51(1), 107-115.

Yu, H. & Huang, Q. (2013). Investigation of the cytotoxicity of food-grade nanoemulsions in Caco-2 cell monolayers and HepG2 cells. *Food Chemistry*, 141(1), 29-33.

Yuan, Y., Gao, Y., Zhao, J. & Mao, L. (2008). Characterization and stability evaluation of β-carotene nanoemulsions prepared by high pressure homogenization under various emulsifying conditions. *Food Research International,* 41(1), 61-68.

Zeeb, B., Herz, E., McClements, D. J. & Weiss, J. (2014). Impact of alcohols on the formation and stability of protein-stabilized nanoemulsions. *Journal of Colloid and Interface Science*, 433, 196-203.

Zhang, J., Field, C., J., Vine, D. & Chen, L. (2015). Intestinal uptake and transport of vitamin B_{12}-loaded soy protein nanoparticles. *Pharmaceutical Research*, 32(4), 1288-1303.

Zhang, Z., Dalgleish, D. G. & Goff, H. D. (2004). Effect of pH and ionic strength on competitive protein adsorption to air/water interfaces in aqueous foams made with mixed milk proteins. *Colloids and Surfaces B: Biointerfaces,* 34, 113–121.

Ziani, K., Fang, Y. & McClements, D. J. (2012). Encapsulation of functional lipophilic components in surfactant-based colloidal delivery systems: vitamin E, vitamin D, and lemon oil. *Food Chemistry*, 134(2), 1106-1112.

Zuidam, N. J. & Shimoni, E. (2010). Overview of Microencapsulates for Use in Food Products or Processes and Methods to Make Them, In Zuidam, N. J. & Nedović, V. (3-30)., *Encapsulation Technologies for Active Food Ingredients and Food Processing* (eds). Springer Science + Business Media, LLC.

APPENDICES

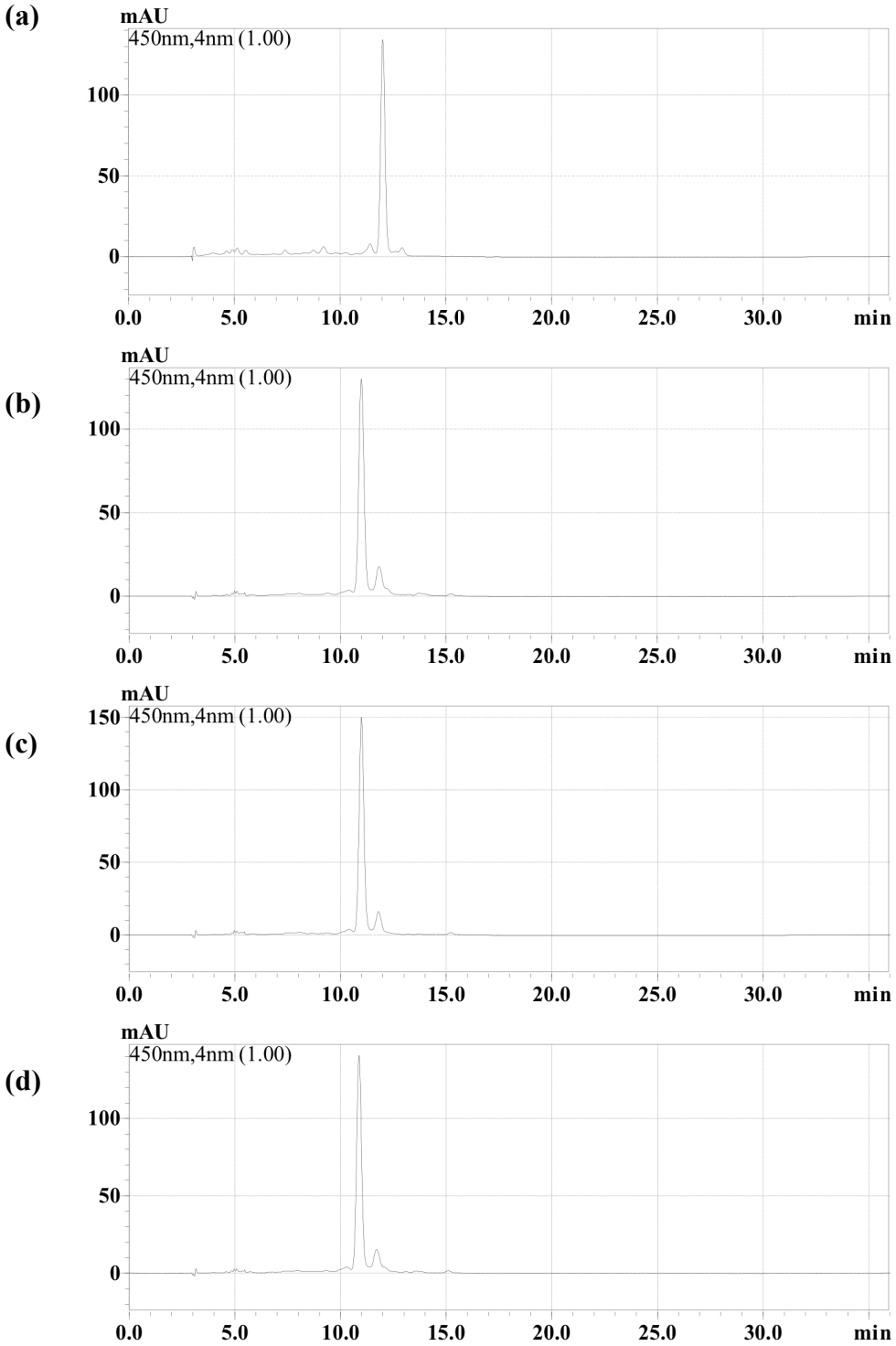

Figure 1 HPLC chromatograms of lutein standard and lutein recovered from emulsions at Day 0: (a) lutein standard in ethyl acetate; (b) WPI-stabilised conventional emulsion; (c) WPI-stabilised nanoemulsions and (d) WPI-lactoferrin stabilised nanoemulsions.

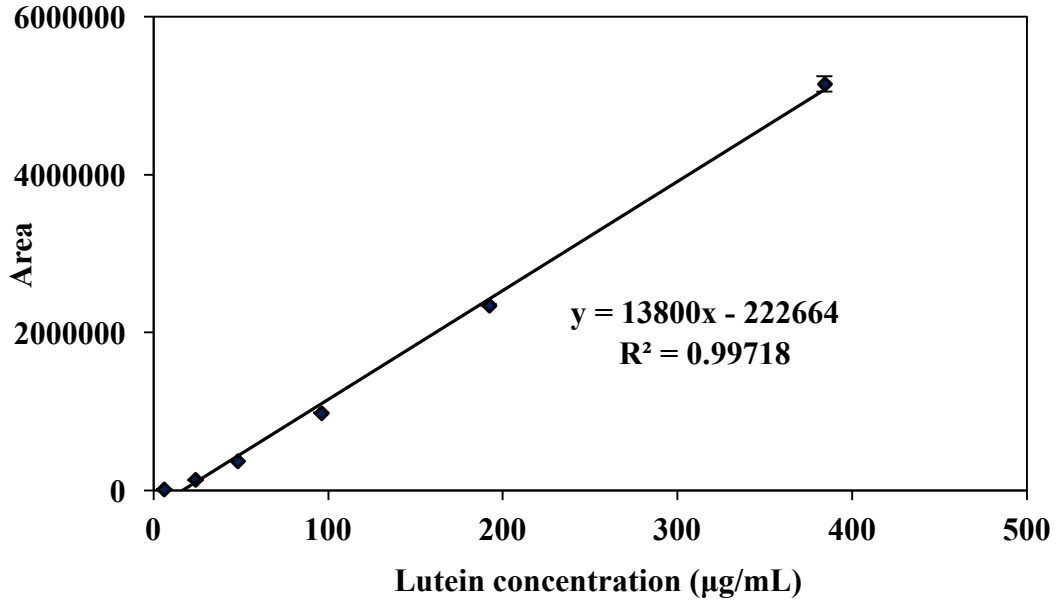

Figure 2 Calibration curve of different concentrations of lutein solutions.

Table 1A Composition of nanoemulsions prepared at organic phase ratio of 10:90.

	Emulsifier concentration											
	0.25%			0.5%			0.75%			1%		
	Before evap.	After evap.	Final compo.	Before evap.	After evap.	Final compo.	Before evap.	After evap.	Final compo.	Before evap.	After evap.	Final compo.
Aqueous phase												
Emulsifier	0.45	0.49	0.23	0.90	0.99	0.45	1.35	1.48	0.68	1.80	1.98	0.90
Water	89.6	98.4	99.3	89.1	97.9	99.1	88.7	97.4	98.8	88.2	96.9	98.6
Organic phase												
Ethyl acetate	9.00	0.00	0.00	9.00	0.00	0.00	9.00	0.00	0.00	9.00	0.00	0.00
Oil	1.00	1.10	0.50	1.00	1.10	0.50	1.00	1.10	0.50	1.00	1.10	0.50
Total	100	100	100	100	100	100	100	100	100	100	100	100

	Emulsifier concentration								
	2%			3%			5%		
	Before evap.	After evap.	Final compo.	Before evap.	After evap.	Final compo.	Before evap.	After evap.	Final compo.
Aqueous phase									
Emulsifier	3.60	4.00	1.80	5.40	5.90	2.70	9.00	9.89	4.50
Water	86.4	95.0	97.7	84.6	93.0	96.8	81.0	89.0	95.0
Organic phase									
Ethyl acetate	9.00	0.00	0.00	9.00	0.00	0.00	9.00	0.00	0.00
Oil	1.00	1.10	0.50	1.00	1.10	0.50	1.00	1.10	0.50
Total	100	100	100	100	100	100	100	100	100

Table 1B Composition of nanoemulsions prepared at organic phase ratio of 20:80.

	Emulsifier concentration											
	0.25%			0.5%			0.75%			1%		
	Before evap.	After evap.	Final compo.	Before evap.	After evap.	Final compo.	Before evap.	After evap.	Final compo.	Before evap.	After evap.	Final compo.
Aqueous phase												
Emulsifier	0.20	0.24	0.05	0.40	0.49	0.10	0.60	0.73	0.15	0.80	0.98	0.20
Water	79.8	97.3	99.5	79.6	97.1	99.4	79.4	96.8	99.4	79.2	96.6	99.3
Organic phase												
Ethyl acetate	18.0	0.00	0.00	18.0	0.00	0.00	18.0	0.00	0.00	18.0	0.00	0.00
Oil	2.00	2.44	0.50	2.00	2.44	0.50	2.00	2.44	0.50	2.00	2.44	0.50
Total	100	100	100	100	100	100	100	100	100	100	100	100

	Emulsifier concentration								
	2%			3%			5%		
	Before evap.	After evap.	Final compo.	Before evap.	After evap.	Final compo.	Before evap.	After evap.	Final compo.
Aqueous phase									
Emulsifier	1.60	1.95	0.39	2.40	2.93	0.59	4.00	4.88	0.98
Water	78.4	95.6	99.1	77.6	94.6	98.9	76.0	92.7	98.5
Organic phase									
Ethyl acetate	18.0	0.00	0.00	18.0	0.00	0.00	18.0	0.00	0.00
Oil	2.00	2.44	0.50	2.00	2.44	0.50	2.00	2.44	0.50
Total	100	100	100	100	100	100	100	100	100

MASSEY UNIVERSITY
GRADUATE RESEARCH SCHOOL

STATEMENT OF CONTRIBUTION
TO DOCTORAL THESIS CONTAINING PUBLICATIONS

(To appear at the end of each thesis chapter/section/appendix submitted as an article/paper or collected as an appendix at the end of the thesis)

We, the candidate and the candidate's Principal Supervisor, certify that all co-authors have consented to their work being included in the thesis and they have accepted the candidate's contribution as indicated below in the *Statement of Originality*.

Name of Candidate: Teo Hwee Ming Anges

Name/Title of Principal Supervisor: Sung Je Lee / Senior Lecturer

Name of Published Research Output and full reference:

Teo, A., Goh, K. K. T. & Lee, S. J. (2014). Nanoparticles and nanoemulsions. In: Noomhorm, A., Ahmad, I. & Anal, A. K., Functional Foods and Dietary Supplements: Processing Effects and Health Benefits (pp. 405-435). United Kingdom: Wiley Blackwell.

In which Chapter is the Published Work: Chapter 2

Please indicate either:

- The percentage of the Published Work that was contributed by the candidate 90%

  and / or
- Describe the contribution that the candidate has made to the Published Work:

Anges Teo — Digitally signed by Anges Teo
Candidate's Signature

9/3/2016
Date

Sung Je Lee — Digitally signed by Sung Je Lee Date: 2016.03.09 14:52:20 +13'00'
Principal Supervisor's signature

9/3/2016
Date

MASSEY UNIVERSITY
GRADUATE RESEARCH SCHOOL

STATEMENT OF CONTRIBUTION TO DOCTORAL THESIS CONTAINING PUBLICATIONS

(To appear at the end of each thesis chapter/section/appendix submitted as an article/paper or collected as an appendix at the end of the thesis)

We, the candidate and the candidate's Principal Supervisor, certify that all co-authors have consented to their work being included in the thesis and they have accepted the candidate's contribution as indicated below in the *Statement of Originality*.

Name of Candidate: Teo Hwee Ming Anges

Name/Title of Principal Supervisor: Sung Je Lee / Senior Lecturer

Name of Published Research Output and full reference:

Teo, A., Goh, K. K. T., Wen, J., Oey, I., Ko, S., Kwak, H. S. & Lee, S. J. (2016). Physicochemical properties of whey protein, lactoferrin and Tween 20 stabilised nanoemulsions: effect of temperature, pH and salt. Food Chemistry, 197(Part A), 297-306.

In which Chapter is the Published Work: Chapter 4

Please indicate either:

- The percentage of the Published Work that was contributed by the candidate 90%

  and / or

- Describe the contribution that the candidate has made to the Published Work:

  The candidate has carried out all the experiments, ~90% of data analysis and 90% of the preparation of the manuscript.

Anges Teo — Candidate's Signature — 9/3/2016 — Date

Sung Je Lee — Principal Supervisor's signature — 9/3/2016 — Date

MASSEY UNIVERSITY
GRADUATE RESEARCH SCHOOL

STATEMENT OF CONTRIBUTION TO DOCTORAL THESIS CONTAINING PUBLICATIONS

(To appear at the end of each thesis chapter/section/appendix submitted as an article/paper or collected as an appendix at the end of the thesis)

We, the candidate and the candidate's Principal Supervisor, certify that all co-authors have consented to their work being included in the thesis and they have accepted the candidate's contribution as indicated below in the *Statement of Originality*.

Name of Candidate: Teo Hwee Ming Anges

Name/Title of Principal Supervisor: Sung Je Lee / Senior Lecturer

Name of Published Research Output and full reference:

Teo, A., S. Dimartino, S. J. Lee, K. K. T. Goh, J. Wen, Indrawati, O., S. Ko & H. S. Kwak (2016). Interfacial structures of whey protein isolate (WPI) and lactoferrin on hydrophobic surfaces in a model system monitored by quartz crystal microbalance with dissipation (QCM-D) and their formation on nanoemulsions. Food Hydrocolloids, 56, 150-160.

In which Chapter is the Published Work: Chapter 6

Please indicate either:

- The percentage of the Published Work that was contributed by the candidate 85%

  and / or

- Describe the contribution that the candidate has made to the Published Work:

  The candidate has carried out all the experiments, data analysis (90%) and preparation of the manuscript (~90%).

Anges Teo — Digitally signed by Anges Teo
DN: cn=Anges Teo, o, ou, email=m.s.a.teo@massey.ac.nz, c=NZ
Date: 2016.03.09 09:11:52 +13'00'

Candidate's Signature — 9/3/2016 — Date

Sung Je Lee — Digitally signed by Sung Je Lee
Date: 2016.03.09 15:02:03 +13'00'

Principal Supervisor's signature — 9/3/2016 — Date